Engineering New Supramolecular Gels:
From Catalysis to Drug Delivery

Dissertation

Zur Erlangung des Doktorgrades

Dr. rer. nat.

an der Fakultät für Chemie und Pharmazie

der Universität Regensburg

vorgelegt von

Jürgen Bachl

aus Rimbach

Regensburg 2014

Dedicated to Mam, Bap, Fab and Theresa

„Try not to become a man of success, but a man of value. Look around at how people want to get more out of life than they put in. A man of value will give more than he receives. Be creative, but make sure that what you create is not a curse for mankind.”

Albert Einstein

Table of Contents

A Summary

The present dissertation evaluates the design, characterization and potential applications of functional supramolecular gel-materials. Gels have attracted tremendous scientific interest as they can be obtained from natural sources or derive from readily available building blocks by facile preparation methods. They have conquered our daily life appearing as constituents of commercial products in the fields of biomedicine, agriculture, cosmetics, food thickeners and many more. Gel-materials exhibit a continuous structure and embody a meta-stable state between liquids and solids. They can be categorized by physical and chemical gels, depending on the forces responsible for their formation. Physical or supramolecular gels are solely held together by weak and non-covalent forces, which provides a potential response to external stimuli and hence they represent the main focus of research conducted in this thesis. In this context, the present work has been divided into three main parts: Introduction, Main part and Supporting Information enclosed on a CD.

The first part of the introduction provides a broader overview on natural and artificial self-assembling systems in order to demonstrate nature´s power of generating well-ordered complex structures with controlled function from available building blocks without human intervention and how we can take lessons for the fabrication of novel materials and devices. A general definition and classification of gels is given in the second part of the introduction in order to get a detailed insight into the diversity of gel-subclasses and to understand the forces necessary to promote the mechanisms of self-assembling gel-formation. The last part of the introduction focuses on high-tech applications of gel-materials in the fields of biomedicine, catalysis and fabrication of nanoparticles of well-defined shape and size. Herein the center of interest lies in the evaluation of potential advantages of 3D gel-environments for applications against already established materials and procedures.

Chapter 1 describes the design and evaluation of gelation properties of novel peptide-based organogelators with side-chain azobenzene modifications. In this context, effective gelation of various organic solvents could be observed at relatively low concentrations without a major effect of the position of the azobenzene-moieties inside the gelator-structure. The presence of azobenzene-functionalities was found to exhibit a

1

positive effect on the gelation properties by lowering minimum gelation concentrations and improving thermal and mechanical stabilities in comparison to control-peptides. Furthermore, photo-induced *gel*-to-*sol* transition could be achieved by UV-irradiation of gel-samples due to a rapid *trans*-to-*cis* isomerization reaction (30-60 min) of the azobenzenes, which was found to be reversible when the samples were left for relaxation. Interestingly, light-driven phase transition was only feasible for peptide-gelators lacking *N*-terminal protecting groups. It is important to mention, that such stimuli-responsive behavior is a key concept for the fabrication of functional materials for biomedical and optoelectronic applications. Additionally, we were delighted to observe a phase selective gelation behavior of our gelators, which could be induced by room temperature gelation protocols for potential application in oil-spill recovery and dye-removal.

Chapter 2 focuses on the exploration of various supramolecular gel-scaffolds as reaction vessels in photo-chemical transformations. Due to the growing demand for sustainability in industrial applications, photochemistry provides efficient and clean alternatives towards conventional processes. Inspired by nature, we investigated the photo-oxidation of a secondary benzyl-alcohol catalyzed by flavin-derivatives in a library of diverse gel-based matrices. Gel-materials provide a well-structured highly porous network and are literally predestinated to serve as nanoreactors, in which alternative selectivities or reaction pathways could be accessible. In this context, we were able to demonstrate that the structure-property relationship of gels derived from both (bio-)polymers and low molecular weight compounds has a direct influence on the kinetics and outcome of the model-reaction. Although it is known that photo-chemical transformation progress less efficient in organic solvents such as acetonitrile, an organogelator proved to be most active to promote the photo-oxidation reactions. Due to the confined gel-network, reaction rates were found to be slightly reduced in comparison to aqueous and micellar environments under non-stirred conditions.

Chapter 3 provides insight into a synergistic computational and experimental approach to improve the hydrogelation-ability of ionene polymer-based gelators. Despite the fact that gels provide numerous potential applications, still the mechanism of self-assembly and gel-formation is not fully understood and hence prediction of physical gel-properties remains challenging. Interestingly, we were able to demonstrate that gelation properties of polyelectrolyte hydrogels could be controlled by simple modification of the core-geometry of the polymers. Conclusions drawn from experimental observations were

successfully confirmed by computational simulation techniques including DFT-calculations. Furthermore, gels based on the most efficient polymer exhibited a transparent appearance and the gel-network was able to disperse single-walled carbon nanotubes to produce organic-inorganic hybrid materials. The poor solubility accompanied by a high affinity towards aggregation is creating a problem for applications of nanotubes as molecular conductors, which could be solved by homogeneous dispersion in gel-materials.

Chapter 4 focuses on the ultrasound enhanced gelation properties of a novel formamidine-based ambidextrous gelator. For a long time, ultrasonic treatment was thought to hinder self-assembling processes in solution. Hence it is very fascinating that treatment of isotropic solutions of the formamidine in various organic solvents resulted in much faster gelation kinetics in comparison to the classical heating-cooling protocol to induce gelation. Additionally, this phenomenon was accompanied by a severe reduction of the minimum gelation concentration and a significant enhancement of thermal and mechanical stabilities. The ambidextrous nature of the formamidine compound was revealed by applying a pH-gradient method to induce gelation in aqueous environments in a pH-range of 4.5-5.5, which could result in potential application in transdermal drug release. Furthermore, organogels revealed a smart colorimetric response towards several heavy metal-ions such as Cu(II), Fe(III) and Ce(IV), which could result in potential applications in sensing.

Finally, chapter 5 deals with isosteric replacement of an amide-moiety inside a known gelator-structure by a triazole. The concept of bioisosteric replacement is well established in the field of biomedicine, but is has so far not been applied in material science. Heterocyclic compounds have been successfully introduced into parental drug systems as they exhibit enhanced stabilities against hydrolysis. Since the development of the copper and ruthenium catalyzed cycloaddition between azides and alkynes, triazoles represent the most common class of heterocycles in isosteric replacement applications. Additionally, triazoles share many common properties with amides such as a high dipole moment and the possibility to create hydrogen-bonds. In this context, gelation abilities of an amphiphilic amide-gelator and its triazole-analogue have been systematically studied. Interestingly, it was found that the amide-containing compound was a more effective gelator for apolar solvents whereas the triazole-compound exhibited superior properties in polar protic environments. Furthermore, hydrogels derived from the triazole were readily

3

degraded in the presence of physiological buffers, which resulted in potential applications of controlled release of a model drug (i.e. vancomycin).

5

B Zusammenfassung

Die vorliegende Dissertation bewertet Studien zur Planung, Charakterisierung und zu möglichen Anwendungen von funktionalen supramolekularen Gel-Materialien. Gele ziehen seit mehreren Jahrzehnten immer mehr Interesse auf sich, da aus ihnen eine Vielzahl von Werkstoffen hergestellt werden kann, die unter anderem in Bereichen der Biomedizin, Katalyse, Landwirtschaft, Kosmetik oder der Lebensmittelindustrie Anwendung finden. Diese Materialien weisen eine kontinuierliche Struktur auf und stellen einen metastabilen Zustand zwischen fest und flüssig dar. Sie können zum Beispiel basierend auf den Wechselwirkungen durch die sie gebildet werden in physikalische oder chemische Gele unterteilt werden. Physikalische, oder auch supramolekulare Gele genannt, besitzen den großen Vorteil, dass sie auf Grund von schwachen Wechselwirkungen potentiell auf äußere Stimuli, wie Wärmeeinfluss oder Bestrahlung mit Licht einer bestimmten Wellenlänge, reversibel reagieren können. Auf Grund dieser herausragenden Eigenschaften liegt der Fokus der vorliegenden Arbeit auf physikalischen Gelen und wurde in drei Teile untergliedert: Einleitung, Hauptteil und Zusatzinformationen auf einer CD.

Der erste Teil der Einleitung vermittelt einen breiten Überblick von natürlichen und synthetischen selbst-assemblierten Systemen. Dies dient zur Veranschaulichung der Fähigkeit der Natur geordnete und komplizierte Strukturen für bestimmte Anwendungen ohne menschliches Zutun herzustellen und zu zeigen, was die Menschheit im Bezug auf die Entwicklung neuer Materialien daraus lernen kann. Gemeinsamkeiten und Unterschiede von gel-basierten Materialien werden im zweiten Teil der Einleitung beschrieben. Besondere Aufmerksamkeit wird hierbei den unterschiedlichen Kräften, die für die Gelbildung verantwortlich sind gewidmet und zugrundelegende Mechanismen werden diskutiert. Mögliche Anwendungen von Gelen in den Gebieten der Biomedizin, chemischen Katalyse und der Herstellung von Nanopartikeln mit kontrollierter Form und Größe werden im abschließenden Teil bearbeitet. Besonderes Interesse liegt hierbei in der Ausarbeitung von möglichen Vorteilen des 3D Gelnetzwerks im Vergleich zu bereits vorhandenen Materialien und Prozessen.

In Kapitel 1 werden neuartige Peptid-basierte Organogelatoren mit Azobenzol-Modifikationen in der Seitenkette vorgestellt. In diesem Zusammenhang wurde festgestellt, dass eine Vielzahl an organischen Lösungsmitteln bei relativ geringen

Gelatorkonzentrationen Gele formten und, dass die Azobenzol-Gruppierungen einen positiven Einfluss auf die Geleigenschaften auswirkten, indem sie eine Erniedrigung der minimalen Gelkonzentration und eine Verbesserung der thermischen und mechanischen Stabilitäten bewirkten. Desweiteren konnten *Gel*-zu-*Sol* Phasenumwandlungen durch UV-Bestrahlung von Gelproben induziert werden, welche auf einer schnellen *trans-cis* Isomerisierung der Azobenzol-Gruppen beruhen. Diese Umwandlungen sind reversibel und Gele können sich durch Relaxation im Dunkeln nach einiger Zeit zurückformen. Interessanterweise konnten nur Peptid-Gelatoren mit freiem *N*-Terminus einer Licht-induzierten Phasenumwandlung unterzogen werden. Zusätzlich konnten wir zu unserer Freude Phasenselektives Gelieren bei Raumtemperaturbedingungen beobachten, was mögliche Anwendungen in der Wasseraufreinigung mit sich bringt.

Kapitel 2 beschäftigt sich mit der Untersuchung von verschiedensten Gel-Materialien für die Verwendung als Reaktionsgefäße in photochemischen Transformationen. Auf Grund des steigenden Bedürfnisses für nachhaltige industrielle Prozesse, stellt insbesondere die Photochemie effiziente und saubere Alternativen zu herkömmlichen Methodiken bereit. Inspiriert von natürlichen Systemen, wurde die Photooxidation eines sekundären Benzylalkohols in diversen Gelmatrizen, katalysiert durch ein Flavinderivat, untersucht. Gelmaterialien stellen ein gut-strukturiertes poröses Netzwerk bereit und sind deshalb geradezu prädestiniert als Reaktionsgefäße verwendet zu werden, worin andere Reaktionswege und Selektivitäten erreicht werden könnten. In diesem Zusammenhang konnte gezeigt werden, dass die Eigenschaften von verschieden strukturierten Gelen (i.e. (Bio-)Polymere und Komponenten mit niedrigem Molekulargewicht) einen direkten Einfluss auf den Reaktionsverlauf und die Reaktionskinetiken ausübten. Interessanterweise, waren die Ergebnisse in einem Organogelnetzwerk am vielversprechendsten, obwohl es bekannt ist, dass photochemische Reaktionen in organischen Lösungsmitteln weniger effizient verlaufen. Im Vergleich zu wässrigen und mizellaren Phasen unter statischen Bedingungen waren die Reaktionskinetiken etwas erniedrigt, was wahrscheinlich an der eingeschränkten Diffusion in Gelen liegt.

Kapitel 3 bereitet einen Einblick zur Verbesserung der Geleigenschaften von ionischen Polymer-Hydrogelatoren an Hand eines Synergismus zwischen experimentellen und computergestützten Methodiken. Obwohl Gele Anwendungen in vielen Bereichen finden, bleibt der Mechanismus der Gelformung nahezu ungeklärt, was eine Vorhersage

der Geleigenschaften stark erschwert. Zu unserer Freude konnte in diesem Zusammenhang gezeigt werden, dass die Geleigenschaften von ionischen Polymer-Hydrogelatoren durch einfache geometrische Veränderungen (i.e. Änderung des Bindungswinkels einer disubstituierten aromatischen Gruppierung) der Polymerstruktur kontrolliert werden können. Experimentelle Befunde konnten erfolgreich durch computergestützte Simulationen wie zum Beispiel DFT-Rechnungen bestätigt werden. Zusätzlich zeigte das effizienteste Polymer die Fähigkeit Kohlenstoff-Nanoröhren homogen zu dispergieren, was zur Bildung von organisch-anorganischen Hybridmaterialen führt. Die schlechte Löslichkeit und der Drang zu aggregieren schränken die Verwendung von Nanoröhren ein, was durch die homogene Verteilung in Gelen vermieden werden kann.

Kapitel 4 beschäftigt sich mit Geleigenschaften eines Formamidine-Derivats, die durch Ultraschallbehandlung verbessert werden können. Lange Zeit wurde angenommen, dass sich Ultraschall negativ auf Selbst-Assemblierungsprozesse in Lösung auswirkt. Es ist deshalb äußerst erstaunlich, dass sich die Beschallung von isotropen Lösungen des Formamidines in diversen organischen Lösungsmitteln durch viel schnellere Gelkinetiken im Vergleich zur herkömmlichen Herstellung von Gelen durch einen Aufheizen-Abkühlen-Zyklus ausdrückt. Zusätzlich konnten Gelatorkonzentrationen erniedrigt und thermische sowie mechanische Stabilitäten erhöht werden. Neben der Fähigkeit Organogele zu formen konnten durch den Aufbau eines pH-Gradienten Hydrogele gebildet werden (pH ~4.5-5.5), was Anwendungen in transdermalem Wirkstofftransport finden könnte. Interessanterweise reagierten Organogele durch die Anwesenheit von Metallsalzen wie Cu(II), Fe(III) oder Ce(IV) mit einem Farbwechsel, was potentielle Anwendung in der Sensorik von Schwermetallen finden könnte.

Das letzte Kapitel beschreibt den isosteren Austausch zwischen einer Amid-Gruppe und einem Triazol und dessen Auswirkung auf die Geleigenschaften eines bekannten Gelator-Gerüsts. Bioisosterer Austausch ist ein häufig gebrauchtes synthetisches Mittel in der Biomedizin, wurde aber bisher nicht im Bereich der Materialwissenschaften angewendet. Insbesondere Heterozyklen wurden oft dazu verwendet Hydrolyse-Empfindlichkeiten von Wirkstoffen zu verbessern und die Flexibilität von bestimmten chemischen Bindungen einzuschränken. Triazole beschreiben die größte Gruppe von Heterozyklen für isosteren Austausch, da sie durch die Entwicklung von Kupfer- und Ruthenium-katalysierten Zykloadditionen zwischen Aziden und Alkinen einfach synthetisch hergestellt werden können. Desweiteren zeigen Triazole ähnliche

Eigenschaften zu Amiden, wie die Möglichkeit Wasserstoff-Brücken auszubilden. In diesem Zusammenhang wurden die Fähigkeiten eines Amid-Gelators und dessen Triazol-Analogons zur Gelformung untersucht. Interessanterweise konnte der Amide-Gelator apolare Lösungsmittel effizienter gelieren, wohingegen der Triazol-Gelator bessere Eigenschaften in polar-protischen Umgebungen zeigte. Zusätzlich konnten Hydrogele des Triazol-Gelators in wässrigen Lösungen abgebaut werden, was dazu genutzt wurde einen Wirkstoff (i.e. Vancomycin) kontrolliert zu transportieren.

C Introduction

1. Natural and artificial self-assembly

One of the most challenging tasks of today´s researchers is to understand processes occurring in natural systems, as this is a key concept for the development of novel compounds, materials and devices under environmentally friendly and mild conditions. An exceptionally exciting and fascinating phenomenon developed by nature is self-assembly, which has attracted tremendous scientific interest already for countless decades. Self-assembly could be described as spontaneous organization of individual components into ordered structures without human intervention and is omnipresent in natural systems involving compounds from the molecular to the planetary scale based on a large set of different interactions.[1] The key processes for molecular self-assembly involve weak, non-covalent interactions (about 0.1-5 kcal/mol) and complementartity in shape amongst the individual components, resulting in materials with dimensions in the nano- and micrometer scale.[2] Hence, this phenomenon is of high interest for material science as it describes a promising approach towards the "bottom up" fabrication of nano-devices exhibiting novel physical properties in comparison to bulk-materials due to quantum mechanical effects.[3] Self-assembly can be seen as a hierarchical process comprising the following steps: a) the formation of molecules with well-defined structures and complexity through sequential covalent synthesis; b) formation of large and stable structurally defined molecular aggregates through non-covalent interactions; and c) the use of multiple copies of one or several constituents to facilitate the synthetic procedure. In order to obtain such stable and well-defined assemblies, it is important that the aggregates are joined by multiple non-covalent interactions to overcome competing interactions with the solvent and entropic dissociation effects.[4] A very illustrative example to demonstrate the concept of hierarchical natural self-assembly is the folding of proteins in aqueous environments. In a first step, a linear polypeptide is covalently synthesized from the 20 natural occurring amino acids by the translation of a sequence present in messenger RNA. As proteins are believed to be thermodynamically stable architectures, it is obvious that the information necessary to promote the final three-dimensional (3D) structure of the protein must be present already in the amino acid sequence. Protein folding is induced by a number of non-covalent

11

Tab. 1 Summary of some examples for natural and artificial self-assembling systems described.

Type of self-assembly	Example	Description
natural	tobacco mosaic virus (TMV)	protein aggregation in a helical manor around a single strand of RNA
natural	mollusc nacre	biomineralization: templated growth of inorganic materials ($CaCO_3$, aragonite) by a composition of pre-organized organic matrices (β-chitin, silk-fibroin proteins and acidic macromolecules)
natural	photosynthesis in chloroplasts	complex assembly of light harvesting and electron-transfer moieties inside the thylakoid membrane
natural	cells	assembly of various aggregates to form complex superstructures with various functions
artificial	peptide ion-channels	protein aggregation of cyclic peptides for trans-membrane ion transport
artificial	cyclodextrins in catalysis	enzyme mimetics (ribonuclease) for regio-selective catalysis (hydrolysis of phosphodiester)
artificial	light harvesting in liposomes	complex assembly of light harvesting and electron-transfer moieties in liposome-membranes coupled with ATP-synthase to mimic natural photosynthesis

interactions- namely hydrogen-bonding, van der Waals, dipole-dipole, electrostatic and π-π interactions amongst others- between structural complementary motifs in the amino acid sequence. A specific influence on the folding process is also provided by the so called "hydrophobic effect", which is based on the interactions between hydrophobic groups in the sequence with water and with each other. Although the information that could be generated by such a sequence is very large (i.e., a polypeptide containing 200 amino acids could generate in principle 20^{200} different sequences), particular amino acid motifs tend to reoccur assembling a small number of local structures such as α-helices or β-sheets through non-covalent forces. Such local structures finally aggregate in the protein to shield non-polar regions from water and to place hydrophilic areas in contact with water, resulting in the formation of the sequence-specific architecture of the protein.[2-5] Proteins also tend to form aggregates amongst each other to form functional associates. A prominent example therefore is the formation of ribosome[4] which is responsible for the translation of RNA to proteins. Another precedence for this phenomenon with a delicate overtone is the formation of amyloid fibrils, whose deposition in various tissues is thought to be responsible for diseases like Alzheimer´s or Parkinson´s disease.[6]
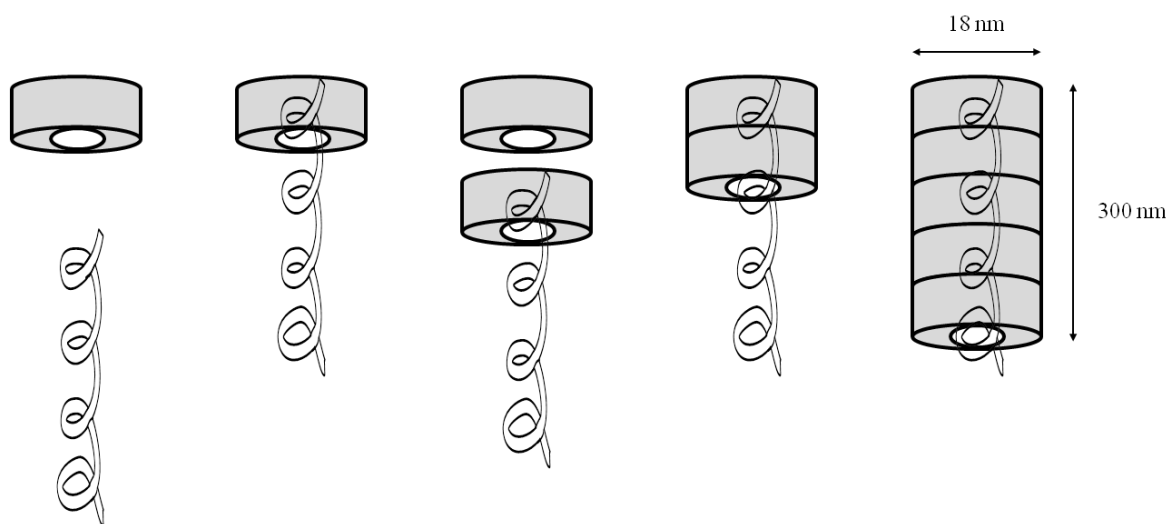
Fig. 1 Step-wise self-assembly of the tobacco mosaic virus.[3, 4]

A more complex, but very well studied system describing natural self-assembly is the tobacco mosaic virus (TMV).[3, 4] This helical virus particle, 300 nm in length and 18 nm in diameter consists of 2130 identical subunits forming a helical surrounding for a single

strand of RNA. As illustrated in Figure 1, each of the protein subunits forms a disk-like sub-assembly, which transforms into a helical structure by insertion of a RNA-strand into the center of the disc. Additional protein discs associate with the growing virus particle by non-covalent forces until completing the assembly process. The non-covalent forces allow the formation process to be dynamic, which makes assembly and disassembly of the subunits facile and results in a self-correcting process. Besides the folding and aggregation of proteins, plenty of other natural molecular self-assembling systems are known. These include for example the formation of the DNA double helix from two complementary strands of oligonucleotides through hydrogen bonding,[2-4, 7] cells[8] or bones.[9] The latter example is special as it comprises self-assembly of a combination of inorganic (hydroxy apatite) and organic materials (mainly collagen), which leads to the complex field of biomineralization. The concept of biomineralization takes advantage of pre-organized discretely self-assembled organic supramolecular templates to transform inorganic compounds like $CaCO_3$, SiO_2 or Fe_3O_4 into precisely controlled complex architectures.[9-15] Like self-assembly itself, biomineralization can be seen as a hierarchical process consisting of several steps which are represented by: a) supramolecular preorganization of the organic template; b) interfacial recognition between inorganic material and organic precursor; c) controlled nucleation and growth of crystals; and d) cellular processing towards high-ordered structures.[10, 11] As discussed earlier the formation of organic supramolecular aggregates is driven by non-covalent interactions such as hydrogen bonding or van der Waals interactions as well as by complementartity of the building blocks and can result in the formation of countless architectures and shapes, which can be transcripted also into biomineralized materials.[2] Some of these "hybrid-materials", like bone or mollusk shells exhibit excellent mechanical strength and/or flexibility and have been developed depending on the needs of the organism in which they are produced.[9, 13, 16 a)] Molecular recognition plays a provital role for the controlled nucleation of inorganic clusters from solution and hence in controlling the final morphologies of biomineralized compounds. The functionalized surfaces of pre-organized organic frameworks induce nucleation by electrostatic, structural and stereochemical complementartity of the inorganic-organic surface, which results in controlled crystallographic structures and orientations.[11] In complex living systems biomineralization templated by self-assembled structures can occur both intra- and extracellular. Inside cells usually protein cages and lipid vesicles are responsible for templated biomineralization, whereas extended protein and polysaccharide networks are common precursors in extracellular environments. Vesicles represent a

14

spherical shaped confined microenvironment for mineralization where the physicochemical conditions can be adjusted due to the permeability of the membrane. Nucleation and crystal growth is caused by spatial charges and accumulation of inorganic materials at localized regions of the cavity surface (metal binding sites) and negatively charged peptides (aspartic or glutamic acid rich areas). Within vesicles the influence on biomineralized materials is quite low and limited mostly to control of the size of the aggregates.[10] In contrast to vesicles, molecular recognition in extracellular extended assemblies allows more complex structuring. The periodic secondary structures of supramolecular organic compounds such as β-sheets control the assembly of nuclei along specific crystallographic directions. These templating polymeric networks usually share common features in structure. They consist of areas which are inert and hydrophobic on the one hand and acidic protein regions (nucleation is supposed to take place here) on the other. Nucleation of a specific crystal face can occur at the mineral-organic interface, if there exists geometric recognition between ion binding sites on the organic surface and the lattice spacing of a corresponding crystal structure.[10]
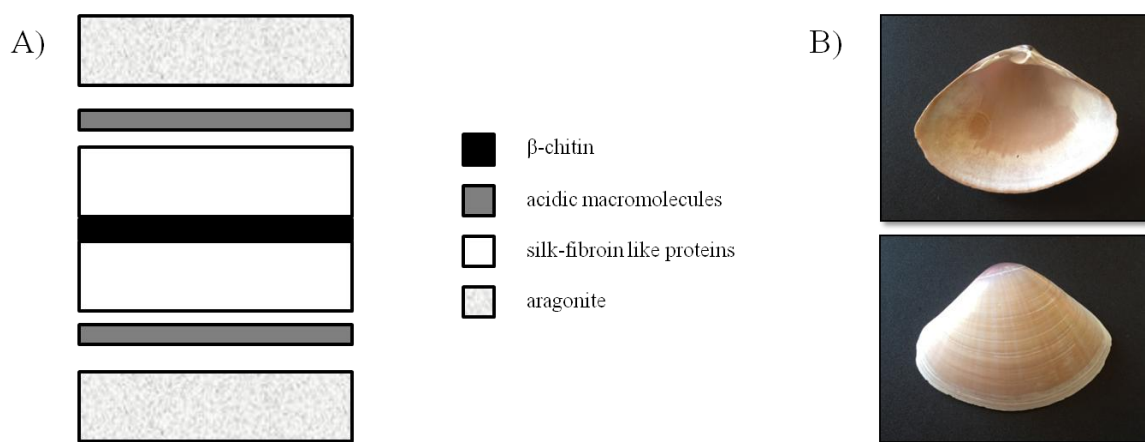
Fig. 2 A) Schematic representation of the composition of nacre from mollusc shells. Acidic nucleation macromolecules are arranged within a framework of hydrophobic biopolymers, forming the organic matrix which is bound by aragonite.[13] B) Digital photograph of a nacre layer (top) from a mollusc shell (bottom).

An illustrative example therefore is the nacre-layer of mollusc shells. Alternating layers of polygonal blocks of aragonite ($CaCO_3$) are intercalated by thin sheets of a protein-polysaccharide matrix in such a way that each aragonite crystal is aligned with its c-axis perpendicular to the plane of the organic sheets. The nucleation sites form repeatedly during life-time of the mollusc through episodic deposition of the matrix surface, resulting

15

in a brick-wall arrangement of the aragonite crystals. The composition of a typical layer of mollusc shell is illustrated in Figure 2.[13] More recently, evidence was found for the presence of amorphous inorganic precursors, replacing the theory of a classical nucleation protocol for the growth of crystalline materials during biomineralization. Amorphous, isotropic materials are in general more soluble and "soft" in comparison to crystals, which provides materials easier to be shaped by pre-organized matrices and could hence represent a reasonable alternate nucleation protocol.[17] Much effort has been spend during the last decades to mimic nature´s self-assembled systems in order to get insight into the phenomenon of self-assembly or to create novel functional materials.[2, 3, 5 a)-d), 7, 8, 16 a), 18] Very interesting approaches have been carried out towards taking advantage of the self-assembly of artificial peptide and protein-based materials for application in the fields of antibiotics, ion-channel mimetics or sensing (view Figure 3 A)).[5 a)-d), 16 a), 18 a)-c), m)] In other attempts, supramolecular scaffolds, such as modified cyclodextrins or calixarenes have been studied to simulate the cavity function of enzymes. These macrocyclic compounds are able to isolate a chemical reaction from the surrounding environment in similarity to enzymes and have been successfully applied for stereo- and enantioselective catalysis (view Figure 3 B)).[16 a), 18 j)-l)] The photosynthetic system is one of the most complex nano-scaled natural self-assembled systems, which converts photonic to chemical energy and is hence essential for living organisms.[16 a), 18 f)-i)] The basis of photosynthesis is a cascade of photo-induced energy and electron transfer amongst donors and acceptors in chloroplasts of plants.[18 i)] Electrons, which are generated by the absorption of photons by chlorophyll and other photopigments are transferred very fast to a number of other molecules in the thylakoid membrane where the photosystems are assembled, resulting in long-live and long-distance charge separation across the membrane, necessary to generate chemical energy.[16 a)] A very sophisticated biomimetic model has been elaborated based on an electron transfer process within the cell-like lipid membrane of liposomes (view Figure 3 C)).[19] The electron transfer system consists of a porphyrine-dye center sandwiched between both an electron donor and acceptor. Absorption of photons by the dye causes charge separation in combination with an electron transfer from the donor to the acceptor moiety. A shuttle molecule, which moves along the membrane, is capable to uptake the electron and transfers protons from the outside of the liposome to the inside once it is reduced. The decreasing pH inside the liposome causes a proton-motive force, which produces an electrochemical potential across the membrane. This potential is utilized by an

incorporated ATP synthase enzyme to produce ATP from ADP, which is the key step in cellular metabolism.
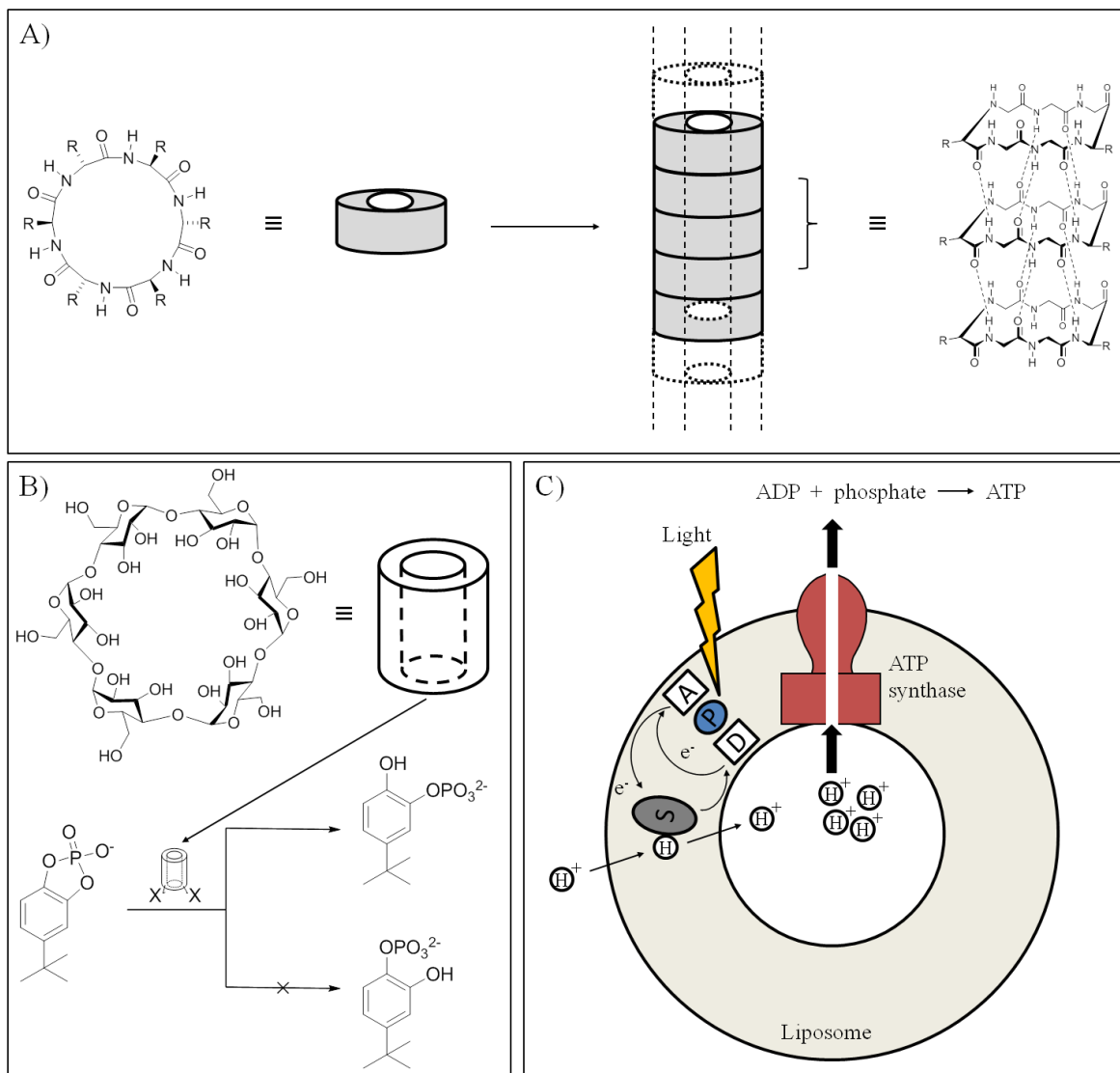
Fig. 3 Examples for artificial self-assembling systems: A) Organic nanotube assembled by hydrogen-bonding from cyclic peptides with alternating *D* and *L* configuration, which can be incorporated into cell-membranes for ion-transport (most of the peptide side-chains have been omitted for clarity).[18 a)] B) Cyclodextrin-derivative modified with imidazole moieties for the regio-selective hydrolysis of a phosphodiester, mimicking the enzyme ribonuclease.[16 a)] C) Schematic representation of an artificial photosynthetic system using a molecular triad in the lipid bilayers membrane of liposomes to generate a proton-motive force to induce ATP production. Abbreviations: A = Acceptor; D = Donor; P = Porphyrine; S = Shuttle.[19]

Chloroplasts in which photosynthesis takes place are rather complex in nature, but only building blocks in the overall compartment of cells, which already gives hint for the huge

complexity of form and function of the latter. Cells are the elemental unit of living systems, which exhibit diverse functionalities arising from an optimized arrangement of components with diverse chemical function.[8] Basic properties of cell-membranes could be reproduced using semi-permeable liposomes,[20] but such materials describe only primitive models to mimic natural cells as they lack the internal architecture of cells namely the cytoplasm and its cytoskeleton. The cytoskeleton is not only responsible for the stability and mobility of the cell, but also contributes towards the regulation of intracellular traffic. As it is composed mainly from protein filaments, simple model systems could be generated by the construction of artificial fibrillar networks within liposomes. Besides approaches based on polymeric gels,[8, 21] self-assembled low molecular weight (LMW) gels[8, 22] provide valuable approaches, as the formation of actin and tubulin filaments building the cytoskeleton proceeds via dynamic self-assembly in similarity to the situation in LMW-gels. LMW-gelators are considered to be small organic compounds that assemble towards the formation of fibers due to non-covalent interactions. These fibers entangle to form a 3D-network in which solvent molecules are trapped by surface tension and capillary forces to form the macroscopic solid-like state of the gel-phase.[23] Their potential stimuli-responsive nature gives raise for applications in various fields such as biomedicine, catalysis, food, cosmetics, agriculture and sensing amongst others.[23, 24] Soft gel-materials represent the main topic of research summarized in this thesis. Therefore, further discussions on their definition, classification and potential applications of these interesting materials will be conducted separately in the following sections.

2. Gels: Definition, classification and formation

The term "gel" was first coined by Thomas Graham[25] in the 1860s to describe colloidal materials that seem to comprise an intermediate state between solids and liquids. Since that, many controversial discussions have been conducted to find a clear definition of gels and gel-like materials. One of the most comprehensive definitions was carried out by Paul Flory[26] in 1974. Based on his statements, a gel is defined as two-component colloidal dispersion with a continuous structure exhibiting macroscopic dimensions that is permanent at least for the duration of an analytical experiment and is solid-like in its rheological behavior. Furthermore, Flory already began to group gels into four different categories based on different structures occurring in gels: 1) well-ordered lamellar

structures (phospholipid-gels, soaps); 2) covalent polymeric networks (vulcanized rubber, polysilicic acid-gels); 3) polymer networks formed through physical aggregation (gelatin-, alginate-gels); and 4) particulate, disordered structures (flocculent precipitates, V_2O_5-gels).[26] Unfortunately, the definition given by Flory is not absolutely correct as many, but not all gel-systems are colloidal in nature.[27] Still, gels have in common, that they consist of a solid three-dimensional (3D) matrix with high surface area, which is constructed by crosslinking of one-dimensional (1D), polymeric fiber-structures of (macro-)molecules by physical and/or chemical forces.[24, 27, 28] The viscoelastic, solid-like macroscopic appearance of gels is the result of entrapment of a solvent in the interstices of the 3D crosslinked and elastic network of gelator-molecules mainly through surface tension and capillary forces (view Figure 4).[23]
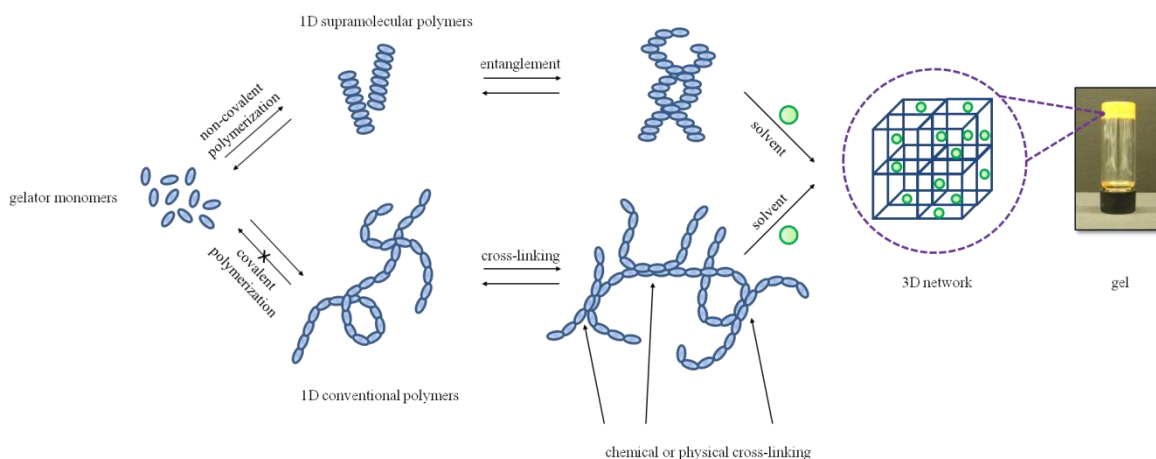
Fig. 4 Schematic representation of the hierarchical self-assembly process resulting in gel-formation for supramolecular and conventional polymers.[28 f), 30]

Hence gels are two-component systems consisting of gelator-molecules and solvent-molecules, which constitute the major part of the structure. In general, the fibrous structure of gels can be divided into a primary, secondary and tertiary structure in similarity to folded proteins, which can help for a better understanding of the complex, hierarchical self-assembling mechanism resulting in gelation.[28 a)] The primary structure (Å-nm scale) is based on molecular recognition driven anisotropic aggregation of the gelator molecules preferable into 1D architectures. The secondary structure (nm-µm scale) is defined as the morphology of the aggregates, which can be expressed as sheets, ribbons, micelles, vesicles, fibers and others. Many interesting models have been elaborated in order to

determine the exact processes responsible for the transition from the molecular scale towards primary and secondary structures.[29] The tertiary structure (μm-mm scale) is based on the interactions of individual aggregates and determines if a gel is finally formed or not. The transition from the secondary to the tertiary structure of gels is strongly dependent on the strength and type of interactions between aggregates such as fibers and gel-formation is a result of both branching and entanglement of the fibers. Gels can be categorized by various criteria depending on their origin (natural and synthetic), constitution (macromolecular and molecular), the forces responsible for crosslinking (chemical or physical) or the solvent entrapped (e.g. hydro-, organo-, xero-, aero-, ionogels).[24 b), 31] Natural gelators are usually macromolecules that form gels by non-covalent crosslinking (e.g. gelatin, chitosan, collagen). On the other hand, gels from synthetic compounds can be classified according to their constitution into macromolecular and molecular gels. Gel-formation from macromolecular compounds can either be a result from chemical crosslinking (chemical gels) or physical interactions (physical or supramolecular gels). Systems based on both types of interactions are also known.[32] Chemical gels are in general not thermoreversible, as they are held together by strong covalent bonds, whereas physical gels, which are built from weak physical interactions, exhibit thermo-reversible properties. Gels derived from low molecular weight (LMW) compounds are supramolecular gels in the strictest sense, as they are formed through self-assembly of gelator molecules into entangled networks driven by non-covalent forces such as hydrogen-bonding, solvophobic forces, π-π stacking, donor-acceptor interaction, metal-coordination and many more.[24 b)]
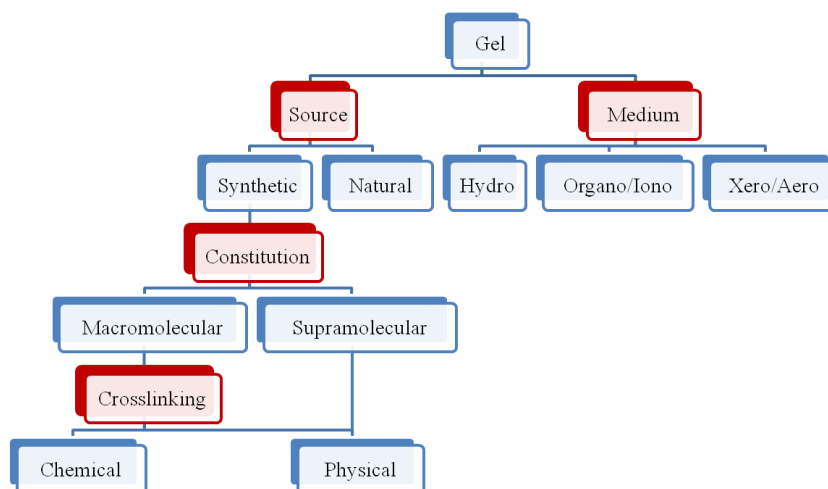
Fig. 5 Schematic representation of the classification of various gel-materials.[24 b)]

With respect to the solvent, which is entrapped in the 3D matrix of gels, they can be further categorized into hydrogels (water), organogels (organic liquids), xero-/aerogels (air) and ionogels (ionic liquids) amongst others. A summary of the different criteria of categorization of gels is represented in Figure 5. Gels have conquered our daily life appearing in various forms as constituents of commercial products such as shampoo, tooth paste, hair-gel, contact-lenses, cosmetic crèmes or food thickeners.[24 b), 28 d), f), 31] Especially macromolecular gels are used in industrial scale for lubrication and other purposes since the 1950s.[33] For a long time, gelation was mainly found by serendipity, but since round about 20 years ago scientists are able to create gelators by rational design, which has lead to countless varieties of gelator-subclasses with tailor-made properties for specific applications (a selection of gelator-structures of various types is given in Figure 6).[24 b), 28 c), d), 34]
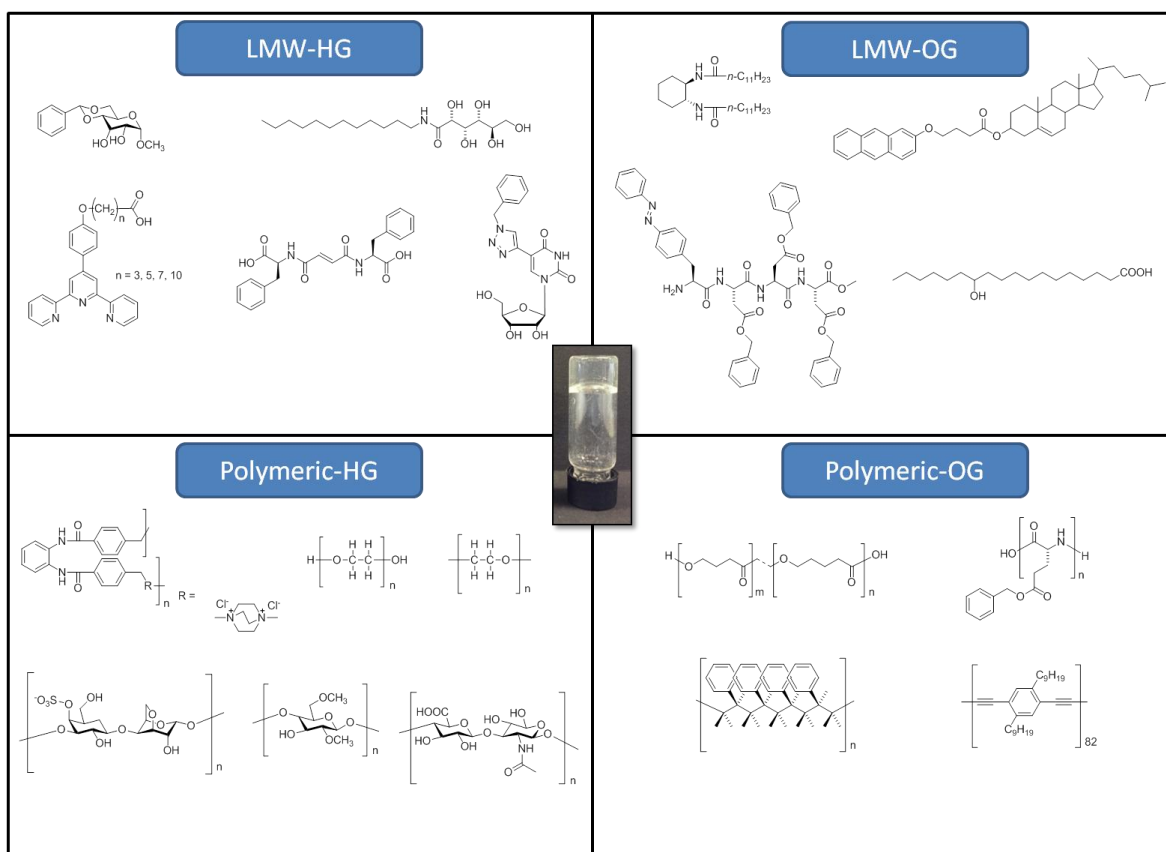
Fig. 6 Selection of various gelator-structures classified by their constitution and entrapped solvent.

On the basis of the latest research on LMW-based gels, concepts were established for the design of gelator-compounds. Hence important features for successful gelation are: 1) the

presence of strong and directional non-covalent intermolecular interactions to promote supramolecular self-assembly; 2) the ability to form intertwined aggregates; and 3) factors that prevent crystallization of the gelator.[28 c)] The last point is of special interest, as it expresses the meta-stable nature of gels and describes, that the key to control the delicate balance between gelation, crystallization and complete solubility is based on proper functionalization of the materials and fine-tuning of the environmental conditions (solvent, pH, ionic strength, etc.).
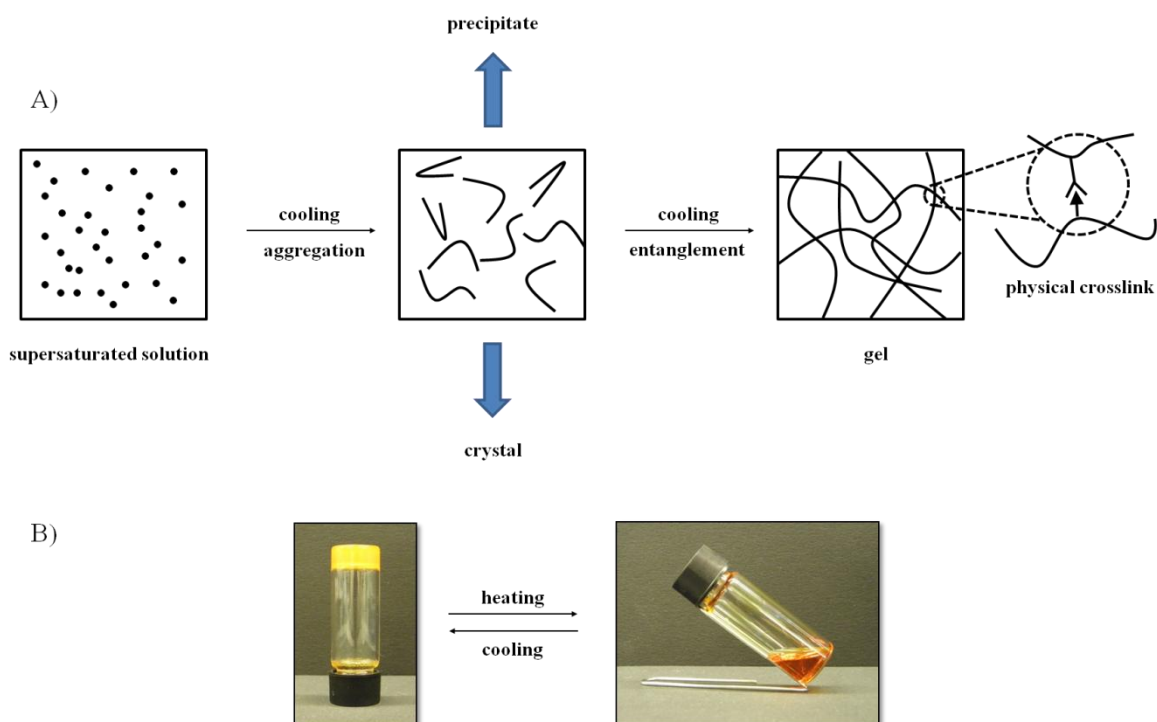
Fig. 7 A) Potential aggregation modes during cooling of a supersaturated solution[24 b), 40] and B) digital photographs to illustrate the thermoreversible nature of a LMW-gelator.

In general, gelators are capable to form stable gels in either aqueous solutions or organic media and only few examples are known to gel both environments.[35] This observation is based on the different types of interactions that are responsible to promote gelation depending on the nature of the solvent. In the case of organogels (OGs), gelation is thought to be driven by dipolar interactions, specific and directional hydrogen bonding (H-bonding) or metal coordination. These forces must balance the increase in free energy that accompanies the loss of translational and rotational freedom of motion during the self-assembling processes.[27, 28 b), e), f)] On the other hand, gelation in hydrogels (HGs) is

established mainly by solvophobic interactions and hence control over hydrophobic interactions is crucial.[28 a), c), d), 33 b)] H-bonds, the most common driving force for organogelation, loose their strength in the presence of water unless they interact in a cooperative manner and are protected from the solvent.[28 a)] During the last 25 years, gels derived from LMW-compounds ($M < 3000$ gmol^{-1}) have drawn more scientific interest in comparison to their macromolecular analogues due to several reasons:[24 b), 28 a)-e), 36] a) huge diversity of gelator-structures is accessible by standard synthetic methods, resulting in varying physical properties suitable for desired application; b) many gelators derive from natural sources and hence have a high potential of being biocompatible and biodegradable (the network formed by LMW-molecules is solely held together by non-covalent forces, which makes them easier biodegradable than polymer gel-systems); c) physically crosslinked gels are thermoreversible (view Figure 7); d) very low minimum gelation concentrations can be found; and e) high tolerance towards salts and other additives. Gels from LMW-compounds are usually prepared by heating the gelator in an appropriate solvent and subsequent cooling of the isotropic supersaturated solution to room temperature.[24 b), 28 c)] It is important to mention in this context, that gelation can be additionally induced by various other stimuli, such as treatment with ultrasound,[37] building a pH-gradient[38] or enzymatically.[39] During cooling, the gelator-molecules start to condense and from a network consisting of fibers as described earlier rather than to undergo phase-separation through crystallization or precipitation (view Figure 7). Such nano-scaled fibers have often found to have a crystalline order and hence it was supposed that their formation is based on a crystallization process including nucleation and growth. Evidence has been found in this context for a specific type of heterogeneous nucleation called "crystallographic mismatch branching" that is responsible for branching and entanglement of the fibers within gels derived from LMW-gelators.[36] Understanding this phenomenon gives raise for the formation of materials with tailor-made properties for various applications. Another key-feature of LMW-gelators towards the fabrication of "smart" materials for sophisticated applications is their facile functionalization by synthetic chemistry. Many gelating-agents have been designed that incorporate photo-sensitive (an example for a gelator exhibiting photo-switchable properties is given in Figure 8), pH-sensitive or molecular recognition moieties for applications in controlled drug-release, sensing, optoelectronics, data storage and many more.[24, 27, 28, 31, 33, 36] A more detailed insight into potential applications of LMW-gelators will be given in the following sections of this thesis.
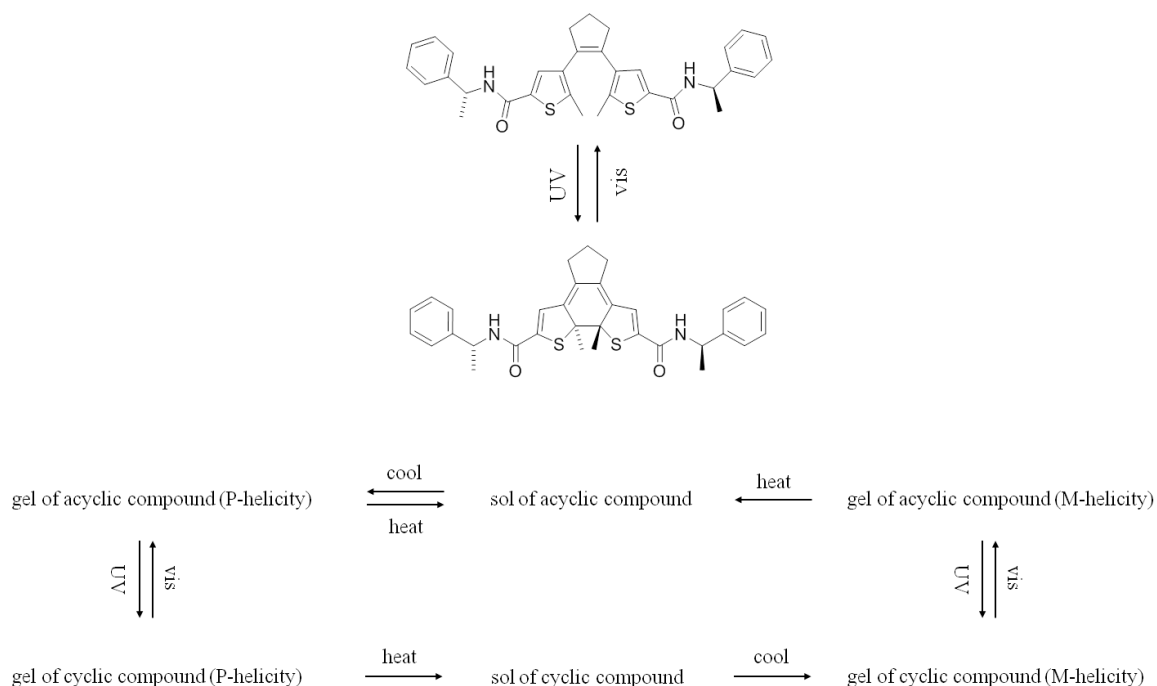
Fig. 8 Photo-sensitive gelator and schematic representation of the switching properties.[24 b)]

3. Potential applications of gel-based materials

3.1. Gels for biomedical applications

Tissue engineering

In modern research, a very strong trend towards interdisciplinary collaborations between medicine, biology, chemistry and material science has developed in order to overcome very delicate and complex sets of issues. Today, we suffer a huge mismatch between the supply and demand of tissues and organs for transplantation. In the United States, currently about 100000 people are waiting on lists for transplants, with an average time of more than 3 years.[41] One promising solution is provided by tissue engineering as a part of the interdisciplinary field of regenerative medicine. In general tissue engineering aims to replace, repair or regenerate damaged tissues or organ functions by creating artificial tissues and arrays for transplantation. Such artificial tissues are based on scaffolds deriving from natural or synthetic sources, which mimic the structure and function of natural

extracellular matrix (ECM). The ECM consists of protein filaments that are semi-flexible crosslinked into networks with different geometries, which is responsible of the mechanical properties of tissues and provides a suitable environment for bioactive materials such as cells.[42] Hence artificial scaffolds must provide a 3D environment to support cell adhesion, migration, proliferation and differentiation for controlled stimuli and signal transmission resulting in successful and directional growth and formation of new, fully operative tissue.[24 c), 41 a), 43] In this context, hydrogels (HGs) have proven to be very suitable scaffolds for biomedical applications such as tissue engineering.[24 b), c), 41-44] The highly hydrated, viscoelastic 3D network present in HGs is a result of interactions between well-defined secondary structural motifs such as ribbons, helices and sheets resembling various types of architectures with defined mechanical properties.[28 a)] Due to their mild and facile preparation from building blocks, that are easily available from chemical synthesis, they exhibit a high mechanical and chemical diversity.[24 b)]

Tab. 2 Criteria to be fulfilled by hydrogels to serve as scaffolds in tissue engineering.

Properties of hydrogels
facile preparation and structural diversity
biocompatible (non-toxic and cell-compatible)
biodegradable (preferable enzymatic)
sterile
mechanical integrity and strength
tolerance against incorporation of bioactive materials (e.g. cells or growth factors)
effective mass transport
control cell function through the presence of cell adhesion moieties (e.g. RGD)

These features allow HGs to act as hydrophilic structural and compositional mimics of biological soft materials and tissues such as the ECM. Furthermore, HGs show a high tolerance against the incorporation of biological active materials such as cells and provide a suitable microenvironment as they are able to create interactions and responses between

functional groups and cellular systems to support cell growth. The porous nature of HGs facilitates high diffusion rates of nutrients and metabolic products of the incorporated cells necessary for mobility and proliferation. Many HGs derive from natural occurring sources, in fact constitutes of the ECM such as collagen or hyaloronic acid are known to be potent hydrogelators with cell-adhesion and signaling domains, which have a high potential of being biodegradable, biocompatible and non-toxic. Additionally, HGs are usually prepared at low concentration and exhibit a high water content resulting in a low amount of potential degradation products.[41-44]
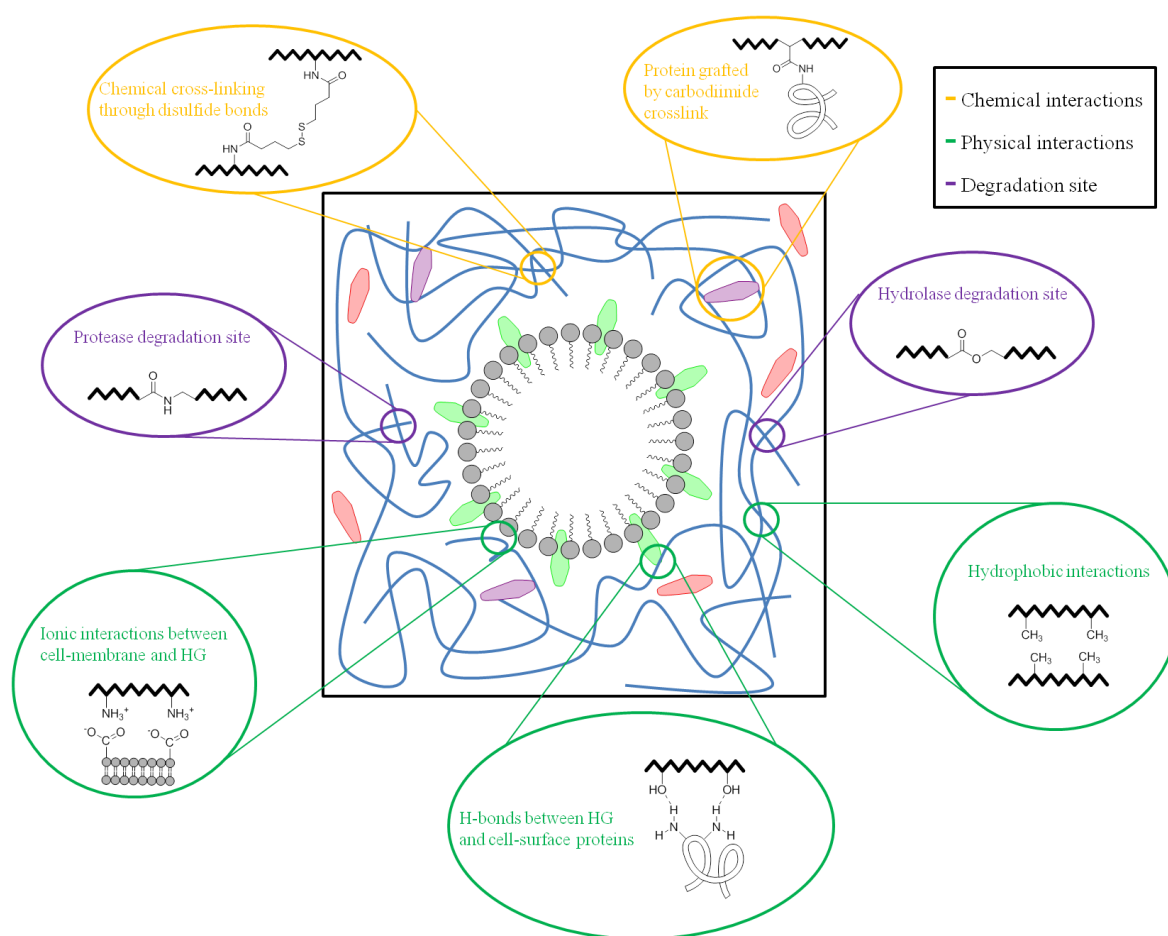
Fig. 9 Simplified schematic representation of the interface between cell (grey) and hydrogel (blue). Cell-receptor proteins (green) are incorporated in the cell-membrane, whereas soluble bioactive materials (red) and covalently linked bioactive proteins (purple) are located in the hydrogel meshes. A set of multiple chemical and physical interactions illustrates the complexity of the cell-hydrogel interface. Degradation can be designed through the incorporation of enzymatic cleavable moieties into the hydrogelator backbone or crosslinks. Bioactivity can be induced by the incorporation of bioactive compounds such as growth factors into the hydrogelator structure.[43 a)]

As every natural tissue has a specific structure and function with unique mechanical properties, suitable HG-scaffolds need to be designed by different criteria for tissue-specific applications. First of all, HGs need to represent 3D space-filling scaffolds with sufficient mechanical integrity and stability to withstand manipulations caused by implantation. The mechanical integrity of HGs is determined by their gel-formation mechanisms and dynamics, mechanical characteristics and degradation. These intrinsic properties are described by the composition and crosslinking characteristics of the HGs.[41 a)] Suitable HGs must be able to support living cells and control cell growth and differentiation by mechanical input for successful tissue formation, which is governed by the dynamics of HGs. Suitable degradation rates of HG-networks shall fit the rate of new tissue formation, especially if processes require controlled resorption to facilitate cell morphogenesis. Degradability can for example be induced by incorporating enzymatic cleavable moieties in the gelator backbone or crosslinks. As a second criterion, HGs must provide suitable pathways for mass transport of gases, nutrients, proteins, cells and metabolic products. Mass transport is primary governed by diffusion and hence dictated by the porosity and pore-size of the 3D HG-network.[41 b)] Finally, HGs must promote desirable cellular functions and tissue formation, which includes adherence, proliferation and differentiation. A well-established approach to design specified adhesive HGs is covalent modification with peptide sequences capable of binding to cellular receptors. The most studied sequence is RGD (arginine-glycine-aspartic acid) deriving from several ECM proteins such as collagen, which has been attached to various types of HG-structures.[41 a), 43 a)] The main features that need to be present for HGs serving as scaffolds in tissue engineering are summarized in Table 2 and Figure 9. It would be desirable to design materials that fulfill all of the mentioned criteria, but this is tough to realize. One very elaborated design-approach by the group of Messersmith matches at least most of the requirements and could be successfully applied on diabetic rats.[45] Polyethylene glycol (PEG) derived hydrogels have been modified with a specific catechol moiety (3,4-dihydroxy-*L*-phenylalanine (DOPA)), known to be responsible for adherence of muscles to wet organic surfaces. DOPA participates in the crosslinking reaction of the PEG hydrogels and additionally forms covalent interactions with nucleophiles such as thiols and imidazoles found in the ECM. Incorporation of extra-hepatic islets and immobilization of the hybrid-material on the surface of the liver of diabetic rates enabled revascularization with minimal inflammation and permitted effective glucose management.[43 a)] In another more simply but still successful example, self-assembled amphiphilic oligopeptides could

27

be applied for recovery of vision.[46] A gelator bearing a Arg-Ala-Asp-Ala repeating sequence was found to enable reconnection of nerve tissue after surgical damaging of the optical tract in the hamster midbrain. It was proposed that the HG is capable of resembling irregular voids, similar to those found in the damaged nerve, and that a close contact between HG fibers and ECM proteins can facilitate cell-scaffold interactions and hence promotes healing. Furthermore, a rapid and complete hemostasis was achieved, which is not tissue-specific. This approach demonstrates that bleeding can be stopped without the application of heat or pressure and give valuable alternatives for bleeding control during surgery.[24 c)]

Controlled drug delivery

Vectorization, which can be defined as the specific and controlled delivery of biologically active substances, such as drugs, to desired organs and tissues by carrier-moieties, provides a very powerful alternative towards conventional drug formulation techniques.[47] Several problems arise from classical drug delivery, which are mainly represented by: 1) the rapid and non-specific delivery of the drug, which can result in overdosage or undesired deposition of the drug in certain tissues or organs and can cause irritations or other side effects; 2) the incapability of drugs to cross barriers in the body due to their specific physico-chemical properties leading to difficulties regarding the drug´s deposition in a desired target area; and 3) the rapid metabolism of many drugs caused by the environment in the body (pH, presence of enzymes).[47, 48] The application of drug carriers can provide valuable solutions to these issues by protecting biological active substances from the environment through encapsulation and improving the specific deposition of the species at desired target areas, hence increasing activities. Furthermore, vectorization represents simple pharmaceutical formulations and convenient administration accompanied with an increased safety due to reduced body dosages to minimize undesired side effects.[47-49] Many types of drug carriers systems such as emulsions or liposomal microspheres have been tested for application in controlled drug release, but they exhibit severe drawbacks such as a low long-term stability, problems with sterilization and low drug-loading capacities.[49 c)] On the other hand, HGs represent highly stable, semi-solid depots with high drug-loading capabilities. They provide a 3D network-support for bio-active substances with a highly homogeneous distribution and sufficient protection from the environment. Furthermore, they consist of a high water content making them biocompatible and their porous nature

allows facile transport and diffusion. As a special feature, the physico-chemical, mechanical and biological properties of HGs can be controlled by the synthesis of functionalized gelator molecules and the method of gel-preparation, which is in general conducted under very mild conditions.[47-50] Controlled drug release from a HG-matrix can be simply driven by diffusion, or induced by changing the gel-structure (including *gel*-to-*sol* transitions) or swelling properties upon environmental changes, resulting in a smart behavior of the matrix as illustrated in Figure 10 A).[48, 50 d)]
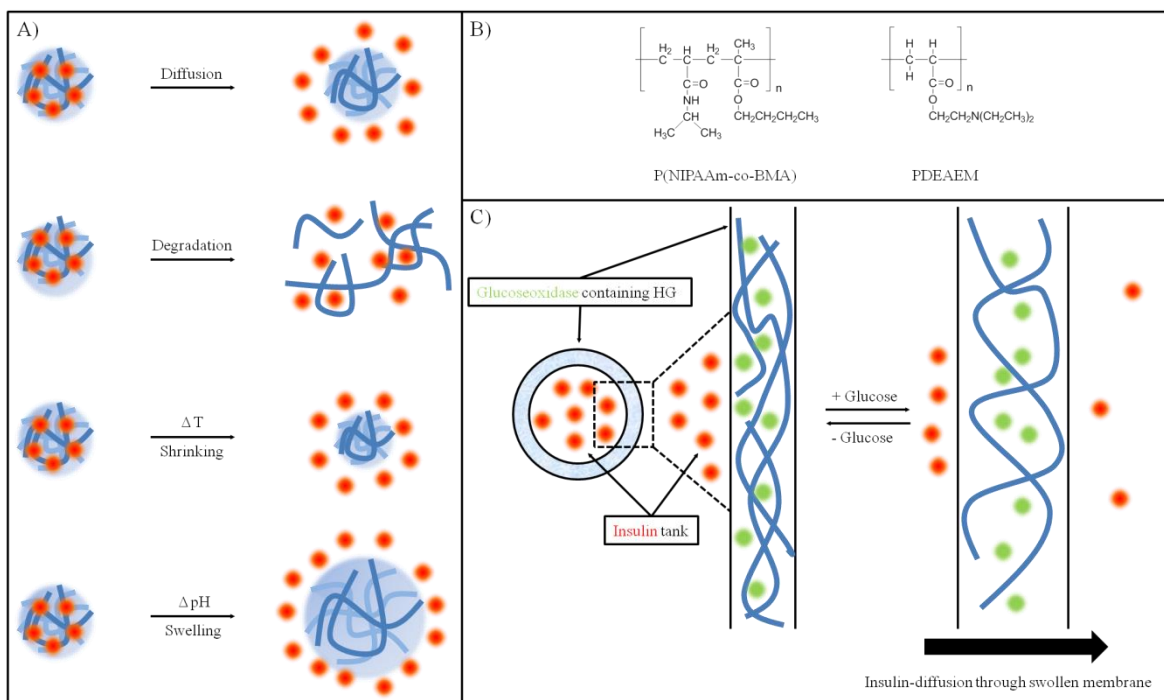
Fig. 10 A) Different strategies for controlled drug release from HGs.[50 d)] B) Chemical composition of block-copolymer P(NIPAAm-co-BMA) and cationic polymer PDEAEM.[48] C) Smart polycationic HG-membranes consisting of PDEAEM for controlled insulin delivery based on glucose concentration.[47, 48]

Probably the most common external stimulus applied in controlled release from HGs is temperature. Most HGs increase their water-solubility when the temperature is increased. Interestingly, some polymeric HGs like block copolymers [P(NIPAAm-co-BMA)] (the structure is shown in Figure 10 B)) derived from crosslinked poly(*N,N'*-isopropylacrylamide) (PNIPAAm) and poly(butylmethacrylate) (PBMA) exhibit an inverse temperature sensitive behavior with a lower critical solution temperature (LCST) close to body temperature. A potential explanation for such behavior could be that with increasing temperature hydrophobic interaction between polymer chains become favored and

accompanied release of hydrating water-molecules results in an entropy driven gelation-mechanism. Further elevation of temperature results in shrinking of the HGs caused by a density increase of the network, which facilitates drug-release by a kind of squeezing event.[48] Another popular stimulus for controlled release, is changing the pH of the surrounding environment. A combination of pH-sensitive polycationic poly(*N,N'*-diethylaminoethyl methacrylate) (PDEAEM) based HGs and glucoseoxidase resulted in the development of very sophisticated insulin-delivery systems. Glucoseoxidase oxidizes glucose to gluconic acid accompanied by a decrease of the environmental pH. A lowering of pH results in swelling of HG-membranes based on polycations, due to ionization and electrostatic repulsion. In general, swollen membranes tend to release more drugs, which results in a self-regulating insulin release based on glucose concentration as illustrated in Figure 10 B), C).[47, 48] It is obvious that most of the gel-systems applied for controlled drug delivery purposes are HGs. Due to their high water-content, HGs exhibit a high potential of being biocompatible. On the other hand, organogels (OGs) prepared from pharmaceutically approved oils represent only a minor important category.[51] Besides valuable applications in tissue engineering and controlled drug release, HGs prepared from polyelectrolytes have the ability to respond to electrical stimuli and can serve as actuators in close similarity to muscles.[52] Additionally, it was reported that derivatives of therapeutic agents can undergo hydrogelation and the corresponding HGs preserve pharmaceutical activity of the parent biological active molecules.[53] The illustrative examples discussed in this section give clear evidence for the high value of HGs in biomedical applications. Hence it is not surprising that much scientific effort is spend at the moment and will for sure be continued in the future in order to design and create novel HG-materials with desired function and properties.

3.2. Gels in catalysis

Only recently, gels from natural occurring sources have found application in the field of catalysis, due to the growing interest in "green chemistry" accompanied by the demand for environmentally friendly and sustainable resourcing and processing. In general gels can derive from a variety of compositions and exhibit well defined conformational preferences, orientations of functional groups and (supramolecular-) chirality.[54, 55] The heterogeneous two-phase nature of gels exhibits a large and highly active surface area between gel fibers

and the entrapped solvent and exposes functional groups to substrates necessary for sufficient performance in catalysis.
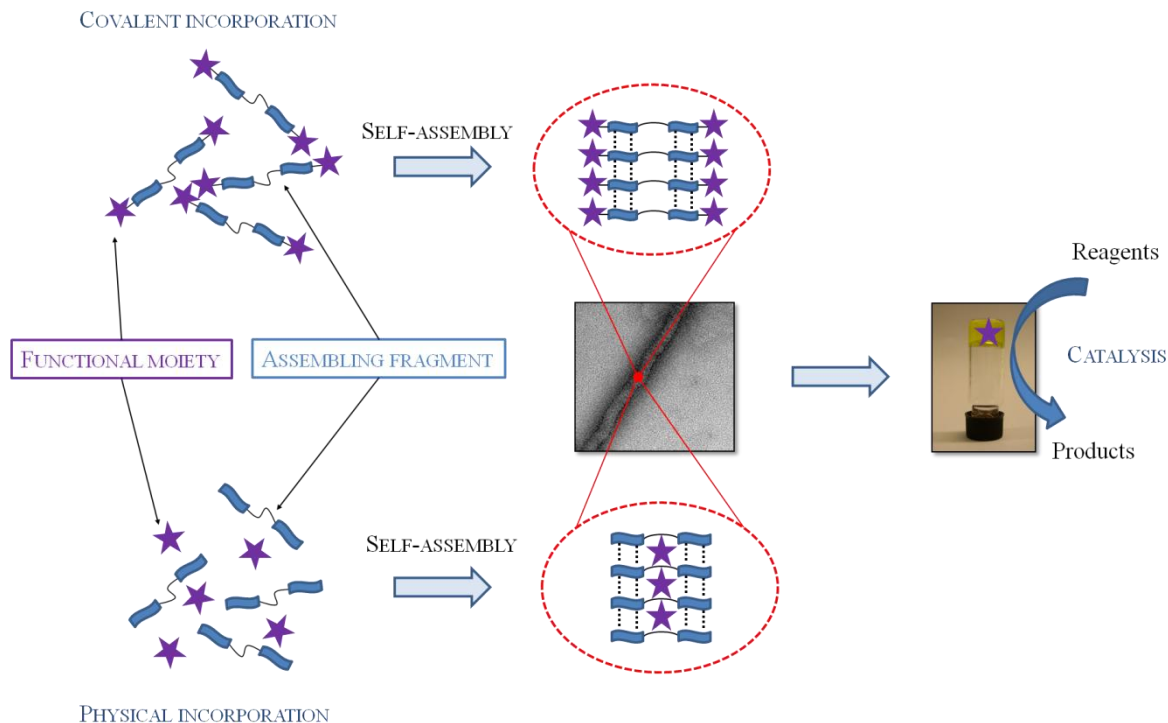
Fig. 11 Design of catalytically active gels by physical or chemical incorporation of functional moieties.[55]

Furthermore, the amphiphilic nature of the gel-environment provides the possibility for effective solubility and separation of substrates and products.[56] The high porosity of the 3D gel-network provides a viscoelastic and dynamic support, which allows fast diffusion of substrates to the catalytic active sites and additional confinement effects could result in advanced catalyst-substrate interactions.[54] The hierarchical assembly of catalytic active moieties by physical or covalent integration into the 3D gel-network can result in additional catalytic features such as polyvalent, neighboring or cooperative effects and the high molecular order may result in regio- and stereoselective transformations (view Figure 11).[54, 55] In this context, smart stimuli-responsive gels could control the accessibility of catalysts by alternating environmental conditions and result in effective catalyst separation and control of the reaction progress for easier processing and work-up.[56] In comparison to most heterogeneous catalysts, gels guarantee a high accessibility of small reagents to the highly solvated network and provide hence valuable and effective alternatives.[54] The classical approach towards the fabrication of catalytically active gel-materials is based on

polymeric materials. Due to recent technological developments, polymer-gels are synthesized exhibiting precisely controlled surface areas, pore volumes and average pore-sizes.[54, 56]
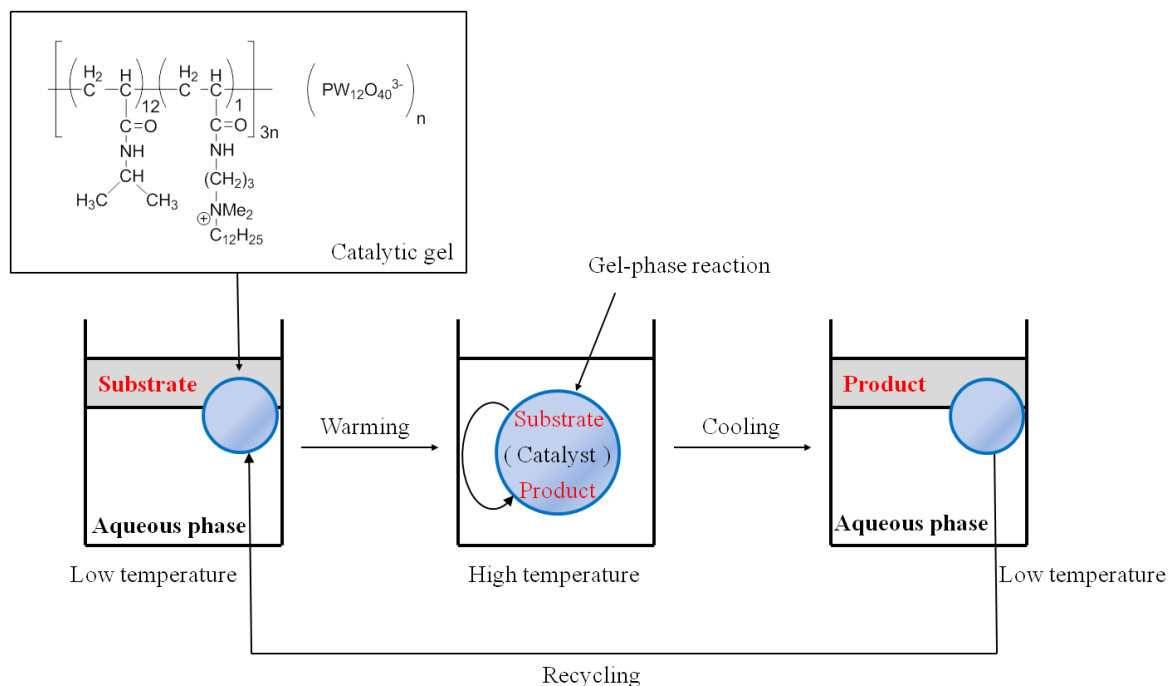
Fig. 12 Thermo sensitive polymeric gels as recyclable heterogeneous catalysts for oxidative cycloaddition of hydrophobic compounds.[56]

As mentioned earlier (see Chapter 3.1), some polymer-gels like PNIPAAm exhibit a thermo sensitive behavior, which allows controllable swelling properties.[48] Such behavior was exploited to prepare recyclable catalytic copolymer-gels from PNIPAAm and an acrylamide bearing quaternary ammonium salts by crosslinking with phosphotungstate anions, which are simultaneously the catalytic active species (view Figure 12).[57] At elevated temperatures, the gel-network is able to soak hydrophobic reactants due to swelling of the gel-matrix. By lowering the temperature after the reaction, products can be released again upon a squeezing event caused by shrinking accompanied by recovery of the catalytic gel. The activity of the gels was demonstrated for the oxidative cyclization of pent-4-en-1-ol, giving conversions of up to 80% even after three consecutive catalytic cycles.[56, 57] Unfortunately polymer-gels are often very brittle and rigid in nature, which makes the availability of catalytic active sites difficult, and hence much effort was spent towards more soft and dynamic materials.[56] Only recently, LMW based gel-materials have

moved to the focus of application in catalysis, as the highly defined mode of self-assembly could be considered as another major advantage against polymeric gels.[54, 55]
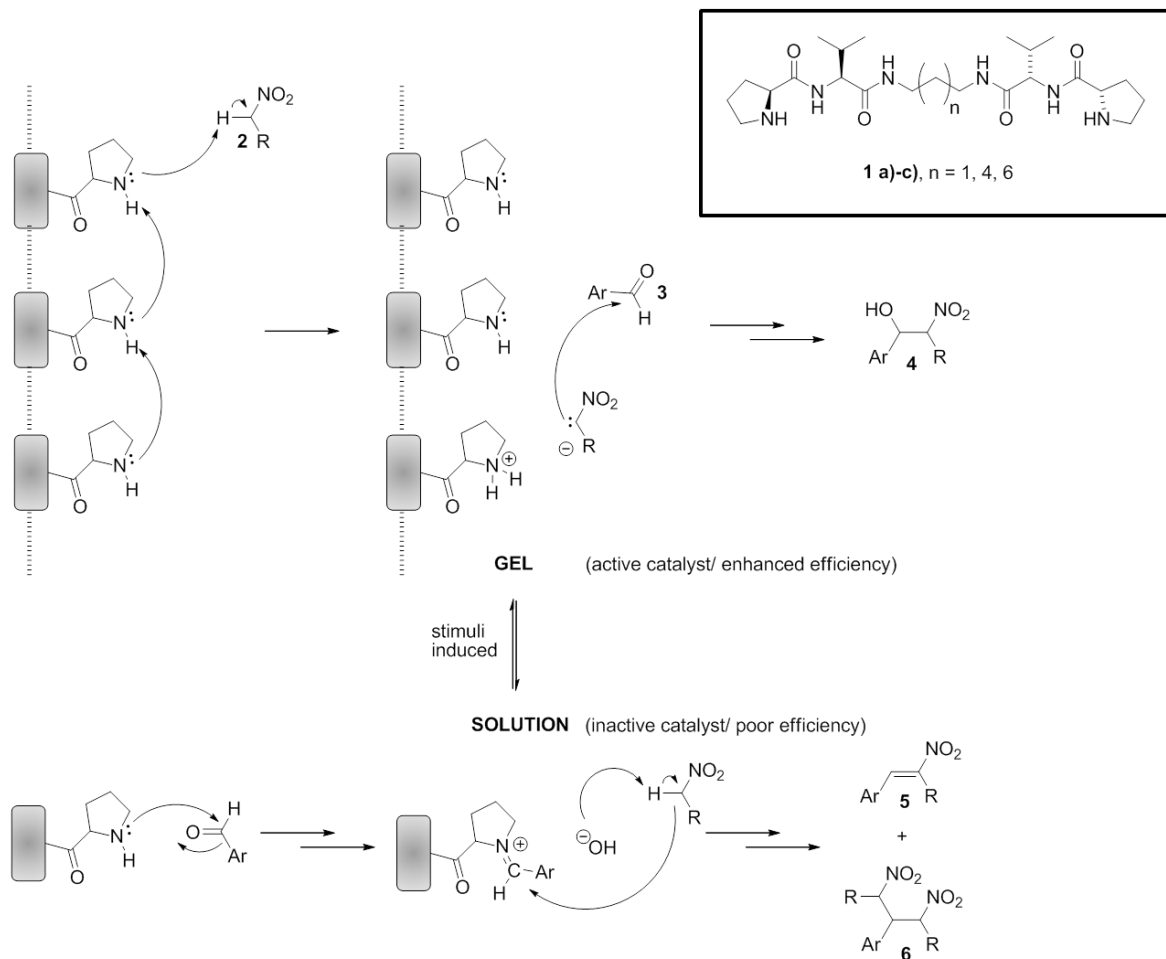
Fig. 13 Proposed mechanism for the Henry reaction using gelators **1 a)-c)** as basic catalysts in the gel- and solution phase.[54]

In this context, Miravet and Escuder have prepared LMW-gelators **1 a)-c)** with pendant *L*-proline-moieties as well studied organocatalytic motif.[58] These gelators were applied for the base-catalyzed Henry nitroaldol reaction between nitroalkanes **2** and aromatic aldehydes **3** to the desired products **4**. Interestingly, in the presence of the gel-state proline moieties act as basic catalysts promoting the Henry reaction via an ionic-pair type mechanism, whereas an iminium-based mechanism seems to be responsible for the formation of dehydrated products **5**, that could further react with a nitroalkanes to yield products **6** in solution (view Figure 13). Unfortunately neither stereo-, nor enantioselectivity could be monitored during these processeses.[54, 55, 58] The examples

illustrated in this section clearly demonstrate that gels provide powerful tools for chemical catalysis, but there are still some issues that need to be overcome for a broader range of applications: 1) taking advantage of supramolecular chirality inside gels in order to induce enantioselective transformations; 2) improvements concerning the loading-capacities of gels; 3) enhancement of the mechanical stabilities of gels; 4) enhancement in understanding how gels can favor certain reaction pathways; 5) understanding the relationship between gel-properties and reaction outcome; and 6) enhancement of the specifity and strength of substrate binding and chemical reactivity of the catalytically active sites.[54]

3.3. Gels with incorporated metal-nanoparticles and quantum dots

Gels provide well-organized 3D structural networks and have been used already for a long time to direct the growth of crystals, nanotubes and other inorganic materials.[59] Especially, gels based on LMW-compounds can comprise a huge diversity of secondary structures such as fibers, sheets, helices or lamellas and templated nanostructures are known to resemble the fibrous structure of certain gel-networks.[60] Metal nanoparticles (NPs) of gold, silver, palladium and others have gained tremendous attention, due to their unique optical, electronic and magnetic properties in comparison to bulk-metal phases, which gives rise for applications in catalysis or sensing.[59-62] Size induced quantum mechanical effects (i.e. electron confinement and surface effects) lead to fascinating inherent properties such as size- and distance-dependant extinction coefficients and size-dependant electron conducting properties.[61] Unfortunately, the long-term storage of metal NPs in solution is still a huge challenge due to low stabilities caused by the their temperature sensitive nature and the high tendency for agglomeration resulting in quenching of the confinement properties.[62, a)] Hence many stabilizers like polymeric matrices or surfactants have been applied to prevent particle agglomeration, but such methodologies often lack a proper size-control of the NPs.[60, 61] In general, gels should be very suitable for the controlled synthesis of NPs as they provide 3D scaffolds with well defined pore sizes, which could control the size of NPs. Indeed, several gel-based materials have been successfully applied for this purpose.[59-62] In this context gels need to be able to properly distribute the NPs in the matrix as a facile electronic communication of individual particles plays an important role for the overall performance and agglomeration of the particles needs to be prevented in order to

keep quantum confined conditions.[63] Furthermore, the stability of the particles and control over their size- and shape-distribution needs to be guaranteed.[59] As many different types of gelator structures are known to efficiently incorporate metal NPs (some gelator-structures are illustrated in Figure 14), it is assumed that the fibrous gel-network itself is responsible for stabilizing NPs rather than specific interactions between the NPs and individual molecular building blocks of gelators.[60 d]
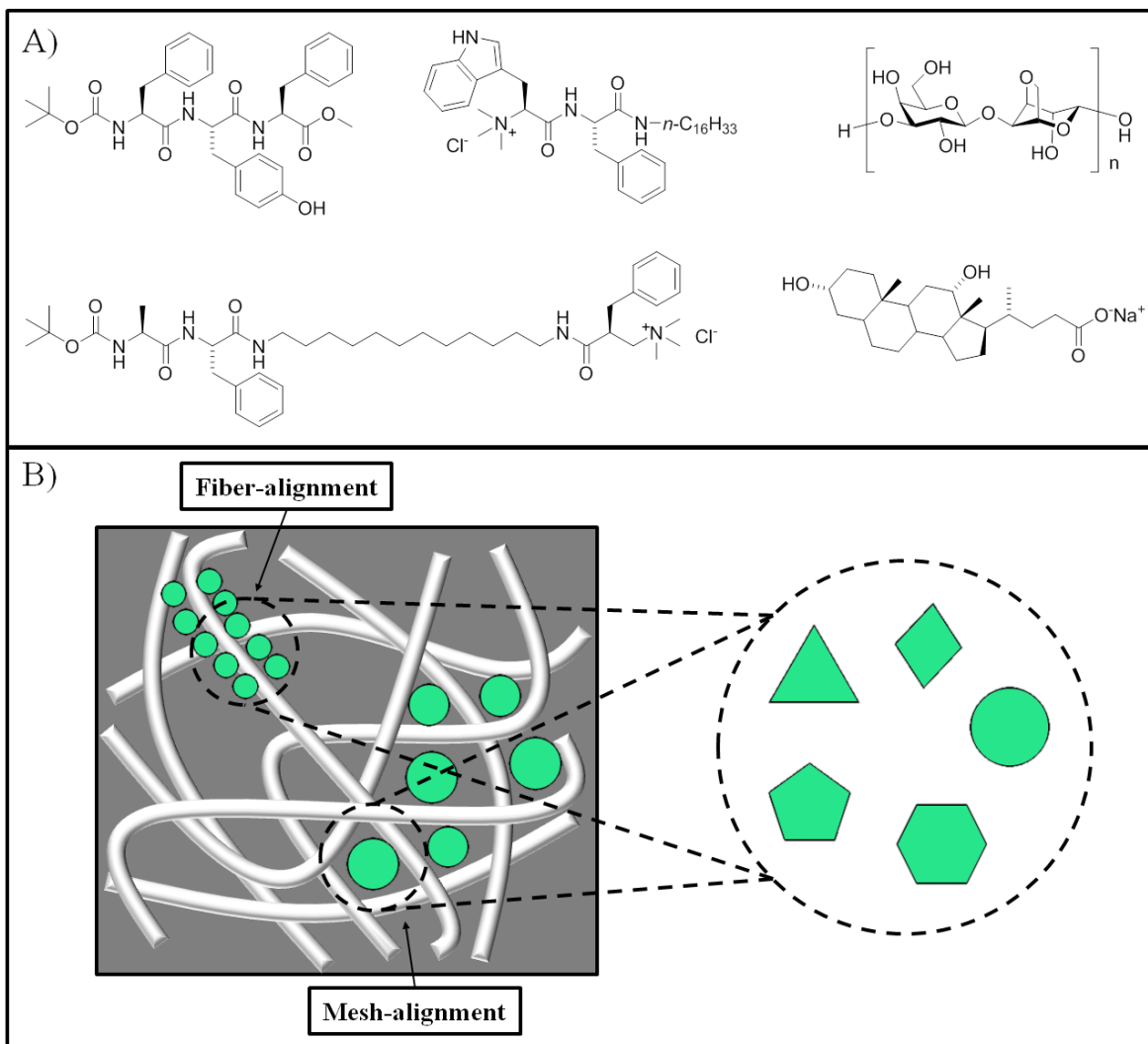
Fig. 14 A) Selection of gelator-structures able to promote controlled growth of metal NPs.[59, 60 a), b), 62] B) Schematic representation of NPs with various shapes in gels with their potential alignments on gel-fibers or in the meshes of the 3D-networks.[60 a), 65 c)]

NPs in gels are usually prepared by the incorporation of suitable metal-salt precursors during the gel-formation procedure and subsequent reduction of the precursors. Reduction towards the formation of NPs can be achieved by the addition of external reducing agents such as NaBH$_4$[61 a)] and ascorbic acid[62 a)] as well as UV-irradiation.[60 d] Another more

sophisticated possibility to prepare NPs in gels is represented by *in situ* reduction of the precursors by the presence of reducing agents inside the gelator structure such as tryptophan, tyrosine or arginine.[59, 60 a)-c)] NPs synthesized in gels exhibit narrow size distribution and the size is strongly correlated to the nature of the 3D gel-environment. Wang and his coworkers[62 a)] demonstrated the influence of agarose-based networks on the size of selenium and silver NPs. Concentration dependant changes in the pore-size of agarose-gels were reflected by smaller NPs located at the interstices of the network at high concentration of agarose as gelator due to an increase in the network density. In this context, it is important to mention that NPs in gels are not always located in the pores of the networks, but they can also be aligned on fibers, which could be useful for the preparation of conducting wires (see Figure 14).[59] Additionally, NPs can exhibit various shapes such as spheres, triangles or hexagons, which is strongly dependent on specific interactions between the NPs and functionalities present in certain gelator structures (see Figure 14).[60 a)-c)] Potential application of NPs in gel-materials for catalysis was for example demonstrated for polyelectrolyte microgels loaded with palladium NPs, which could efficiently reduce *p*-nitrophenol to *p*-aminophenol.[61 b)] Besides the incorporation of metal NPs, gels are also able to support fluorescent semiconductor quantum dots (QDs).[63-65] In similarity to metal NPs, QDs exhibit unique properties due to quantum confinement such as narrow and size-dependent emission, multicolor excitation and excellent photo-stabilities, which results in numerous applications such as fluorescence markers, electronic or optical devices.[63, 64] The most common semiconductor QDs are represented by cadmium-chalcogenides (e.g. CdSe) or metal-oxides (e.g. ZnO) due to their easy synthesis and handling. Homogeneous distribution of such QDs into gel-matrices is mainly conducted by physical entrapment of pre-synthesized and stabilized QDs.[64] In a very sophisticated approach, fluorescence properties of a double-network nanogel with entrapped ZnO-QDs have been applied for glucose-sensing.[63] One of the networks was modified with a phenylboronic acid, which is known for glucose-binding ability. In the presence of glucose swelling of the gel-matrix is induced by an increase of the charge density caused by the formation of a boronate ester, which is proportional to the glucose-concentration. It is assumed that swelling induces an increase in the elastic tension of the polymer network, which could stretch the polymer-QD interface and propagate the strain to the surface of bound QDs and create surface states responsible for quenching fluorescence. Such phenomenon can be utilized to quantify glucose-levels by simple spectroscopic techniques as illustrated in Figure 15.[63]
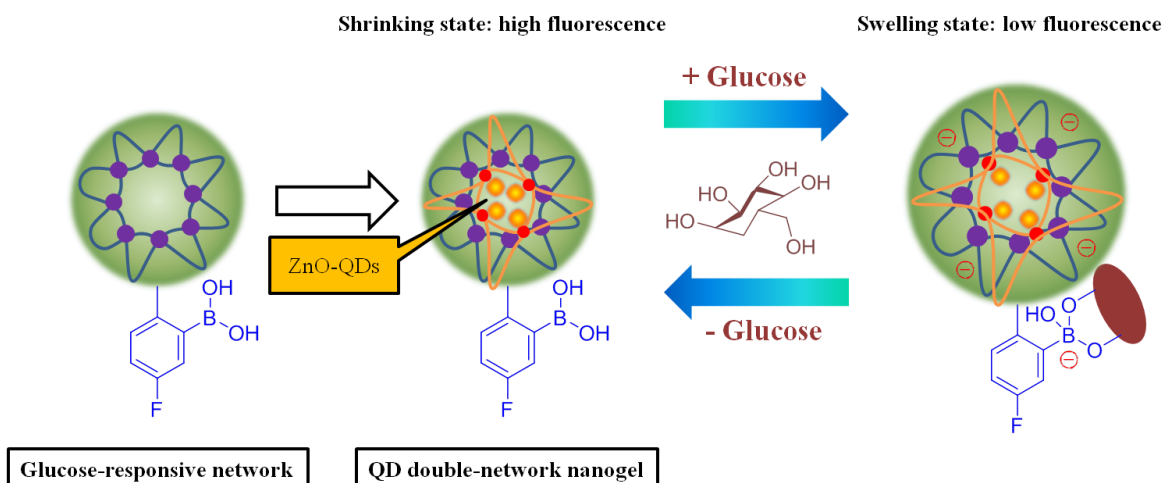
Fig. 15 Glucose-sensor based on double-network nanogel with incorporated fluorescent ZnO-QDs.[63]

It is important to mention, that gels find plenty more applications, but to treat all of them would simply go beyond the scope of this discussion. Hence some further applications will be just mentioned and in case of further interest references are given for each case. Due to the unique property of physical gels to respond to external stimuli, such materials have found broad application in chemical analysis[66] and sensing.[67] Gels based on conducting materials are used for the generation of nanowires in molecular electronics.[68] Gels can serve for scaffolds in the directed growth of inorganic nanotubes[24 a), b)] or crystals.[69] A few gelators are even capable of selectively gel organic phases from two-component water-oil mixtures for water purification purposes.[70] Some gelator-molecules investigated during the studies conducted in this thesis exhibit huge potential for some of the above mentioned applications and the results obtained will be discussed in the following chapters.

4. References

[1] G. M. Whitesides and B. Grzybowski, *Science*, 2002, **295**, 2418-2421.

[2] S. Zhang, D. M. Marini, W. Hwang and S. Santoso, *Curr. Opin. Chem. Biol.*, 2002, **6**, 865-871.

[3] D. Philp and J. F. Stoddart, *Angew. Chem. Int. Ed.*, 1996, **35**, 1154-1196.

[4] G. M. Whitesides, J. P. Mathias and C. T. Seto, *Science*, 1991, **254**, 1312-1319.

[5] a) A. M. Kushner and Z. Guan, *Angew. Chem. Int. Ed.*, 2011, **50**, 9026-9057; b) D. W. P. M. Löwik and J. C. M. van Hest, *Chem. Soc. Rev.*, 2004, **33**, 234-245; c) X. Zhao and S. Zhang, *Macromol. Biosci.*, 2007, **7**, 13-22; d) S. Zhang, *Biotechnol. Adv.*, 2002, **20**, 321-339; e) Y. Levy and J. N. Onuchic, *Annu. Rev. Biophys. Biomol. Struct.*, 2006, **35**, 389-415.

[6] I. Cherny and E. Gazit, *Angew. Chem. Int. Ed.*, 2008, **47**, 4062-4069.

[7] C. Lin, Y. Liu and H. Yan, *Biochemistry*, 2009, **48**, 1663-1674.

[8] A. M. Brizard and J. H. van Esch, *Soft Matter*, 2009, **5**, 1320-1327.

[9] P. Fratzl, *J. R. Soc. Interface*, 2007, **4**, 637-642.

[10] S. Mann, *Nature*, 1993, **365**, 499-505.

[11] S. Mann and G. A. Ozin, *Nature*, 1996, **382**, 313-318.

[12] S. Mann, D. D. Archibald, J. M. Didymus, T. Douglas, B. R. Heywood, F. C. Meldrum and N. J. Reeves, *Science*, 1993, **261**, 1286-1292.

[13] S. Mann, *Nature*, 1988, **332**, 119-124.

[14] S. Mann, *Angew. Chem. Int. Ed.*, 2000, **39**, 3392-3406.

[15] a) A. H. Heuer, D. J. Fink, V. J. Laraia, J. L. Arias, P. D. Calvert, K. Kendall, G. L. Messing, J. Blackwell, P. C. Rieke, D. H. Thompson, A. P. Wheeler, A. Veis and A. I. Caplan, *Science*, 1992, **255**, 1098-1105; b) W. Kunz and M. Kellermeier, *Science*, 2009, **323**, 344-345; c) S. Mann, *Chem. Commun.*, **1**, 2004, 1-4; d) E. C. Samano, M. Pilo-Pais, S. Goldberg, B. N. Vogen, G. Finkelstein and T. H. LaBean, *Soft Matter*, 2011, **7**, 3240-3245; e) C.-L. Chen and N. L. Rosi, *Angew. Chem. Int. Ed.*, 2010, **49**, 1924-1942.

[16] a) P. Ball, *Nanotechnology*, 2002, **13**, R15-R28; b) H. S. Gupta, J. Seto, W. Wagermaier, P. Zaslansky, P. Boesecke and P. Fratzl, *PNAS*, 2006, **103**, 17741-17746; c) I. S. Bayer, A. Ghosh, M. Labriola, A. S. Biris, E. Dervishi, F. Watanabe, T. Wang, C. Slaboch, T. C. Ovaert and A. Biswas, *RSC Adv.*, 2013, **3**, 20315-20323; d) Y. Cai and R. Tang, *J. Mater. Chem.*, 2008, **18**, 3775-3787.

[17] a) L. B. Gower, *Chem. Rev.*, 2008, **108**, 4551-4627; b) L. Addadi, S. Raz and S. Weiner, *Adv. Mater.*, 2003, **15**, 959-970.

[18] a) D. T. Bong, T. D. Clark, J. R. Granja and M. R. Ghadiri, *Angew. Chem. Int. Ed.*, 2001, **40**, 988-1011; b) S. Zhang, *Nat. Biotechnol.*, 2003, **21**, 1171-1178; c) X. Zhao, F. Pan, H. Xu, M. Yaseen, H. Shan, C. A. E. Hauser, S. Zhang and J. R. Lu, *Chem. Soc. Rev.*, 2010, **39**, 3480-3498; d) M. P. Lutolf and J. A. Hubbell, *Nat. Biotechnol.*, 2005, **23**, 47-55; e) J. H. Collier, J. S. Rudra, J. Z. Gasiorowski and J. P. Jung, *Chem. Soc. Rev.*, 2010, **39**, 3413-3424; f) D. G. Nocera, *Accounts Chem. Res.*, 2012, **45**, 767-776; g) M. R. Wasielewski, *Accounts Chem. Res.*, 2009, **42**, 1910-1921; h) M. R. Wasielewski, *J. Org. Chem.*, 2006, **71**, 5051-5066; i) H. Imahori, Y. Mori and Y. Matano, *J. Photoch. Photobio. C*, 2003, **4**, 51-83; j) O. Hayden, P. A. Lieberzeit, D. Blaas and F. L. Dickert, *Adv. Funct. Mater.*, 2006, **16**, 1269-1278; k) Z. Dong, Q. Luo and J. Liu, *Chem. Soc. Rev.*, 2012, **41**, 7890-7908; l) B. Linton and A. D. Hamilton, *Chem. Rev.*, 1997, **97**, 1669-1680; m) L. E. R. O´Leary, J. A. Fallas, E. L. Bakota, M. K. Kang and J. D. Hartgerink, *Nat. Chem.*, 2011, **3**, 821-828.

[19] a) G. Steinbach-Yfrach, P. A. Liddell, S.-C. Hung, A. L. Moore, D. Gust and T. A. Moore, *Nature*, 1997, **385**, 239-241; b) G. Steinbach-Yfrach, J.-L. Rigaud, E. N. Durantini, A. L. Moore, D. Gust and T. A. Moore, *Nature*, 1998, **392**, 479-482.

[20] a) I. Tsogas, D. Tsiourvas, G. Nounesis and C. M. Paleos, *Langmuir*, 2006, **22**, 11322-11328; b) M. Edidin, *Annu. Rev. Biophys. Biomol. Struct.*, 2003, **32**, 257-283; c) R. G. King and R. M. Marchbanks, *Nature*, 1980, **287**, 64-65.

[21] a) E. An, C. B. Jeong, C. Cha, D. H. Kim, H. Lee, H. Kong, J. Kim and J. W. Kim, *Langmuir*, 2012, **28**, 4095-4101; b) H. J. Kwon and J. P. Gong, *Curr. Opin. Colloid In.*, 2006, **11**, 345-350; c) B. Jeong, S. W. Kim and Y. H. Bae, *Adv. Drug Deliver. Rev.*, 2002, **54**, 37-51.

[22] a) H.-K. Lee, S. Soukasene, H. Jiang, S. Zhang, W. Feng and S. Stupp, *Soft Matter*, 2008, **4**, 962-964; b) A. Brizard, M. Stuart, K. van Bommel, A. Friggeri, M. de Jong and J. H. van Esch, *Angew. Chem. Int. Ed.*, 2008, **47**, 2063-2066; A. Heeres, C. van der Pol, M. Stuart, A. Friggeri, B. L. Feringa and J. H. van Esch, *J. Am. Chem. Soc.*, 2003, **125**, 14252-14253.

[23] A. Ajayaghosh, V. K. Praveen and C. Vijayakumar, *Chem. Soc. Rev.*, 2008, 37, 109-122.

[24] a) J. H. Jung, M. Park and S. Shinkai, *Chem. Soc. Rev.*, 2010, **39**, 4286-4302; b) N. M. Sangeetha and U. Maitra, *Chem. Soc. Rev.*, 2005, **34**, 821-836; c) A. R. Hirst, B.

Escuder, J. F. Miravet and D. K. Smith, *Angew. Chem. Int. Ed.*, 2008, **47**, 8002-8018; d) D. D. Díaz, D. Kühbeck and R. J. Koopmans, *Chem. Soc. Rev.*, 2011, **40**, 427-448.

[25] T. Graham, *J. Chem. Soc.*, 1864, **17**, 318-327.

[26] P. J. Flory, *Faraday Discuss.*, 1974, **57**, 7-18.

[27] D. J. Abdallah and R. G. Weiss, *Adv. Mater.*, 2000, **12**, 1237-1247.

[28] a) L. A. Estroff and A. D. Hamilton, *Chem. Rev.*, 2004, **104**, 1201-1217; b) P. Terech and R. G. Weiss, *Chem. Rev.*, 1997, **97**, 3133-3159; c) P. Dastidar, *Chem. Soc. Rev.*, 2008, **37**, 2699-2715; d) M. de Loos, B. L. Feringa and J. H. van Esch, *Eur. J. Org. Chem.*, 2005, **17**, 3615-3631; e) M. George and R. G. Weiss, *Acc. Chem. Res.*, 2006, **39**, 489-497; f) M. Suzuki and K. Hanabusa, *Chem. Soc. Rev.*, 2010, **39**, 455-463.

[29] a) J. M. Schnur, *Science*, 1993, **262**, 1669-; b) N. Nandi and B. J. Bagchi, *J. Am. Chem. Soc.*, 1996, **118**, 11208-11216.

[30] G. Yu, X. Yan, C. Han and F. Huang, *Chem. Soc. Rev.*, 2013, **42**, 6697-6722.

[31] J. W. Steed, *Chem. Commun.*, 2011, **47**, 1379-1383.

[32] E. R. Zubarev, M. U. Pralle, E. D. Sone and S. I. Stupp, *Adv. Mater.*, 2002, **14**, 198-203

[33] a) D. K. Smith, *Chem. Soc. Rev.*, 2009, **38**, 684-694; b) E. A. Appel, J. del Barrio, X. J. Loh and O. A. Sherman, *Chem. Soc. Rev.*, 2012, **41**, 6195-6214.

[34] a) J. H. van Esch, *Langmuir*, 2009, **25**, 8392-8394; b) J. L. Drury and D. J. Mooney, *Biomaterials*, 2003, **24**, 4337-4351; c) K. Y. Lee and D. J. Mooney, *Chem. Rev.*, 2001, **101**, 1869-1879.

[35] a) P. K. Vemula, U. Aslam, V. Ajai Mallia and G. John, *Chem. Mater.*, 2007, **19**, 138-140; b) C. Boettcher, B. Schade and J. H. Fuhrhop, *Langmuir*, 2001, **17**, 873-877; c) P. Gao, C. Zhang, L. Liu, Y. Zhou and M. Liu, *Chem. Commun.*, 2004, **10**, 1174-1175.

[36] a) X.-Y. Liu, *Top. Curr. Chem.*, 2005, **256**, 1-37; b) J.-L. Li and X.-Y. Liu, *Adv. Funct. Mater.*, 2010, **20**, 3196-3216.

[37] a) G. Cravotto and P. Cintas, *Chem. Soc. Rev.*, 2009, **38**, 2684-2697; b) D. Bardelang, *Soft Matter*, 2009, **5**, 1969-1971.

[38] a) O. E. Philippova, D. Hourdet, R. Audebert and A. R. Khokhlov, *Macromolecules*, 1997, **30**, 8278-8285; b) T. D. Nguyen, K. C.-F. Leung, M. Liong, C. D. Pentecost, J. F. Stoddart and J. I. Zink, *Org. Lett.*, 2006, **8**, 3363-3366.

[39] Z. Yang and B. Xu, *Adv. Mater.*, 2006, **18**, 3043-3046.

[40] S. Nayak and L. A. Nyon, *Angew. Chem. Int. Ed.*, 2005, **44**, 7686-7708.

[41] a) J. L. Drury and D. J. Mooney, *Biomaterials*, 2003, **24**, 4337-4351; b) B. V. Slaughter, S. S. Khurshid, O. Z. Fisher, A. Khademhosseini and N. A. Peppas, *Adv. Mater.*, 2009, **21**, 3307-3329.

[42] I. Levental, P. C. Georges and P. A. Janmey, *Soft Matter*, 2007, **3**, 299-306.

[43] a) D. Seliktar, *Science*, 2012, **336**, 1124-1128; b) N. A. Peppas, J. Z. Hilt, A. Khademhosseini and R. Langer, *Adv. Mater.*, 2006, **18**, 1345-1360; c) A. D. Metcalfe and M. W. J. Ferguson, *J. R. Soc. Interface*, 2007, **4**, 413-437.

[44] a) A. S. Hoffman, *Adv. Drug. Deliver. Rev.*, 2002, **54**, 3-12; b) B. Xu, *Langmuir*, 2009, **25**, 8375-8377; c) N. E. Federovich, J. Alblas, J. R. de Wijn, W. E. Hennink, A. J. Verbout and W. J. A. Dhert, *Tissue Eng.*, 2007, **13**, 1905-1925; d) S. van Vlierberghe, P. Dubruel and E. Schacht, *Biomacromolecules*, 2011, **12**, 1387-1408.

[45] a) C. E. Brubaker, H. Kissler, L.-J. Wang, D. B. Kaufman and P. B. Messersmith, *Biomaterials*, 2010, **31**, 420-427; b) H. Lee, B. P. Lee and P. B. Messersmith, *Nature*, 2007, **448**, 338-342.

[46] S. Zhang, T. C. Holmes, C. M. DiPersio, R. O. Hynes, X. Su and A. Rich, *Biomaterials*, 1995, **16**, 1385-1393.

[47] E. Soussan, S. Cassel, M. Blanzat and I. Rico-Lattes, *Angew. Chem. Int. Ed.*, 2009, **48**, 274-288.

[48] Y. Qiu and K. Park, *Adv. Drug Deliver. Rev.*, 2001, **53**, 321-339.

[49] a) L. Yu and J. Ding, *Chem. Soc. Rev.*, 2008, **37**, 1473-1481; b) B. Jeong, S. W. Kim and Y. H. Bae, *Adv. Drug Deliver. Rev.*, 2002, **54**, 37-51; c) A. Hatefi and B. Amsden, *J. Control. Release*, 2002, **80**, 9-28.

[50] a) P. Calvert, *Adv. Mater.*, 2009, **21**, 743-756; b) N. A. Peppas, P. Bures, W. Leobandung and H. Ichikawa, *Eur. J. Pharm. Biopharm.*, 2000, **50**, 24-46; c) Y. Li, J. Rodrigues and H. Tomás, *Chem. Soc. Rev.*, 2012, **41**, 2193-2221; d) A. V. Kabanov and S. V. Vinogradov, *Angew. Chem. Int. Ed.*, 2009, **48**, 5418-5429.

[51] A. Vintiloiu and J.-C. Leroux, *J. Control. Release*, 2008, **125**, 179-192.

[52] M. T. Cortés and J. C. Moreno, *E-Polymers*, 2003, **41**, 1-42.

[53] F. Zhao, M. L. Ma and B. Xu, *Chem. Soc. Rev.*, 2009, **38**, 883-891.

[54] D. D. Díaz, D. Kühbeck and R. J. Koopmans, *Chem. Soc. Rev.*, 2011, **40**, 427-448.

[55] B. Escuder, F. Rodríguez-Llansola and J. F. Miravet, *New. J. Chem.*, 2010, **34**, 1044-1054.

[56] A. Döring, W. Birnbaum and D. Kuckling, *Chem. Soc. Rev.*, 2013, **42**, 7391-7420.

57 H. Hamamoto, Y. Suzuki, H. Takahashi and S. Ikegami, *Adv. Synth. Catal.*, 2007, **349**, 2685-2689.

58 a) F. Rodríguez-Llansola, J. F. Miravet and B. Escuder, *Chem. Commun*, 2009, **47**, 7303-7305; b) F. Rodríguez-Llansola, J. F. Miravet and B. Escuder, *J. Am. Chem. Soc.*, 2009, **131**, 11478-11484.

59 S. Ray, A. K. Das and A. Banerjee, *Chem. Commun.*, 2006, **26**, 2816-2818.

60 a) D. Das, S. Maiti, S. Brahmachari and P. K. Das, *Soft Matter*, 2011, **7**, 7291-7303; b) R. N. Mitra and P. K. Das, *J. Phys. Chem. C*, 2008, **112**, 8159-8166; c) T. Kar, S. Dutta and P. K. Das, *Soft Matter*, 2010, **6**, 4777-4787; d) C. S. Love, V. Chechik, D. K. Smith, K. Wilson, I. Ashworth and C. Brennan, *Chem. Commun.*, 2005, **15**, 1971-1973.

61 a) A. Pal, A. Srivastava and S. Bhattacharya, *Chem. Eur. J.*, 2009, **15**, 9169-9182; b) Y. Mei, Y. Lu, F. Polzer and M. Ballauff, *Chem. Mater.*, 2007, **19**, 1062-1069.

62 a) J.-L. Li, X.-Y. Liu, X.-G. Wang and R.-Y. Wang, *Langmuir*, 2011, **27**, 7820-7827; b) J.-S. Shen, Y.-L. Chen, J.-L. Huang, J.-D. Chen, C. Zhao, Y.-Q. Zheng, T. Yu, Y. Yang and H.-W. Zhang, *Soft Matter*, 2013, **9**, 2017-2023.

63 J. Fan, X. Jiang, Y. Hu, Y. Si, L. Ding and W. Wu, *Biomater. Sci.*, 2013, **1**, 421-433.

64 a) J. Liu, G. Chen, M. Guo and M. Jiang, *Macromolecules*, 2010, **43**, 8086-8093; b) X. Yan, Y. Cui, Q. He, K. Wang and J. Li, *Chem. Mater.*, 2008, **20**, 1522-1526.

65 a) J. Li, X. Hong, Y. Liu, D. Li, Y. Wang, J. Li, Y. Bai and T. Li, *Adv. Mater.*, 2005, **17**, 163-166; b) D. Bardelang, Md. B. Zaman, I. L. Moudrakovski, S. Pawsey, J. C. Margeson, D. Wang, X. Wu, J. A. Ripmeester, C. I. Ratcliffe and K. Yu, *Adv. Mater.*, 2008, **20**, 4517-4520; c) P. D. Wadhavane, M. A. Izquierdo, F. Galindo, M. I. Burguete and S. V. Luis, *Soft Matter*, 2012, **8**, 4373-4381; d) L. Korala, L. Li and S. L. Brock, *Chem. Commun.*, 2012, **48**, 8523-8525.

66 H. J. van der Linden, S. Herber, W. Olthuis and P. Bergveld, *Analyst*, 2003, **128**, 325-331.

67 a) G. R. Hendrickson and L. A. Lyon, *Soft Matter*, 2009, **5**, 29-35; b) A. Kavanagh, R. Byrne, D. Diamond and K. J. Fraser, *Membranes*, 2012, **2**, 16-39.

68 D. B. Amabilino and J. Puigmartí-Luis, *Soft Matter*, 2010, **6**, 1605-1612.

69 a) A. Moreno, B. Quiroz-García, F. Yokaichiya, V. Stojanoff and P. Rudolph, *Cryst. Res. Technol.*, 2007, **42**, 231-236; b) L. A. Estroff, L. Addadi, S. Weiner and A. D. Hamilton, *Org. Biomol. Chem.*, 2004, **2**, 137-141; c) J. A. Foster, M.-O. M. Piepenbrock, G. A. Lloyd, N. Clarke, J. A. K. Howard and J. W. Steed, *Nat. Chem.*, 2010, **2**, 1037-1043.

[70] a) S. Bhattacharya and Y. K. Gosh, Chem. Commun., 2001, **2**, 185-186; b) D. R. Trivedi, A. Ballabh, P. Dastidar and B. Ganguly, *Chem. Eur. J.*, 2004, **10**, 5311-5322; c) D. R. Trivedi and P. Dastidar, *Chem. Mater.*, 2006, **18**, 1470-1478; d) J. Peng, K. Liu, X. Liu, H. Xia, J. Liu and Y. Fang, *New J. Chem.*, 2008, **32**, 2218-2224; e) D. Bardelang, F. Camerel, J. C. Margeson, D. M. Leek, M. Schmutz, M. B. Zaman, K. Yu, D. V. Soldatov, R. Ziessel, C. I. Ratcliffe and J. A. Ripmeester, *J. Am. Chem. Soc.*, 2008, **130**, 3313-3315; f) T. Kar, S. Debnath, D. Das, A. Shome and P. K. Das, *Langmuir*, 2009, **25**, 8639-8648; g) M. Xue, D. Gao, K. Liu, J. Peng and Y. Fang, *Tetrahedron*, 2009, **65**, 3369-3377; h) S. R. Jadhav, P. K. Vemula, R. Kumar, S. R. Raghavan and G. John, *Angew. Chem. Int. Ed.*, 2010, **49**, 7695-7698.

D Main part

1. Multistimuli responsive supramolecular organogels formed by low-molecular-weight peptides bearing side-chain azobenzene moieties[i]
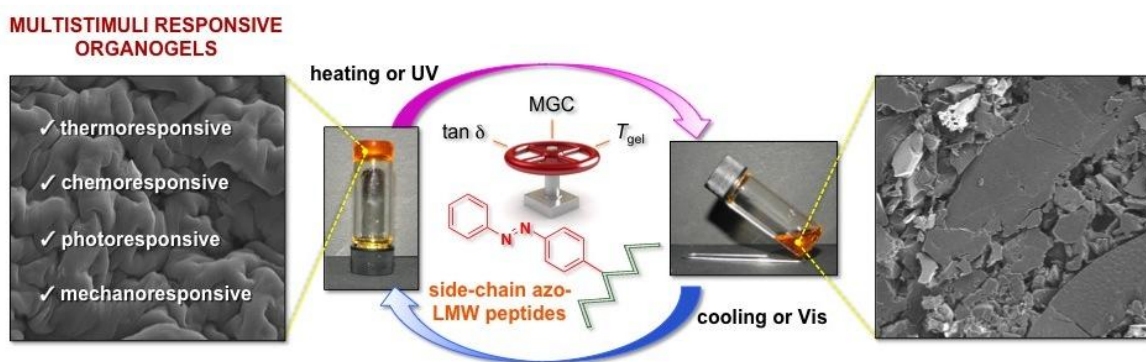
This work demonstrates that the incorporation of azobenzene residues into the side-chain of low-molecular-weight peptides can modulate their self-assembly process in organic solvents leading to the formation of stimuli responsive physical organogels. The major driving forces for the gelation process are hydrogen-bonding and π–π interactions, which can be triggered either by thermal or ultrasound external stimuli, affording materials having virtually the same properties. In addition, a predictive model for gelation of polar protic solvent was developed using Kamlet-Taft solvent parameters and experimental data. The obtained viscoelastic materials exhibited interconnected multistimuli responsive behaviors including thermal-, photo-, chemo- and mechanical responses. All of them displayed thermoreversability with *gel*-to-*sol* transition temperatures established between 33-80 ºC and gelation times from minutes to several hours. Structure-property relationship studies of a designed peptide library have demonstrated that the presence and position of the azobenzene residue can be operated as a versatile regulator to reduce the critical gelation concentration and enhance both the thermal stability and mechanical strength of the gels, as demonstrated by comparative dynamic rheology. The presence of *N*-Boc protecting group in the peptides showed also a remarkable effect on the formation and

properties of the gels. Despite numerous examples of peptides-based gelators known in the literature, this is the first time in which low-molecular-weight peptides bearing side-chain azobenzene units are used for the synthesis of 'intelligent' supramolecular organogels. Compared to other approaches, this strategy is advantageous in terms of structural flexibility since it is compatible with a free, unprotected amino terminus and allows placement of the chromophore at any position of the peptide sequence.[ii]

1.1. Introduction

The ability of natural systems to alter function in direct response to environmental conditions has inspired many scientists to fabricate 'smart' materials that respond to temperature, light, pH, electro/magnetic field, mechanical stress and/or chemical stimuli. These responses are usually manifested as remarkable changes from the molecular (e.g. conformational state, hierarchical order) to the macroscopic level (e.g. shape, surface properties).[1] Among many types of stimuli responsive materials, self-assembled viscoelastic gels[2] of both organic solvents (organogels) and water (hydrogels) have been recognized as promising materials for bottom-up nanofabrication tools in various fields such as biomedicine, catalysis, sensors, cosmetics, foods and environmental remediation.[3] As soft materials, gels are continuous in structure and solid-like in rheological behavior.[4] In contrast to chemical gels,[5] which are based on covalent bonds (usually cross-linked polymers unable to redissolve), physical (also called supramolecular) gels[6] are made of either low-molecular-weight (LMW) compounds or polymers -so called gelators- through extensive non-covalent interactions such as hydrogen-bonding, van der Waals, charge-transfer, donor-acceptor, dipole-dipole, π–π stacking and coordination interactions. The solid-like appearance of the gels is the result of the entrapment of the liquid (major component) in the interstices of a solid 3D matrix of large surface area (minor component), usually through surface tension and capillary forces.[3f), 7] In the case of LMW gelators, the formation of the viscoelastic matrix is a consequence of the entanglement of one dimensional (1D) supramolecular fibers, which is typically induced by cooling their hot

---

[ii] The synthesis of the compounds described in Schemes 1, 2 and Figure 1 has been conducted by P. Fatás and S. Oehm. Temperature dependent FT-IR, photo-response and dye-removal studies as described in Figures 6, 12 and 18 have been conducted by S. Oehm and J. Bachl. All other experiments have been carried out by J. Bachl.

isotropic solutions to room temperature. Due to the weakness of the non-covalent interactions that maintain the dynamic supramolecular structure, physical gels are usually thermoreversible. Moreover, the *sol*-to-*gel* (and/or *gel*-to-*sol*) phase transition can also be triggered by other stimuli such as light irradiation if a suitable chromophore is present. This has been proven to be useful for understanding gelation mechanisms and for advanced applications like drug delivery and switchable devices with memory function.[8] The simplest molecular design principle in this case is to incorporate one or more light responsive units in the structure of the respective gelating moiety. Azobenzene is the photochromic group[9] most widely used to generate photoresponsive gels,[10] probably due to its facile incorporation into organic structures and its well-studied *trans*-to-*cis* photoisomerization. In addition to the photoresponsive behavior, aromatic $\pi-\pi$ stacking and other non-covalent interactions have been found to cooperatively stabilize some organogel structures.[11] However, it should be considered that the simple incorporation of switchable azo units into LMW gelators does not warrant a rapid, if any, macroscopic response of the gel material upon light irradiation because photo-induced isomerization is very sensitive to the gel structure.[12] Indeed, very slow kinetics have generally been documented for supramolecular organized systems where the azobenzene moieties are tightly packed.[13] Nevertheless, exceptions to this rule have been also reported in the case of gels made from azobenzene dendrons and aliphatic amide units.[14] In addition, one should consider that incorporation of relatively large stimuli responsive moieties in the structure of a gelator may cause an important disruption of the gelation ability and/or modification of the gel properties as a consequence of the delicate equilibrium between crystallization and solubility that usually defines the metastable gel state.[15] Peptides are among the most popular gelating moieties, with numerous examples of LMW peptide-based gelators being reported in recent years.[16] However, only a few works[14a), 17] have focused on compounds of this type that contain azobenzene groups for the preparation of photoresponsive gel materials. In most of such reports, the azobenzene unit is incorporated into the peptide backbone blocking the terminal amino moiety. Additionally, in some cases,[17a), e)] hydrocarbon chains are also attached to the molecule to promote self-assembly through hydrophobic interactions, so that the compounds cannot be considered strictly as peptides but rather as peptide-conjugates or peptide-hybrid materials. A different approach to generate photoresponsive LMW peptide gelators while completely keeping the peptide nature of the system can be the use of amino acids that bear an azobenzene group in the

47

side chain. This strategy seems advantageous in terms of structural flexibility since it is compatible with a free, unprotected amino terminus and allows placement of the chromophore at any position of the peptide sequence. We report herein the ability of small peptides bearing a side-chain azobenzene moiety to form stable supramolecular gels that are responsive to several stimuli, among which light. In particular, we have synthesized and studied the gelation properties and responsiveness of tetrapeptides containing *p*-(phenylazo)-l-phenylalanine, that is, the l-phenylalanine (Phe) derivative formally resulting from the attachment a phenylazo group to the *para* position of the aromatic ring[18] (azoPhe in the abbreviated form; Figure 1). After the pioneering studies of Goodman[19] on the chirooptical and conformational properties of high-molecular-weight homo- and copolymers based on azoPhe, a number of works[20] have dealt with this azobenzene-containing amino acid but none of them is related to the design of peptide gelators.

1.2. Results and discussion

Peptide design and synthesis: In the course of an investigation on the structural behavior of peptides composed of azoPhe and Asp(OBzl) (l-aspartic acid with a side-chain benzyl ester) residues, we observed that the intermediate tetrapeptide Boc-azoPhe-[Asp(OBzl)]$_3$-OMe (**A4** in Figure 1) exhibited a high propensity to form a gelatinous material. We decided to investigate the gelation properties of this compound and extended the study to the analogous sequences **B4**, **C4** and **D4** (Figure 1), differing in the position occupied by the azobenzene-containing residue (azoPhe) within the peptide backbone. Given the different solubility expected for tetrapeptides bearing an *N*-Boc protected (Boc = *tert*-butoxycarbonyl) vs. a free amino group, the study was also applied to the corresponding unprotected derivatives (name preceded by **H-** in Figure 1). Additionally, to evaluate the extent to which the gelation ability of these compounds depends on the presence of the azobenzene moiety, we considered the replacement of the azoPhe residue by Phe in the peptide sequences mentioned. Clearly, the compounds incorporating Phe (named as **F-** in Figure 1) will not be photosensitive but their gelation capacity could be similar or even superior to that of the corresponding azoPhe-containing counterparts depending on whether the additional *p*-(phenylazo) group is beneficial or detrimental to the gelation process. The absence of both Phe and azoPhe was evaluated by considering **Z4** while the tripeptide **A3**

48

was included in the study to check whether **A4** is the shortest sequence exhibiting gelation capacity. Finally, we wondered about the effect produced when the side-chain azobenzene group acts as a bridge to connect two peptide chains. This possibility was explored for the **A4** and **D4** sequences, linked in this way to give rise to **bis-A4** and **bis-D4**, respectively (Figure 1).
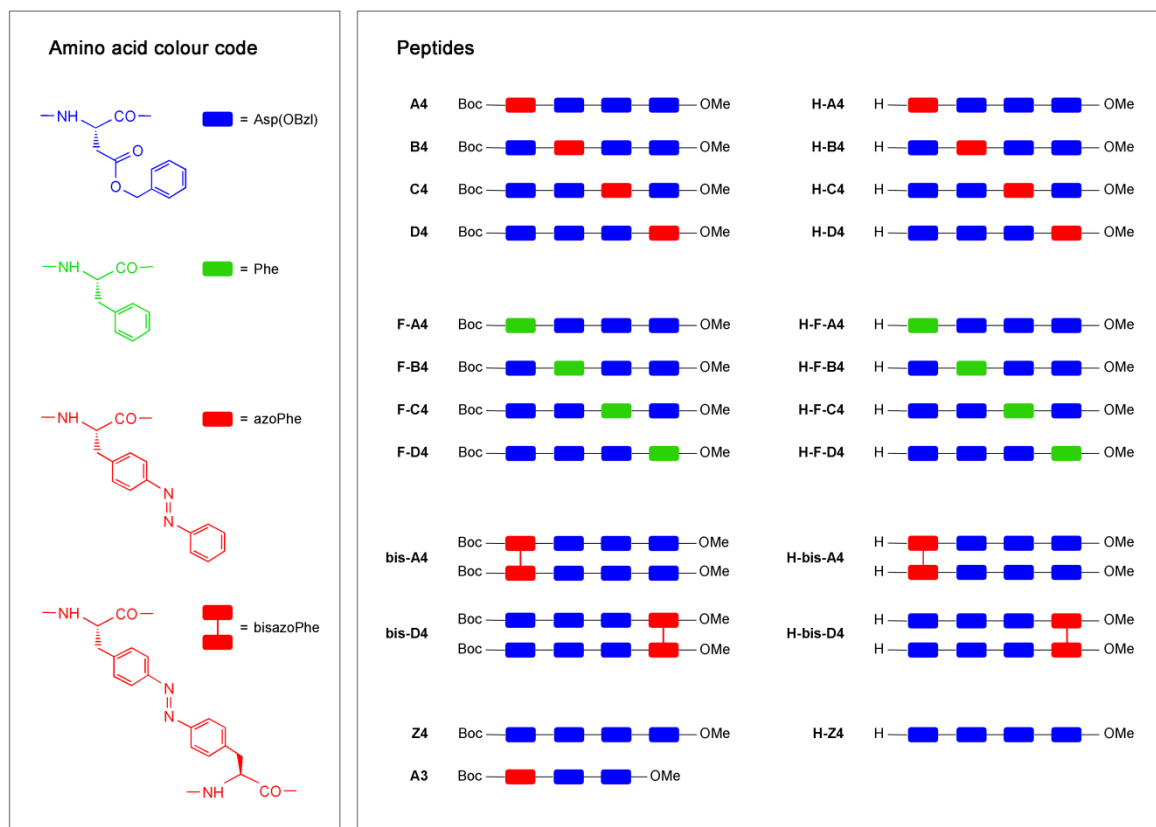
Fig. 1 Library of LMW peptides bearing side-chain azoPhe synthesized for this work (*right*). A code according to key moieties was adopted in order to simplify the representation of the peptides (*left*). The nomenclature used for naming the peptides was based on the position of the azoPhe group with respect to the *N*-terminal group (i.e. **A**, **B**, **C**, **D**), the length of the peptide (i.e. tripeptides = **3**; tetrapeptide = **4**). Definition of other abbreviations: **F** = Phe; **H** = absence of *N*-Boc protecting group; **Z** = control peptide without azoPhe or Phe moieties.

The azobenzene-based amino acids azoPhe and bisazoPhe were synthesized in the *N*-Boc-protected form appropriate for subsequent peptide synthesis, Boc-azoPhe-OH (**1**) and Boc-bisazoPhe-OH (**2**), using commercial *N*-Boc-(*p*-nitro)-l-phenylalanine (**3**) as a common precursor (Scheme 1). In both cases, the synthetic strategy involved condensation of a

nitroso and an amino moiety, similarly to that described by Goodman for the preparation of unprotected azoPhe.[19] [a)] Catalytic hydrogenation of *N*-Boc-(*p*-nitro)-l-phenylalanine (**3**) yielded the *p*-amino derivative **4**, which was further reacted with nitrosobenzene in acetic acid to afford the desired Boc-azoPhe-OH (**1**) (Scheme 1). To generate the bisazoPhe derivative, **4** was also used as the amino component while the nitroso moiety (**5**) was obtained from **3** upon reduction with zinc and subsequent treatment with iron trichloride. Condensation of the two fragments in acetic acid yielded the bis(amino acid) bearing a Boc group in both amino termini (**2**) (Scheme 1). This methodology is more straightforward than the one previously reported by Sewald,[21] which required additional protection and deprotection steps. It should be noted that the α carbon atom(s) in amino acids **1** and **2** exhibit an l stereochemistry (equivalent to *S*), as in the precursor **3**.[22]
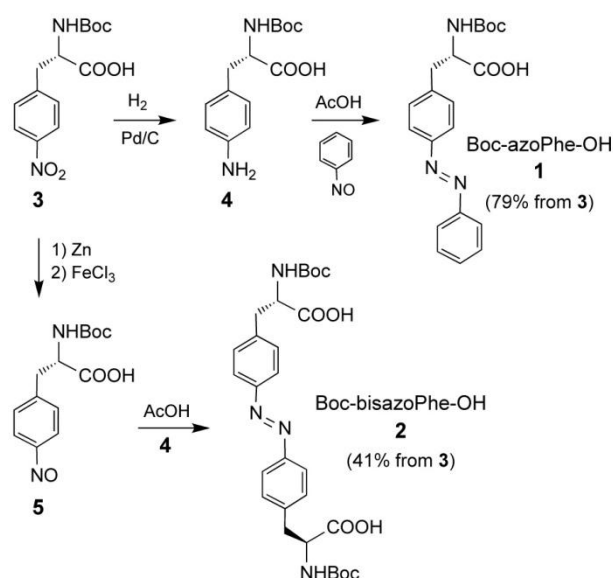
Scheme 1 Synthesis of the azobenzene-based amino acids Boc-azoPhe-OH (**1**) and Boc-bisazoPhe-OH (**2**). Abbreviations: Boc, *tert*-butoxycarbonyl.

All peptides in Figure 1 were prepared following standard procedures of peptide synthesis in solution,[23] using Boc as a temporary protection for the amino function and EDC/HOBt as coupling agents (EDC = *N*-(3-dimethylaminopropyl)-*N*'-ethylcarbodiimide hydrochloride; HOBt = 1-hydroxybenzotriazole). The *C*-terminal methyl esters were prepared by reaction of the corresponding *N*-Boc-protected amino acid with methyl iodide in the presence of potassium carbonate. Boc deprotection was carried out by treatment with a 4:6 (v/v) TFA/dichloromethane mixture (TFA = trifluoroacetic acid). When bisazoPhe

was involved, the two amino or carboxylic acid groups in the bis(amino acid) (or the bisazoPhe-containing peptide chain) were made react simultaneously. All *N*-Boc-protected intermediate derivatives and final peptides were purified by column chromatography and fully characterized by NMR spectroscopy and high-resolution mass spectrometry. Isolation of the final peptides exhibiting a free amino terminus (those denoted with **H-** in Figure 1) was accomplished by removal of the Boc protecting group in the corresponding precursor under standard conditions and further neutralization of the trifluoroacetate formed. As a model example, the preparation of **A4**, **H-A4** and **bis-A4** is shown in Scheme 2.
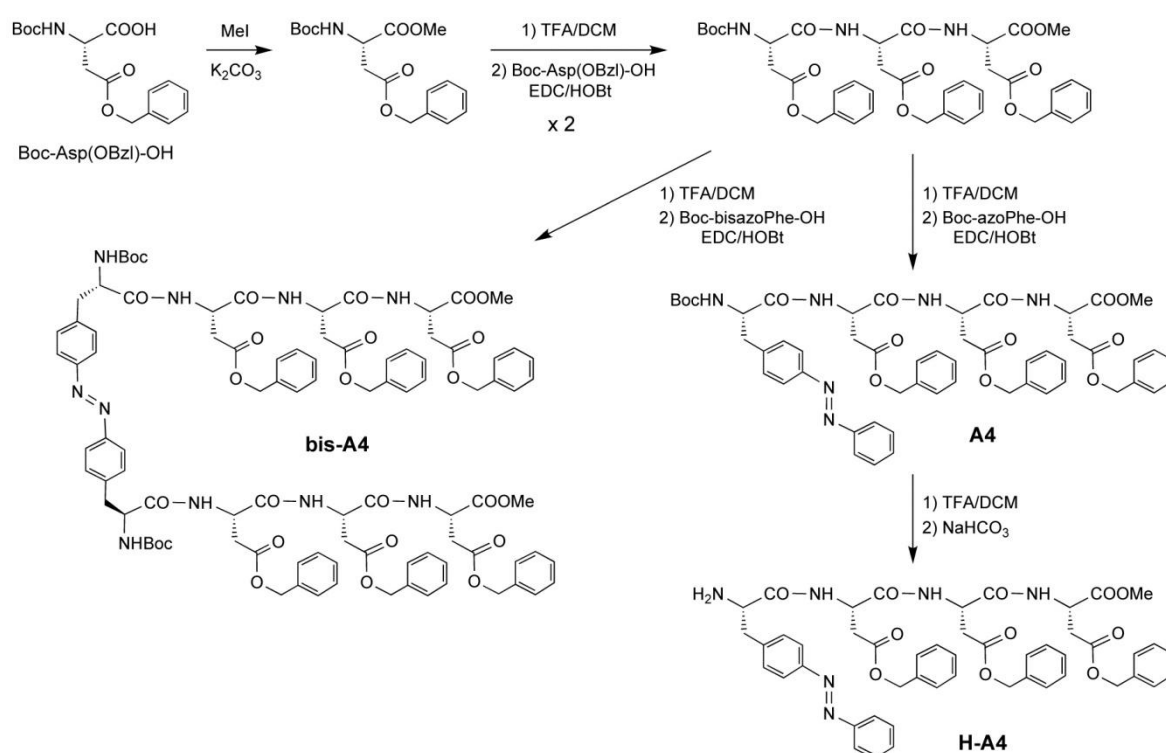
Scheme 2 Synthesis of azoPhe-based peptides **A4**, **H-A4** and **bis-A4**. Abbreviations: Boc, *tert*-butoxycarbonyl; Bzl, benzyl; EDC, *N*-(3-dimethylaminopropyl)-*N'*-ethylcarbodiimide hydrochloride; HOBt, 1-hydroxybenzotriazole; TFA, trifluoroacetic acid.

Gelation ability and solubility considerations: The gelation ability of the peptide library (Figure 1) was systematically studied for 20 solvents of different nature (polar protic, polar aprotic or non-polar) using the classical thermal (heating-cooling) treatment. This provided a 2D rectangular matrix of 460 elements (ESI, Table S1). The state of the material was examined by the "stable-to-inversion" method,[22] and the gel condition of the samples that

did not show gravitational flow upon turning the vial upside-down was further confirmed by dynamic rheological measurements (*vide infra*). All peptides studied in this work were found to be insoluble in water, n-hexane and glycerol upon heating and/or intense ultrasound treatment. In contrast, the use of dimethyl sulfoxide, acetonitrile, acetone, dichloromethane, ethyl acetate, tetrahydrofuran, chloroform or 1,4-dioxane resulted in complete solubilization of most of the peptides upon heating-cooling or ultrasound treatment. Among these solvents, only a few exceptions were observed for acetonitrile (**A4**, **B4**, **D4**, **F-C4, bis-A4, H-bis-D4**) and ethyl acetate (**H-B4**, **H-C4**, **bis-A4**, **H-bis-A4**, **bis-D4**), in which inhomogeneous or homogeneous opaque gels were obtained.[22] Conversely, precipitate formation was observed in some solvents like methanol (**A4**, **H-A4**, **H-B4**, **H-C4**) and diethyl ether (**D4**, **F-A4**, **F-B4**) after cooling down the corresponding isotropic solutions to room temperature. However, no apparent correlation was found between the parameters of the above solvents and the structure of the different peptides that formed either gels or precipitates. Besides occasional gels observed in non-protic solvents (acetonitrile, ethyl acetate, diethyl ether), gelation was effective in aromatic solvents (toluene, benzene, xylene) with very few exceptions (ESI, Table S1). Excluding the solvents that did not provide any gel and the reference peptides **A3**, **Z4** and **H-Z4**, 60% of the matrix elements afforded stable gels. In the case of alcohols, a remarkable enhancement of the gelation ability of the peptides was observed when increasing the molecular weight (MW) of the solvent, probably due to additional hydrophobic interactions stabilizing the aggregates. Thus, methanol was gelled by 15% of the peptides, ethanol by 50% and higher MW alcohols (isopropanol, 2-butanol, 1-hexanol) by 75-95%. Moreover, the azoPhe-containing peptides showed greater gelation ability than their Phe counterparts both in aromatic and alcoholic solvents (e.g. **A4** vs. **F-A4**; **H-A4** vs. **H-F-A4**; **B4** vs. **F-B4**; **C4** vs. **F-C4**; **H-C4** vs. **H-F-C4**; ESI, Table S1). On the other hand, tripeptide **A3** showed gelation only in two aromatic solvents, which asserts the tetrapeptides as the shortest sequence leading to efficient azobenzene-based peptide organogelator of this type. Notably enough, control tetrapeptides **Z4** and **H-Z4** (containing no azoPhe or Phe residue) provided gels only in 1-hexanol or toluene, respectively. These results highlight the important role of π–π stacking interactions of aromatic residues in the side-chain in promoting peptide supramolecular assembly in organic solvents.[24] It is worth noting that both **Z4** and **H-Z4** bear a benzyl group attached to the side-chain of each Asp residue (Figure 1). The fact that replacement of a single Asp(OBzl) residue in **Z4** or **H-Z4**,

at any position of the peptide sequence, by Phe brings about a dramatic increase in gelating capacity means that, at least for the kind of peptides under study, the benzyl moiety in Phe is much more effective in providing π-π stacking interactions than the one present in Asp(OBzl). This distinct effect could be related to the closer proximity of the aromatic group to the peptide backbone in the case of Phe, which in turn results in a more restricted flexibility.

Appearance of the gels: All organogels formed at the MGC by the peptides containing an azobenzene group showed a characteristic yellow-orange color (Figure 2).

Fig. 2 Representative digital photographs of upside-down vials containing organogels obtained from different peptides in toluene or isopropanol. Gels were prepared at their MGC as indicated in Table S1 (ESI). In isopropanol: **A4**, 2% w/v; **B4**, 4% w/v; **C4**, 6% w/v; **D4**, 10% w/v; **bis-D4**, 2% w/v; **F-A4**, 4% w/v; **F-D4**, 5% w/v. In toluene: **A4**, 2% w/v; **B4**, 1.5% w/v; **C4**, 2% w/v; **D4**, 4% w/v; **bis-D4**, 1% w/v; **H-A4**, 7% w/v; **F-D4**, 9.5% w/v; **H-F-D4**, 2.5% w/v.

The formation of aggregates smaller than λ = 400-700 nm (visible wavelength range) was routinely observed in non-aromatic solvents, as indicated by the complete opacity of the

materials. In general, gels derived from bisazoPhe-based peptides were more yellowish and pale than those made of the analogous azoPhe derivatives, in which the ratio of amino acid residues per azobenzene moiety is higher. In the case of alcohols, the degree of opacity was independent of the solvent structure (methanol, ethanol, isopropanol, 2-butanol, 1-hexanol). However, translucent or transparent orangish gels were always obtained in aromatic solvents. The same opacity behavior was also observed for gels prepared from peptides lacking the azobenzene units (**F-** series).[22] Such marked optical differences point out the importance of the interactions established between gelator and solvent molecules for the growth of supramolecular aggregates.

Correlations with solvent properties: In order to evaluate possible correlations between gelation ability, gel properties and solvent nature, we paid attention to the study of the Kamlet-Taft solvent parameters.[25] Kamlet-Taft solvatochromic parameters measure separately the acidity or hydrogen bond donor ability (α-parameter), hydrogen bond acceptor (β-parameter) and dipolarity/polarizability (π*-parameter) properties of the solvent as contributing to overall solvent polarity. Previous studies with physical gels have demonstrated the usefulness of these parameters to categorize the interactions between solvent and gelator molecules.[26] The results of these studies indicate that α-parameter plays a key role during the formation of hydrogen-bonded gel networks, β-parameter affects the thermal stability of the gel and π*-parameter relates to the stabilization of charges and dipoles associated to peripheral groups (solvation) and interactions between fibers at the nanoscale. In our case, it was possible to build an appropriate fitting Gaussian-model based on theoretical and experimental data distribution that accounts for the gelation ability of the peptide library in polar protic solvents (Figure 3).[22] Thus, the protic solvents with higher tendency to form stable gels were those presenting simultaneously relatively high and balanced hydrogen bond donor and acceptor abilities (e.g. $\alpha \sim 0.75$, $\beta \sim 0.85$), as well as intermediate polarizability (e.g. π* ~ 0.5). In this scenario, solvents like MeOH, water or glycerol with much higher α-values and much lower β-values should hinder initial steps of the gelation process affording either precipitation or clear solutions. On the other hand, both the high gelation efficiency of the peptide library and similar Kamlet-Taft parameters in the case of aromatic solvents caused a size population data too small to build a statistically significant model for the gelation ability. Regardless the solvent, no significant differences could be observed for the distribution of gel properties such as the

gel-to-*sol* transition temperature (T_{gel}) or the minimum gelation concentration (MGC = lowest concentration of the gelator at which gelation occurs) in function of α, β or π^*-parameters. However, we could elucidate some general trends by comparing directly these properties with the structure of the peptide-based gelators (*vide infra*).
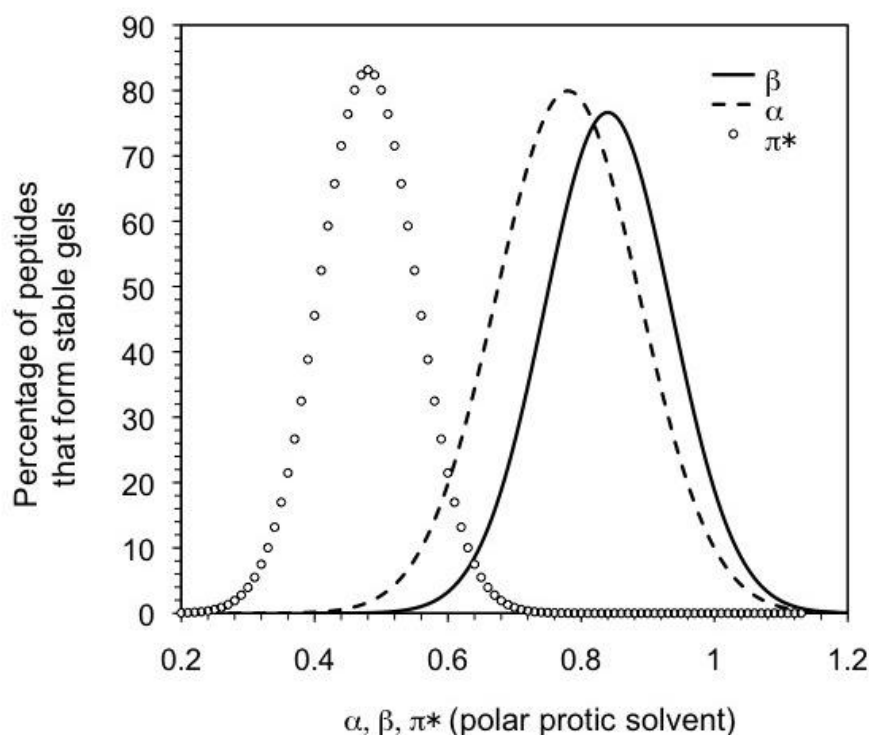
Fig. 3 General Gaussian-based predictive model built from the correlation between Kamlet-Taft solvent parameters and gelation ability of the peptide library in polar protic solvents (2-butanol, isopropanol, 1-hexanol, ethanol, methanol, water, glycerin). Note: Gaussian distributions reflect the normal probability of the peptides to form gels in protic solvents. Thus, highest probability is achieved when all Kamlet-Taft parameters of a given solvent are simultaneously at the X-coordinate of the corresponding maximum.

Interestingly, we also found that gel formation could be also achieved by ultrasound treatment during 5-30 min at room temperature of the initial [gelator + solvent] mixture instead of the typical heating-cooling process without major alteration of the MGC. In general, gels prepared at the same concentration by both methods did not show major differences in terms of T_{gel} values and morphology. However, the gelation times were considerably lower and the opacity somewhat higher for gels prepared by ultrasound treatment, suggesting the eventual formation of larger aggregates. Rheological experiments

also confirmed slightly higher strength within the linear regime for gels prepared by thermal process (*vide infra*). From a mechanistic point of view, ultrasound has been proven to activate non-covalent interactions (e.g. hydrogen-bonding, π–π stacking, van der Waals) via cavitation of the solvent, which can eventually dissolve the gelator molecules and trigger the gelation phenomenon.[27]

Minimum gelation concentration and *gel*-to-*sol* phase transition temperature: MGC values were established in most cases between 1-10% w/v (weight/volume, i.e. 1% w/v = 1 g of solute per 100 mL of solution). These values involve the immobilization between hundreds and thousands of solvent molecules per gelator molecule.[22] The *gel*-to-*sol* transition temperatures (Tgel) of the gels were obtained by the "inverse flow method" (IFM).[28]
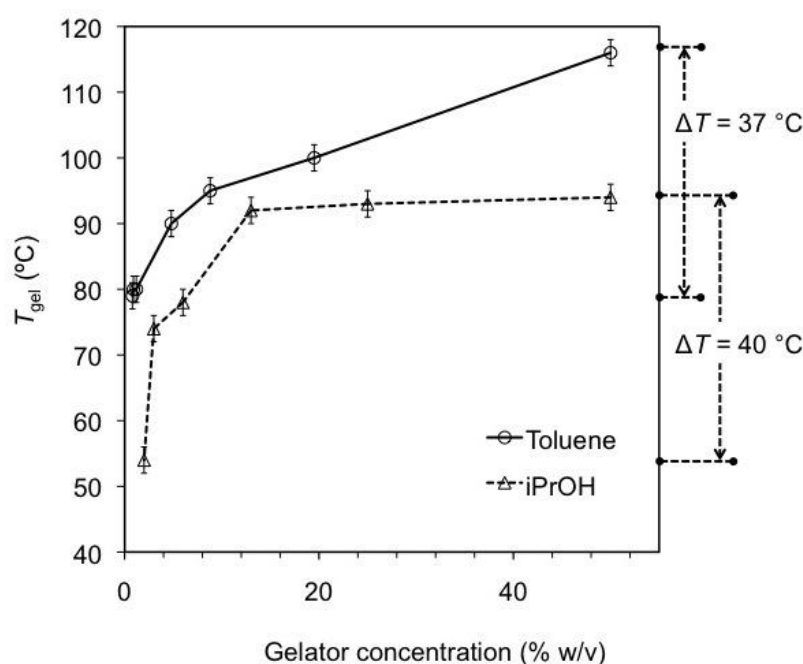
Fig. 4 Phase boundaries defined by the evolution of T_{gel} as a function of gelator concentration for **bis-D4** in isopropanol (bp = 82.5 °C) and toluene (bp = 110.6 °C). The plateau value in isopropanol was virtually reached after increasing 6.5-fold the concentration with respect to MGC (i.e. 2% w/v).

However, as Tgel values determined by IFM strongly depend on factors such as cooling rate, aging time, thermal history and degree of hysteresis, among others,[29] they were correlated for model examples with the first endothermic transition observed by modulated differential scanning calorimetry (DSC).[22] As typical feature of supramolecular gels, Tgel

56

increased considerably with increasing initial gelator concentration (ΔTgel ~ 35-40 ºC, Figure 4), indicating that self-assembly is driven by strong intermolecular interactions affording closely packed 3D networks. Remarkably, gelator concentration could be increased in many cases until 50% w/v affording homogeneous gels, which retained stability well above the boiling point of the solvent. The impossibility to prepare more concentrated isotropic solutions in those cases prevented the detection of the typical plateau region before collapse of the gel. As expected, gelation time also decreased with increasing gelator concentration.[22] In terms of thermal responsiveness, all organogels were found to be fully thermoreversible and stable to several cycles of heating and cooling, without affecting the gelation ability. Moreover, they remained homogeneous, without significant change in mechanical strength (e.g. caused by microcrystallization of the gelator), reconstitution ability, color or appearance for several months when stored in sealed glass vials at room temperature.

Structure-property relationship studies: Figure 5 outlines an overview of the T_{gel} and MGC values corresponding to the gels prepared with all peptides in two of the most statistically relevant solvents, namely isopropanol (polar protic) and toluene (non-polar). The results show that the presence of the side-chain azoPhe unit in **A4**-**D4** leads to the formation of organogels in isopropanol that exhibit higher thermal stability (ΔT_{gel} ~ 10-20 ºC) in comparison to the analogous gelators containing Phe (Figure 5A). However, this effect was not evident in toluene for the above series or when considering bisazoPhe-based gelators (Figure 5A). The presence of an N-Boc protecting group generally resulted in slightly higher T_{gel} values for the gels prepared with the azoPhe series in isopropanol (Figure 5A, C). This effect was nearly irrelevant in toluene, except for the gels made with **H-A4** that were intriguingly more thermostable (ΔT_{gel} ~ 14 ºC) than those made with **A4**. A much higher gelation tendency was also observed for the N-Boc protected in the **F-** series, although no clear correlation was found between solvent nature and gelation ability for the latter. Moreover, the bisazoPhe-based gels usually displayed T_{gel} values superior to those of the corresponding azoPhe-based gels (ΔT_{gel} ~ 15-30 ºC) with little influence of the solvent or presence/absence of N-Boc protection. In general, the position of the azoPhe or Phe residue within the peptide sequence did not have a major impact on the T_{gel} of the gel materials. Conversely, MGC values were typically lower in toluene than in isopropanol, regardless the gelator family in the case of N-Boc protected peptides, except for **F-D4** for which the opposite was unexpectedly observed (Figure 5B). Much lower MGC were also

57

achieved in the case of bisazoPhe-containing peptides. In general, location of azoPhe at the **A** or **B** position in *N*-Boc protected peptides provided lower MGC values, especially in isopropanol. This effect was even more marked in the **F-** series. For instance, **F-B4** formed gels in isopropanol and toluene at 1.0 and 0.5% w/v respectively, whereas **F-C4** required 13.5 and 7.0% w/v respectively.
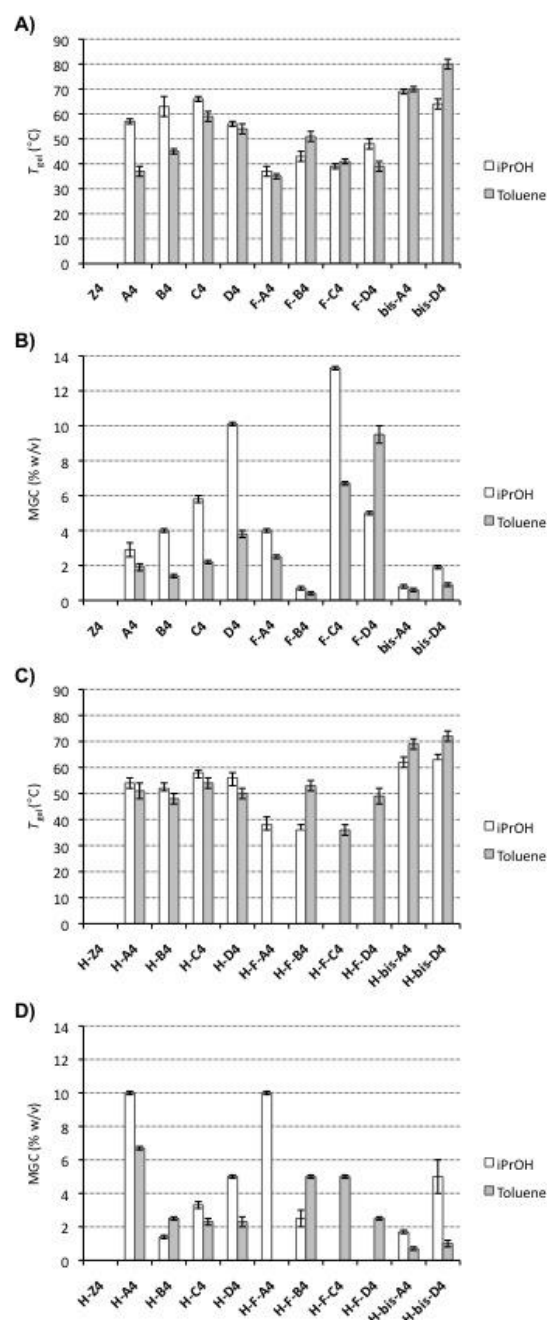
Fig. 5 Bar graphs showing the influence of peptide structure on T_{gel} and MGC for freshly prepared gels in two representative solvents (isopropanol, toluene).

Interestingly, the absence of *N*-Boc protection in the gelator structure of the azoPhe-based peptides resulted in a lower MGC value, especially in isopropanol,[30] with the exception of **H-A4** (Figure 5D). In contrast, complete inhibition of the gelation was observed for some peptides of the **H-F-** series in isopropanol (**H-F-C4**, **H-F-D4**). These results support the importance of remote groups on fine-tuning the properties of physical gels.[31]

Driving force study

Temperature-dependent FT-IR experiments: We carried out temperature-controlled FT-IR experiments in order to classify the major driving forces for the gelation phenomenon. As expected, intensity of the bands involving the amides groups were found to be much higher in the gel samples compared to the solid gelator indicating more efficient interactions of these groups in the gel phase.[22] In order to induce the *gel*-to-*sol* transition, the samples were submitted to a controlled increase of temperature.
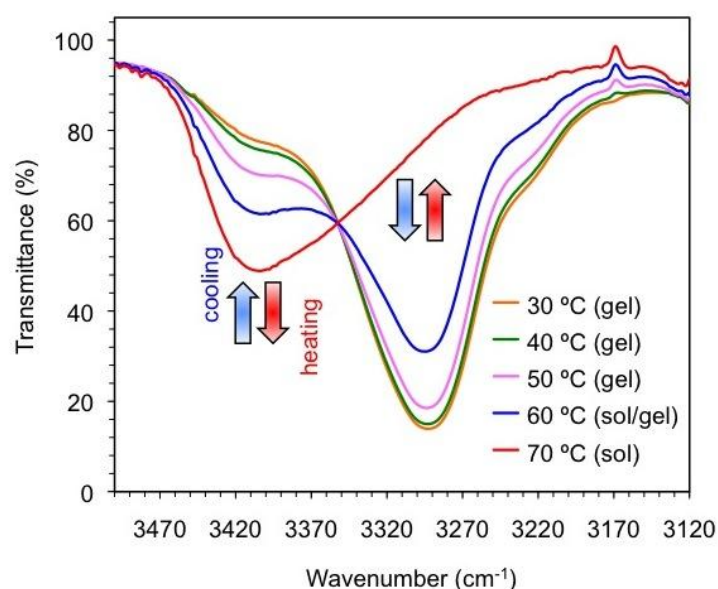
Fig. 6 Typical temperature-controlled FT-IR spectra showing blue shift and intensity change of the -NH stretching vibration band during the *gel*-to-*sol* transition upon heating. Experiment performed with peptide **C4** in toluene at the MGC (2% w/v). The T_{gel} of the material was 59 ± 2 ºC as determined by IFM. The arrows indicate the directions of motion.

Figure 6 shows a very remarkable shift observed in the region of the –NH stretching vibrational bands upon heating the gel made from the model azopeptide **C4**. The spectra of the isotropic solution ($T = 70$ ºC) displayed the characteristic –NH stretching band at 3391

cm^{-1}, which is broadened and 109 cm^{-1} blue shifted in comparison to the hydrogen-bonded gel state (T = 30 ºC). The evolution of the spectra showed a drastic change over 60 ºC, which corresponds to the T_{gel} of the material. Less dramatic lower-energy shift ($\Delta\lambda_{max}$ = 39 cm^{-1}) attributed to the amide I (80% –C=O stretching) resonance band were also observed in the gel compared to the solution phase (λ_{max} = 1643 cm^{-1}). Overlapped noise in the region 1515-1550 cm^{-1} did not allow a clear distinction between the bands associated to the amide II (60% –NH bending) resonance. Similar observations were made for other azopeptide gelators.[22] These results point out the key role of hydrogen-bonded amide groups during the formation of the 3D supramolecular gel network, besides the great stabilization effect of side-chain aromatic residues via π–π stacking interactions (this is in agreement with the poor gelation ability of control peptides such as **Z4**, *vide supra*). [31 e), 32]

Temperature-dependent ^{1}H-NMR experiments: In order to gain insight into the protons involved in the stabilization of the self-assembled network, we recorded ^{1}H-NMR spectra of different model azoPhe-based gels in d_8-toluene within a temperature range comprising both gel and solution states. Previous studies have demonstrated that the signals of gelator molecules forming part of the gel network cannot be observed due to long correlation times. Hence, any observed ^{1}H-NMR signal of a gel is a consequence of small amounts of gelator molecules, either aggregated or disaggregated, dissolved in the immobilized solvent. Thus, the increase of gelator signals upon heating is due to the enhancement of molecular mobility and dissociation of the gel network.[31 d), 33] As a model example, Figure 7 shows the chemical shift variation of the amide proton (Boc-CO-N*H*-) of **B4** upon heating the corresponding gel. In general, a gradual improvement of the signals resolution and slight chemical shift displacements were observed as the temperature increased. This observation was made at different levels for all protons.[22] Both aromatic and benzyl ester protons (PhC*H$_2$*O–) shifted upfield, practically in a linear manner, upon heating from 25 ºC (gel state) to 60 ºC (solution state) ($\Delta\delta / \Delta T \approx 6.7 \times 10^{-4}$ - 1.0×10^{-3} ppm K^{-1}). However, the most significant variations were observed for –N*H* amide protons and the closest –NH-C*H*-C*H$_2$*-R protons ($\Delta\delta / \Delta T \approx 3.5 \times 10^{-3}$ ppm K^{-1}). In these cases, downfield shift ($\Delta\delta / \Delta T \approx 7.1 \times 10^{-4}$ ppm K^{-1}) was first observed in the range 25-45 ºC, followed by a more evident upfield shift ($\Delta\delta / \Delta T \approx 2.8 \times 10^{-3}$ ppm K^{-1}) in the range 45-60 ºC. The inflection point of the curve at 318 K (44.85 ºC) matched with the T_{gel} of the material calculated by IFM (45 ºC ± 1 ºC). This behavior has been already attributed by others[34] to the existence of a different type of disassembly process during the initial heating period, and it is overall in

60

agreement with the split of hydrogen-bonding as the major driving force of the gelation process.
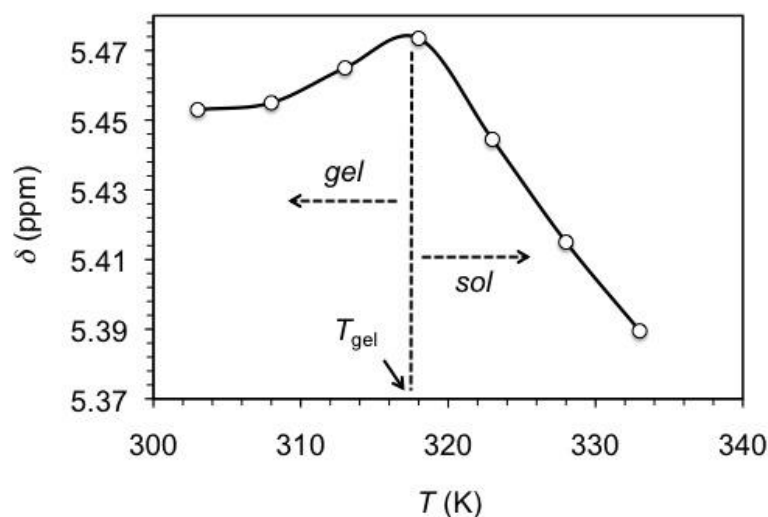
Fig. 7 Representative temperature-induced chemical shift of Boc-CO-NH- proton of **B4** in d_8-toluene (1.5% w/v). The inflection point corresponds to the T_{gel}.

Morphological characterization: In order to gain visual insights into the microscopic morphologies of the organogels, we conducted transmission electron microscopy (TEM) observations of the corresponding xerogels (Figure 8). The photographs showed characteristic fibrillar networks in all cases regardless the position of the Phe, azoPhe or bisazoPhe residue in the peptide gelator or the free or protected state of the N-terminus. Most of the fibers presented lengths on the micrometer scale and relatively uniform diameters in the range of 10-60 nm (smallest feature). Typically, the high aspect ratio of the entangled networks is a consequence of a strong anisotropic growth process, which indicates a well-ordered molecular packing to form the unit nanofiber. In general, the more densely entangled fibrous structure of some samples was in agreement with their higher thermal stability and intermolecular cohesiveness as indicated by the T_{gel} values (e.g. Figure 8 A-B: T_{gel} (**A4** in toluene) = 37 ºC; T_{gel} (**A4** in isopropanol) = 57 ºC - see ESI, Table S1-). In contrast to the materials prepared in toluene, those in isopropanol presented somehow numerous patches that made the observation of the fibers generally more difficult. No evident morphological differences were observed by TEM analysis of a given azoPhe-based gel and its analogous Phe-derived material.[22] In order to ensure that the

61

observed fibrillar structures were not artifacts, we also recorded atomic force microscopy (AFM) height images of the xerogels,[22] which were in good agreement with the TEM photographs (Figure 8 A vs. G). 3D surface topographic images showed fiber bundles and established average heights in the range of 250-350 nm for the largest individual feature (Figure 8 H).
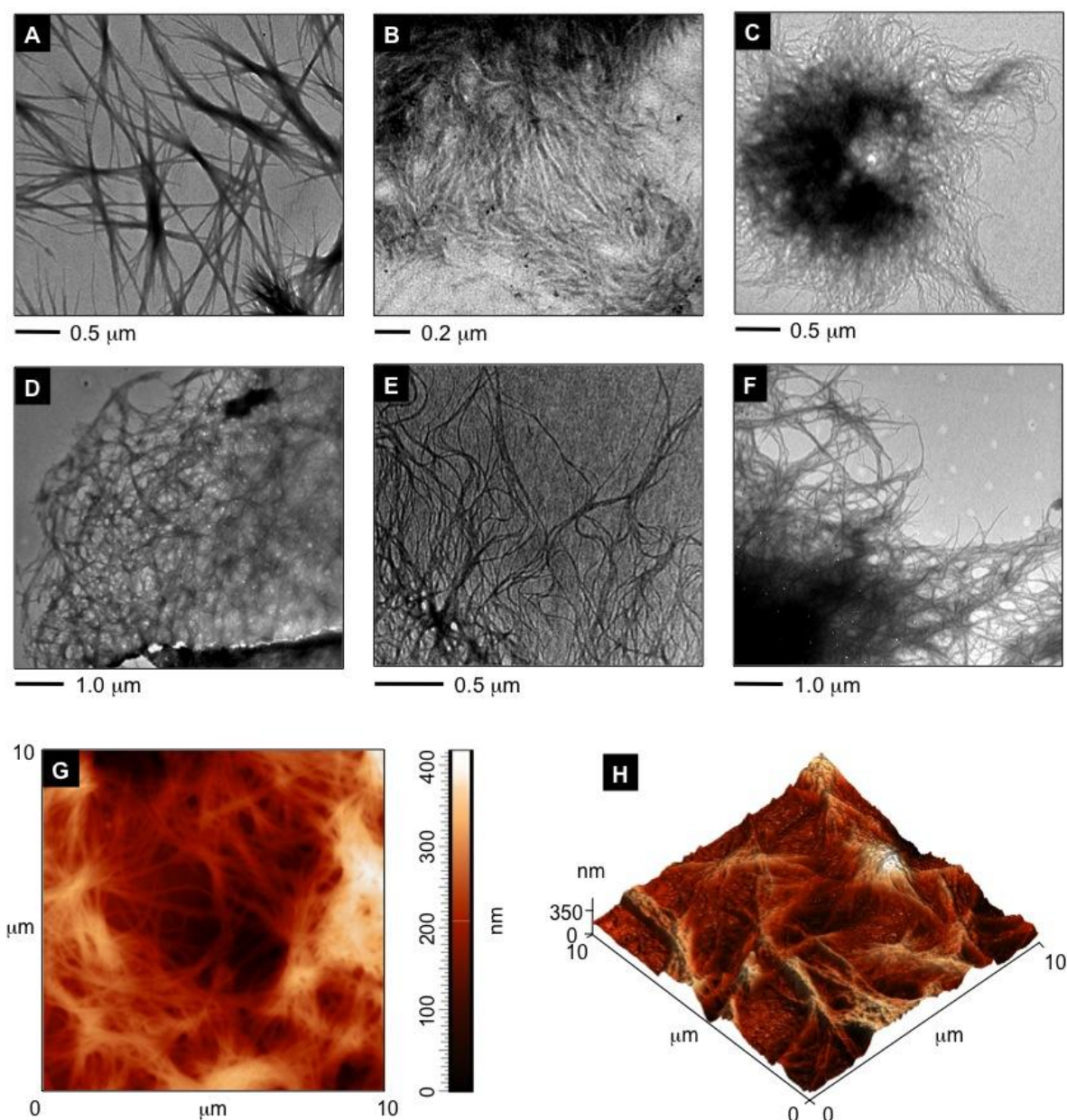
Fig. 8 Representative TEM and AFM images of xerogels obtained from the corresponding organogels prepared at their MGC as described in Table S1 (ESI). TEM: A) **A4** in toluene (2% w/v); B) **A4** in isopropanol (2% w/v); C) **C4** in toluene (2% w/v); D) **C4** in isopropanol (6% w/v), E) **D4** in toluene (4% w/v); F) **bis-A4** in toluene (0.6% w/v). AFM: G) **A4** in toluene (2% w/v); H) **B4** in toluene (1.5% w/v).

Furthermore, scanning electron microscopy (SEM) of the corresponding xerogels revealed a 3D appearance of the surface structure of the samples resembling lava flows or wrinkles in drapery (Figure 9).
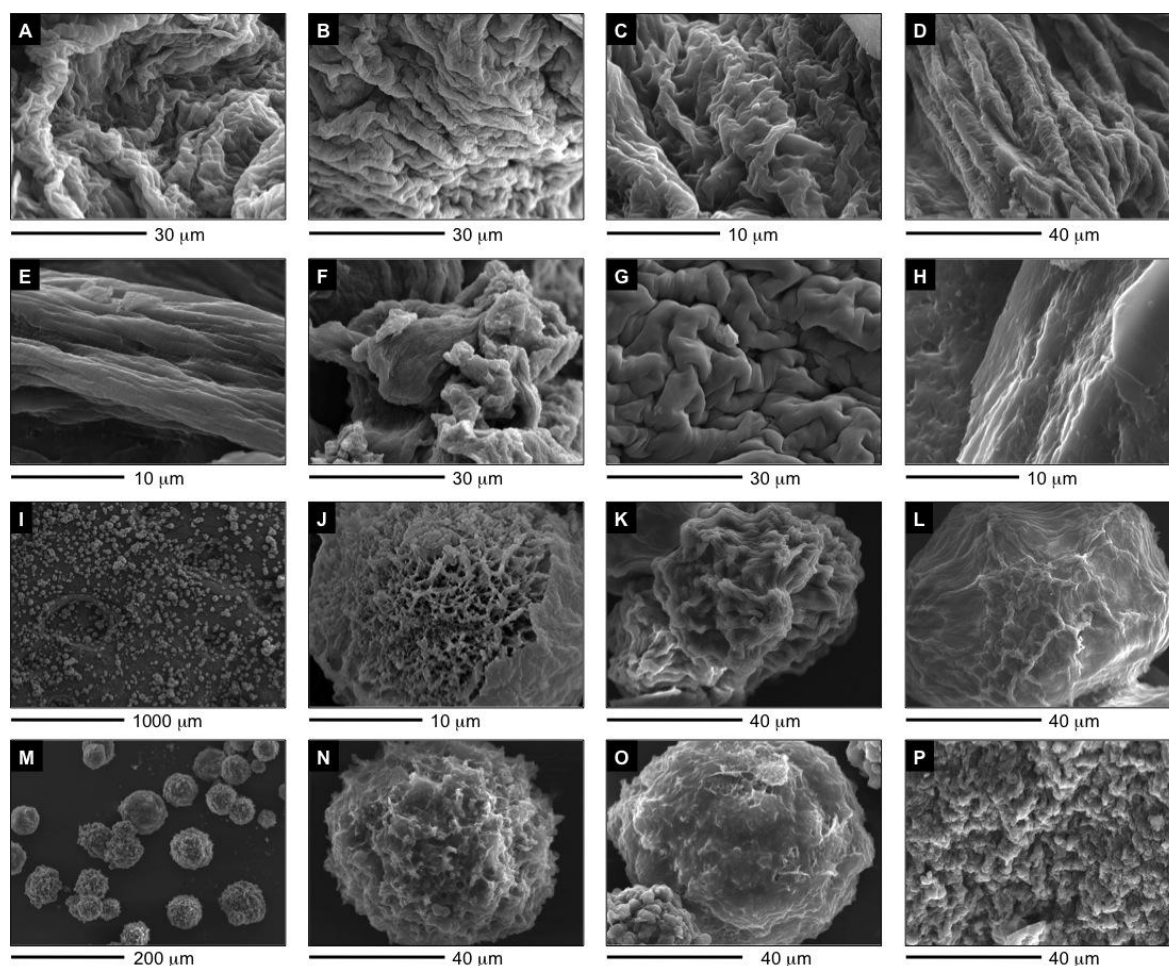
Fig. 9 Representative SEM images of xerogels obtained by freeze-drying the corresponding organogels prepared at their MGC as described in Table S1 (ESI). A: **A4** in toluene (2% w/v); B: **B4** in toluene (1.5% w/v); C: **C4** in toluene (2% w/v); D: **D4** in toluene (4% w/v); E: **D4** in toluene (4% w/v); F: **H-A4** in toluene (7% w/v); G: **F-A4** in toluene (2.5% w/v); H: **bis-A4** in toluene (0.6% w/v); I: **A4** in isopropanol (2% w/v); J: **A4** in isopropanol (2% w/v); K: **C4** in isopropanol (6% w/v); L: **C4** in isopropanol (6% w/v); M: **D4** in isopropanol (10% w/v); N: **D4** in isopropanol (10% w/v); O: **D4** in isopropanol (10% w/v); P: **bis-A4** in isopropanol (1% w/v).

It was common to observe numerous fibers fused to form large longitudinal fibrillar architectures with diameters of ca. 10-40 mm. Such morphologies were routinely observed when the gels were prepared in toluene regardless the presence of a Phe or an azoPhe

residue and its position in the peptide. However, rougher surfaces were somehow observed in the case of gels made of peptides bearing an azoPhe moiety (Figure 9A vs. 7G). Interestingly, when protic solvents such as isopropanol were used for the preparation of the gels, the SEM images showed the presence of well defined spherical structures resembling a cluster of marine sponges with diameters of ca. 35-70 mm (Figure 9I-O). At least two levels of surface roughness were observed within this globular population (Figure 9N-O). The cross-section view of one of these large structures revealed a highly interconnected porous (Ø = 30-70 mm) and fibrillar network of the inner part. Nevertheless, it should emphasized that due to the drying process such structures may not necessarily always represent those in the gel phase, and, therefore, any potential relationships should be relativized within this context. Indeed, more detailed research is still needed to explain the differences observed in morphology.

Dynamic rheological properties: Oscillatory rheological measurements unequivocally confirmed the viscoelastic gel state of the materials that did not show gravitational flow upon turning the vial upside-down.[22] Thus, their storage modulus G' (energy storage modulus) and loss modulus G'' (energy loss modulus) were first measured at room temperature as a function of angular frequency ω (dynamic frequency sweep experiment, DFS) and shear strain (dynamic strain sweep experiment, DSS) to determine the linear viscoelastic regime associated to the material (Figure 10A). Relatively constant tan d (G''/G') values during the frequency sweep indicate a good tolerance of the gels to external forces. Within the linearity limits of deformation (solid-like response), the storage modulus was always about one order of magnitude higher than the loss modulus during the flow experiment (e.g. $G' \approx 26.6 \pm 0.3$ kPa, $G'' \approx 2.4 \pm 0.01$ kPa, for the gel made of **A4** in toluene). Further dynamic time sweep (DTS) measurements at 0.1% strain and 1 Hz frequency confirmed the stability (no phase transition) of the gel materials as a function of the ageing time at room temperature (Figure 10B). In general, the tan δ values between random measurements of the same material were reproducible and increased with the concentration of the gelator, suggesting an enhancement of the mechanical damping properties. Notably enough, the replacement of the Phe unit in the **F-** series by azoPhe caused an increase of the internal resistance of the gels, as evidenced by the lower tan d value for the azobenzene-containing peptides.[22] Such reduction of tan δ was ca. 60-70% in gels prepared from azoPhe-based gelators in toluene. In isopropanol, the reduction was estimated in ca. 40%. Tan δ also increased slightly upon removal of the *N*-Boc protection

for gels prepared in toluene. Interestingly, the opposite tendency was observed for some isolated cases in isopropanol, probably due to additional non-covalent interactions established between the gelator and solvent molecules. For the case of azoPhe-peptides bearing an *N*-Boc group, increased relative elasticity of the gel network was routinely observed for the gels prepared in toluene when compared to those in isopropanol. The influence of the position occupied by the Phe or azoPhe residue within the peptide sequence on the mechanical damping properties of the materials was found to be irrelevant except for the **D** gelators. Thus, a slight increase in tan δ was observed for both **D4** and **F-D4**.[22]
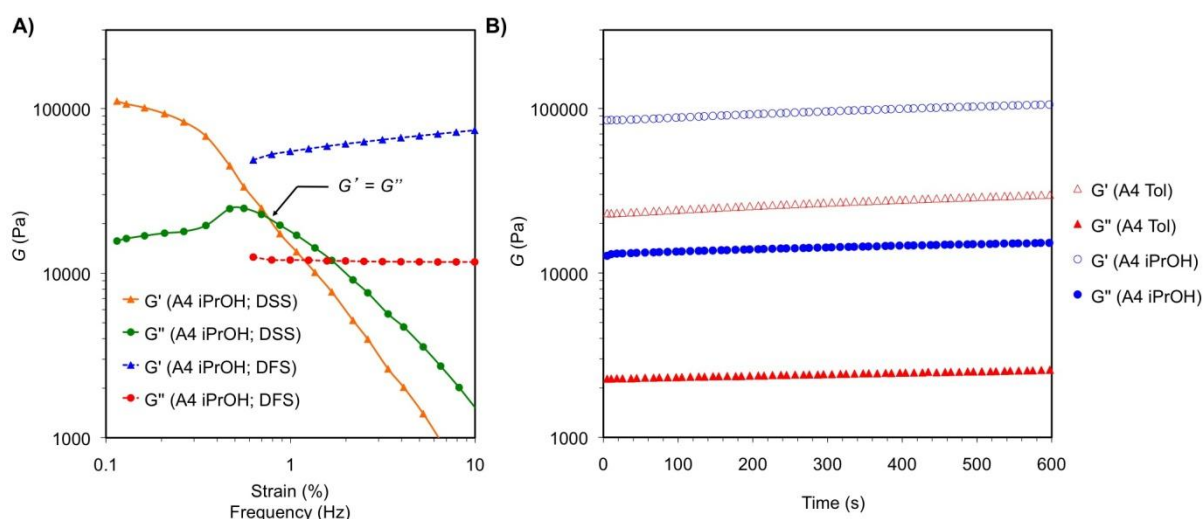
Fig. 10 Oscillatory rheological measurements of model gels: A) Representative DSS and DFS experiments of the gel made from A4 in isopropanol (2% w/v). B) Representative DTS experiments of gels prepared from A4 in toluene or isopropanol (2% w/v). All gels were prepared at their MGC as indicated in Table S1 (ESI). Tol = toluene.

Remarkably, we also found a smart thixotropic response of all azoPhe-based gels to external large straining. The phenomenon of thixotropy was properly described for the first time by Peterfi in 1927[35] and, nowadays, it is considered a key property for real-life applications of gel-based materials.[36] Figure 11 shows a simple thixotropy three-step rheological loop test[37] for the organogel made of D4 in toluene (3.8% w/v). The experiment is based on successive cycles involving the following steps: 1) application of a

shear strain as defined by DTS experiments (gel state, $G' > G''$), 2) increase of the shear strain until the gel fractures (viscous solution, $G' < G''$) and 3) return at the same rate to the initial strain % value (recovered gel state, $G' > G''$).[22] In the model example shown in Figure 11, the gel displayed more than 90% recovery in its G' value in only 5 seconds after the second cycle. Moreover, a similar behavior was observed in other solvents like isopropanol (the recovery of the initial G' value was ca. 85%) and regardless the method of preparation (i.e. heating-cooling, ultrasound). The dramatic loss of viscosity and recovery of the gel state were also macroscopically observed in a standard glass vial upon a vigorous shaking-resting process.
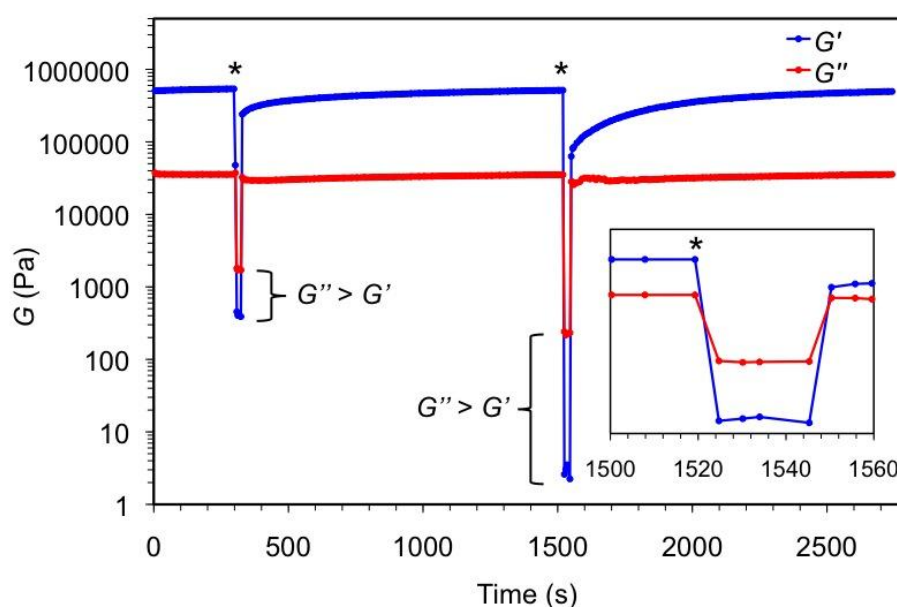
Fig. 11 Typical thixotropy loop test of the model gel made from D4 in toluene (3.8% w/v). The strain for each step during shear was first increased from 0.1% (linear viscoelastic regime - gel state -) to 100% (rupture of the gel - solution state -) and subsequently returned to the original value (recovery of the gel state). Asterisks indicate the increase of the shear strain at the time scale.

Responsiveness to light: The expected *trans*-to-*cis* photoisomerisation was observed in solution for all peptides containing azoPhe or bisazoPhe upon irradiation with UV light at room temperature. Moreover, light-induced reversible *gel*-to-*sol* transition was achieved for all azoPhe-based peptides exhibiting a free amino terminus upon exposure of the gel material to the appropriate wavelength. An appropriate experimental set up ruled out any temperature effect on *gel*-to-*sol* transition caused by the irradiation process.[22] As shown in

Figure 12 for **H-C4** as a model example, UV irradiation at λ_{max} = 366 nm of the gel made in toluene resulted in photoisomerization of the side-chain azobenzene moiety from the *trans* to the *cis* state, as indicated by the gradual decrease of the π-π^* transition band at 328 nm and concomitant increase of the n-π^* transition centered at λ_{max} = 439 nm. Such *trans*-to-*cis* photoisomerization led to a *gel*-to-*sol* transition of the material after 10 min of UV irradiation.
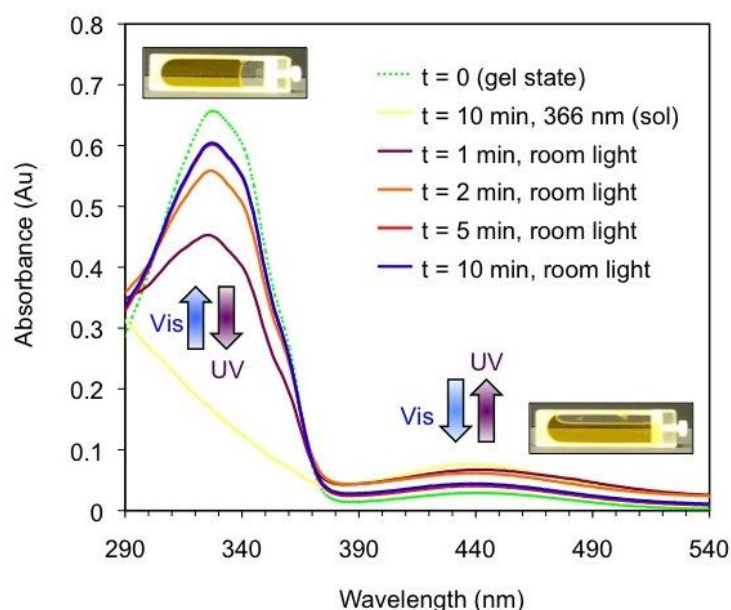
Fig. 12 Reversible changes in the UV-vis absorption spectra of the gel made from **H-C4** in toluene (2.5 % w/v; 0.1 mm path length). The transition from the *trans*-rich gel state to the *cis*-rich solution state was induced by UV irradiation at 366 nm for 10 min. The *sol*-to-*gel* transition was further achieved by exposure of the cuvette to ambient visible light. The arrows indicate the directions of motion. Original gel state (t = 0); solution state upon 10 min irradiation at 366 nm (t = 10 min, 366 nm); progressive solution-to-gel phase transition under visible light (t = 1, 2, 5, 10 min, room light).

Moreover, *cis*-to-*trans* back isomerization of the azobenzene unit also took place upon exposure of the cuvette to room light. These reversible transitions could be repeated for several cycles. These results indicate that the isomerization toward the *trans*-form of the azobenzene residue is gradually hindered by the growth of the supramolecular fibrillar network. The final content of the *trans*-isomer after irradiation was estimated by integrating the difference of the curves in ca. 15-20% of the original content in the gel state. Despite the fast *trans*-to-*cis* and *cis*-to-*trans* isomerization processes, the complete

67

gel-to-*sol* and *sol*-to-*gel* transitions, respectively, required prolonged exposure times to light of appropriate wavelength. Thus, complete macroscopic *gel*-to-*sol* transition in toluene was observed within 30-60 min of UV irradiation, whereas complete *sol*-to-*gel* was achieved after exposing the material to visible light for 3-8 h.[22] The absolute values are specific for each case as the time required for isomerization is both solvent and concentration dependent (e.g. the response times of gels made in isopropanol were found to be longer than those in toluene).[22] The isosbestic points of the solution and gel states are centered at 290 and 378 nm, where the absorbance values differ in ca. 0.03 ± 0.01 (Au) with respect to the intermediate states achieved during irradiation. As these values are within the standard deviation of absorbance for replicate measurements, only two absorbing species (i.e. *trans-* and *cis-* azobenzene-containing molecules) are likely to be involved during the light-induced *gel* $\Leftrightarrow$ *sol* transition. The absorption corresponding to the π-π^* transition band exhibited a narrow 3 nm red-shift in the gel state with respect to the solution state (i.e. 1 min after exposure to room light), which based on the exciton theory suggests that azobenzene groups likely packed into 1D J-aggregates instead of H-aggregates.[38, 39] Remarkably, light-induced *gel*-to-*sol* transition was only observed for azobenzene-based organogels lacking the *N*-Boc protection. In general, this process was also faster in aromatic solvents than in alcohols. In agreement with previous studies in other systems,[13] this may be due to some sterically hindered spatial conformation of the aggregates that prevents the *trans*-to-*cis* isomerization of the azoPhe moiety when the *N*-Boc protection is present.

Multiresponsive map: Figure 13 summarizes the study carried out with the model peptide **H-D4**, which is insoluble in toluene at room temperature (2.5% w/v) (A). An isotropic solution could be achieved upon heating (B), which led to the thermoreversible formation of a stable organogel upon cooling (C). Vigorous shaking of the vial afforded a viscous fluid state (H), which returned to the precedent gel state upon resting (thixotropy). Ultrasound could be also used to dissolve **H-D4** and generate a dense fibrillar gel material (E), which was also liquefied upon heating affording a clear solution (F). Solutions F and B were found to be equivalent according to both thermal and mechanical properties of the corresponding gels (C, G). Additionally, the existence of a free amino terminus in the peptide gelator allowed for a light-induced *gel*-to-*sol* transition (I), which was reversible (C). High-resolution FE-SEM images demonstrated the complete destruction of the fibrillar network upon UV-irradiation (K, L vs. M), as well as the general preservation of

the gel morphology for materials prepared either by thermal or ultrasound treatment (K vs. L).
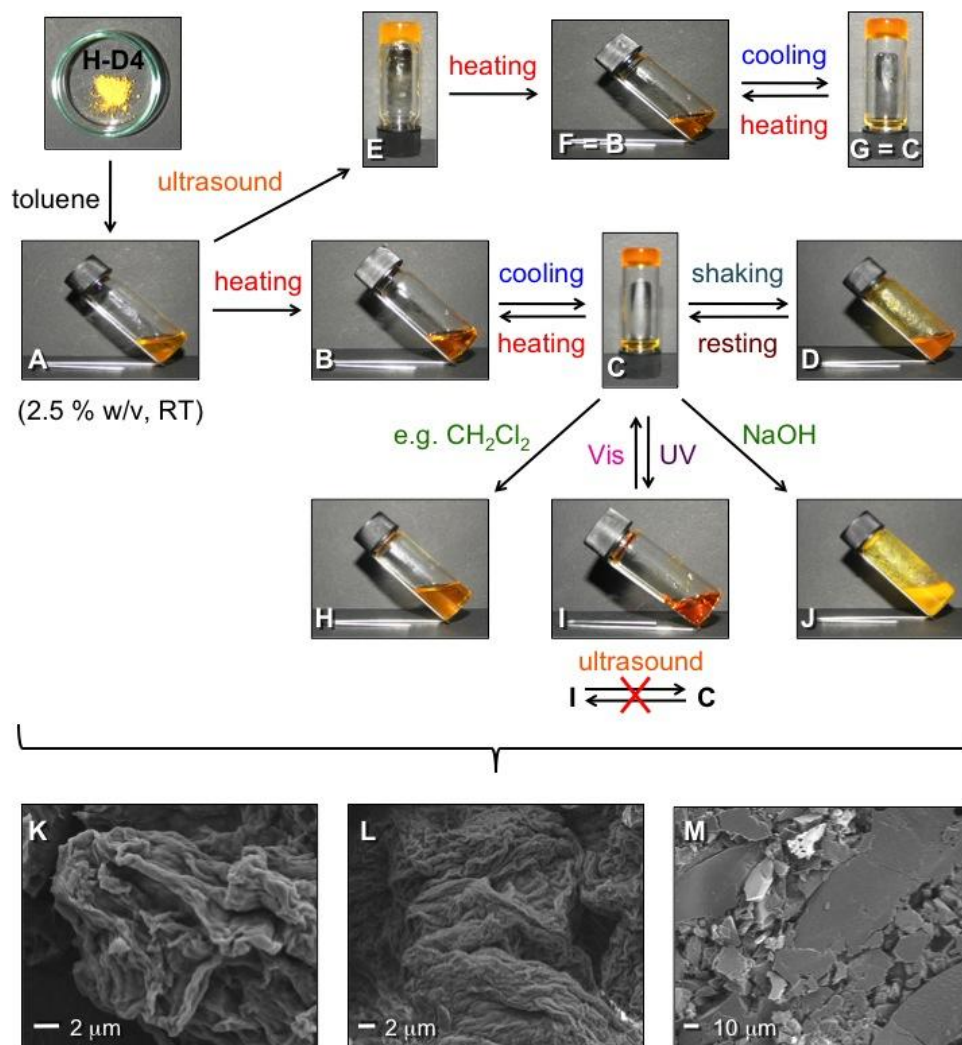
Fig. 13 Diagram showing the preparation of multistimuli responsive organogels from the azoPhe-containing peptide **H-D4** and the interrelated response between different materials. T_{gel} values: E = 47 ± 1 ºC; C = 50 ± 1 ºC; G = 49 ± 2 ºC. Tan *d* values: E = 0.47; C = 0.41; G = 0.42. Gelation times: A → E = 2-3 min; B → C = 5-10 min; F → G = 5-10 min; I → C = 10-12 h. Liquefaction times: C → I = 45-60 min; C → D = 20-30 min; C → J = 10-30 min. Selected FE-SEM images are shown at the bottom: K: gels prepared by heating-cooling (G' = 1.78 × 10^5 Pa; tan *d* = 0.42); L: gel prepared by ultrasound treatment (G' = 1.21 × 10^5 Pa, tan *d* = 0.49); M: solution obtained upon UV-irradiation of gel K.

On the other hand, transition from I to C was not assisted by ultrasound within minutes under visible light, as occurs for the A → E transformation. Hence, ultrasound treatment of

peptide solution does not accelerate the *cis*-to-*trans* isomerization of the azobenzene group. Responsiveness to chemical stimuli was also observed (H, J). This behavior, exemplified in Figure 13 for **H-D4**, was general for all the organogels prepared regardless the gelator family and solvent. Thus, addition of some solvents in which gelation did not take place led to the formation of clear solutions. For instance, when the gels made of **C4**, **H-D4** or **F-A4** or **H-D4** were overlaid with tetrahydrofuran, 1,4-dioxane or dichloromethane (gel volume : additional solvent volume = 1:1), they were dissolved within 20-30 min without shaking. In contrast, the gels were stable for several days in the presence of solvents like pentane. Moreover, the gels were transformed into either solutions or dispersions upon gentle shaking in the presence of 0.1 M aqueous NaOH within 10-30 min.[22] Solvent evaporation (B-I) and drying of the residue under vacuum allowed full recovering of **H-D4**, which could be reused without losing its properties. In addition, the structural anisotropies of the organogels observed by electron microscopy switched on their birefringence under polarized light,[22] which could be also switched off upon *gel*-to-*sol* transition. Such fine birefringence control is important for a number of optical device applications.[40]

1.3. Conclusion

The foregoing results have showed that the incorporation of azobenzene residues into the side-chain of LMW peptides can modulate their self-assembly in organic solvents leading to the formation of stimuli responsive supramolecular organogels. The synthetic strategy is advantageous in terms of structural flexibility since it is compatible with a free, unprotected amino terminus and allows placement of the chromophore at any position of the peptide sequence. The major driving forces for the observed gelation process are hydrogen-bonding and π–π interactions, which can be triggered either by thermal or ultrasound external stimuli. In addition, a predictive model for gelation of polar protic solvent was developed using Kamlet-Taft solvent parameters and experimental data. Remarkably, the obtained viscoelastic materials exhibited interconnected multistimuli responsive behaviors including thermal-, photo-, chemo- and mechanical responses. Structure-property relationship studies have demonstrated that the presence and position of the azobenzene residue can be operated as a versatile regulator to reduce MGC and

enhance both the thermal stability and mechanical strength of the gels. To the best of our knowledge, this is the first time in which LMW peptides bearing side-chain azobenzene units are used for the synthesis of 'intelligent' supramolecular organogels. This investigation opens new perspectives for the rational design of tunable multiresponsive physical gels from small peptides. Efforts towards potential applications of the described materials, as well as structural and charge modifications of the peptides in order to expand the scope to biocompatible hydrogels are currently underway in our laboratories.

1.4. Addendum: Phase selective gelation behavior for oil-spill recovery

Recent years have witnessed plenty natural disasters of environmental water-pollution originated from oil-spills. The major concerns arising from such events are based on the environmental impacts of volatile hydrocarbons on climate changes and the effects of toxic oil residues on the marine ecosystem.[41] Amongst other types of materials,[42] phase selective organogelators (PSOGs), that can selectively congeal the oil-phase from two-phase systems of water and oil, represent a promising alternative for oil-spill recovery.[43]
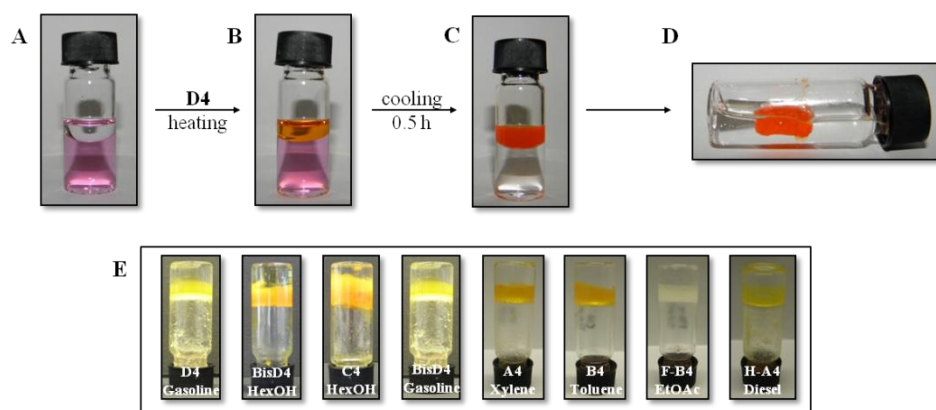
Fig. 14 Representative digital photographs demonstrating the procedure applied to induce of PSG using compound **D4** and a biphasic system consisting of water and toluene (2:1 (v/v)). The aqueous phase has been stained with a dye (ruthenium red) for better visualization of the two-phase nature. (A) Two phase mixture of toluene and water before the gelator is added. (B) Two-component liquid system prepared by adding **D4** (4.0 % w/v) and gentle heating. (C) Selective gelation of the toluene layer accompanied by complete removal of the dye from the aqueous phase. (D) Floating gel-body after mechanical agitation to remove the former from the walls of the vial. (E) Additional digital photographs of upside-down vials containing materials prepared by PSG. The concentration of gelator applied is the corresponding MGC as indicated in Table 1.

In this context we are delighted to report the discovery of selective and quantitative gelation of the organic phase of various aqueous-oil mixtures caused by the peptide-based gelators we described earlier.[44] Adding any of the gelator compounds (except from control compounds **Z4** and **H-Z4**) to a 2:1 mixture of water and a non water-miscible organic phase and applying a classical heating-cooling protocol resulted in the selective gelation of the organic layer (view Figure 14). It was found that compounds can be grouped together due to very similar behavior of the physical properties of the gels and hence model compounds for each group have been selected. **A4** is used as representative for all azo-containing compounds with Boc-protected or free *N*-terminus, **bis-A4** represents all compounds of the bis-series and **F-A4** represents all Phe-based peptides. Very interestingly, the presence of the side-chain azo moiety in the gelator structure (also compounds of the bis-series) allowed to achieve phase selective gelation (PSG) at the same concentration as the described MGC for pure organic phase (POP). In contrast, the use of Phe-based gelators required an approximate 1.5-fold increased concentration making the azo-containing compounds more favorable for the application in PSG. Additionally, the presence of water during PSG seems to have no significant negative effect on the thermal, mechanical and morphological properties of gels based on azo-containing compounds as determined by T_{gel}, dynamic rheological measurements and electron microscopy (SEM, TEM) (view Table 1 and Figure 15). We also investigated potential PSG of water-soluble organic solvents like MeCN, EtOH and *i*-PrOH where gelation of POP was observed before. Very interestingly we found gelation of the whole water-organic solvent mixture to result in the formation of quasi-hydrogels with a total content of organic phase being 33% (v/v) in combination with a change in morphologies of the materials (view Figure 15 (D)). In the presence of water gelation at very low concentrations in comparison to POP can be observed (0.7 %w/v and 2.0 %w/v using *i*-PrOH as organic phase), which gives rise for further investigation in optimization of the total content of the organic phase for potential application in controlled drug-release. Unfortunately the heating-cooling method for inducing PSG is very impractical for the removal of oil-spills due to the flammability of most oil-phases. Taking advantage of our previous observation of ultrasound-induced gelation we were able to successfully transfer this concept to PSG. Further investigations on RT-induced PSG lead to the development, that adding concentrated (20-40 %w/v) warm solutions of the gelators in an oil-phase to a mixture of the same oil and water

resulted in effective PSG at the same MGC as determined for POP and PSG induced by a classical heating-cooling treatment (view Table 2).
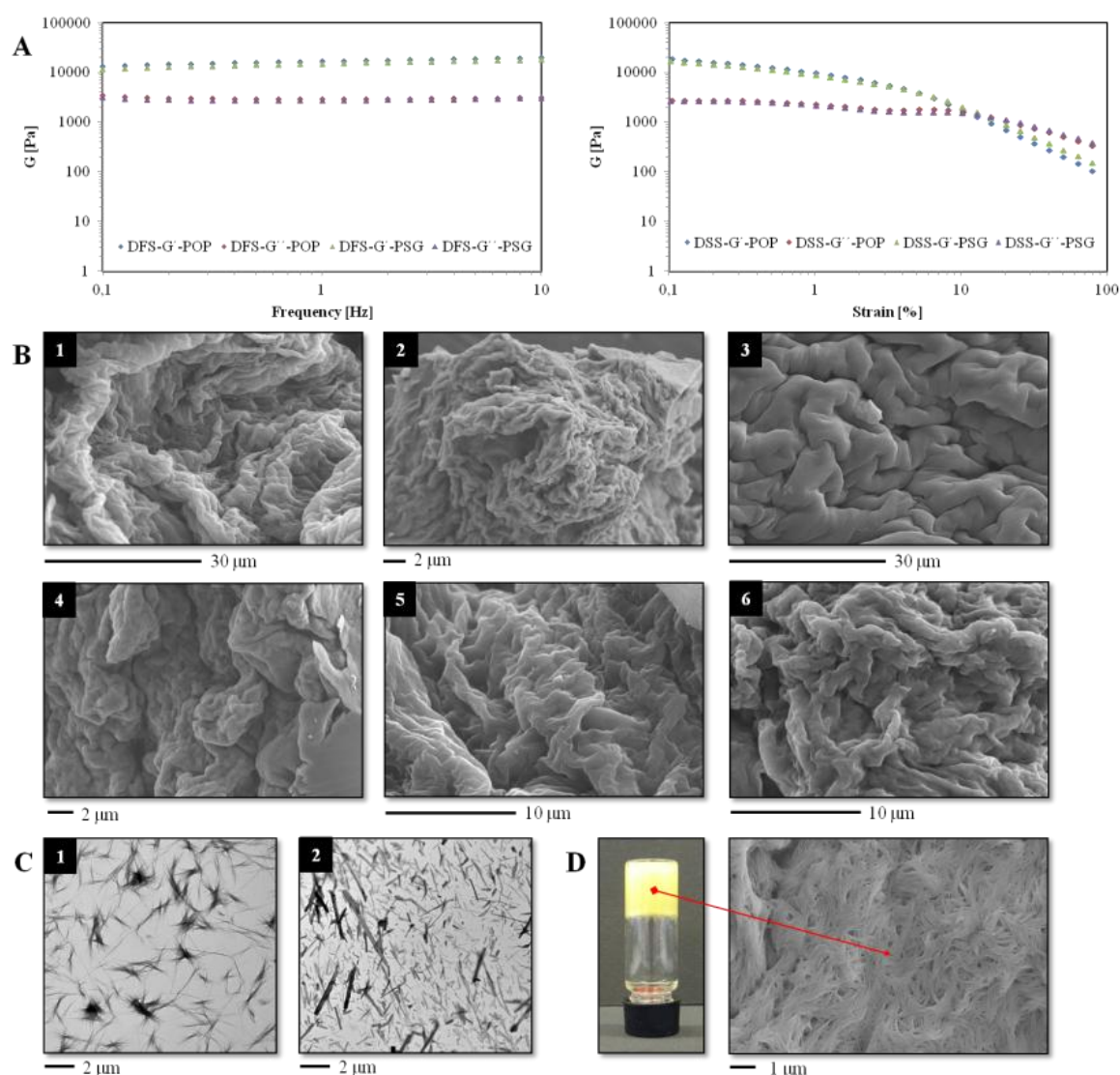
Fig. 15 (A) Dynamic oscillatory rheology experiments (DFS and DSS) of gels from A4 in toluene (2.0 %w/v) prepared from POP and PSG respectively. Absolute values of G' (16.5±1.97 and 14.7±1.89 kPa) and G'' (3.0±0.12 and 2.8±0.11 kPa), as well as tan δ (0.18±0.0028 and 0.19±0.0019) and maximum strain at break (16±2.0 and 13±1.5 %) stay the same within the limits of error independent on the material. (B) SEM-images of cryogels prepared by the freeze-drying method of corresponding gel-materials at the MGC: (1) **A4** in toluene (POP); (2) **A4** in toluene (PSG); (3) **F-A4** in toluene (POP); (4) **F-A4** in toluene (PSG); (5) **bis-A4** in toluene (POP); (6) **bis-A4** in toluene (PSG). (C) TEM-images of cryogels prepared by the freeze-drying method of corresponding gel-materials at the MGC: (1) **A4** in toluene (POP); (2) **A4** in toluene (PSG). (D) Kind of hydrogel from *i*-PrOH-water mixture (1:2) using **A4** (0.7 %w/v) and FE-SEM image of the isolated cryogel.

Multistimuli responsive supramolecular organogels formed by low-molecular-weight peptides bearing side-chain azobenzene moieties

Tab. 1 Comparing physical properties of PSG and gels derived from pure organic phases. [a]

Entry	Solvent	Gelator	MGC [% w/v]		T_{gel} [°C] [b]	
			POP	PSG	POP	PSG
1	2-BuOH	**A4**	2.8 (0.3)	3.0 (0.4)	55 (1)	54 (2)
2	BMIM·PF$_6$	**A4**	4.0 (0.3)	4.0 (0.3)	78 (2)	76 (1)
3	Toluene	**A4**	1.9 (0.2)	2.0 (0.2)	37 (2)	39 (1)
4	Xylene	**A4**	7.0 (0.5)	7.0 (0.5)	59 (1)	62 (2)
5	Olive Oil	**A4**	1.3 (0.2)	1.5 (0.2)	93 (2)	89 (1)
6	Gasoline	**A4**	2.2 (0.2)	2.4 (0.2)	52 (2)	53 (2)
7	Diesel	**A4**	2.0 (0.2)	2.0 (0.2)	62 (1)	61 (1)
8	2-BuOH	**F-A4**	10.0 (1.0)	13.0 (1.5)	57 (1)	52 (2)
9	BMIM·PF$_6$	**F-A4**	-	-	-	-
10	Toluene	**F-A4**	2.5 (0.3)	4.0 (0.3)	35 (1)	44 (1)
11	Xylene	**F-A4**	2.0 (0.2)	3.2 (0.3)	37 (1)	36 (2)
12	Olive Oil	**F-A4**	2.0 (0.2)	2.8 (0.3)	72 (2)	71 (1)
13	Gasoline	**F-A4**	3.3 (0.3)	4.5 (0.5)	54 (2)	57 (2)
14	Diesel	**F-A4**	1.8 (0.2)	2.4 (0.2)	56 (2)	54 (1)
15	2-BuOH	**bis-A4**	0.8 (0.1)	1.0 (0.1)	62 (2)	63 (1)
16	BMIM·PF$_6$	**bis-A4**	2.2 (0.2)	2.2 (0.2)	69 (1)	68 (2)
17	Toluene	**bis-A4**	0.6 (0.1)	0.5 (0.1)	70 (1)	70 (2)
18	Xylene	**bis-A4**	3.3 (0.2)	3.5 (0.3)	76 (2)	74 (2)
19	Olive Oil	**bis-A4**	0.5 (0.1)	0.5 (0.1)	104 (2)	101 (2)
20	Gasoline	**bis-A4**	2.5 (0.2)	2.5 (0.2)	56 (1)	55 (2)
21	Diesel	**bis-A4**	1.8 (0.2)	2.0 (0.2)	59 (2)	61 (1)

[a] Values in brackets indicate experimental errors from at least two random measurements. Abbreviations: PSG = phase selective gelation; POP = pure organic phase; MGC = minimum gelation concentration; T_{gel} = thermal gel-to-sol transition temperature. [b] T_{gel}-values have been determined using the "inverse-flow-method" (IFM). [45]

Tab. 2 Comparison of the MGC necessary to induce PSG for different methods in some oil-phases. [a]

Entry	Solvent	Gelator	MGC [% w/v]			
			POP	PSG (H-C)	PSG (US)	PSG (CSM)
1	Toluene	**A4**	1.9 (0.2)	2.0 (0.2)	2.0 (0.2)	2.0 (0.2)
2	Gasoline	**A4**	2.2 (0.2)	2.4 (0.2)	2.4 (0.2)	2.4 (0.2)
3	Diesel	**A4**	2.0 (0.2)	2.0 (0.2)	2.0 (0.2)	2.0 (0.2)
4	Toluene	**bis-A4**	0.6 (0.1)	0.5 (0.1)	0.5 (0.1)	0.5 (0.1)
5	Gasoline	**bis-A4**	2.5 (0.2)	2.5 (0.2)	2.5 (0.2)	2.5 (0.2)
6	Diesel	**bis-A4**	1.8 (0.2)	2.0 (0.2)	2.0 (0.2)	2.0 (0.2)

[a] Values in brackets indicate experimental errors from at least two random measurements. Abbreviations: PSG = phase selective gelation; POP = pure organic phase; MGC = minimum gelation concentration; H-C = heating cooling method; US = ultrasound induced method; CSM = inducing PSG by adding a concentrated solution of the corresponding gelator in an oil-phase to the water-oil mixtures.

These findings result in a much more practical situation of the azobenzene modified peptides in the recovery of oil-spills as usually other types of gelators have to be predissolved in water-soluble cosolvents, which can be of potential toxic nature and hence can exhibit negative influence on the marine eco-system.[43 a), b)] The complete removal of the oil-phase from water-oil mixtures was ensured by ^{1}H-NMR-spectroscopy using D_2O as aqueous phase containing DMF (0.1 mmol) as internal standard. No indication of signals referring to toluene or xylene could be found in the corresponding NMR-spectra as indicated in Figure 16 when compound **A4** (2.0 %w/v and 7.0 %w/v) was used in PSG induced by the classical heating-cooling method. Additionally also only little indication for the presence of non-gelled gelator **A4** (below 2% of the initially applied concentration) in the aqueous phase was found. The excellent properties of azobenzene containing peptides in PSG made us curious to know whether the compounds can be applied for natural oil-spill recovery. A comparison of MGC for the induction of PSG for some specific oil-water mixtures with fresh water, 3.3 % NaCl and river water (from the Donau in Regensburg) revealed that the gelation-efficiency is the same for all these biphasic systems (view Table 3). Interestingly the presence of NaCl or impurities in river water did not affect the gelation-ability.
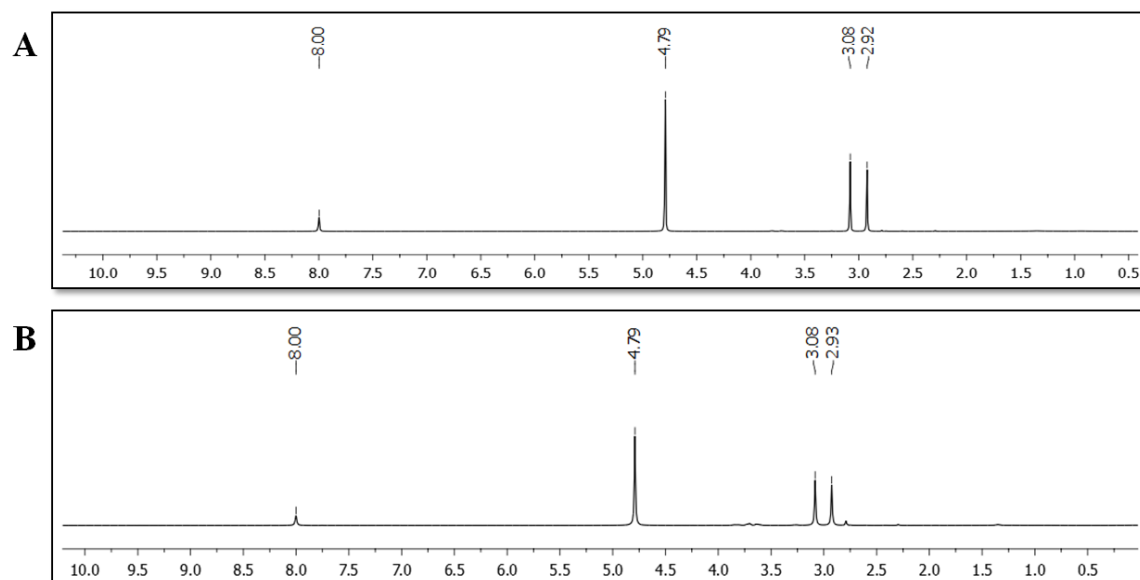
Fig. 16 ^{1}H-NMR spectra of D_2O containing DMF (0.1 mmol) as internal standard when compound **A4** was used in experiments to induce PSG by the heating-cooling method. (A) A D_2O-toluene mixture (2:1 v/v) was used with a concentration of **A4** being 2.0 %w/v. (B) A D_2O-toluene mixture (2:1 v/v) was used with a concentration of **A4** being 7.0 %w/v.

Tab. 3 Comparison of MGC necessary to induce PSG for different aqueous phases for some model cases. [a]

Entry	Solvent	Gelator	MGC [% w/v]		
			pure water	3.3 % NaCl	river water
1	Toluene	**A4**	2.0 (0.2)	2.0 (0.2)	2.0 (0.2)
2	Gasoline	**A4**	2.4 (0.2)	2.4 (0.2)	2.4 (0.2)
3	Diesel	**A4**	2.0 (0.2)	2.0 (0.2)	2.0 (0.2)
4	Toluene	**bis-A4**	0.5 (0.1)	0.5 (0.1)	0.5 (0.1)
5	Gasoline	**bis-A4**	2.5 (0.2)	2.5 (0.2)	2.5 (0.2)
6	Diesel	**bis-A4**	2.0 (0.2)	2.0 (0.2)	2.0 (0.2)

[a] Values in brackets indicate experimental errors from at least two random measurements. The heating-cooling method to induce PSG was applied.

In order to illustrate the potential application in oil-spill recovery, a model scenario was set up as demonstrated in Figure 17 by adding toluene (5 mL) to a compared large volume of aqueous 3.3 % NaCl-solution (40 mL). The aqueous layer was stained with $CuSO_4$ for

better visualization of the two-phase nature of the mixture. The toluene-layer could be effectively gelled by adding a warm and concentrate solution of compound **A4** (27.5 %w/v) in toluene in a small volume (0.4 mL) resulting in a concentration of the gelator of 2.0 %w/v in the overall toluene-phase. The resulting gel-phase can be easily separated by filtration, melted by heating and destilled to recover about 82 % of the toluene by volume. This experiment can also be repeated using other oil phases like gasoline and Diesel with similar results for the recovery of the oils (80 and 76 % respectively). The relative high mechanical strength of the gel-materials as demonstrated in Figure 15 (A) in combination with a high temporal stability (inverted vials containing PSG can keep the weight of the aqueous phase for at least 2 month while remaining stable) make them very interesting alternative for the application in oil spill recovery.
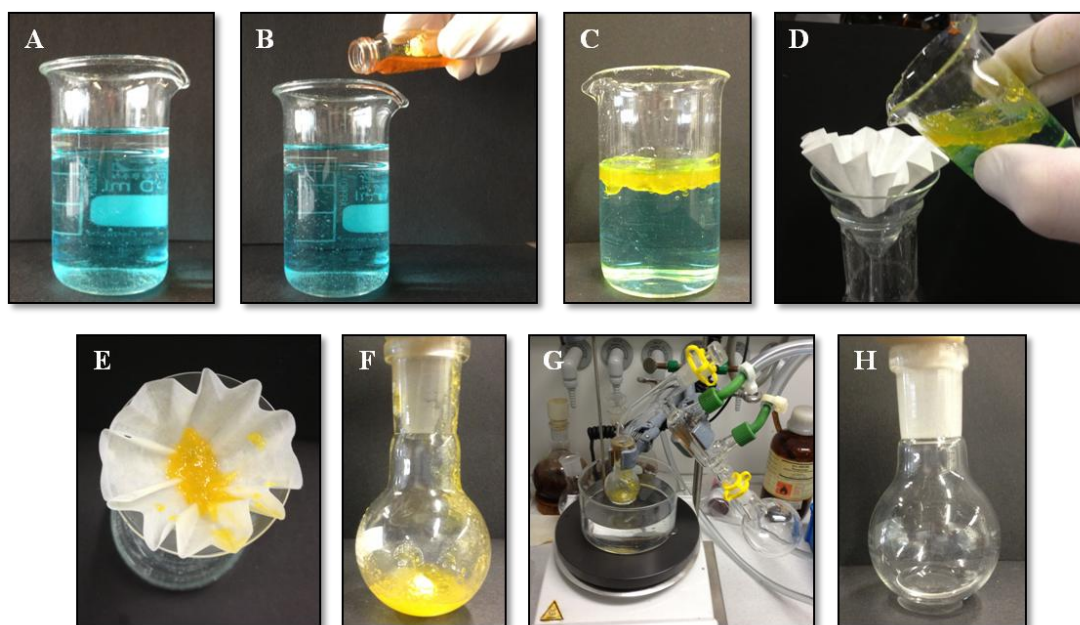
Fig. 17 Model scenario for oil-spill recovery using PSG properties of azo-containing peptides. Compound **A4** (2.0 %w/v) was used as a model. (A) Biphasic mixture of toluene (5 mL) and aqueous 3.3 % NaCl (40 mL) stained with $CuSO_4$. (B) Addition of a warm and concentrate solution of compound **A4** in toluene (27.5 %w/v; 0.4 mL). (C) Complete PSG of the toluene layer at a concentration of 2.0 %w/v of the gelator with respect to the overall volume of the oil-phase. (D-G) Separation of the oil-phase by filtration and subsequent distillation. (H) Recovered toluene after distillation (82 % in volume).

Taking advantage of such a PSG property we were additionally able to use these peptide gelators to quantitatively remove water-soluble dyes[46] (e.g. ruthenium red, crystal violet)

from aqueous mixtures within minutes, which constitutes a subject for further investigation (view Figure 18). In a model example compound **bis-D4** (1.0 %w/v) was able to remove crystal violet (1.0×10^{-5} molL^{-1}) from an aqueous solution using a toluene-water biphasic system within 15 min.
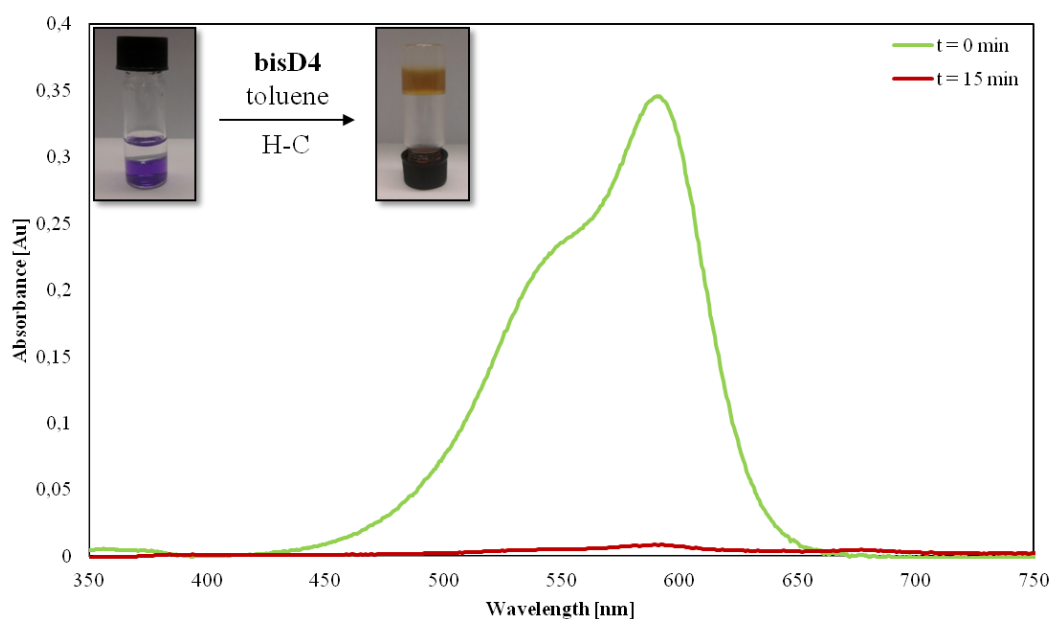
Fig. 18 Absorption spectra of crystal violet (1.0×10^{-5} molL^{-1}; t = 0) in water and of the aqueous phase after PSG using **bis-D4** (1.0 %w/v) in toluene (water:toluene = 2:1 v/v; t = 15 min). H-C = heating-cooling.

→ Compound synthesis and characterization, general remarks on gel-formation and preparation, additional photographs and gel-characterization and a collection of ^{1}H and ^{13}C-spectra of the synthesized compounds can be found in the electronic supplementary information (ESI) on the enclosed CD.

1.5. References

[1] a) P. Bawa, V. Pillay, Y. E. Choonara and L. C. du Toit, *Biomed. Mater.*, 2009, **4**, 22001-22016; b) M. A. C. Stuart, W. T. S. Huck, J. Genzer, M. Müller, C. Ober, M. Stamm, G. B. Sukhorukov, I. Szleifer, V. V. Tsukruk, M. Urban, F. Winnik, S. Zauscher, I. Luzinov and S. Minko, *Nature Mater.*, 2010, **9**, 101-113; c) M. W. Urban, *Handbook of Stimuli-Responsive Materials*, Wiley-VCH, Weinheim, 2011.

[2] a) X. Y. Liu, *Top Curr. Chem.*, 2005, **256**, 1-37; b) R. G. Weiss, P. Terech, *Molecular Gels: Materials with Self-Assembled Fibrillar Networks*; Springer: New York, 2006; c) M. George, R. G. Weiss, *Acc. Chem. Res.*, 2006, **39**, 489-497; d) G. C. Maity, *J. Phys. Sci.,* 2007*,* **11**, 156-171; e) S. Banerjee, R. K. Das, U. Maitra, *J. Mater. Chem.,* 2009, **19**, 6649-6687.

[3] a) D. Derossi, Y. Kajiwara and Y. Osada, *Polymer Gels: Fundamentals and Biomedical Applications*, Plenum Press, New York, 1991, and references therein; b) J. H. Jung and S. Shinkai, *Top. Curr. Chem.,* 2004, **248**, 223-260; c) N. M. Sangeetha and U. Maitra, *Chem. Soc. Rev.,* 2005, **34**, 821-836; d) R. V. Ulijn and A. M. Smith, *Chem. Soc. Rev.,* 2008, **37**, 664-675; e) A. R. Hirst, B. Escuder, J. F. Miravet and D. K. Smith, *Angew. Chem. Int. Ed.,* 2008, **47**, 8002-8018; f) M. O. M. Piepenbrock, G. O. Lloyd, N. Clarke and J. W. Steed, *Chem. Rev.,* 2010, **110**, 1960-2004; g) D. D. Diaz, D. Kühbeck and R. J. Koopmans, *Chem. Soc. Rev.*, 2011, **40**, 427-448.

[4] a) J. H. van Esch and B. L. Feringa, *Angew. Chem.*, 2000, **112**, 2351-2354; *Angew. Chem. Int. Ed.*, 2000, **39**, 2263-2266, and references therein; b) F. M. Menger and K. L. Caran, *J. Am. Chem. Soc.*, 2000, **122**, 11679-11691; c) O. Gronwald, E. Snip and S. Shinkai, *Curr. Opin. Colloid Interface Sci.*, 2002, **7**, 148-156; d) M. de Loos, B. L. Feringa and J. H. van Esch, *Eur. J. Org. Chem.*, 2005, 3615-3631; e) E. Zaccarelli, *J. Phys. Condens. Matter*, 2007, **19**, 323101.

[5] a) T. Tanaka, *Sci. Am.*, 1981, **244**, 124; b) Y. Osada and A. R. Khokhlov, *Polymer Gels and Networks*, Marcel Dekker, New York, 2002; c) S.-K. Ahn, R. M. Kasi, S.-C. Kim, N. Sharma and Y. Zhou, *Soft Matter*, 2008, **4**, 1151-1157.

6   a) L. A. Estroff and A. D. Hamilton, *Chem. Rev.*, 2004, **104**, 1201-1218, and references therein; b) B. Xie and R. Zhang, *J. Mater. Chem.*, 2005, **15**, 2529-2550; c) M. George, R. Mathew and R. G. Weiss, *Molecular Gels*, 2006, 449-551; d) D. K. Smith, *Chem. Commun.*, 2006, 34-44; e) D. J. Adams, *Macromol. Biosci.*, 2011, **11**, 160-173; f) A. Dawn, T. Shiraki, S. Haraguchi, S. Tamaru and S. Shinkai, *Chem. Asian J.*, 2011, **6**, 266-282; g) X. Yang, G. Zhang and D. Zhang, *J. Mater. Chem.*, 2012, **22**, 38-50.

7   A. Ajayaghosh, V. K. Praveen and C. Vijayakumar, *Chem. Soc. Rev.*, 2008, **37**, 109-122.

8   a) A. Aggeli, M. Bell, N. Boden, J. N. Keen, P. F. Knowles, T. C. B. McLeish, M. Pitkeathly and S. E. Radford, *Nature*, 1997, **386**, 259-262, and references therein; b) K. Inoue, Y. Ono, Y. Kanekiyo, T. Ishi-i, K. Yoshihara and S. Shinkai, *Tetrahedron Lett.*, 1998, **39**, 2981-2984; c) T. Oya, T. Enoki, A. Y. Grosberg, S. Masamune, T. Sakiyama, Y. Takeoka, K. Tanaka, G. Wang, Y. Yilmaz, M. S. Feld, R. Dasari and T. Tanaka, *Science*, 1999, **286**, 1543-1545; d) C. Renner and L. Moroder, *ChemBioChem*, 2006, **7**, 868-878.

9   S. Bhattacharya and S. K. Samanta, *Langmuir*, 2009, **25**, 8378-8381.

10 a) T. Ishi-I and S. Shinkai, *Top Curr. Chem.*, 2005, **258**, 119-160, and references therein; b) D. Inoue, M. Suzuki, H. Shirai and K. Hanabusa, *Bull. Chem. Soc. Jpn.*, 2005, **78**, 721-726; c) S. Yagai, T. Iwashima, K. Kishikawa, S. Nakahara, T. Karatsu and A. Kitamura, *Chem. Eur. J.*, 2006, **12**, 3984-3994; d) Y. Zhou, M. Xu, T. Yi, S. Xiao, Z. Zhou, F. Li and C. Huang, *Langmuir*, 2007, **23**, 202-208; e) G. Palui and A. Banerjee, *J. Phys. Chem. B*, 2008, **112**, 10107-10115; f) D. Chen, H. Liu, T. Kobayashi and H. Yu, *J. Mater. Chem.*, 2010, **20**, 3610-3614; g) R. Rajaganesh, A. Gopal, T. M. Das and A. Ajayaghosh, *Org. Lett.*, 2012, **14**, 748-751.

11 a) K. Murata, K. Aoki, T. Nishi, A. Ikeda and S. Shinkai, *J. Chem. Soc. Chem. Commun.*, 1991, 1715-1718; b) K. Murata, M. Aoki, T. Suzuki, T. Harada, H. Kawabata, T. Komori, F. Ohseto, K. Ueda and S. Shinkai, *J. Am. Chem. Soc.*, 1994, **116**, 6664-6676.

12 a) J. Mamiya, K. Kanie, T. Hiyama, T. Ikeda and T. Kato, *Chem. Commun.*, 2002, 1870-1871; b) H. Kobayashi, A. Friggeri, K. Koumoto, M. Amaike, S. Shinkai and D. N. Reinhoudt, *Org. Lett.*, 2002, **4**, 1423-1426.

[13] a) S. Shinkai, K. Matsuo, M. Sano, T. Sone and O. Manabe, *Tetrahedron Lett.*, 1981, **22**, 1409-1412; b) S. Shinkai, K. Matsuo, A. Harada and O. Manabe, *J. Chem. Soc. Perkin Trans. 2*, 1982, 1261-1265; c) X. Song, J. Perlstein and D. G. Whitten, *J. Am. Chem. Soc.*, 1997, **119**, 9144-9159; d) S. van der Laan, B. L. Feringa, R. M. Kellogg and J. van Esch, *Langmuir*, 2002, **19**, 7136-7140.

[14] a) Y. Ji, G. C. Kuang, X. R. Jia, E. Q. Chen, B. B. Wang, W. S. Li, Y. Wie and J. Lei, *Chem. Commun.*, 2007, 4233-4235; b) J. H. Kim, M. Seo, Y. J. Kim and S. Y. Kim, *Langmuir*, 2009, **25**, 1761-1766.

[15] I. Kapoor, E.-M. Schön, J. Bachl, D. Kühbeck, C. Cativiela, S. Saha, R. Banerjee, S. Roelens, J. J. Marrero-Tellado and D. D. Díaz, *Soft Matter*, 2012, **8**, 3446-3456.

[16] For recent reviews, see: a) E. Gazit, *Chem. Soc. Rev.*, 2007, **36**, 1263-1269, and references therein; b) I.W. Hamley, *Angew. Chem.*, 2007, **119**, 8274-8295; *Angew. Chem. Int. Ed.*, 2007, **46**, 8128-8147; c) J. P. Jung, J. Z. Gasiorowski and J. H. Collier, *Biopolymers (Pept. Sci.)*, 2010, **94**, 49-59; d) X. Yan, P. Zhu and J. Li, *Chem. Soc. Rev.*, 2010, **39**, 1877-1890; e) D. W. P. M. Lçwik, E. H. P. Leunissen, M. van den Heuvel, M. B. Hansen and J. C. M. van Hest, *Chem. Soc. Rev.*, 2010, **39**, 3394-3412; f) E. K. Johnson, D. J. Adams and P. J. Cameron, *J. Mater. Chem.*, 2011, **21**, 2024-2027.

[17] a) L. Li, H. Jiang, B. W. Messmore, S. R. Bull and S. I. Stupp, *Angew. Chem.*, 2007, **119**, 5977-5980; *Angew. Chem. Int. Ed.*, 2007, **46**, 5873-5876, and references therein; b) Y. Matsuzawa and N. Tamaoki, *J. Phys. Chem. B*, 2010, **114**, 1586-1590; c) X. Li, Y. Gao, Y. Kuang and B. Xu, *Chem. Commun.*, 2010, **46**, 5364-5366; d) Y. Huang, Z. Qiu, Y. Xu, J. Shi, H. Lina and Y. Zhang, *Org. Biomol. Chem.*, 2011, **9**, 2149-2155; e) Y. Lin, Y. Qiao, P. Tang, Z. Li and J. Huang, *Soft Matter*, 2011, **7**, 2762-2769; f) Z.-X. Liu, Y. Feng, Z.-C. Yan, Y.-M. He, C.-Y. Liu and Q.-H. Fan, *Chem. Mater.*, 2012, **24**, 3751-3757.

[18] Note that azoPhe can also be viewed as the result of linking an azo-benzene moiety to the methyl side chain of l-alanine.

[19] a) M. Goodman and A. Kossoy, *J. Am. Chem. Soc.*, 1966, **88**, 5010-5015; b) M. Goodman and M. L. Falxa, *J. Am. Chem. Soc.*, 1967, **89**, 3863-3867; c) E.

Benedetti, A. Kossoy, M. L. Falxa and M. Goodman, *Biochemistry*, 1968, **7**, 4234-4242.

[20] a) J. C. Rodríguez-Cabello, M. Alonso, L. Guiscardo, V. Reboto and A. Girotti, *Adv. Mater.*, 2002, **14**, 1151-1154, and references therein; b) N. Muranaka, T. Hohsaka and M. Sisido, *FEBS Lett.*, 2002, **510**, 10-12; c) K. Nakayama, M. Endo and T. Majima, *Chem. Commun.*, 2004, 2386-2387; d) K. Nakayama, E. Masayuki and M. Tetsuro, *Bioconjugate Chem.*, 2005, **16**, 1360-1366; e) M. Bose, D. Groff, J. Xie, E. Brustad and P. G. Schultz, *J. Am. Chem. Soc.*, 2006, **128**, 388-389; f) C. Aleman, G. Revilla-Lopez, A. Laurent, E. A. Perpete, D. Jacquemin, J. Torras and X. Assfeld, *J. Phys. Chem. B*, 2011, **115**, 1232-124220.

[21] J. Juodaityte and N. Sewald, *J. Biotechnol.*, 2004, **112**, 127-138.

[22] See the Supporting Information for further details.

[23] M. Bodanszky and A. Bodanszky, *The Practice of Peptide Synthesis*, Springer, Berlin, 1994.

[24] Y. Wu, S. Wu, G. Zoua and Q. Zhang, *Soft Matter*, 2011, **7**, 9177-9183.

[25] M. J. Kamlet, J. L. M. Abboud, M. H. Abraham and R. W. Taft, *J. Org. Chem.*, 1983, **48**, 2877-2887.

[26] a) K. S. Partridge, D. K. Smith, G. M. Dykes and P. T. McGrail, *Chem. Commun.*, 2001, 319-320; b) A. R. Hirst and D. K. Smith, *Langmuir*, 2004, **20**, 10851-10857; c) W. Edwards, C. A. Lagadec and D. K. Smith, *Soft Matter*, 2011, **7**, 110-117.

[27] a) G. Cravotto and P. Cintas, *Chem. Soc. Rev.*, 2009, **38**, 2684-2697; b) L. Sambri, F. Cucinotta, G. De Paoli, S. Stagni and L. De Cola, *New J. Chem.*, 2010, **34**, 2093-2096; c) S. Maity, P. Kumar and D. Haldar, *Soft Matter*, 2011, **7**, 5239-5245.

[28] A. Takahashi, M. Sakai and T. Kato, *Polym. J.*, 1980, **12**, 335-341.

[29] a) L. Lu, T. M. Cocker, R. E. Bachman and R. G. Weiss, *Langmuir*, 2000, **16**, 20-34; b) J. Becerril, B. Escuder, J. F. Miravet, R. Gavara and S. V. Luis, *Eur. J. Org. Chem.*, 2005, 481-485.

[30] We could identify a tendency of N-deprotected peptides toward decomposition in solutions of polar protic solvents regardless of the position of the azoPhe or Phe residue. TLC, in situ NMR spectroscopy and mass spectroscopy

preliminary experiments suggested the possible formation of a lactam intermediate, which could be further ring-opened by a good nucleophilic solvent, like methanol or ethanol. However, this propensity was found to be apparently negligible in the gel phase.

31 a) K. Hanabusa, R. Tanaka, M. Suzuki, M. Kimura and H. Shirai, *Adv. Mater.*, 1997, **9**, 1095-1097; b) A. K. Das, P. P. Bose, M. G. B. Drew and A. Banerjee, *Tetrahedron*, 2007, **63**, 7432-7442; c) U. Hahn, A. R. Hirst, J. L. Delgado, A. Kaeser, B. Delavaux-Nicot, J.-F. Nierengarten and D. K. Smith, *Chem. Commun.*, 2007, 4949-4945; d) A. R. Hirst, I. A. Coates, T. Boucheteau, J. F. Miravet, B. Escuder, V. Castelletto, I. W. Hamley and D. K. Smith, *J. Am. Chem. Soc.*, 2008, **130**, 9113-9121; e) A. Banerjee, G. Palui and A. Banerjee, *Soft Matter*, 2008, **4**, 1430-1437.

32 For selected studies concerning the role of π-stacking interactions of Phe units in self-assembly and gel formation, see: a) V. L. Sedman, L. Adler-Abramovich, S. Allen, E. Gazit and S. J. B. Tendler, *J. Am. Chem. Soc.*, 2006, **128**, 6903-6908; b) P. Tamamis, L. Adler-Abramovich, M. Reches, K. Marshall, P. Sikorski, L. Serpell, E. Gazit and G. Archontis, *Biophys. J.*, 2009, **96**, 5020-5029; c) M. Ma, Y. Kuang, Y. Gao, Y. Zhang, P. Gao and B. Xu, *J. Am. Chem. Soc.*, 2010, **132**, 2719-2728; d) A. Duttaa, D. Chattopadhyay, and A. Pramanik, *Supramol. Chem.*, 2010, **22**, 95-102.

33 a) V. Caplar, M. Zinic, J.-L. Pozzo, F. Fages, G. Mieden-Gundert and F. Vögtle, *Eur. J. Org. Chem.*, 2004, 4048-4059; b) B. Escuder, M. Llusar and J. F. Miravet, *J. Org. Chem.*, 2006, **71**, 7747-7752; c) L. Frka-nec and M. Zinic, *Chem. Commun.*, 2010, **46**, 522-537.

34 a) J. Makarevic, M. Jokic, Z. Raza, Z. Stefanic, B. Kojic-Prodic and M. Zinic, *Chem. Eur. J.*, 2003, **9**, 5567-5580; b) F. Allix, P. Curcio, Q. N. Pham, G. Pickaert and B. Jamart-Grégoire, *Langmuir*, 2010, **26**, 16818-16827.

35 T. Peterfi, *Arch. Entwicklungsmech. Org.*, 1927, **112**, 680-686.

36 P. Kirilov, F. Gauffre, S. Franceschi-Messant, E. Perez and I. Rico-Lattes, *J. Phys. Chem. B*, 2009, **113**, 11101-11108.

37 a) H. A. Barnes, *J. Non-Newtonian Fluid Mech.*, 1997, **70**, 1-33; b) G. Mezger, *The Rheology Handbook*, Vincentz Network, Hannover, Germany, 2011.

38 N. Koumura, M. Kudo and N. Tamaoki, *Langmuir*, 2004, **20**, 9897-9900.

39 Y. Zhou, M. Xu, J. Wu, T. Yi, J. Han, S. Xiao, F. Li and C. Huang, *J. Phys. Org. Chem.*, 2008, **21**, 338-343.

40 R. E. Fischer, B. Tadic-Galeb and P. R. Yoder, *Optical System Design*, McGraw Hill, 2nd Ed., 2008.

41 A. Prathap and K. M. Sureshan, *Chem. Commun.*, 2012, **48**, 5250-5252.

42 a) R. J. Swannell, K. Lee and M. McDonagh, *Microbiol. Rev.*, 1996, **60**, 342-365; b) R. J. Fiocco and A. Lewis, *Pure Appl. Chem.*, 1999, **71**, 27-42; c) H. Zhu, S. Qiu, W. Jiang, D. Wu and C. Zhang, *Environ. Sci. Technol.*, 2011, **45**, 4527-4531, and references cited therein.

43 a) S. Bhattacharya and Y. K. Gosh, *Chem. Commun.*, 2001, 185-186; b) D. R. Trivedi, A. Ballabh, P. Dastidar and B. Ganguly, *Chem. Eur. J.*, 2004, **10**, 5311-5322; c) D. R. Trivedi and P. Dastidar, *Chem. Mater.*, 2006, **18**, 1470-1478; d) J. Peng, K. Liu, X. Liu, H. Xia, J. Liu and Y. Fang, *New J. Chem.*, 2008, **32**, 2218-2224; e) D. Bardelang, F. Camerel, J. C. Margeson, D. M. Leek, M. Schmutz, M. B. Zaman, K. Yu, D. V. Soldatov, R. Ziessel, C. I. Ratcliffe and J. A. Ripmeester, *J. Am. Chem. Soc.*, 2008, **130**, 3313-3315; f) T. Kar, S. Debnath, D. Das, A. Shome and P. K. Das, *Langmuir*, 2009, **25**, 8639-8648; g) M. Xue, D. Gao, K. Liu, J. Peng and Y. Fang, *Tetrahedron*, 2009, **65**, 3369-3377; S. R. Jadhav, P. K. Vemula, R. Kumar, S. R. Raghavan and G. John, *Angew. Chem. Int. Ed.*, 2010, **49**, 7695-7698.

44 P. Fatás, J. Bachl, S. Oehm, A. I. Jiménez, C. Cativiela and D. D. Díaz, *Chem. Eur. J.*, 2013, **19**, 8861-8874.

45 J. E. Eldrige, J. D. Ferry, *J. Phys. Chem.*, 1954, **58**, 992-995.

46 S. Debnath, A. Shome, S. Dutta and P. K. Das, *Chem. Eur. J.*, 2008, **14**, 6870-6881.

2. Organophotocatalysis in nanostructured soft gel materials as tunable reaction vessels: Comparison with homogeneous and micellar solutions[i]
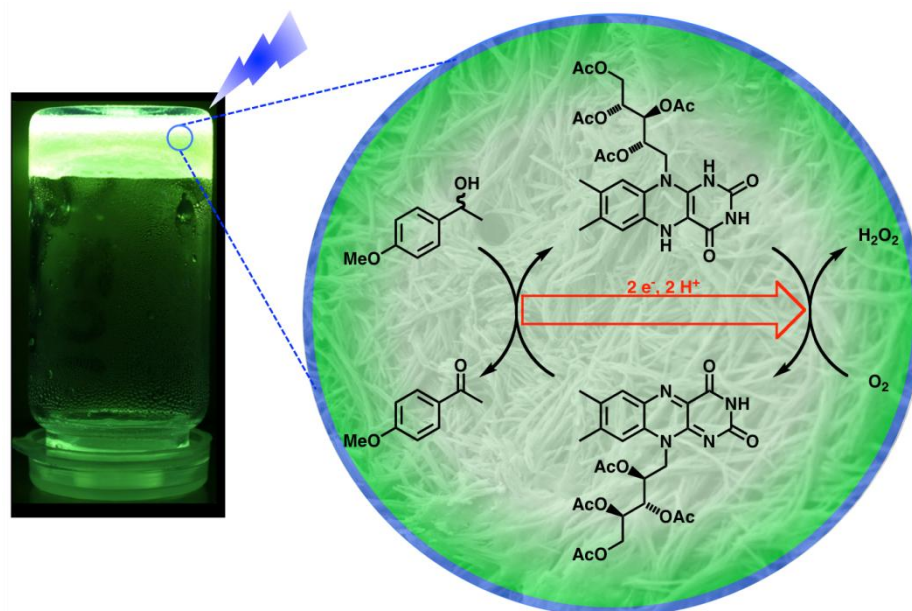
Riboflavin tetraacetate-catalyzed aerobic photooxidation of 1-(4-methoxyphenyl)ethanol was investigated as a model reaction under blue visible light in different soft gel materials, aiming to establish their potential as reaction vessels for photochemical transformations. Three strategies involving different degrees of organization of the catalyst within the gel network were explored, and the results compared to those obtained in homogeneous and micellar solutions. In general, physical entrapment of both the catalyst and the substrate under optimized concentrations into several hydrogel matrices (including low-molecular-weight and biopolymer-based gels) allowed the photooxidation with conversions between 55-100% within 120 min (TOF ~ 0.045-0.08 min^{-1}; k_{obs} ~ 0.011-0.028 min^{-1}), albeit with first-order rates *ca.* 1-3-fold lower than in solution under comparable non-stirred conditions. Remarkably, the organogel made of a cyclohexane-based bisamide gelator in CH$_3$CN not only prevented the photo degradation of the catalyst but also afforded full conversion in less than 60 min (TOF ~ 0.167 min^{-1}; k_{obs} ~ 0.073 min^{-1}) without the need of additional proton transfer mediators (*e.g.*, thiourea) as it occurs in CH$_3$CN solutions. In general, the gelators could be recycled without detriment of their gelation ability and

—

---

[i] Reproduced with permission from: J. Bachl, A. Hohenleutner, B. B. Dhar, C. Cativiela, U. Maitra, B. König and D. D. Díaz, *J. Mater. Chem. A*, 2013, **1**, 4577-4588. Copyright 2013 The Royal Society of Chemistry.

reaction rates. Moreover, kinetics could be fine-tuned according to the characteristics of the gel media. For instance, entangled fibrillar networks with relatively high mechanical strength were usually associated to lower reaction rates, whereas wrinkled laminated morphologies seemed to favor the reaction. In addition, the kinetics results showed in most cases a good correlation with the aeration efficiency of the gel media.[ii]

2.1. Introduction

Inspired by nature, much effort has been devoted over the last decade to the study of meso-, micro- and nano-scale reactors. The main reason for this is the fact that many chemical reactions take place with high efficiency in natural confined environments where the motions of reactant molecules are restricted to that in free solution. Through biomimetic principles, a significant number of self-assembled and compartmentalized molecular (*e.g.*, micelles, vesicles, microemulsions, multilayered capsules, inorganic frameworks), macromolecular (*e.g.*, polymersomes, polymer micelles) and biomacromolecular nanoreactors (*e.g.*, viruses, protein cages) have been investigated in the context of chemical reactivity and highlighted in several excellent reviews.[1-9] Therein, numerous advantages have been attributed to the use of synthetic nanoreactors including, among others, the possibility of tailoring additional functionalities, organization and orientation of solvent, catalyst and reactant molecules, controllable molecular diffusion, large surface area to volume ratios and reduction of overheating/concentration effects. Thus, an improved control over the efficiency and selectivity of reactions carried out in constrained spaces compared to conventional solution or heterogeneous media has been demonstrated in many of those examples. Nevertheless, predicting the outcome of a chemical process in a potential nanoreactor continues being a scientific challenge mainly due to the number of thermodynamic and interfacial effects that should be considered and rationalized.[10]

Looking now at the plethora of chemical processes, photocatalysis constitutes undoubtedly a subject of increasing technological and economic importance owed to its critical role in many of today's energy and environmental concerns. Also here, the

---

[ii] Compounds 10 and 12 in Figure 1 have been prepared by A. Hohenleutner. Compound 15 in Figure 4 has been prepared both by A. Hohenleutner and J. Bachl. Kinetic data (k_{obs}) represented in Tables 1-3 and Figure 6 have been cross-checked by B. Dhar. All other experiments were carried out by J. Bachl.

literature contains numerous investigations directed towards understanding photochemical processes in nanophotoreactors based on either porous inorganic structures or organized molecular assemblies (*e.g.*, titania spheres, lipid vesicles, foams, oil-in-water emulsions), which demonstrate the importance of these studies in the field of materials chemistry.[11] On the other hand, soft gel materials[12] have been also studied as structured reaction vessels and reusable catalysts,[13, 14] although truly biomimetic catalysis[3] has not yet been demonstrated with these materials. In addition, the study of photochemical processes in gel media, involving embedded reactants that do not participate in the assembly of the viscoelastic network has been scarcely explored.[13, 15] In this sense, Bhat and Maitra published the most relevant study in 2007,[16] showing that the photodimerization of acenaphthylene occurs with higher *syn/anti* selectivity in bile acid-based hydrogels than in micellar solutions. Two years later, Shinkai and co-workers reported the selective photocyclodimerization of anthracene derivatives within an organogel matrix.[17] Eswaramoorthy, George and co-workers have demonstrated that clay-dye hybrid supramolecular hydrogels can act as efficient light-harvesting soft materials[18] to promote Förster resonant energy transfer.[19] Haldar and co-workers have also reported the successful formation of a charge-transfer complex between a tripeptide-based gelator and picric acid in gel phase.[20] Very recently, Biradha's group has described different effects of crystalline and gel states on the photodimerization of unsymmetrical olefins.[21] These few reports envisage the significant influence that the properties of the gel media and the local microenvironment may have on the outcome of a photochemical reaction.

From our point of view, the reduced number of photocatalytic studies inside metal-free gels is leastwise surprising if we consider, for example, that hydrogels and natural cells (including those where light-driven reactions take place) have been found to share many features such as dynamic nature, water structuring, exclusion of solutes via phase-transition, physical consistency, multiple cooperative non-covalent interactions,[22] and therefore self-adaptivity.[23] Motivated by this paradigm and the appearance of new forms of gel bio-inspired materials with great potential for coacervate domains,[24] we aimed here to gain insights into the impact of different gels on both kinetics and selectivity of flavin-mediated aerobic photooxidation of benzyl alcohols as model photocatalytic reaction. A comparative analysis was also made with the reaction performed in homogeneous and micellar systems.

2.2. Experimental section

2.2.1   Materials

Unless otherwise specified, all reagents, starting materials and solvents (p.a. grade) were purchased from commercial suppliers and used as received without further purification. See ESI† for detailed information about instrumentation, synthetic procedures, compounds and material characterization.

2.2.2   Gelation experiments

In a typical gelation experiment (approach I), a weighted amount of all the required components (*i.e.*, gelator, substrate, and catalyst) and the appropriate solvent system (1 mL) were placed into a 4 mL screw-capped glass vial (4.5 cm length × 1.2 cm diameter) and heated gently with a heat gun until an isotropic solution was formed. In some cases, sonication of the mixture in an ultrasound bath for 30 s before heating allowed a faster dissolution of the solids. The resulting homogeneous solution was then allowed to slowly cool down to RT and left for at least 12 h to ensure equilibration. After this time, the so-formed soft materials were preliminary classified as "gels" if they did not exhibit gravitational flow upon upside-down the vial. The gel state was further confirmed by oscillatory rheological measurements. The gels were kept overnight in the dark for stabilization purposes before irradiation. Experimental details on other strategies (approaches II and III) are given in ESI†.

2.2.3   Typical procedures for catalytic photooxidations

Each experimental data point used for kinetics calculations represents the average value from at least two randomized measurements.

Representative reaction in homogeneous solutions

Riboflavin tetraacetate (**RFT**) (10.9 mg, 0.02 mmol) and 1-(4-methoxyphenyl)ethanol (**1**) (30.4 mg, 0.2 mmol) were placed into a conical flask and the mixture diluted with H_2O/DMSO or CH_3CN to reach a total volume of 40.0 mL containing 2% (v/v) DMSO. The mixture was stirred for 30 min in the dark to allow complete solubilization of both the catalyst and the substrate under aerobic conditions (without additional saturation with O_2).[25] Thiourea (0.5 mM) was used in some experiments as electron-transfer mediator to enhance reaction rates in CH_3CN solutions (Table 1).[26] The homogenous solution was split into several plastic-capped vials (4 cm length × 1.9 cm diameter; total volume of solution = 1 mL) equipped with a magnetic stirring bar. The reaction mixture was irradiated during the desired time under stirring (250 rpm) by means of a light-emitting diode (LED) (λ_{max} = 440 nm, 3 W). The vial was placed vertically above the aperture of the LED and the temperature of the mixture was held at 20 ± 1 °C during the experiments via a custom made cooling apparatus (see ESI†). Work-up for reactions made in aqueous solutions: Reaction mixtures were diluted with brine (5 mL) and extracted with CH_2Cl_2 (5 x 5 mL). The combined organic phases were dried over Na_2SO_4, filtered and the solvent was evaporated under reduced pressure (≤ 250 mbar). The obtained residue was redissolved in $CDCl_3$ (0.7 mL) for subsequent NMR analysis. Work-up for reactions made in CH_3CN solutions: Solvent was directly evaporated to dryness under reduced pressure and the residue redissolved in $CDCl_3$ (0.7 mL) for NMR analysis.

Representative reaction in micellar solutions

RFT (10.9 mg, 0.02 mmol), **1** (30.4 mg, 0.2 mmol) and sodium deoxycholate (**11**)[27] (199 mg, 480 mmol) were placed into a conical flask, diluted with H_2O (40.0 mL total volume) and the mixture stirred for 3 h in the dark to allow micelle formation and solubilization of both the catalyst and the substrate (resulting concentrations in the micellar solution: **11** = 12.0 mM, **RFT** = 0.5 mM, **1** = 5 mM). The homogeneous solution was then split into several sample vials (4 cm length × 1.9 cm diameter; total volume of solution = 1 mL) and submitted to LED irradiation (λ_{max} = 440 nm, 3 W) under stirring at 20 ± 1 °C (see ESI†). After irradiation, the samples were diluted with brine (5 mL), and extracted with CH_2Cl_2 (5 × 5 mL). The combined organic phases were dried over Na_2SO_4, filtered, and concentrated. The obtained residue was redissolved in $CDCl_3$ (0.7 mL) for NMR analysis or in iPrOH (1 mL) for HPLC-analysis after filtration through a PTFE filter.

90

Representative reaction in gel media

RFT (50 μL from a 0.01 M solution in CH_2Cl_2) and **1** (50 μL from a 0.1 M solution in CH_2Cl_2) were added to a 5 mL sample vial (4 cm height, 1.9 cm diameter) containing the specified amount of the respective gelator. The solvent was then allowed to slowly evaporate, and the mixture diluted with the appropriate solvent system for gelation (1 mL). The gels were prepared as described above. Alternatively, the gelator was weighed into a vial and **1** (50 μL from a 0.1 M solution in CH_2Cl_2) was added. After evaporation of the solvent, resuspension of the mixture and gel formation, **RFT** (50 μL from a 0.1 M solution in CH_2Cl_2) was carefully added on top of the gel and allowed to diffuse overnight. After an equilibration period (12 h), the samples were submitted to LED irradiation (λ_{max} = 440 nm, 3 W) at 20 ± 1 °C (see ESI†). For kinetics calculations, irradiation was stopped after a certain time and the gels dissolved by dilution, heating, and mechanical agitation. The solutions of the destroyed gels were extracted with CH_2Cl_2 (5 × 5 mL). The combined organic phases were dried over Na_2SO_4, filtered, and evaporated. The residue was redissolved in $CDCl_3$ for NMR analysis or in iPrOH for HPLC-analysis as described for micellar systems.[28]

2.3. Results and discussion

Flavin cofactors such as riboflavin (vitamin B2), flavin adenine mononucleotide (FMN), and flavin adenine dinucleotide (FAD) are well known as versatile catalysts in both one-electron and two-electron redox processes, playing a key role in a number of light-regulated biological processes.[29] Moreover, riboflavin-based organocatalysis has recently gained much attention as a green and economic alternative to the corresponding metal-catalyzed reactions.[30-33] For this investigation, we selected 1-(4-methoxyphenyl)ethanol(**1**) as a model activated substrate to study its photo induced oxidation in different media upon irradiation with blue visible light (λ_{max} = 440 nm) in the presence of **RFT** as non-toxic photocatalyst and aerial O_2 as terminal oxidant (Scheme 1). As it occurs with other flavin-derivatives, **RFT**-mediated photooxidation of benzyl alcohols[25, 26, 34-38] takes advantage of the increased oxidation power of the chromophore in its oxidized state (**RFT$_{ox}$**) upon excitation by visible light.[25] In the presence of an electron-donor (*e.g.*, benzyl alcohol), triplet-excited **RFT$_{ox}$** undergoes a subsequent two-electron reduction and protonation to

91

generate the corresponding dihydroflavin (**RFT$_{red}$**). Finally, **RFT$_{red}$** is rapidly and stoichiometrically reoxidized to **RFT$_{ox}$** by aerial O_2, yielding H_2O_2 as the sole byproduct.[39]
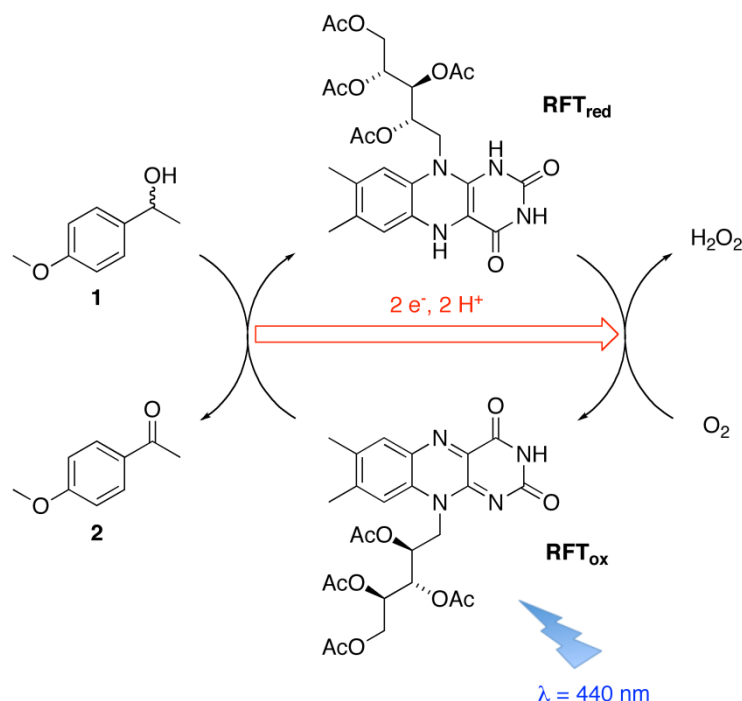
Scheme 1 Catalytic cycle of aerobic photooxidation of **1** under blue visible light catalyzed by **RFT**.

In order to draw meaningful comparisons, the reaction kinetics was first studied in homogeneous and micellar solutions as a reference scenario, and subsequently in several gel systems including those made from low-molecular-weight (LMW) and biopolymer-based gelators. Both aqueous and organic environments were also considered in this investigation. All reactions were performed under aerobic conditions using commercially available LEDs with emission maximum centered at $\lambda_{max} = 440$ nm as light source, which corresponds roughly to the longest wavelength absorption maximum of **RFT$_{ox}$**.

2.3.1.   Photooxidation in homogeneous and micellar solutions

For comparative purposes, the maximum catalyst loading (*i.e.*, 10 mol%) in these experiments was chosen based on the ability of the gel systems to integrate the catalyst without mayor disruption of the fibrillar gel network (*vide infra*). Under these conditions,

the kinetics of the reaction was studied in both aqueous and CH_3CN solutions (Table 1, entries 1-5).[28] Apparent first order rate constants (k_{obs}) were estimated from the slopes of ln[**1**] against time plots.[40] In agreement with previous observations made by some of us,[25, 26] almost complete conversion of **1** into ketone **2** upon irradiation with blue visible light was achieved without formation of byproducts[41] within 30 min in aqueous stirred solution, whereas only 5% conversion was reached in CH_3CN after the same reaction time.[28] Thus, the catalyst activity (average TOF) resulted 33-fold higher in aqueous than in CH_3CN solution under comparable conditions (Table 1, entry 1 *vs* 3). As expected, the addition of thiourea (0.5 mM) as proton transfer mediator for the first reaction step caused a remarkable enhancement of the photooxidation rate in CH_3CN by a factor of *ca.* 12 under the conditions described in Table 1 (entry 3 *vs* 4), although catalyst deactivation was observed after 40 min (*ca.* 50% conversion).[25, 26]

Table 1 Kinetic parameters of **RFT**-catalyzed photooxidation of **1** in homogeneous and micellar solutions, and effect of stirring[a]

entry	solvent system[b]	[1] (mmolL^{-1})	[RFT] (mol%)	[TU] (mmolL^{-1})	[NaDC] (mmolL^{-1})	IT (min)	conversion (%)	TON	TOF (min^{-1})	k_{obs} (× 10^{-3} min^{-1})	$t_{1/2}$ (min)
1	H_2O/DMSO[c]	5	10	-	-	30	100	10.0	0.33	154.2±7.71	4.5±0.21
2	H_2O/DMSO[c,d]	5	10	-	-	90	100	10.0	0.11	37.3±0.78	18.6±0.38
3	CH_3CN	5	10	-	-	240	25	2.5	0.01	1.3±0.07	533.2±2.86
4	CH_3CN	5	10	0.5	-	120	69	6.9	0.06	15.5±0.57	44.7±1.59
5	CH_3CN[d]	5	10	0.5	-	240	43	4.3	0.02	2.6±0.07	266.6±6.99
6	H_2O	5	10	-	12.0	20	100	10.0	0.50	251.9±9.33	2.8±0.10
7	H_2O[d]	5	10	-	12.0	90	100	10.0	0.11	60.6±3.47	11.4±0.62

[a] Reaction conditions: T = 20 ± 1 °C; light source = LED blue visible light (λ_{max} = 440 nm, 3 W); stirring at 250 rpm unless otherwise indicated. Abbreviations: **RFT** = riboflavin tetraacetate; **TU** = thiourea; **NaDC** = sodium deoxycholate = **11**; IT = irradiation time; TON = turnover number (catalyst productivity); TOF = turnover frequency (catalyst activity); k_{obs} = rate constant; $t_{1/2}$ = half life. Square brackets refer to concentration. [b] Total solvent volume = 1 mL. [c] 2% (v/v) DMSO was here necessary for complete solubilization of all components. [d] Reactions carried out without stirring. [e] Reaction conversion over time for kinetics calculations was determined by ^{1}H NMR analysis. Estimated error = ± 1.5%. For additional catalyst/substrate molar ratios, see ESI†.

On the other hand, previous investigations have demonstrated that performing photochemical reactions in the presence of bile salt micelles could significantly alter their course and selectivity.[42, 43] For this reason, and considering the wide use of bile salts also as LMW gelators,[44] we additionally performed the above reaction as comparative control in micellar solutions of sodium deoxycholate (**NaDC**) (Table 1, entries 6-7). Micellar medium was prepared by adjusting the concentration of **NaDC** to 12 mM as previously described.[27] In this case, the micellar medium allowed complete solubilization of both the substrate and the catalyst without the need of organic co-solvents like DMSO, achieving quantitative conversion within 20 min under stirring conditions. Thus, the micellar medium caused a modest enhance of the rate constant (*ca.* 1.6-fold increase) in comparison to that in H_2O/DMSO solution.

Nevertheless, it is important to remark that the catalyst activity in the above media underwent a 3-6-fold drop when carried out without moderate stirring (Table 1, entries 2, 5 and 7), which is in good agreement with previous observations[25] and suggests the existence of non-homogeneous microphases and a more complex nature of the kinetics. Moreover, HPLC analysis of the reaction mixture showed that the chiral microenvironment provided by **NaDC** did not induce any enantioselective oxidation of ($\pm$) **1**.[28]

2.3.2.   Photooxidation in gel media

In principle, we could expect both diffusion-controlled and electron-transfer processes to be altered within viscoelastic gels due to constrained molecular mobility and light scattering phenomena.[45] However, among a number of potential advantages of gel materials as reaction vessels,[13] their two-phase nature and highly solvated 3D-network could facilitate the separation of catalysts and products, provide a much higher accessibility of small reactants in comparison to other heterogeneous catalysts, and/or promote different orientations of the chromophore.

In this work we considered three different strategies in order to assess the actual potential of nanostructured soft gel materials as tunable reaction vessels for the **RFT**-catalyzed photooxidation of **1** under irradiation with blue visible light: Use of systems with the photocatalyst physically entrapped into the gel matrices (approach I); systems where

the photocatalyst is covalently attached to a complementary gelator structure (approach II);
and bicomponent gelator systems, in which one of the complementary partners needed for
building the 3D gel network is the own photocatalyst (approach III).

• *Approach I:* For this strategy we considered a number of known bio-based polymers (*i.e.*,
Figure 1: methylcellulose (**3**), κ-carrageenan (**4**), gelatin (**5**)), and LMW gelators (*i.e.*,
Figure 1: compounds **6**-**12**) with distinctive properties in order to evaluate their possible
effects on both selectivity and reaction kinetics. In the case of **NaDC** (**11**), the micellar
concentration was *ca.* 4-fold increased to reach the minimum gelation concentration
(MGC, 48.25 mM).
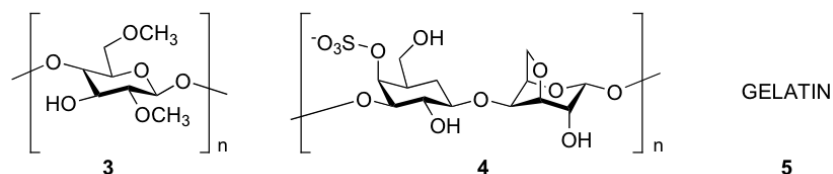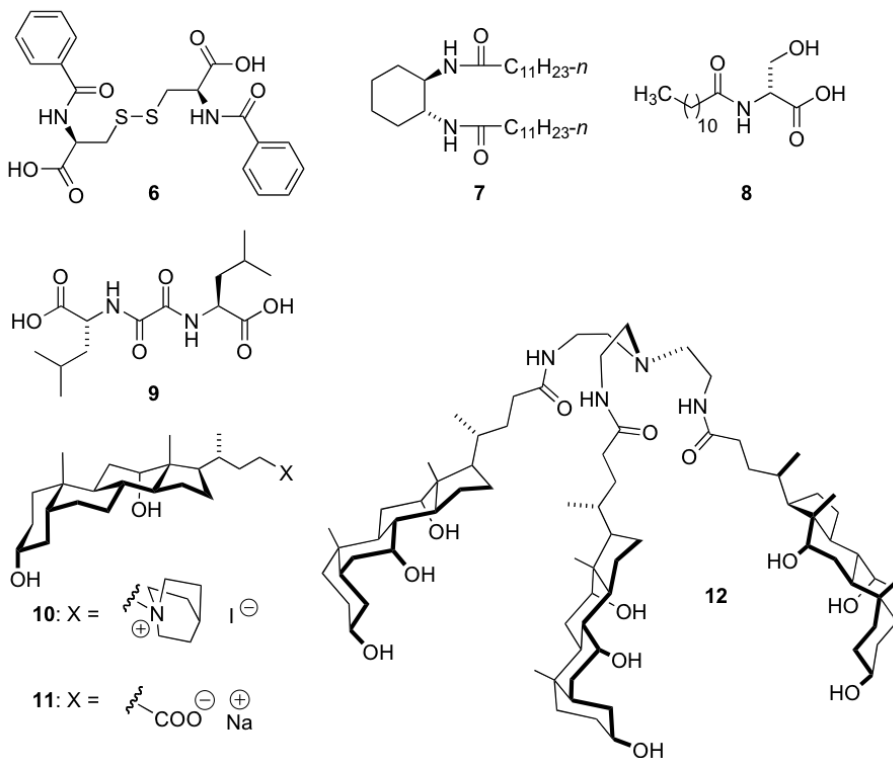
Fig. 1 Library of structurally diverse gelators used to study **RFT**-catalyzed photooxidation of **1** in gel media
(approach I).

All compounds could form stable hydrogels under different conditions, except bisamide **7** that was selected as a versatile organogelator for comparison with the less efficient reaction in CH$_3$CN solutions. Moreover, chiral hydrogelators were selected in order to investigate also any possible enantioselective recognition of the racemic substrate enabled by attractive forces with the self-assembled fibers. Such possible interactions[46] may provide regions of lower polarity within a chiral environment, in which photosensitizers and/or substrates with moderate water-solubility could be preorganized in a selective manner.[47-49] In principle, a similar reasoning could be also made for the approaches II and III.

Initially, a series of experiments were necessary to define the conditions (*e.g.*, concentration of components, solvent system) to entrap both the catalyst and the substrate into the gel matrices without causing major disruption of their microstructure and viscoelastic properties. As shown in Figure 2, the relative opacity of the pure gels was also preserved upon incorporation of **RFT** and **1**. In general, the opacity of the materials made from gelators **7-10** suggested the formation of aggregates smaller than the visible wavelength range. The use of a custom made cooling apparatus (see ESI†) was especially important for the kinetics experiments under LED irradiation (λ_{max} = 440 nm, 3 W). Thus, a constant reaction temperature far below the *gel*-to-*sol* phase transition temperatures (T_{gel}) was ensured to prevent disruption of the organized self-assembled fibrillar networks by a thermal shock and further melting of the gels. The stability of the bulk materials upon doping and irradiation was confirmed by the absence of visible liquid phase, as well as FT-IR analyses before and after irradiation. In general, the spectra showed no significant modification of the H-bonding pattern (*e.g.*, amide I at ν = 1638-1740 cm^{-1}, amide II at ν = 1525-1635 cm^{-1}, H-bound OH stretching at ν = 3315-3335 cm^{-1}) after doping the materials (under optimized concentrations), and during irradiation.[27] Furthermore, the absorption properties of **RFT** were in general maintained upon incorporation into the gel matrices as demonstrated by UV-vis spectroscopy.[28] Minor disruption of the nanostructures was also confirmed by electron microscopy imaging (*vide infra*).[28] We were delighted to observe that **RFT**-catalyzed photooxidation of **1** proceeded, under the above conditions, with conversions in the range 23-100% (Table 2). Regardless the reaction media, control experiments carried out in the absence of **RFT** or light irradiation (λmax = 440 nm) showed no conversion of substrate **1**. In addition, quantitative analysis of different sections of gel samples demonstrated a reasonably homogeneous distribution of the reaction

product, which was in agreement with the intrinsic dynamic nature of the gels and a relatively uniform irradiation along the bulk materials.[28] However, it should be noted that potential gradient of light intensity in the case of larger reaction volumes could influence catalyst activation. As expected for diffusion-controlled processes, photooxidation rates of **1** in hydrogel media were on average 10-20-fold lower than those in stirred solution, but only 1-3-fold lower under non-stirred conditions, which represents to some extent a more similar scenario to the reactions inside the gels.
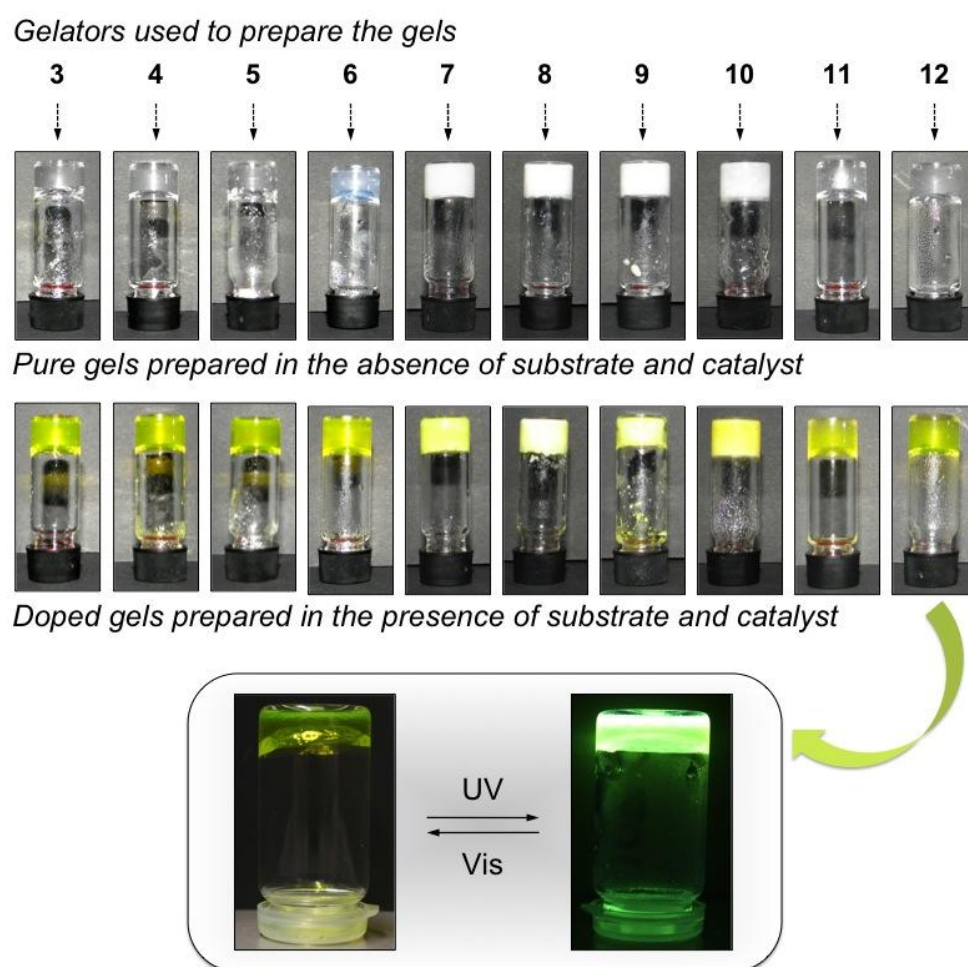
Fig. 2 Photographs of upside-down vials containing stable gels prepared with each gelator (*i.e.*, **3-12**) at given concentration (see Table 2) in the absence and presence of substrate **1** (5 mM) and **RFT** catalyst (10 mol%) using 1 mL of solvent (optimized conditions). The bright yellow color is derived from the catalyst. Solvent used in each case: [**3-5, 8-9**] = H_2O; [**6**] = H_2O/DMSO (95/5 v/v); [**7**] = CH_3CN; [**10**] = 0.5 M NaCl; [**11**] = phosphate buffer; [**12**] = H_2O/AcOH (80/20 v/v). Note that compounds **6, 10, 11** and **12** did not form stable hydrogels in pure water. Bottom: Example of fluorescent hydrogel made of **12** under visible and UV-light.

Only hydrogels made of bile salt-based gelator **10** in 0.5 M NaCl (Table 2, entry 9) resulted inefficient as reaction vessels (*i.e.*, conversion < 5%), probably due to the sensitivity of the excimer fluorescence towards microenvironmental changes. On the other hand, one of the most surprising and interesting results was the rapid reaction observed in the organogel made of bisamide gelator **7** in CH_3CN (Table 2, entry 6). In contrast to the reaction carried out in CH_3CN solution, the gel environment not only prevented deactivation of the catalyst, but also afforded full conversion in less than 60 min without the need of thiourea and stirring. This result suggests the existence of favorable interactions between gel fibers and substrate and/or catalyst, and will constitute the focus of a further detailed study. A potential role of secondary amides as proton transfer mediators, similar to thiourea, in solvents like CH_3CN[26] was disproved in control experiments.[28]

As it occurs in solution, some of the doped gels showed significant bleaching during irradiation at λ_{max} = 440 nm due to photo degradation of the **RFT** catalyst.[50] In the case of translucent gels, such process could be easily confirmed by UV-vis spectroscopy (Figure 3). Visual monitoring of the degree of bleaching during the experiments was in good agreement with the decrease of the reaction rate and stagnation of the process after certain irradiation time.[28]
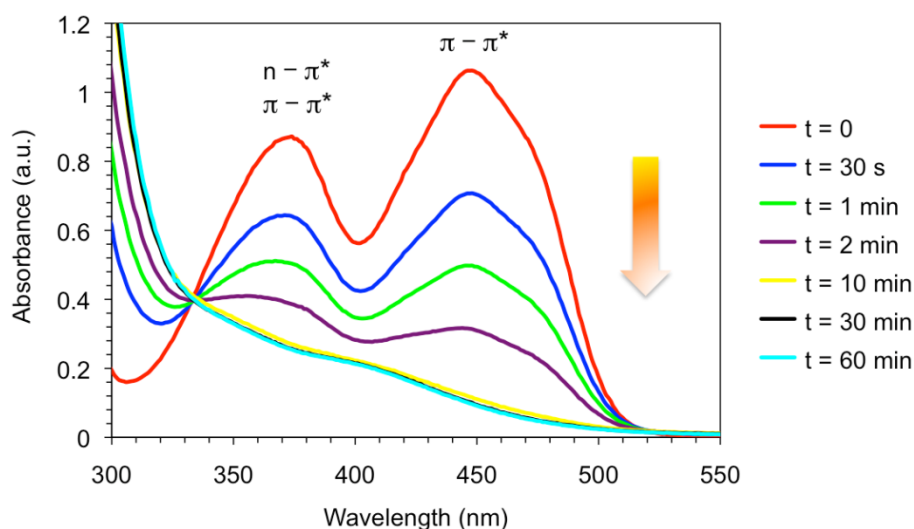
Fig. 3 Evolution of the UV-vis spectrum of the doped gel made from gelator **3** during irradiation with LED blue visible light (λ_{max} = 440 nm, 3 W). Signals at λ_{max} = 373 and 445 nm are characteristic of the **RFT** catalyst. Note that time values in the spectra do not correlate to real bleaching rates observed during kinetics experiments due to different light pathways. For additional details and examples, see ESI†.

Table 2 Kinetic parameters of **RFT**-catalyzed photooxidation of **1** in different gel media under optimized conditions[a]

entry	gelator system	solvent system[b]	[gelator] (% w/v)	[1] (mmol L^{-1})	[RFT] (mol%)	IT (min)	conversion (%)[c]	TON	TOF (min^{-1})	k_{obs} (× 10^{-3} min^{-1})	t$_{1/2}$ (min)
1	**3**	H$_2$O	5.0	5	10	120	83	8.3	6.9	17.3±0.07	40.1±0.16
2	**4**	H$_2$O	2.0	5	10	120	90	9.0	7.5	20.8±0.49	33.3±.78
3	**3+4**[d]	H$_2$O	2.0	5	10	120	96	9.6	8.0	28.2±2.76	24.6±2.19
4	**5**	H$_2$O	1.5	5	10	120	76	7.6	6.3	12.3±0.42	56.4±1.86
5	**6**	H$_2$O/DMSO[g]	0.3	5	10	120	23	2.3	1.9	2.7±0.21	256.7±18.53
6	**7**	CH$_3$CN	0.5	5	10	60	100	10.0	16.7	72.6±8.34	9.6±0.98
7	**8**	H$_2$O	3.0	5	10	120	70	7.0	5.8	11.0±0.07	63.0±0.40
8	**9**	H$_2$O	3.0	5	10	120	69	6.9	5.8	11.5±0.57	60.3±2.85
9	**10**	0.5 M NaCl[h]	2.0	5	10	360	14	1.4	0.4	0.5±0.07	1386.3±19.4
10	**11**	PBS[i]	2.0	5	10	120	55	5.5	4.6	19.3±3.18	35.9±5.08
11	**12**	H$_2$O/AcOH[j]	2.0	5	10	120	100	10.0	8.3	19.7±0.64	35.2±1.11
12	**15+11**[e]	PBS[i]	2.0	5	10	120	54	5.4	4.5	18.7±0.07	37.1±0.14
13	**RFT+16**[f]	H$_2$O	3.5	5	10	480	63	6.3	1.3	13.5±1.48	51.3±5.07

[a] Reaction conditions: T = 20 ± 1 °C; light source = LED blue visible light (λ_{max} = 440 nm, 3 W). Abbreviations: **RFT** = riboflavin tetraacetate; IT = irradiation time; TON = turnover number (catalyst productivity); TOF = turnover frequency (catalyst activity); k_{obs} = rate constant; t$_{1/2}$ = half life. Square brackets refer to concentration. [b] Total solvent volume = 1 mL. [c] Reaction conversion over time for kinetics calculations was determined by ^{1}H NMR analysis. Estimated error = ± 1.5%. [d] Weight ratio = 1:1. [e] Molar ratio of gelator system [**15** : **11**] = 1 : 96.5. [f] Molar ratio of gelator system [**RFT** : **16**] = 1 : 1. [g] Volume ratio = 95/5. [h] Although these gels could be also formed in the presence of up to 20% of organic solvents such as MeOH or DMSO, no enhancement of the conversion was observed. [i] Phosphate buffer solution, pH 7.5. [j] Volume ratio = 80/20.

It is also worth to mention that both LMW and polymer gelators could be easily recovered (*i.e.*, 92-98% of the original weight) after the photochemical reaction and reused for further experiments without any appreciable deterioration of the gelation ability and photoconversion rates. The purity of recycled materials was confirmed by ^{1}H NMR spectroscopy. In general, recycling experiments in the case of hydrogels involved

lyophilization, liquid-solid extraction of the corresponding xerogels, and drying under vacuum. In the case of organogels, the first two steps were replaced by solvent evaporation and subsequent recrystallization of the gelator.[28] On the other hand, it should be considered that, in contrast to other immobilized flavins,[25] the use of doped photoluminescent xerogels (produced from the corresponding doped gels by the freeze-drying method) is not appropriate for the purposes of this work due to visible leaching of the **RFT** catalyst when swollen in aqueous or organic solutions (even under non-stirred conditions), and in sufficient amounts to catalyze the reaction.[28]

• *Approach II:* In order to gain additional insights into the effects of the gel-like microenvironment of the chromophore on the catalytic activity, we also explored a second strategy based on flavin-based catalysts covalently tethered to a complementary gelator structure. In principle, such systems may provide a different catalyst-gel network interface compared to the previous non-covalent approach, which could have an impact on the catalytic process.
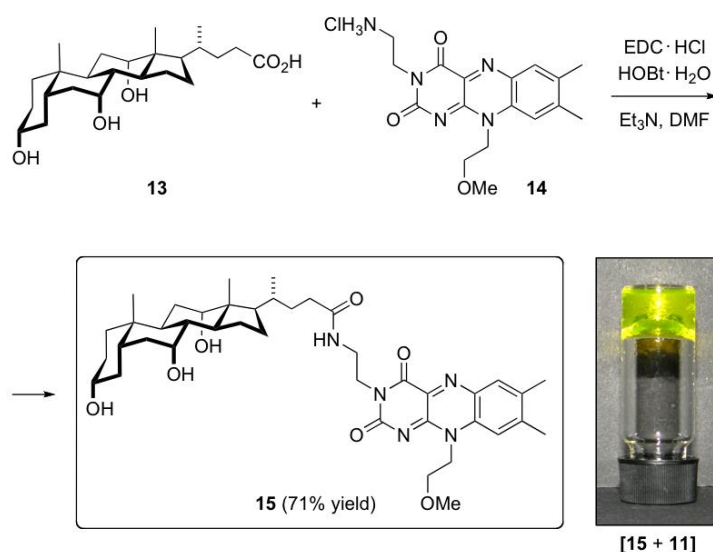
Fig. 4 Synthesis of catalyst **15** and hydrogel formation upon being co-assembled with gelator **11** (approach II). Substrate **1** was incorporated into the gel for comparative kinetic experiments as described in Table 2.

Herein, we synthesized conjugate **15** by EDC-coupling of cholic acid (**13**) and flavin derivative **14** bearing an ethylene linker with a primary amine (Figure 4). Although **15** did not present gelation ability, its design allowed further co-assembly with structurally related gelator **11** (sodium deoxycholate) under adequate concentrations in order to obtain stable

100

hydrogels. UV-vis and fluorescence spectra of this hybrid showed no shift of the characteristic absorption and emission bands, respectively, in comparison to the solution state. In terms of scope, this behavior was also found with alternative conjugates (*e.g.*, [**15** + **12**]).[28] Therefore, although no firm conclusions could be drawn regarding the hydrophobicity of the chromophore environment in the gel matrix, preservation of the spectroscopic properties made this type of hydrogels also suitable as reaction vessel for testing the photooxidation of **1**. However, at least in our case, the expected better organization of the catalyst within the gel network defined by gelator **11** did not show a significant effect on the photooxidation rate (Table 2, entry 12 *vs* 10).

• *Approach III:* Finally, photooxidation of **1** was also studied using gel-based materials in which the flavin-based catalyst was forming part, as an indispensable component, of the supramolecular gel network. This approach was inspired in a recent report from Nandi and co-workers, in which the formation of a highly fluorescent H-bounded complex between riboflavin and 6-methyl-1,3,5-triazine-2,4-diamine (**16**) (1:1 molar ratio) was described to prepare a stable hydrogel.[51] We found that riboflavin could be also exchanged by **RFT** (Figure 5) to form an analogous hydrogel, which was more appropriate as a model medium for our studies. Interestingly, the use of **RFT** instead of riboflavin allowed the formation of hydrogels with higher thermal-mechanical stability, and without significant bleaching even after 2 h of irradiation.[28] In general, the results obtained with this system (Table 2, entry 13), even at much higher catalyst loading, showed *ca.* 4-6-fold reduction of the catalyst activity in comparison to the values obtained using the approach I.[28] Thus, the degree of participation of the photocatalyst in the construction of the gel network resulted inversely correlated to its catalytic activity. Kinetic studies revealed a lower reaction conversion even under 4-fold increased irradiation times (*i.e.*, 63% conversion after 480 min), which could be explained by unfavorable substrate-catalyst interactions, significant restricted diffusion of reagents and/or hindered excimer formation.

Control experiments were done with related hydrogels made of riboflavin or **RFT** and salicylic acid instead of acetoguanamine. In these cases, the different H-bonding moieties caused quenching of photoluminescence due to a less efficient formation of a hydrophobic core based on p-stacking interactions, which seems to be responsible for the stabilization of the excited state by resonance.[51] As a consequence, the photooxidation of **1** was completely inhibited in these hydrogels,[28] pointing out the importance of the specific

H-bonding pattern (involving the isoalloxazine moiety of the riboflavin catalyst) in this approach.
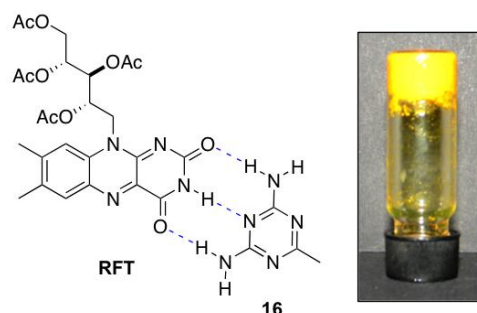
Fig. 5 Bicomponent supramolecular hydrogel made of an equimolar mixture of **RFT** and **16** (approach III). Substrate **1** was incorporated into the gel for comparative kinetic experiments as described in Table 2.

A comparative analysis of the first-order kinetics plots[28] (Figure 6) clearly demonstrated the possibility of fine-tuning the photooxidation kinetics (*i.e.*, k_{obs} range ~ 0.005-0.073 min^{-1}) depending on the characteristics of the gel media (see next section for extended discussion). In addition, it should be noted that both substrate enantiomers were equally photooxidated, as confirmed by HPLC,[28] in all gel media tested in this work. This result suggests the absence of favored hydrophobic interactions between one specific enantiomer and the corresponding gel network.
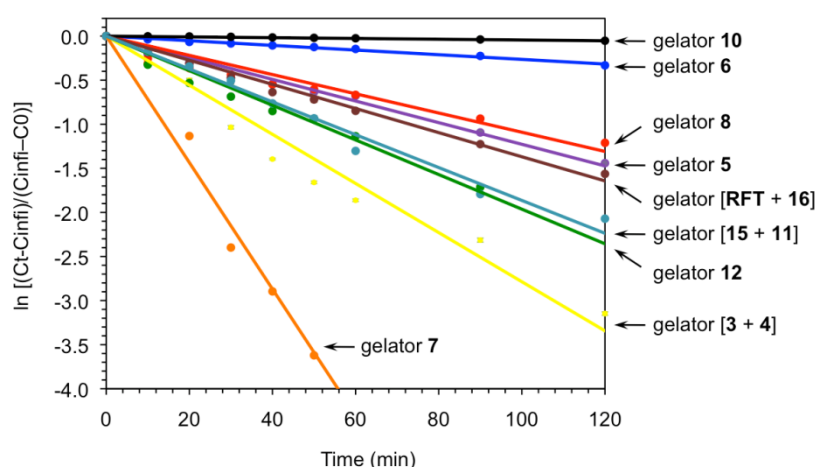
Fig. 6 First-order kinetics plots of **RFT**-catalyzed photooxidation of **1** in different gel media according to selected entries in Table 2. Each data point represents the average of two independent measurements. Abbreviations: Cinfi = final concentration, at infinite time; Ct = concentration at a given time t; C0 = initial concentration, at t = zero time.

102

Gel properties and relationships with kinetics

Mechanical, thermal, morphological and aeration efficiency of all gels were studied as part of their characterization, and to identify any underlying connection with the reaction kinetics (Table 3). Thus, oscillatory rheological experiments confirmed the viscoelastic nature of all systems, showing an average storage modulus (G') with low dependence on the frequency (*i.e.*, $G' \sim \omega^{0.01\text{-}0.06}$), and at least one order of magnitude higher than the loss modulus (G'') within the linear regime.[28] The higher internal resistance was observed for some biopolymer-based hydrogels (Table 3, entries 2, 4 $\Rightarrow$ gelators **4**, **5**) according to the lower loss factors (tan $\delta \leq 0.1$). Interestingly, similar damping properties were also found for the bicomponent supramolecular hydrogel (Table 3, entry 13 $\Rightarrow$ gelator [**RTF** + **16**]), whereas other LMW hydrogels were slightly weaker (Table 3, entries 5, 8-9 $\Rightarrow$ gelators **6**, **9**, **10**). In contrast, methylcellulose, some bile acid and serine based LMW gelators (Table 3, entries 1, 7, 10-11 $\Rightarrow$ gelators **3**, **8**, **11**, **12**) presented poorer mechanical strength.

In general, the same tendency was observed after incorporation of reagents (under optimized concentrations) into the gel matrices, albeit with a certain detriment of the thermal stability. For instance, the decrease of the T_{gel} value upon doping was in general relatively small ($\Delta T_{gel} \sim 5\text{-}15\%$) suggesting preservation of the global gel structure, which was further confirmed by field emission electron scanning microscopy (FESEM).[28] The only exception was found with the hydrogel made of cystine-based gelator **6** ($\Delta T_{gel} \sim 42\%$), which was also found useless as reaction vessel. If necessary, a possibility to compensate the thermal destabilization of the gels after doping would be to enhance the gelator concentration, which in some cases could be 4-foldincreased without causing major changes on the rate constants.

Figure 7 provided some insights on the microstructure of the different gel systems. Interestingly, well-defined and entangled fibrillar networks were in general associated to lower reaction rates in the case of LMW hydrogels ($k_{obs} < 0.005$ min^{-1}; *e.g.*, Figures 7d, 7h), whereas extended or wrinkled laminated structures with visible porosity or secondary clusters seemed to favor the reaction in both LMW and polymer gels (0.005 min$^{-1} < k_{obs} <$ 0.03 min^{-1}; *e.g.*, Figures 7a, 7c, 7f, 7j-l). The only exceptions to the rule were the fastest kinetics observed in the densely packed fibrillar organogel made of **7** (Figure 7e), and the relatively slow reaction in the hydrogel made of **11** in PBS (Figure 7i). Nevertheless, one

103

should be very prudent regarding specific conclusions based on SEM images, as solvation in the gel phase may modify the structural packing in comparison to the dried state.[21, 52]
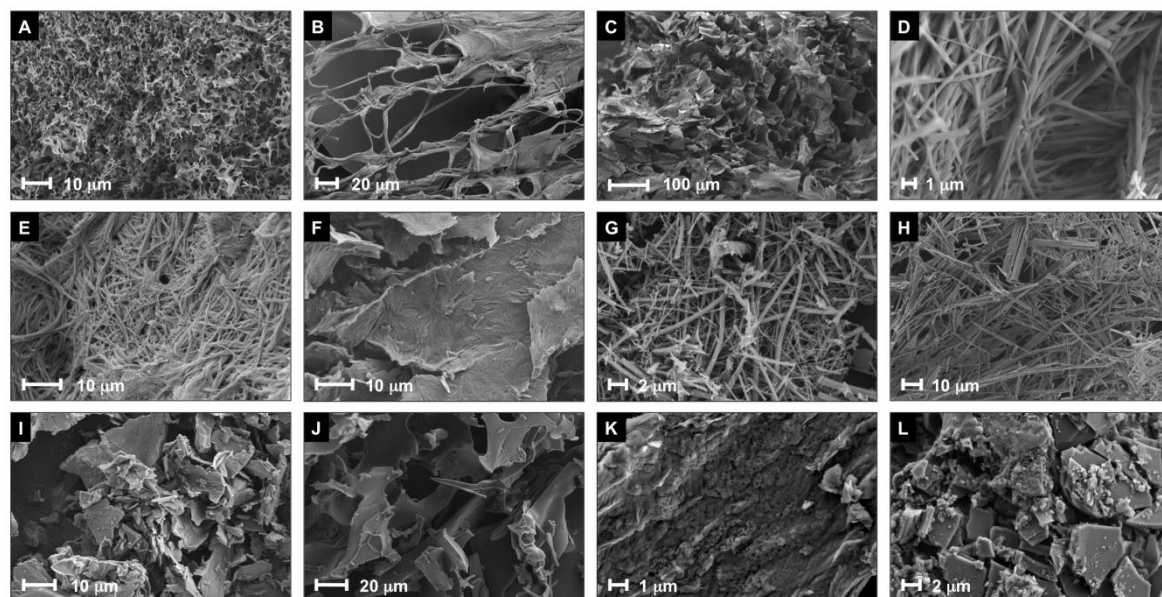
Fig. 7 Selected FESEM images of xerogels prepared by the freeze-drying method from the corresponding doped gels (*i.e.*, prepared in the presence of substrate/catalyst under optimized conditions as described in Table 2). Gelator concentrations are given in parentheses: A) xerogel made of **3** (5% w/v); B) xerogel made of **4** (2% w/v); C) xerogel made of **5** (1.5% w/v); D) xerogel made of **6** (0.3% w/v); E) xerogel made of **7** (0.5% w/v); F) xerogel made of **8** (3% w/v); G) xerogel made of **9** (3% w/v); H) xerogel made of **10** (2% w/v); I) xerogel made of **11** (2% w/v); J) xerogel made of **12** (2% w/v); K) xerogel made of [**15** + **11**] (2% w/v); L) xerogel made of [**RFT** + **16**] (3.5% w/v). See ESI† for additional images of both pure and doped gels.

Finally, although material rigidity could not be directly associated to product yield, the lower conversions were obtained in LMW gels of relatively high strength (*e.g.*, Table 3, entries 5, 9). However, contrasting results obtained with other LMW and polymer gels (*e.g.*, Table 3, entries 1, 8, 11) suggested the influence of more complex variables connected to the diffusion of reagents and/or excimer formation. Indeed, a reasonably good correlation was found between reaction rates and the aeration efficiency of most of the gels before saturation. This may be in agreement with better availability of O_2 molecules for the photocatalytic cycle inside the materials. This trend was typically observed for both LMW and polymer gels when they were considered separately, suggesting a multivariate dependence of the aeration phenomenon. Thus, an increase of the aeration efficiency was

generally accompanied by an increment, albeit not proportionally, of both conversion and reaction rate.[28]

Table 3 Representative thermo-mechanical properties and aeration efficiency of gels used as reaction vessels for **RFT**-catalyzed photooxidation of **1**.[a]

entry	gelator system	solvent system	G' (Pa)[b]	G'' (Pa)[b]	tan δ	Tgel ($\pm$ 2 °C) (pure)[c]	Tgel ($\pm$ 2 °C) (doped)[d]	Aeration coef. (s^{-1})[e]	conv. (%)[f]	k_{obs} ($\times$ 10^{-3} min^{-1})
1	**3**	H$_2$O	119$\pm$39	81$\pm$64	0.64$\pm$0.33	34	31	0.041	83	17.3$\pm$0.07
2	**4**	H$_2$O	2471$\pm$338	192$\pm$31	0.08$\pm$0.03	51	43	0.066	90	20.8$\pm$0.49
3	**3+4**[d]	H$_2$O	1549$\pm$46	245$\pm$48	0.16$\pm$0.04	38	36	0.069	96	28.2$\pm$2.76
4	**5**	H$_2$O	166$\pm$31	6$\pm$3	0.04$\pm$0.02	53	46	0.029	76	12.3$\pm$0.42
5	**6**	H$_2$O/DMSO[g]	11020$\pm$1483	1494$\pm$231	0.14$\pm$0.04	72	42	0.047	23	2.7$\pm$0.21
6	**7**	CH$_3$CN	26229$\pm$868	5207$\pm$1180	0.20$\pm$0.04	80	72	0.093	100	72.6$\pm$8.34
7	**8**	H$_2$O	162927$\pm$8676	72969$\pm$511	0.45$\pm$0.02	57	53	0.051	70	11.0$\pm$0.07
8	**9**	H$_2$O	329206$\pm$22091	82532$\pm$1403	0.14$\pm$0.01	91	78	0.066	69	11.5$\pm$0.57
9	**10**	0.5 M NaCl[h]	28995$\pm$1371	2809$\pm$151	0.12$\pm$0.03	98	93	0.034	14	0.5$\pm$0.07
10	**11**	PBS[i]	293$\pm$24	240$\pm$2	0.85$\pm$0.03	56	47	0.050	55	19.3$\pm$3.18
11	**12**	H$_2$O/AcOH[j]	235$\pm$21	85$\pm$21	0.36$\pm$0.06	64	53	0.065	100	19.7$\pm$0.64
12	**15+11**[e]	PBS[i]	196$\pm$61	160$\pm$47	0.82$\pm$0.01	56	49	0.057	54	18.7$\pm$0.07
13	**RFT+16**[f]	H$_2$O	21803$\pm$4052	1734$\pm$7	0.08$\pm$0.02	92	79	0.052	63	13.5$\pm$1.48

[a] See ESI† for additional information. [b] Average values calculated from randomized DTS (dynamic time sweep) experiments carried out within the linear viscoelastic regime as defined by DFS (dynamic frequency sweep) and DSS (dynamic strain sweep) measurements. Conditions: Frequency = 1 Hz, strain = 0.1%, temperature = 25 °C. [c] Gels prepared in the absence of substrate and catalyst, using the gelator concentration shown in Table 2. [d] Concentration values: Substrate **1** (doped gels) = 5.0 mmol L^{-1}, **RFT** catalyst (doped gels) = 10 mol%, total solvent volume = 1 mL, and gelator concentration as defined in Table 2. Irradiation time = 120 min, except for the organogel made in CH$_3$CN (entry 6) that was 60 min. All T_{gel} values were determined by IFM. [e] Aeration coefficient determined using dissolved oxygen microelectrode at T = 23 $\pm$ 1 °C and a constant air flow rate at 0.06 bar. Estimated error = $\pm$ 3 $\times$ 10^{-3} s^{-1}. Note that this coefficient does not represent a measurement for the reaction rate within the bulk material. [f] Reaction conditions: Light source = LED blue visible light (λ_{max} = 440 nm, 3 W); T = 20 $\pm$ 1 °C. Reaction conversion over time for kinetics calculations was determined by ^{1}H NMR analysis. Estimated error = $\pm$ 1.5%. [g] Weight ratio = 1:1. [h] Molar ratio of gelator system [**15** : **11**] = 1 : 96.5. [i] Molar ratio of gelator system [**RFT** : **16**] = 1 : 1. [j] Volume ratio = 95/5. [k] Phosphate buffer solution, pH 7.5. [l] Volume ratio = 80/20. Abbreviations: G' = storage modulus; G'' = loss modulus; tan δ = loss factor; conv. = conversion; k_{obs} = rate constant.

2.4. Summary and conclusion

The foregoing results demonstrated that both micellar and soft gel media, including LMW and biopolymer-based gels, may serve as tunable reaction vessels for the **RFT**-catalyzed aerobic photooxidation of 1-(4-methoxyphenyl)ethanol (**1**) under LED blue visible light irradiation (λ_{max} = 440 nm). Photooxidation rates of **1** in hydrogel media were on average 10-20-fold lower than those in stirred solutions, but only 1-3-fold lower under non-stirred conditions. Moreover, the gelators could be recycled without detriment of their gelation ability and reaction conversion. Detailed kinetics studies confirmed first-order rates and the possibility to be fine-tuned according to the characteristics of the confined media. In general, physical entrapment of both the catalyst and the substrate under optimized concentrations into various hydrogel matrices (approach I) permitted reaction conversions between 55-100% within 120 min (TOF ~ 0.045-0.08 min^{-1}), albeit with kinetics rates *ca.* 1-3-fold lower than in solution under equivalent non-stirred conditions. Remarkably, in contrast to the reaction in CH_3CN solution, the fibrillar organogel medium made of bisamide gelator **7** not only prevented photo degradation of the catalyst but also afforded full conversion in less than 60 min (TOF ~ 0.167 min^{-1}; k_{obs} ~ 0.073 min^{-1}) without the need of thiourea. Other strategies (approaches II, III) based on a higher degree of organization of the catalyst within the gel network led to slower reaction rates in comparison to the first approach. In addition, despite the presence of a chiral environment (approaches I, II) both substrate enantiomers were equally oxidized, suggesting the absence of selective interactions with the fibrillar gel structure. Although no unambiguous associations could be made between reaction kinetics and morphology of the gels, the former was generally in good agreement with the relative aeration efficiency of the gel media. This study constitutes one of the few reports so far dealing with photochemical reactions inside gels. The comprehensive kinetics analyses and the demonstrated influence of the local environment may help to design new gel materials as biomimetic nanoreactors for photochemical transformations.

→ Additional information on compound synthesis and characterization, gel characterization and kinetic experiments can be found in the ESI on the enclosed CD.

2.5. References

1   D. M. Vriezema, M. C. Aragonés, J. A. A. W. Elemans, J. J. L. M. Cornelissen, A. E. Rowan and R. J. M. Nolte, *Chem. Rev.*, 2005, **105**, 1445-1489.

2   S. A. Bode, I. J. Minten, R. J. M. Nolte and J. J. L. M. Cornelissen, *Nanoscale*, 2011, **3**, 2376-2389.

3   L. Marchetti and M. Levine, *ACS Catal.*, 2011, **1**, 1090-1118.

4   J. Rebek, *Acc. Chem. Res.*, 2009, **42**, 1660-1668.

5   B. Breiner, J. K. Clegg and J. R. Nitschke, *Chem. Sci.*, 2011, **2**, 51-56.

6   V. Ramamurthy and A. Parthasarathy, *Isr. J. Chem.*, 2011, **51**, 817-829.

7   M. Yoshizawa, J. Klosterman and M. Fujita, *Angew. Chem. Int. Ed.*, 2009, **48**, 3418-3438.

8   Y. Inokuma, M. Kawano and M. Fujita, *Nature Chem.*, 2011, **3**, 349-358.

9   R. K. O'Reilly, *Phil. Trans. R. Soc. A*, 2007, **365**, 2863-2878.

10   A. Ostafin and Y.-C. Chen, in *Kirk-Othmer Encyclopedia of Chemical Technology*, John Wiley and Sons, 2009, pp. 1-18.

11   For selected examples, see: a) A. Maldotti, A. Molinari and R. Amadelli, *Chem. Rev.,* 2002, **102***, 3811-3836; b) D. G. Shchukin and D. V. Sviridov, *J. Photochem. Photobiol. C*, 2006, **7**, 23-39; c) J. Matsumoto, T. Matsumoto, Y. Senda, T. Shiragami, M. Yasuda, *J. Photochem. Photobiol. A,* 2008, **197**, 101–109; d) C. Harris and P. V. Kamat, *ACS Nano*, 2009, **3**, 682-690; e) B. Cojocaru, S. Neatu, V. I. Parvulescu, K. Dumbuya, H.-P. Steinrück, J. M. Gottfried, C. Aprile, H. Garcia and J. C. Scaiano, *Phys. Chem. Chem. Phys.*, 2009, **11**, 5569–5577; f) F. A. Leibfarth, K. M. Mattson, B. P. Fors, H. A. Collins and C. J. Hawker, *Angew. Chem. Int. Ed.*, 2013, **52**, 199-210.

12   For selected reviews on gel materials and applications, see: a) L. A. Estroff and A. D. Hamilton, *Chem. Rev.*, 2004, **104**, 1201-1218; b) N. M. Sangeetha and U. Maitra, *Chem. Soc. Rev.*, 2005, **34**, 821-836; c) P. Xie and R. Zhang, *J. Mater. Chem.*, 2005, **15**, 2529-2550; d) M. George and R. G. Weiss, *Acc. Chem. Res.*, 2006, **39**, 489-497; e) G. C. Maity, *J. Phys. Sci.*, 2007*, **11**, 156-171; f) R. V. Ulijn and A. M. Smith, *Chem. Soc. Rev.*, 2008, **37**, 664-675; g) A. R. Hirst, B. Escuder, J. F. Miravet and D. K. Smith, *Angew. Chem. Int. Ed.*, 2008, **47**, 8002-8018; h) S. Banerjee, R. K. Das and U. Maitra, *J. Mater. Chem.*, 2009, **19**, 6649-6687; i) M. O. M. Piepenbrock, G. O. Lloyd, N. Clarke, J. W.

Steed, *Chem. Rev.*, 2010, **110**, 1960-2004; f) D. J. Adams, *Macromol. Biosci.*, 2011, **11**, 160-173; g) A. Dawn, T. Shiraki, S. Haraguchi, S. Tamaru and S. Shinkai, *Chem. Asian J.*, 2011, **6**, 266-282; h) X. Yang, G. Zhang and D. Zhang, *J. Mater. Chem.*, 2012, **22**, 38-50; i) A. Noro, M. Hayashi and Y. Matsushita, *Soft Matter*, 2012, **8**, 2416-2429.

[13] a) D. D. Díaz, D. Kühbeck and R. J. Koopmans, *Chem. Soc. Rev.*, 2011, **40**, 427-448, and references therein; b) A. Shumburo and M. C. Biewer, *Chem. Mater.*, 2002, **14**, 3745-3750.

[14] M. Pagliaro, R. Ciriminna and G. Palmisano, *Chem. Soc. Rev.*, **2007**, *36*, 932-940; b) F. Rodríguez-Llansola, J. Miravet and B. Escuder, *Chem. Eur. J.*, 2010, **16**, 8480-8486; c) P. D. Wadhavane, M. A. Izquierdo, F. Galindo, M. I. Burguete and S. V. Luis, *Soft Matter*, **2012**, *8*, 4373-4381.

[15] There is a vast literature dealing with photoresponsive moieties covalently incorporated in gelator structures for tuning either the *sol*-to-*gel* phase transition or the mechanical robustness of the material upon light-induced isomerization or polymerization reactions. For representative examples, see those collected in reference 13.

[16] S. Bhat and U. Maitra, *Molecules*, 2007, **12**, 2181-2189.

[17] A. Dawn, N. Fujita, S. Haraguchi, K. Sada and S. Shinkai, *Chem. Commun.*, 2009, 2100-2102; b) A. Dawn, N. Fujita, S. Haraguchi, K. Sada, S.-i. Tamaru and S. Shinkai, *Org. Biomol. Chem.*, 2009, **7**, 4378-4385.

[18] For selected examples of light-harvesting studies in hybrid non-covalent assemblies, see: a) M. Kercher, B. König, H. Zieg and L. De Cola, *J. Am. Chem. Soc.*, 2002, **124**, 11541-11551; b) H. F. M. Nelissen, M. Kercher, L. De Cola, M. C. Feiters and R. J. M. Nolte, *Chem. Eur. J.*, 2002, **8**, 5407-5414; c) M. Braun, S. Atalick, D. M. Guldi, H. Lanig, M. Brettreich, S. Burghardt, M. Hatzimarinaki, E. Ravanelli, M. Prato, R. van Eldik and A. Hirsch, *Chem. Eur. J.*, 2003, **9**, 3867-3875; d) B. Ferrer, G. Rogez, A. Credi, R. Ballardini, M. T. Gandolfi, V. Balzani, Y. Liu, H.-R. Tseng, and J. F. Stoddart, *Proc. Natl. Acad. Sci. U.S.A.*, 2006, **103**, 18411-18416; e) K. V. Rao, K. K. R. Datta, M. Eswaramoorthy and S. J. George, *Chem. Eur. J.*, 2012, **18**, 2184-2194, and references therein.

[19] K. V. Rao, K. K. R. Datta, M. Eswaramoorthy and S. J. George, *Angew. Chem. Int. Ed.*, 2011, **50**, 1179-1184.

[20] P. Jana, S. Maity, S. K. Maity, P. K. Ghorai and D. Haldar, *Soft Matter*, 2012, **8**, 5621-5628.

21   S. Samai, P. Ghosh and K. Biradha, *Chem. Commun.*, 2013, DOI: 10.1039/C2CC34901A.

22   G. H. Pollack, Cells, Gels and the Engines of Life: A New, Unifying Approach to Cell Function, Ebner & Sons, Seattle WA, USA, 2001.

23   B. Rybtchinski, *ACS Nano*, 2011, **5**, 6791-6818.

24   J. N. Hunt, K. E. Feldman, N. A. Lynd, J. Deek, L. M. Campos, J. M. Spruell, B. M. Hernandez, E. J. Kramer and C. J. Hawker, *Adv. Mater.*, 2011, **23**, 2327-2331.

25   Additional saturation with O_2 has been proven to quench the flavin excited state, see: H. Schmaderer, P. Hilgers, R. Lechner and B. König, *Adv. Synth. Catal.*, 2009, **351**, 163-174.

26   J. Svoboda, H. Schmaderer and B. König, *Chem. Eur. J.*, 2008, **14**, 1854-1865.

27   For the study of other photochemical reactions in micellar solutions of NaDC, see: M. Pattabiraman, L. S. Kaanumalle and V. Ramamurthy, *Langmuir*, 2006, **22**, 2185-2192.

28   See ESI for details.

29   V. Massey, *Biochem. Soc. Trans.*, 2000, **28**, 283-296, and references therein.

30   Y. Imada, T. Kitagawa, T. Ohno, H. Iida and T. Naota, *Org. Lett.*, 2010, **12**, 32-35, and references therein.

31   R. Lechner, S. Kümmel and B. König, *Photochem. Photobiol. Sci.*, 2010, **9**, 1367-1377, and references therein.

32   J. F. Teichert, T. den Hartog, M. Hanstein, C. Smit, B. ter Horst, V. Hernandez-Olmos, B. L. Feringa and A. J. Minnaard, *ACS Catal.*, 2011, **1**, 309-315.

33   Y. Imada, H. Iida, T. Kitagawa and T. Naota, *Chem. Eur. J.*, 2011, **17**, 5908-5920.

34   J. Dad'ová, E. Svobodová, M. Sikorski, B. König and R. Cibulka, *ChemCatChem.*, 2012, **4**, 620-623.

35   R. Lechner and B. König, *Synthesis*, 2010, **10**, 1712-1718.

36   W. A. Massad, Y. Barbieri, M. Romero and N. A. Garcia, *Photochem. Photobiol.*, 2008, **84**, 1201-1208.

37   O. Lu, G. Bucher and W. Sander, *Chem. Phys. Chem.*, 2004, **5**, 47-56.

38   R. Cibulka, R. Vasold and B. König, *Chem. Eur. J.*, 2004, **10**, 6223-6231, and references therein.

39   For a detailed mechanistic study, see: U. Megerle, M. Wenninger, R.-J. Kutta, R. Lechner, B. König, B. Dick and E. Riedle, *Phys. Chem. Chem. Phys.*, 2011, **13**, 8869-8880.

40   Although the data of a few examples suggested a complex kinetic in nature (see ESI†), first-order assumptions provided the best fit in each case. For our experiments in air, and

from a mechanistic point of view, this was also consistent with an O_2 concentration well above the saturating concentration for the reaction with the excited state of the sensitizer.

[41] In general, photooxidation of benzyl alcohols in aqueous and acetonitrile solutions yields the corresponding aldehydes as the sole product. However, traces of benzoic acids have been occasionally observed with immobilized flavins due to overoxidation (see ref. 24).

[42] M. Pattabiraman, L. S. Kaanumalle and V. Ramamurthy, *Langmuir,* 2006, **22**, 2185-2192.

[43] M. Marchena and F. Sanchez, *Prog. React. Kinet. Mech.,* 2010, **35**, 27-80.

[44] H. Svobodová, V. Noponen, E. Kolehmainen and E. Sievänen, *RSC Adv.*, 2012, **2**, 4985-5007.

[45] H. Koshima, W. Matsusaka and H. Yu, *J. Photochem. Photobiol. A*: *Chem.*, 2003, **156**, 83-90.

[46] M. I. Burguete, M. A. Izquierdo, F. Galindo and S. V. Luis, *Chem. Phys. Lett.,* 2008, **460**, 503-506, and references therein.

[47] J. Svoboda and B. König, *Chem. Rev.*, 2006, **106**, 5413-5430.

[48] For the use of chiral host molecules for enantioselective photoreactions via chirality transfer, see for example: P. Selig and T. Bach, *J. Org. Chem.*, 2006, **71**, 5662-5673, and references therein.

[49] Molecular aggregation has been also found to play an important role in some catalytic processes dealing with chirality amplification, see for example: D. G. Blackmond and M. Klussmann, *Chem. Commun.,* 2007, 3990-3996.

[50] Detailed fotodegration studies of riboflavin derivatives have been carried out under different conditions. For selected examples, see: a) I. Ahmad, Q. Fasihullah and F. H. M. Vaid, *Photochem. Photobiol. Sci.*, 2006, **5**, 680-685, and references therein; b) I. Ahmad, Q. Fasihullah and F. H. M. Vaid, *J. Photochem. Photobiol. B: Biol.,* 2006, **82**, 21-27; c) H. Görner, *J. Photochem. Photobiol. B: Biol.,* 2007, **87**, 73-80; d) I. Ahmad, S. Ahmed, M. A. Sheraz and F. H. M. Vaid, *J. Photochem. Photobiol. B: Biol.,* 2008, **93**, 82-87; e) I. Ahmad, S. Ahmed, M. A. Sheraz, F. H. M. Vaid and I. A. Ansari, *Int. J. Pharm.*, 2010, **390**, 174-182; f) M. Insinska-Rak, A. Golczak and M. Sikorski, *J. Phys. Chem. A*, 2012, **116**, 1199-1207.

[51] Saha, B. Roy, A. Esterrani and A. K. Nandi, *Org. Biomol. Chem.*, 2011, **9**, 770-776.

[52] K. A. Houston, K. L. Morris, L. Chen, M. Schmidtmann, J. T. A. Jones, L. C. Serpell, G. O. Lloyd and D. J. Adams, *Langmuir*, 2012, **28**, 9797-9806.

111

3. Synergistic computational-experimental approach to improve ionene polymer-based functional hydrogels[i]
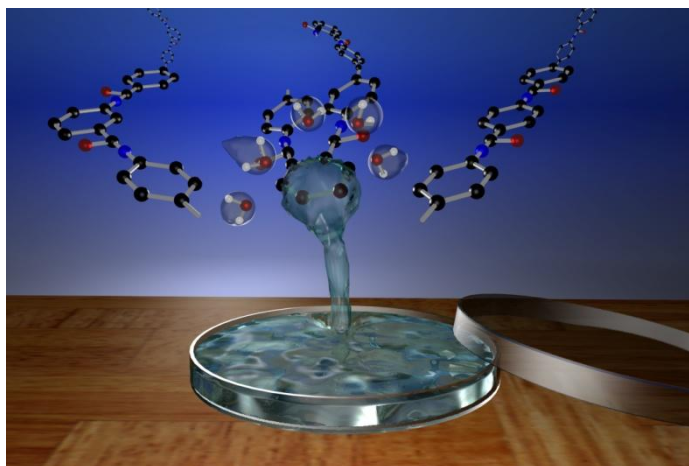
The manifold applications of ionene-based materials such as hydrogels in daily life, biomedical sciences and industrial processes are a consequence of their unique physical and chemical properties, which are governed by a judicious balance between multiple non-covalent interactions. However, one of the most critical aspects identified for a broader use of different polyelectrolytes is the need of raising their gelation efficiency. In this work, we focus on surfactant-free ionene polymers **1**-**3** containing DABCO and *N,N'-(x-phenylene)dibenzamide* (*x = ortho-/meta-/para-*) linkages as model systems to develop a combined computational-experimental approach to improve the hydrogelation through a better understanding of the gelation mechanism. Molecular dynamics simulations of isomeric ionenes **1**-**3** with explicit water molecules point out remarkable differences in the assembly of the polymeric chains in each case. Interchain regions with high degree of hydration (i.e., polymer···water interactions) and zones dominated by polymer···polymer interactions are evident in the case of *ortho-* (**1**) and *meta-* (**2**) isomeric ionenes, whereas domains controlled by polymer···polymer interactions are practically inexistent in **3**. In excellent agreement,

ortho-ionene **1** provides experimentally the best hydrogels with unique features such as thixotropic behavior and dispersion ability for SWNTs.[ii]

3.1. Introduction

Polyelectrolytes are of fundamental and practical importance since many of them play critical biological functions in nature.[1-3] Within this type of macromolecules, synthetic ionenes represent an important subgroup in which the ionic groups form part of the polymer backbone.[4-10] In general, the term refers to polycations carrying quaternary ammonium as the charged species. From a synthetic point of view, ionenes are typically accessible either by (1) chain or step polymerization of suitable monomers (e.g., Menshutkin reaction between bis-tertiary amines and activated dihalides, self-polyaddition of aminoalkylhalides) or (2) cationic functionalization of reactive precursor polymers.[11, 12] Since the first synthesis of an ionene more than 80 years ago by Marvel and co-workers,[13, 14] they have been the subject of intensive investigations in diverse fields including chemistry, biology, physics, medicine and materials science. Such tremendous research activity has culminated with the development of manifold applications of these macromolecular materials in daily life, biosciences and industrial processes (e.g., as antibacterial agents or building blocks for the preparation of chromatography stationary phases, symplexes or functional gels, among other uses).[4] The unique physical and chemical properties of these polymers are the result of a judicious balance between multiple interactions including hydrophobic, charge transfer and long-ranged electrostatic interactions. As for all polycations, besides the density and charge distribution along the

---

[ii] All results related to computational and mechanistic studied as illustrated in Figures 3, 4 and 10 in sections 3.2.2. and 3.2.4. have been conducted by D. Zanuy, D. E. López-Pérez and G. Revilla-López. All other experiments have been carried out by J. Bachl.

backbone, the nature of the counterion, the molecular weight, flexibility and H-bonding capability of the polymer chain are also critical aspects that may markedly influence the conformation and dynamics of polymer chains. Additionally, their considerable structural versatility (e.g., achievable via counterion exchange, chemical modification of monomers, polymerization method) and key features such as electrostatic stabilization of colloids and tunability of their mechanical properties can be used to induce the formation of stable polyelectrolyte hydrogels for applications in biomedicine, engineering and food science.[15,] [16] Yet one of the critical technical issues identified for the practical use of a broader range of organic polyelectrolytes is the necessity of increasing the efficiency of gelation.[17] However, despite numerous efforts to establish structure-property relationships, the understanding of the gelation mechanism of such complex systems remains a major challenge. This is mainly due to (1) non-uniform distribution of ionic groups along the polymer chain,[18, 19] and (2) the fact that several experimental results are typically poorly described from a microscopic point of view, which makes difficult the prediction of gelation properties through simple theoretical models and the rational design of more efficient gelling agents. In this sense, conversely to other polyelectrolytes, ionenes constitute ideal systems to study ionic aggregation phenomena since the ionic sites are precisely situated along the macromolecular unit. On the other hand, theoretical description of polyelectrolyte hydrogels at the atomistic level is very challenging because of the conformational complexity of polymer chains, which increases with the number of degrees of freedom in repeat units, the description of excluded volume interactions involved in these hydrophilic polymeric networks containing large amounts of water, and the huge dimensions of the systems necessary to represent these water-swollen ionic aggregates.[20] Thus, in spite of the interest in polyelectrolyte hydrogels, the intrinsic complexity of gelated systems and the significant amount of computational resources needed to describe

their chemical details and physical properties, have severely restricted their atomistic

modeling. However, in the last few years, computational advances (i.e., parallel computer

architectures and efficient scalability of computer programs) have allowed the study of

some of the most important polymeric hydrogels.[21-25] Because of these recent advances,

approaches combining computer simulations and experimental methodologies are currently

expected to be successful in the rational design of hydrogels with advanced properties.

Herein, we reasoned that using different structural isomers of phenylenediamine as

molecular core for the construction of ionene polymers would lead to different types of

cross-linked networks in water and, hence, potential superior hydrogels. We demonstrate

that a combined computational-experimental approach can be used to rationally design

more efficient ionene hydrogelators in terms of gelation kinetics as well as mechanical and

functional properties of the resulting hydrogels.

3.2. Results and discussion

Hydrogels based on surfactant-free linear ionenes having *N,N'-(-para-*
phenylene)dibenzamide linkages were first described by Yoshida and co-workers.[26]
Motivated by the remarkable properties and potential applications shown by these systems,
we envisioned the possibility to develop a combined computational-experimental paradigm
with the aim of enhancing the gelation efficiency of these valuable functional materials.
Among the number of tertiary diamines that can be used as spacers for building the ionenes
we focused for this work on 1,4-diazabicyclo[2.2.2]octane (DABCO), as this moiety has
also proven useful in the development of polycations for other applications such as
template synthesis of porous nanomaterials[27] and gene delivery.[28] Our approach takes
advantage of the structural isomerism of the phenylenediamine core (view Figure 1).
Depending on the substitution pattern of the phenyl ring, it is possible to grow the two
polymeric arms of the ionene forming different angles to each other (i.e., $\theta = 60°$, 120° or
180°). Such well-defined topological variations not only impact the net dipole moment of

115

the polymers but also their inter- and intramolecular interactions, which are expected to influence significantly the gelation phenomenon. Thus, information provided by advanced computational modeling of these interactions at the atomistic level combined with experimental parameters of the ionenes could serve as a versatile and accurate tool to predict their hydrogelation ability.
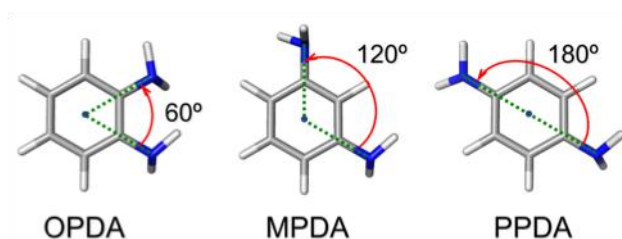
Fig. 1 Phenyl ring substitution angles in phenylenediamine structural isomers: OPDA = *ortho*-phenylenediamine; MPDA = *meta*-phenylenediamine; PPDA = *para*-phenylenediamine. Different net dipole moments derive from vector addition of the moments of the respective monosubstituted compounds.

3.2.1.   Synthesis and characterization of ionenes

Following the general procedure reported by Yoshida and co-workers, the ionenes **1**-**3** (view Figure 2) were rapidly synthesized via a two-step reaction sequence. Briefly, amidation of isomeric phenylenediamines OPDA, MPDA and PPDA with 4-(chloromethyl)benzoyl chloride in the presence of Et$_3$N in CH$_2$Cl$_2$ afforded the corresponding bis-benzamides (dielectrophilic monomers) in good yields (87-96%) upon recrystallization (Scheme S1). Their subsequent step-growth copolymerization with DABCO (dinucleophilic monomer) under equimolar conditions in DMF at 80 ºC gave the desired polycations **1**-**3** as precipitates within 2-3 days in good yields (69-98%) after a simple filtration, washing and drying protocol (ESI). Fundamental structural analyses of ionenes **1**-**3** were carried out by NMR, FT-IR, elemental analysis, SEC, TGA, and DSC measurements (Figures S1-S7). ^{1}H-NMR spectra in D$_2$O clearly distinguished the expected three sets of broad resonances for each pure polymer corresponding to aromatic protons (d ~ 7.1-8.0 ppm), benzylic methylene protons (d ~ 4.1-4.7 ppm), and methylene protons bonded to quaternized nitrogen atoms (d ~ 2.9-3.9 ppm). In agreement, FT-IR measurements exhibited broadening of the bands centered at ca. 1650 cm^{-1} (C=O

116

stretching, amide I) and 3310 cm^{-1} (N-H stretching) in comparison to precursor monomers, and new resonance features at ca. 980-1130 cm^{-1} associated to C-N$^+$ stretching vibration. In order to achieve adequate solubility and mobility of the polymers for GPC/SEC measurements (thus, avoiding undesired polymer-column interactions), counteranion exchange of chloride by bis(trifluoromethanesulfonyl)amide (TFSA) anions was carried out using LiTFSA in hot water.[29] The results for our polymer batches showed dispersity values ($Đ = M_w/M_n$) ranged from 2.1 to 2.9, which is expected for ionenes made via step-growth polymerizations and fairly consistent with previous data.[26] In principle, the differences in the observed average molecular weights for a given batch of ionenes (i.e., 8.1×10^3 Da for **1**·TFSA; 1.2×10^4 Da for **2**·TFSA; 1.7×10^4 Da for **3**·TFSA, with degrees of polymerization $n \leq 10$), could have a certain impact on the thermal, mechanical and/or gelation properties (*vide infra*).
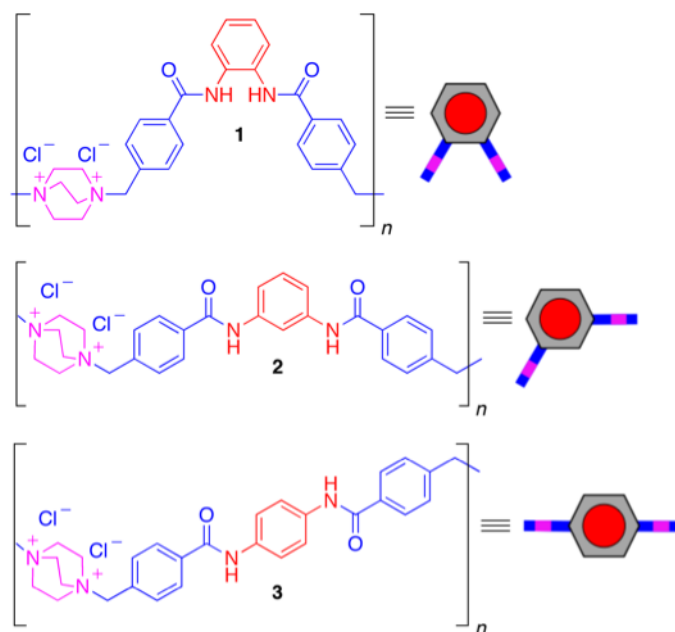
Fig. 2 Synthesized DABCO-containing ionene polymers **1-3** with *N,N'*-(*x*-phenylene)dibenzamide linkages (*x = ortho-/meta-/para-*). A symbolic representation of each ionene is given for ease of reading and interpretation.

Moreover, the lack of optical birefringence domains under crossed nicols reflected the isotropic nature of the solid polymers. Simultaneous TGA-DSC analysis of the three ionenes revealed similar thermal stability with a series of events associated to (1)

endothermic moisture/solvent loss (weight loss ~ 5-7%, T ~ 78-80 ºC) and (2) multi-step thermal degradation of the polymers. In general, the primary degradation pathway of these high charge density polymers begins at temperatures around 200-250 ºC, which correspond to the dequaternization (Hofmann elimination) of backbone nitrogens.[30] Specifically, the starting degradation temperature for **1**, **2** and **3** was estimated from the first endothermic transition in the DSC traces after solvent loss at ca. 234 for **1** and 254-255 ºC for **2-3**. In concordance with the SEC results, the higher starting decomposition temperature observed for **2** and **3** is attributed to their higher molecular weight (hence, a higher content of quaternized nitrogen groups) in comparison to **1**. These results point out the hygroscopic and amorphous nature of the polymers, as well as a relative indirect influence of the core topology on the thermal stability due to the different degree of polymerization obtained using OPDA, MPDA or PPDA. In this sense, the ionic aggregation is more prevalent when the molecular weight is higher, and hence more thermal energy is needed to dissociate the aggregates.

3.2.2.   Computational studies

With the aim of using computer simulations as a predictive tool for the hydrogelation of isomeric ionenes, we performed atomistic molecular dynamics (MD) simulations of **1–3** using molecular models formed by two polymer chains with $n = 6$ immersed in a simulation box filled with explicit water molecules. Initially, two identical ionene polymer molecules were placed at a distance of approximately 9 Å. Figure 3 provides representative snapshots of the simulated systems during the production trajectory (i.e., after thermalization and density relaxation). Apparently the assembly between the two chains of **1** and **2** is different than that of **3**. Thus, although both **1** and **2** show regions between the two chains with a high degree of hydration, zones dominated by polymer···polymer interactions are also evident. In contrast, polymer···water are practically the only intermolecular interactions in **3**, polymer···polymer interactions being very scarce (i.e., domains controlled by polymer···polymer are practically inexistent). These observations are corroborated in Figure 4a, which displays the radial distribution function for pairs of carbon atoms belonging to different chains, $g_{C-C}(r)$. Thus, the shape of the $g_{C-C}(r)$ profile is largely influenced by the molecular architecture of the ionene polymers. **2** shows a very

high and well defined peak centered at 4.2 Å reflecting that intermolecular interactions between two polymer molecules are relatively strong. This peak is less intense but still prominent in **1**, remaining centered at 4.2 Å, which is consistent with a slight reduction in the strength of polymer⋯polymer interactions with respect to **2**. However, **1** shows other well defined peaks centered at 6.2 and 9.7 Å and a shoulder at 8.2 Å, which are not detected in **2**, suggesting that the assembly formed by the two polymer chains is very stable. In contrast, **3** only shows a broad shoulder centered at 5.2 Å suggesting that interactions between the two ionene chains are very weak, or even practically inexistent.
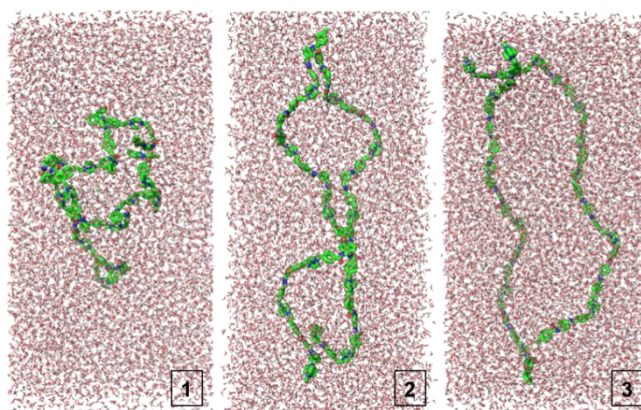
Fig. 3 Representative snapshots of the three simulated systems. The numbers refer to the ionene polymer in each case. For each case, only the central zone of the simulation box, which contains the polymer chains, is displayed while the rest has been omitted for the clarity.

Similar conclusions are reached by analyzing the existence of intermolecular polymer⋯polymer hydrogen bonding and π-π stacking interactions. Intermolecular hydrogen bonds in **1**–**3** have been examined through the radial distribution functions for N⋯O pairs belonging to different chains, $g_{N-O}(r)$, which are represented in Figure 4b. The peak centered at 3.7 Å, which reflects the formation of intermolecular N–H⋯O hydrogen bonds, is higher for **2** than for **1**, whereas the peak found for **3** is shifted to 4.2 Å and significantly smaller than for the other two systems. Quantitative analysis of the number of intermolecular hydrogen bonds with a N⋯O distance ≤ 4 Å indicates that this kind of

interactions are 1.3 and 3.3 times more abundant for **2** than for **1** and **3**, respectively. In order to compare the stability of these interactions, the life time (i.e., amount of time in which a given interaction remains formed without any disruption) of each detected interaction has been evaluated. After this, hydrogen bonds have been categorized in n groups, which reflect the number of interactions (N) with a life time comprised between (n-1)·500 ps and n·500 ps. Thus, hydrogen bonds belonging to groups with n= 1, 2, 3 or 4 refer to interactions with life times comprised within the following intervals: [0-0.5 ns], [0.5-1.0 ns], [1-1.5 ns] or [1.5-2.0 ns], respectively. Figure 4c, which depicts N against n for the three simulated systems, indicate that 46% / 35% / 6% of hydrogen bonds found in **1** show life times higher than 0.5 ns / 1.0 ns / 1.5 ns. In contrast, 91% of hydrogen bonds detected in **2** display life times lower than 0.5 ns while only 4% of such interactions remain for a time comprised between 1.0 and 1.5 ns. Finally, hydrogen bonds in **3** are not only scarce but also relatively unstable (i.e., only 5% exceed 0.5 ns and none reached 1.0 ns). According to these results, N,N'-(-*para*-phenylene)dibenzamide linkages affect not only to the abundance of intermolecular hydrogen bonds but also to the stability of such interactions. On the other hand, the radial distribution functions calculated for pairs of centers of masses of aromatic rings belonging to different chains, $g_{Xcm-Xcm}$ (i.e., X_{cm} refers to the center of masses of aromatic rings), has been used to explore the possible existence of intermolecular π-π stacking interactions. As it can be seen in Figure 4d, $g_{Xcm-Xcm}$ shows a high and relatively sharp peak centered at 3.9 Å for **2**, which becomes smaller for **1**. The practically flat profile obtained for **3** suggests that this kind of interactions is very scarce for polymers with N,N'-(*para*-phenylene)dibenzamide linkages. According to these results, the number of intermolecular π-π stacking interactions grows in the following order: **3** < **1** < **2**. Considering a threshold distance r < 6 Å, the number of interactions detected for **2** is 2.1 and 4.4 times higher than that found for **1** and **3**, respectively. Analysis of the angles

(θ) formed by the planes of two interacting rings led to an average value of 47 ± 33º, 26 ± 14º and 67 ± 26º for **1**, **2** and **3**, respectively, evidencing important differences in the relative orientation of the two aromatic entities. More specifically, π-π stacking interactions in **2** are essentially dominated by a parallel disposition of the aromatic rings (i.e., relatively close to the ideal planar configuration with $\theta \approx 0$º) while rings prefer a perpendicular arrangement in **3** (i.e., relatively close to the ideal T-shaped configuration with $\theta \approx 90$º). Interestingly, the average angle displayed by **1**, as well as its large deviation, reflects an intermediate situation, suggesting the coexistence of parallel and perpendicular configurations. Categorization of the π-π stacking interactions according to the life time is provided in Figure 4e. As it can be seen, the life time of 88% of the interactions found in **2** is lower than 0.5 ns while 72% / 50% / 23% of the π-π stacking interactions detected in **1** show life times larger than 1.0 ns / 1.5 ns / 2.0 ns. Overall these results clearly indicate that the topological constraints derived from the substitution of the phenyl ring affects very significantly to the intermolecular interactions pattern (i.e., abundance and stability of both hydrogen bonds and π-π stackings), which is also expected to have a large influence on the gelation phenomenon. The average life times calculated for intermolecular hydrogen bond / π-π stacking interactions of **1**, **2** and **3** are 0.7 / 1.7, 0.1 / 0.3 and 0.2 / 0.2 ns, respectively. These averages combined with results displayed in Figure 4 allow us to conclude that the stability of the assemblies predicted by MD simulations decreases as follows: **1** > **2** >> **3**. On the other hand, the formation of specific hydrogen bonding interactions between the polymer chains and the explicit solvent molecules has been analyzed snapshot-by-snapshot. Figure 4e represents the number of water molecules hydrogen bonded to the amide groups contained in the polymer chains of each system against the number of analyzed snapshots. As it can be seen, the maximum of hydrogen-bonded waters is 45, 40 and 45 for **1**, **2** and **3**, respectively, even though such high number is only observed in one

snapshot. Moreover, only 145, 235 and 154 snapshots are able to retain 10 or more water

hydrogen bonded to the amide groups of **1**, **2** and **3**, respectively. These results indicate

that the hydration of polymer chains, which is illustrated in Figure 3, essentially occur

through non-specific water···polymer interactions. Moreover, the inset displayed in Figure

4e clearly shows that the formation of water···amide interactions is slightly more favored

for **2** than for **1** and **3**.
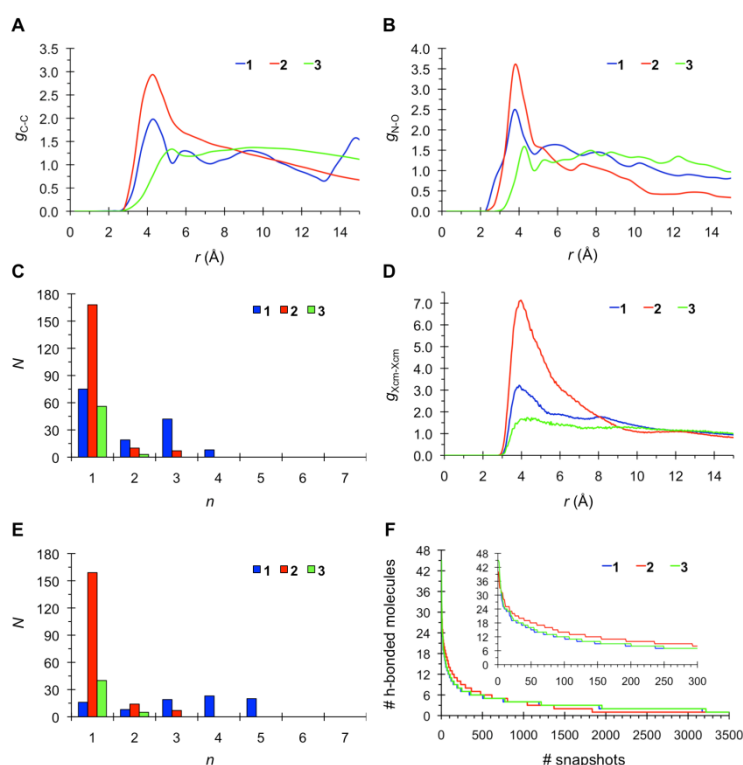
Fig. 4 Radial distribution functions for the A) C···C and B) N···O pairs of atoms belonging to different

ionene polymer chains. C) Number of N···O hydrogen bonds (*N*) with life times comprised between 0 and

0.5 ns (*n* = 1), 0.5 and 1.0 ns (*n* = 2), 1.0 and 1.5 ns (*n* = 3) and 1.5 and 2.0 ns (*n* = 4). D) Radial distribution

functions for pairs of centers of masses of aromatic rings belonging to different ionene polymer chains. E)

Number of π-π stacking interactions (*N*) with life times comprised between 0 and 0.5 ns (*n* = 1), 0.5 and 1.0

ns (*n* =2), 1.0 and 1.5 ns (*n* = 3), 1.5 and 2.0 ns (*n* = 4) and 2.0 and 2.5 ns (*n* = 5). F) Number of water

molecules involved in hydrogen bonding interactions with the amide groups of the polymer chains against

the number of snapshots (a decreasing order is displayed for the three evaluated systems).

The temporal evolution of the radius of gyration (R_g) has provided qualitative information of the molecular flexibility of **1–3** (Figure S14). The resulting average R_g value $\pm$ 2·standard deviation is 21.1 $\pm$ 3.56 Å, 27.8 $\pm$ 4.36 and 35.8 $\pm$ 2.81 Å for **1**, **2** and **3**, indicating that the flexibility grows in the following order: **3** < **1** < **2**. Evaluation of the hydrodynamic radius (R_H) leads to similar conclusions, the average value being 21.5 $\pm$ 1.5 Å, 24.6 $\pm$ 2.0 and 28.8 $\pm$ 1.2 Å for **1**, **2** and **3**, respectively. Correlation of these structural parameters with the intermolecular interactions discussed above allows us to predict that the ability to form polymer assemblies increases with the molecular flexibility, which in turn is directly related with the structural isomerism of the phenylenediamine core. However, the stability of the formed polymer assemblies is also significantly affected by the molecular flexibility, as is clearly evidenced by the analyses of the residence times. More specifically, although **1** shows less intermolecular interactions than **2**, the molecular flexibility of the latter perturbs their strength and stability, which are weaker than those of **1**. Accordingly, the hydrogelation capacity is controlled by the density of intermolecular interactions, which allows to discriminate **3** with respect to **2** and **1**, and also by the stability of such interactions, which is significantly higher for **1** than for **2**. In order to examine the reliability of the studied models, additional simulations were carried out using an extended system of **2** (model **2e**), which was selected because of its abundant intermolecular interactions. Results obtained for model **2e** (Figure S16 and S17), which consists of four polymer chains with *n* = 6 immersed in a simulation box with 98498 explicit water molecules (Figure S15), are fully consistent with those reported in Figure 4 for **2** corroborating the assembling ability predicted for the system with *N,N'-(meta-phenylene)dibenzamide* linkages). Thus, enlargement of the number of polymer chains does not alter the structural organization and the main characteristics of the interaction pattern obtained for **2**, which is based on the coexistence of regions dominated by a large

123

number of polymer⋯polymer with hydrated polymer zones. The maximum number of water molecules forming hydrogen bonds with the polymer chains is 10 and 15 per molecule of **2** and **2e**, respectively. However, the average R_g and R_H values calculated **2e** (32.6 ± 3.6 and 31.4 ± 1.5 Å, respectively) indicate that, as expected, the length of the molecular chain increases slightly with the number of assembled molecules while the flexibility decreases. On the other hand, the influence of the molecular weight in the hydrogelation ability of ionenes **1** and **2** has been evaluated by considering models made of two polymer chains with $n = 8$ (**1w** and **2w**, respectively) immersed in a simulation box filled with explicit water molecules, respectively. Results obtained for **1w** and **2w** (Figure S18) are similar to those displayed in Figure 4, this feature being particularly outstanding for the latter system. Accordingly, the assembly behavior discussed above for the polymer with *N,N'*-(*meta*-phenylene)dibenzamide and *N,N'*-(*ortho*-phenylene)dibenzamide linkages are practically independent of the number of repeat units in terms of abundance and stability of the intermolecular polymer⋯polymer interactions. Density Functional Theory (DFT) calculations using small model dimers, which are described in the ESI, were carried in both the gas-phase and aqueous solutions to get additional information on the relative hydrophobicity and hydrogelation ability of the three investigated systems. Evaluation of the free energies of solvation (ΔG_{sol}) indicated that the interaction of such dimers with the solvent is more favorable for **3** than for **2** and **1** by 0.8 and 3.6 kcal mol^{-1}, respectively. Accordingly, the relative hydrophobicity of these dimers, which decreases with increasing separation the aromatic rings containing in the repeat unit, follows the same order that the gelation ability: **1** > **2** > **3**. This feature together with the calculated binding energies and intermolecular geometries (Table S1 and Figure S20) indicate that the hydrogelation ability of **1** and **2** are higher than that of **3**. Moreover, the complex and dense network of hydrogen

bonding and π-π stacking interactions found for **1** (Figure S20) suggest that *N,N'-(ortho-phenylene)dibenzamide* linkages are the most appropriated to form stable hydrogels.

3.2.3.   Experimental hydrogelation

Ionenes **1**-**3** were subjected to thermal hydrogelation tests that consisted in cooling to RT the isotropic solutions of a weighted amount of a given ionene in 1 mL of doubled-distilled water (organogelation tests were negative). The material phase was first classified as a gel if no gravitational flow was observed upon turning the vial upside-down, and further confirmed by rheological measurements. **1** induced the most effective gelation at the lowest critical gelation concentration (CGC = 25 ± 2 g L^{-1}), which corresponded to a ca. 4-fold and 2-fold drop with respect to **2** and **3**, respectively (view Figure 5). All hydrogels were thermoreversible over several heating-cooling cycles without any noticeable detriment of their properties. A typical hysteresis loop between gel-to-sol and sol-to-gel transition temperatures of 10-15 ºC was also observed under controlled heating-cooling rates. Remarkably, and in agreement with the rheological data (*vide infra*), we observed that the gel-to-sol transition of the hydrogel made of **1** could be also induced by sonication instead of heating as external stimulus, and the gel phase restored upon quiescence. In sharp contrast, sonication treatment of the hydrogels made of **2** or **3** lead to a heterogeneous mixture of solvent, precipitate and pieces of jelly-like material that did not returned to a uniform hydrogel over time. Simple changes in the molecular geometry of the ionenes not only influenced the CGC, but also the gelation kinetics. Figure 5 suggests complex decay kinetics of the supramolecular assembly with increasing concentration of a given ionene. Ln-Ln plots revealed that for an equivalent increment in concentration with respect to the CGC the materials based on **3** and **2** evolved ca. 1.7-fold and 1.5-fold faster, respectively, than **1** to reach gelation within ca. 2-3 min (Figure 5). However, in absolute terms, the much lower CGC of **1** makes this ionene the best choice to achieve rapid gelation within a wide range of concentrations. For instance, the gelation times achieved at 100 g L^{-1} were ca. 5 min, 1.3 h and 21 h for **1**, **3** and **2**, respectively. Even at the CGC, **1** showed the faster gelation (e.g., ca. 19 h for **1** vs. 47 h for **3**).
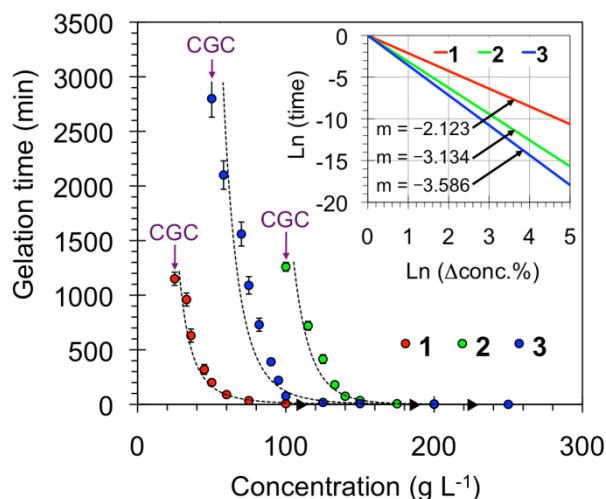
Fig. 5 Gelation kinetics for each ionene gelator. Inset: Normalized Ln-Ln plot of the gelation time against the corresponding percentage increases in concentration.

Physical properties of hydrogels

Anticipating unique structure-property relationships, the hydrogels made of each ionene were subsequently characterized in terms of their thermal-mechanical stability, optical and morphological properties. The thermal stability of the hydrogels prepared from the isomeric ionenes at a concentration of 100 g L^{-1} (this corresponds to the CGC of **2**, which is the largest CGC value among the three ionenes) was comparable between **2** and **3**, and slightly superior in ca. 5-6 ºC for **1**. However, a more realistic vision could be obtained by looking at the percentage increases of the variable over the entire range of permitted concentration until reaching a plateau value of T_{gel}. As expected for physical gels, the gel-to-sol transition temperature (T_{gel}) values increased considerably with the gelator concentration. Very interestingly, homogeneous and stable hydrogels could be formed at very high concentrations, defined by the solubility limit of the ionene in hot water, following the order **1** (1500 g L^{-1}) > **2** (750 g L^{-1}) > **3** (400 g L^{-1}) (view Figure 6A). This feature allowed for the preparation of hydrogels with a wide range of T_{gel} values (ΔT_{gel} = 58-74 ºC) even well above the boiling point of water. The Ln-Ln plot of the percentage increases before the plateau regions showed an almost perfect linear relationship between the increment in the gelator concentration and the consequent increment in the T_{gel} with respect to the initial values at the CGC (Inset Figure 6A). Thus, within the end-limits defined by the CGCs and the maximum T_{gel} values, the slopes of these straight lines

126

indicated that **3** causes a 1.2-fold and 1.6-fold higher percentage increment of T_{gel} than **2** and **1**, respectively.
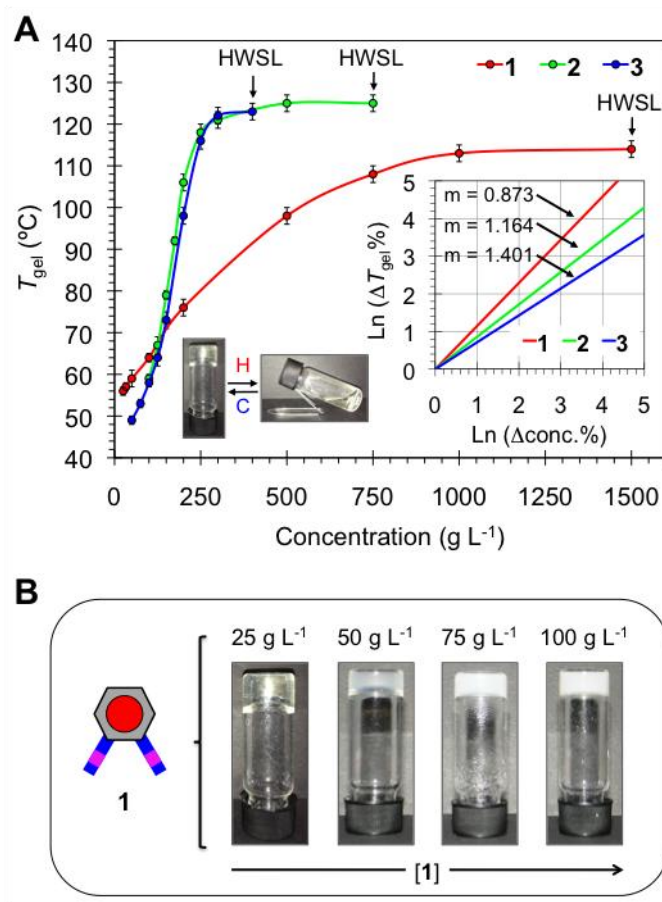
Fig. 6 A) Evolution of T_{gel} with ionene concentration. Inset plot: Normalized Ln-Ln graphic of the corresponding percentage increases. Inset photographs: Representative phase thermoreversible transition for the hydrogel prepared from **1** at 25 g L^{-1}. Abbreviation: HWSL = hot-water solubility limit; m = slope; H = heating; C = cooling. B) Increment of opacity with the ionene concentration for the hydrogel prepared from **1**.

Oscillatory rheological measurements confirmed the viscoelastic gel state of the materials. Their storage modulus (G') and loss modulus (G'') were first measured at RT as a function of the frequency (dynamic frequency sweep experiment, DFS) and shear strain (dynamic strain sweep experiment, DSS) to determine the linear viscoelastic regime (solid-like response) associated to each material (view Figure 7A and 7B). Reproducible and relatively constant dissipation factors (tan $\delta = G''/G' \approx 0.1$) during the dynamic frequency sweep indicate a good tolerance of the hydrogels to external forces. Within the linearity

127

limits of deformation, G' was always about one order of magnitude higher than G'' over the
entire range of frequencies. Further dynamic time sweep (DTS) measurements at critical
strain at yield ($\gamma = 0.1\%$) and 1 Hz frequency confirmed the stability of the hydrogels as a
function of the ageing time at RT.
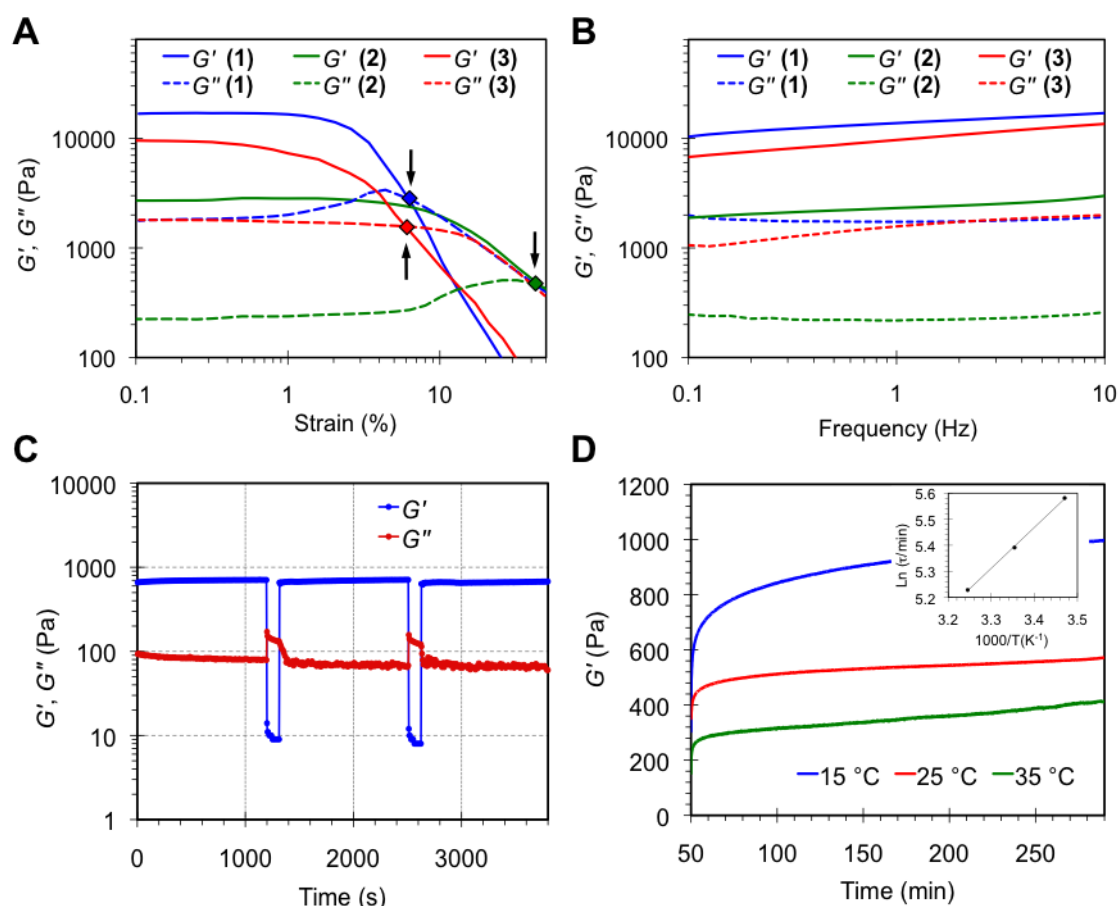
Fig. 7 Rheological characterization of hydrogels made from **1**-**3** at the same concentration ($c = 100$ g L^{-1}). A)
DSS test at 1 Hz frequency and RT. B) DFS tests at 0.1% strain and RT. C) Thixotropy-loop test of the
hydrogel prepared from **1** at CGC. D) Evolution of the storage modulus at different temperatures after
termination of the large stress (t = 30 min). Inset: Arrhenius plot of the relaxation time.

In general, for the same ionene G' increased and tan δ decreased with increased
concentration, whereas the crossover point of G' and G'' shifted to lower strain, indicating
an enhancement of the mechanical damping properties and brittle nature of the materials
(Figure S9). It is worth mentioning that both thermal and flow properties of hydrogels
based on oligomeric electrolytes are also influenced by the salt content.[31] Focusing on the

effect of the polymer topology, the mechanical strength of the hydrogels prepared from ionenes **1-3** at 100 g L^{-1} (higher CGC among the studied ionenes) decreased in the order **1** ($G' \approx 14$ kPa) > **3** ($G' \approx 11$ kPa) > **2** ($G' \approx 2.5$ kPa). However, when the hydrogels were prepared at their respective CGC the tan δ increased in the order **2** < **1** < **3**, which indicates that concentration affects differently to the gel properties depending on the topology of the ionene polymer (Figure S10). Remarkably, we also found that only the hydrogel made of **1** displayed a thixotropic response against the mechanical stress caused by large-amplitude oscillations. Figure 7C shows a loop test based on successive cycles of low-high strain separated by enough time to ensure complete gel-to-sol ($G' < G''$) and sol-to-gel ($G' > G''$) transitions while minimizing inertial effects between the steps. The results showed that the original gel properties were fully recovered within 220 ± 3 min after termination of the large stress. The enthalpy change for the exothermic gel-recovery was found to be $\Delta E_H = -13.0 \pm 0.5$ kJ mol^{-1} from the Arrhenius equation (Figure 7D). Such self-healing behavior at RT was also macroscopically observed within ca. 16 h after a vigorous shaking-resting process applied directly to the glass vial containing the hydrogel. These results suggest that ionene **1** behaves similarly to other ionene gelators (i.e., poly[pyridinium-1,4-diyliminocarbonyl-1,4-phenylene-methylene chloride),[32] albeit the underlying relationship between ionene structure and thixotropic behavior still remains unclear pending further investigation. In terms of optical appearance, the difference in the CGC values associated to each ionene was accompanied by the formation of transparent gels from **1**, whereas opaque white gels were obtained in the case of **2** and **3** at their respective CGC (Table S1 and Figure S8). As expected, an increase in the concentration of **1** increased also the opacity of the hydrogel (Figure 6B), suggesting the gradual formation of aggregates greater than the wavelength of visible light (ca. 380-780 nm). Moreover, the hydrogels showed distinctive birefringence domains under crossed nicols depending on the ionene structure and concentration (view Figure 8 and Figure S13), indicating the presence of different anisotropic aggregates. The reduced birefringence observed for the hydrogels made of **2** in comparison to **1** and **3** at the same concentration suggested the formation of less extended networks in the former, which was in agreement with their weaker mechanical strength (*vide supra*). Noteworthy is that the possibility of tuning the optical properties of these thermo-sensitive hydrogels based on the topology of the ionene gelator may help to expand also their range of potential applications to optoelectronic devices.[33]
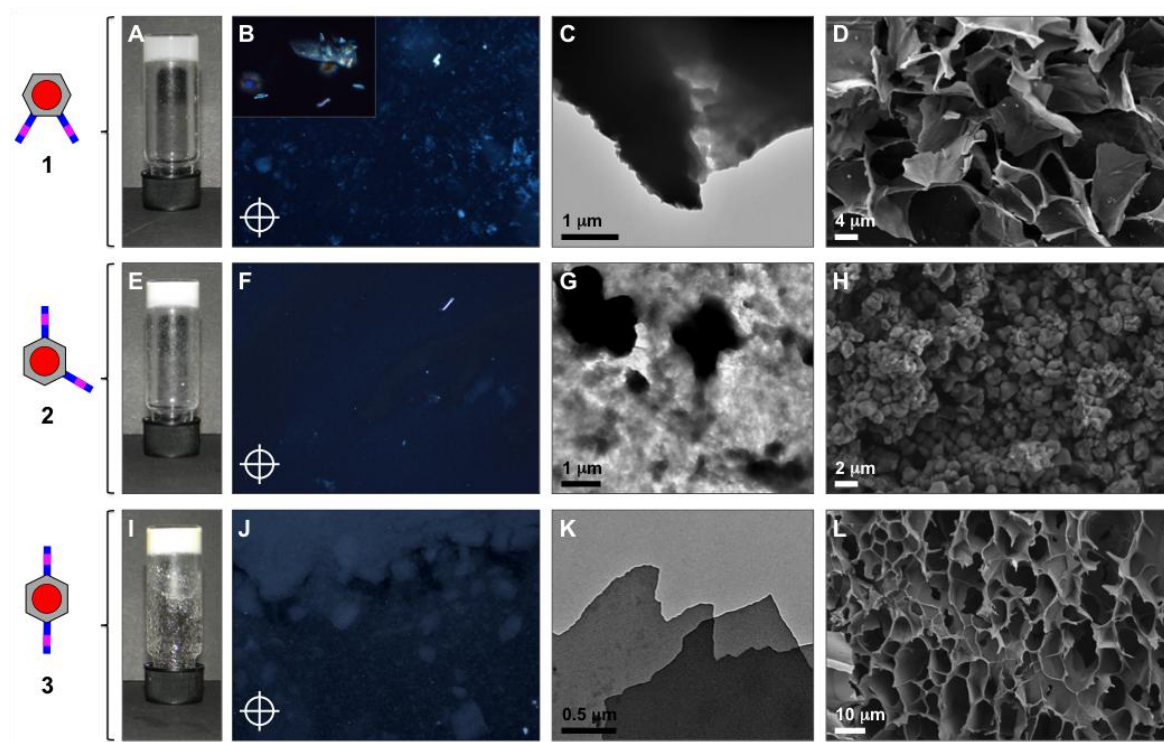
Fig. 8 Optical and morphological features of hydrogels prepared from ionenes **1** (A-D), **2** (E-H) and **3** (I-J) at
$c = 100$ g L^{-1}. (A, E, I) Digital photographs of upside-down vials with the hydrogels. (B, F, J) Optical images
(10×) of the hydrogel films under crossed nicols. Inset in (B): Optical image (50×) of the hydrogel prepared
from **1** at CGC ($c = 25$ g L^{-1}). (C, G, K) TEM and (D, H, L) FE-SEM microphotographs of the corresponding
xerogels.

Further electron microscopy imaging of the xerogels, obtained by freeze-drying the
corresponding hydrogels, confirmed the induction of different anisotropic morphologies
caused by each ionene (Figure 8). TEM images clearly revealed overlapped laminar
structures consisting on large and homogeneous sheets for the xerogels from **1** and **3**,
whereas the xerogel from **2** showed a complete different morphology consisting on rough
domains without discernible fibrillar or laminar regions. In good agreement, further FE-
SEM images of the specimens confirmed the described morphology in greater detail. Thus,
dense macroporous networks formed by connected leaf-like structures with interlaminar

distances in the range of ca. 5-10 μm were observed for the xerogels from **1** and **3**. In sharp contrast, globular shaped agglomerates resembling pebble stones ($\varnothing \approx 0.5\text{-}1$ μm for individual particles) were characteristic of the xerogel obtained from **2**. Augment of the cross-linking density and loss of anisotropy was observed in all cases upon extensive increase of ionene concentration, as evidenced by the formation of distorted microstructures of reduced birefringence.

Dispersion of single-walled carbon nanotubes (SWNTs)

The insolubility of SWNTs in aqueous solutions due to entanglement and hydrophobic association of the nanotubes is considered one of the major practical limitations of these promising materials, especially in fields such as biomedical engineering and biochemistry.[34, 35] Hence, a considerable research effort has been devoted during the last decade to the development of cost-effective methods to readily disperse SWNTs either by covalent or non-covalent strategies that preserve their functional properties.[36] Within non-covalent approaches different research groups have explored the use of surfactants[37] and polycations[38-40] as dispersants. Moreover, the preparation of SWNTs-hydrogel composites has also received a growing interest due to the potential synergic combination of properties from both materials.[36, 41-43] In comparison to ionenes **1-3**, other polyelectrolyte dispersants are built either from a different rigid core or different spacers. During our research, we were delighted to confirm that the modification of the substitution angle in the phenylenediamine core of DABCO-containing ionene gelators resulted also crucial to provide such additional functionality to these specific hydrogels (i.e., use of DABCO as molecular spacer). Despite the structural similarities with other polyelectrolyte dispersants, in which the planar π-surface of the phenylene core seems to be crucial for the π-stacking interaction with the carbon nanotubes,[26] opaque hydrogels based on ionenes **2** and **3** at

131

their CGC were unable to hold a dispersion of SWNTs. However, the use of the ionene gelator **1** at CGC allowed for the facile preparation of thermoreversible and homogeneous SWNTs-hydrogel composites (view Figure 9A).
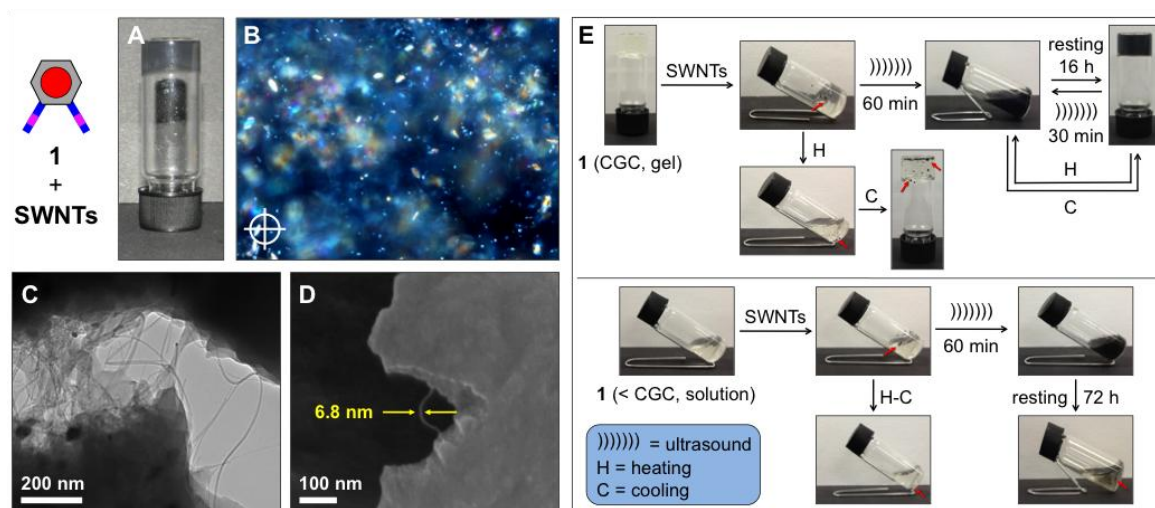
Fig. 9 Optical and morphological characterization of SWNTs-hydrogel composite made of **1** (c = 25 g L^{-1}) and SWNTs (c = 0.1 g L^{-1}). A) Upside-down vial containing the hybrid hydrogel. B) Optical image (20×) of the composite film under crossed nicols. C) TEM and D) FE-SEM images of the hybrid xerogel. (E) *Top*: General preparation of SWNTs-hydrogel composite and its reversibility. *Bottom*: Dispersion of the SWNTs was not possible by sonication or heating-cooling treatment of the mixtures at concentrations of **1** below CGC.

Interestingly, other transparent hydrogels obtained using flexible diamine spacers (e.g., *N,N,N′,N′*-tetramethyl-1,6-hexanediamine, *N,N,N′,N′*-tetramethyl-1,3-propanediamine) and PPDA showed a similar dispersion ability. In general, an increase of the gelator concentration leading to more opaque gels was accompanied by a gradual detriment of the dispersibility. Thus, the aggregates size and morphology seem to play a key role among the parameters influencing the dispersion of SWNTs within surfactant-free ionene hydrogels. In contrast to previous systems,[26] hybrid hydrogels could be prepared by addition of the SWNTs on top of the hydrogel made of **1** followed by sonication and a final quiescent state

at RT (Figure 9E). The so-prepared materials maintained the same T_{gel} either upon heating-cooling or sonication-resting cycles. Interestingly, we observed that the use of the preformed hydrogel was crucial in order to disperse by sonication the over layered SWNTs and form the stable hybrid gel. Thus, the addition of the SWNTs to an isotropic solution of **1** at the CGC (prepared by heating or sonication) resulted in the hydrogel formation with precipitated instead of dispersed SWNTs (Figure 9E, top). The use of concentrations higher than CGC accelerated in all cases the gelation process but, as mentioned above, it did not improve the dispersion of the nanotubes. Thus, the hydrogel prepared from **1** at CGC behaves as a unique system for the dispersion of SWNTs and subsequent formation of SWNTs-hydrogel composites. It is worth to mention that although sonication usually leads to transient exfoliation of the nanotubes, the favorable interaction with the ionene gelator, like with other polymeric dispersants, may stabilize the exfoliated tubes preventing further aggregation.[44] Moreover, sonication-induced sol-to-gel transition could be repeated several times, without the necessity of the heating-cooling process, which indicated the preservation of the thixotropic gel network. The maximum concentration of SWNTs that could be homogenously dispersed was 0.1 g L^{-1}, which did not cause a major change on the thermal-mechanical stability of the gel matrix (i.e., $\Delta T_{gel} \approx$ 2-5 °C; $\Delta \tan \delta \approx 0.04$) (Figure S11 and S12). Under these conditions, the gel-like SWNTs dispersions showed vis-NIR absorption (Figure S13), maintained the uniform black color for several months (e.g., no precipitation of nanotubes was observed after 3 months) and displayed birefringence under polarized light (Figure 9B). Precipitation of the SWNTs and a clear supernatant solution were obtained when the dispersion was attempted by sonication or heating in the presence of **1** below the CGC (i.e., c = 10 g L^{-1}) (Figure 9E, bottom). Therefore, the gel network (and not only the polyelectrolyte) provides the necessary microenvironment for the optimal stabilization of the nanotubes dispersion. Moreover, electron microscopy imaging (i.e.,

TEM, FE-SEM) of the specimens clearly visualized the perfect embedment of the SWNTs within the highly dense gel matrix (Figure 9C and 9D). The above results were in concordance with both the conserved anisotropy of the gel phase and the high stability of these dispersions without aggregation of the nanotubes.[45]

3.2.4.   Mechanistic considerations

It has been already anticipated that cooperative hydrogen bonding, π-π, cation-π, and other electrostatic interactions may play an important role in the gelation mechanism of ionenes.[26] In fact, the bonding energy for only H-bonding (ca. 20 kJ mol^{-1}) is much higher than the global activation energy for the gel formation estimated by rheology. As expected, comparative FT-IR spectra confirmed the expected participation of hydrogen-bonded amides and aromatic interactions during the gelation process. Thus, hydrogen bonding in the ionene hydrogels shifted both CO and NH resonances to lower energy with respect to the solid ionene (e.g., from ca. 1656 to 1531 cm^{-1} for amide I bands, and from ca. 3390 to 3275 cm^{-1} for NH stretching bands). Although the gel-to-sol transition occurred with increasing temperature, the IR bands arising from hydrogen-bonded amide groups decreased only slightly in the isotropic solution indicating that these interactions are already significant in the solution phase (ESI). In agreement with previous observations,[46] additional contributions arising from dynamic interactions between amide groups and water molecules through the chloride anions is also reasonable based on the observation of amide proton signals at ca. 12.3 ppm in the NMR spectrum in DMSO-d_6 (ESI). Moreover, anion/cation-π interactions in these ionenes should also be considered, especially in a polar medium where most other intermolecular forces are considerably attenuated. In this sense, it is important to realize that strongly associated ion pairs can diminish the strength of the cation-π bonding by up to 80%.[47] In our case, this interaction could be rather important in the gelation mechanism because the ionenes were unable to form hydrogels upon exchange of chloride by TFSA anions, which should hinder the ammonium-π interactions due to the expected stronger association of the TFSA-tetraalkylammonium ionic pair in comparison to chloride-tetraalkylammonium in water. In order to get more conclusive information

about the gelation mechanism, MD results for the three simulated ionene polymers have been used to examine the possible existence of interactions different to those discussed above (i.e., intermolecular hydrogen bonds and intermolecular π-π stacking in Figure 4b and 4c, respectively). Figure 10a and 10b represent the radial distribution functions for $N^+ \cdots X_{cm}$ ($g_{N+/X}$) and $Cl^- \cdots X_{cm}$ ($g_{Cl-/X}$) pairs, respectively, where X_{cm} refers to the center of masses of aromatic rings. It is worth noting that $g_{N+/X}(r)$ and $g_{Cl-/X}(r)$ are related with the formation of cation-π and anion-π interactions, respectively. The number of pairs with a $N^+ \cdots X_{cm}$ distance lower than 5.0 Å is very low for **1** and **2**, the only system with a peak below such threshold distance being **3**. Indeed, cation-π interactions are 5.2 and 7.5 times more abundant for **3** than for **1** and **2**, respectively. Combination of this result with the experimental evidences discussed above suggests that the importance of cation-π interactions in the gelation process is relatively low. In order to corroborate this feature, the $g_{N+/X}(r)$ profile was calculated for **2e**, results being included in Figure 10a. Comparison of the profiles obtained for **2** and **2e** indicates that number and strength of cation-π interactions decreases and increases, respectively, with the number of polymer chains contained in the model. Despite of this, the strength of such kind of interactions is significantly lower for **2e** than for **3**, confirming their little influence in the gel formation. The $g_{Cl-/X}(r)$ profiles calculated for **1**-**3** (Figure 10b) are relatively similar, evidencing the existence of $Cl^- \cdots X_{cm}$ pairs at distances as short as 3.22 Å. From a quantitative point of view, the population of $Cl^- \cdots X_{cm}$ pairs at distances shorter than 5.0 Å is similar for **1** and **2** (i.e., 4% larger for the latter) but 15% lower for **3** than for **2**. Furthermore, the amount of anion-π interactions in **2** is 1.1 times higher than the number of cation-π interactions in **3**. Comparison of the profiles obtained for **2** and **2e** indicates that both the strength and the amount of Cl⁻-π interactions do not change when the number of polymer molecules in the simulated model increases from two to four. Although the amounts of anion-π interaction detected for the three molecular systems show differences that are smaller than for intermolecular hydrogen bonds and π-π stacking, they grow as displayed in Figure 4 for the latter interactions (i.e., **2** > **1** > **3**), Accordingly, anion-π interactions may play a crucial role in the gelation mechanism since their strength is not negligible as compared to intermolecular hydrogen bonding and π-π stacking interactions.[48,49] The average residence time for anion-π interactions is 431, 173 and 316 ps for **1**, **2** and **3**, respectively. Attractive interactions between the N–H of amide groups and the π-cloud of aromatic rings belonging to different chains have been also invoked to explain the gelation mechanisms. The

135

possible existence of such kind of intermolecular interactions in **1-3** has been analyzed by examining the radial distribution functions for (N–)H $\cdots X_{cm}$ pairs, $g_{H-X}(r)$, which are displayed in Figure 10c. As it can be seen, no peak is detected for **3** evidencing that the formation of such kind of interactions is not particularly favored in the polymer N,N'-(para-phenylene)dibenzamide linkages. In contrast, **1** and **2** show a well-defined peak centered at 4.17 and 4.32 Å, respectively. The height of the peak is significantly more pronounced for **2** than for **1** evidencing that N–H$\cdots\pi$ interactions are considerably more abundant in the former than in the latter. More specifically, integration of the area of the peaks within the distance interval defined by the crossing of the two profiles at r = 7.47 Å indicates that the population of N–H$\cdots\pi$ interactions through the trajectories is 60% higher for **2** than for **1**, even though the average residence time is slightly higher for the latter than for the former (i.e., 368 and 319 ps for **1** and **2**, respectively). Inspection of the $g_{H-X}(r)$ profile calculated for **2e** (Figure 10c) indicates that the preference of the ionene polymer with *N,N'*-(meta- phenylene)dibenzamide linkages is practically independent of the number of explicit molecules used in the simulated model. Thus, a pronounced peak centered at 4.17 Å, similar in high to that found for **2**, is also detected for **2e**. On the other hand, detailed analyses of the stored snapshots evidenced that the amount of weak specific interactions at the intramolecular level (i.e., hydrogen bond, π-π stacking and N–H$\cdots\pi$) is very small or practically null. This feature reflects that the role of intramolecular interactions in the gelation of the three ionenes studied in this work is null. This result combined with both the experimental observations previously discussed and the radial distribution functions represented in Figure 4 and 10 indicate that the hydrogels studied in this work results from the combination of multiple specific intermolecular interactions. Specifically, hydrogen bonding, π-π stacking, anion-π and N–H$\cdots\pi$ interactions play a fundamental role in the formation of **1**-**3** hydrogels. Furthermore, the stability of the formed assemblies is also crucial for understanding the gelation ability. Accordingly, interactions are clearly more numerous in **2** than in **1** while, in opposition, they are more stable in **1** than in **2**, **3** being the less favored in all cases. These results clearly reflect the large influence of the substituted phenylenediamine isomerism in the strength, abundance and stability of intermolecular interactions, being responsible of the differences observed in the gelation of such ionene systems. It is worth mentioning that we have also observed a superior ability of **1** to gel not only water but also HCl solutions, which constitute the subject of a separate investigation.
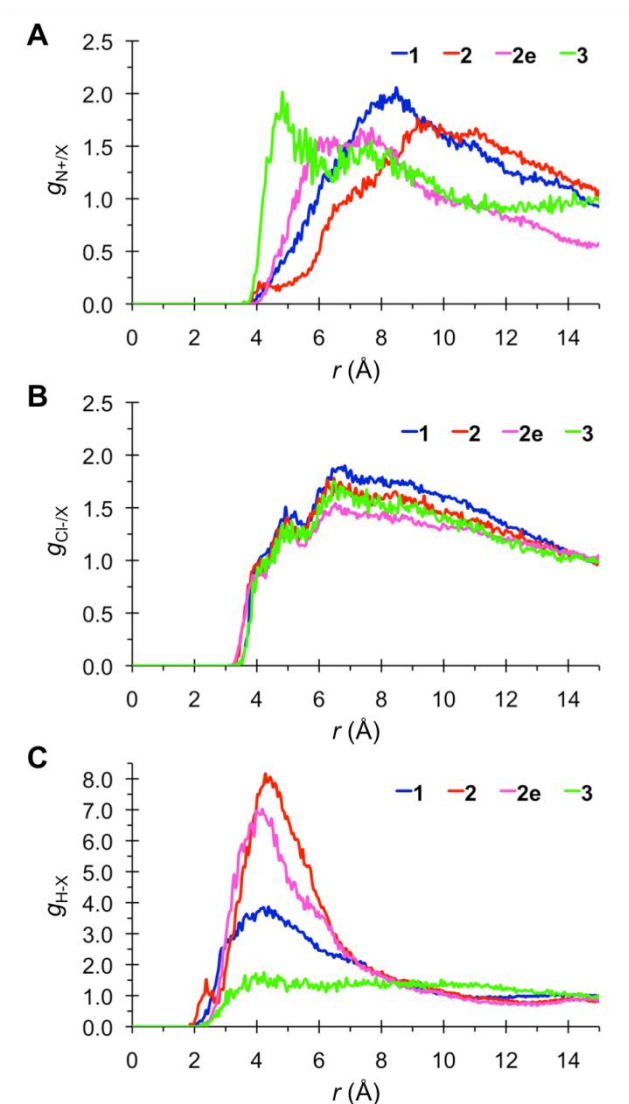
Fig. 10 Radial distribution functions for the A) $N \cdots X_{cm}$, B) $Cl^- \cdots X_{cm}$ and C) $(N–)H \cdots X_{cm}$ pairs, belonging to different ionene polymer chains, where X_{cm} refers to the center of masses of aromatic rings.

3.3. Conclusion

In conclusion, a combined computational-experimental approach can be applied to optimize the structure of ionene polymers in order to enhance their gelation efficiency and achieve hydrogels with superior properties without adding external additives. As a proof of concept, surfactant-free ionene polymers **1**-**3** containing DABCO and *N,N'-(x-* phenylene)dibenzamide linkages (*x = ortho-/meta-/para-*) were used as model systems.

Molecular dynamics simulations of the isomeric ionenes with explicit water molecules allowed for the comparison of polymer···water and polymer···polymer interactions (i.e., hydrogen bonding, π-π stacking, cation-π, anion-π) in each case through the corresponding radial distribution functions. The results showed that the topological constraints derived from the substitution pattern of the core aromatic ring drastically affects the intermolecular interactions pattern, which is also expected to have a large influence on the gelation phenomenon. Specifically, although domains with high degree of hydration were visualized for the three systems, polymer···polymer interactions were only evident in the case of *ortho-* (**1**) and *meta-* (**2**) isomeric ionenes. The predictive models were consistent upon a range of repeating units and explicit polymer chains. In good agreement with the theoretical assembly models, **1** provided experimentally the best hydrogels among the three ionenes **1**-**3**. Heating-cooling treatment allowed for the preparation of thermoreversible hydrogels in each case, but only in the case of **1** sonication was also found to induce gelation very efficiently. Moreover, **1** displayed the lowest critical gelation concentration (CGC = 25 ± 2 g L^{-1}), the highest thermal stability at CGC, superior optical properties, a rapid gelation kinetics within a wide range of concentration, a self-healing behavior, and the ability to disperse pristine SWNTs. Neither optical transparence, nor self-healing, nor dispersibility of SWNTs could be achieved with *meta-* (**2**) and *para-* (**3**) DABCO-containing ionenes. In principle, this approach could be applied for the topological optimization of other gelators based on either polymers or low-molecular-weight compounds in order to tune the molecular self-assembly and achieve multifunctional gels with superior properties. Detailed investigations on additional properties of gelator **1**, property-ionization state relationship studies, and the preparation of biohybrid materials are currently underway in our laboratories.

3.4. Addendum: Enhanced gelation properties in dilute aqueous solutions of hydrochloric acid

Potential gelation of acids by hydrogelator-compounds is an interesting topic of research, due to the harmful properties of the acids on natural environments and practical applications of corresponding materials.[50] Unfortunately, only little reports exist on effective gelation of dilute mineral acids in the literature so far.[26, 51] Probable explanations

138

for this phenomenon could be the presence of labile moieties inside the structures of gelating agents and their potential cleavage in the presence of acidic media or simple protonation events. As reported by Yoshida *et al.*,[26] a surfactant free ionic polymer based on a *N,N'*-(p-phenylene)dibenzamide linkage bearing a flexible spacer (**5·Cl**) exhibits such interesting property of gelating dilute HCl-solution (0.1 M), unfortunately lacking further investigations on the effects of the acid-medium on the physical properties of the resulting hydrogels. Due to the structural similarities with compounds we describe in this section, we were curious on further investigating such phenomenon. Interestingly we found effective gelation of dilute HCl-solution (0.1 M) for compounds **1** and **3** at their corresponding critical gelation concentration (CGC) in pure water (25 and 48 mg/mL) in similarity to compound **5·Cl**, while compound **2** was lacking such behavior even when increased concentrations (up to 200 mg/mL) were applied.

Tab. 1 Effect of different aqueous environments containing various acid and Cl$^-$-ion sources on the gelation ability of compounds **1**-**3** in respect to the CGC in pure aqueous solution. [a]

Medium	CGC [mg/mL]		
	1	**2**	**3**
H$_2$O	25 (2.0)	100 (10.0)	48 (5.0)
HCl (0.1 M)	22 (2.0)	-	33 (3.0)
AcOH (0.1 M)	43 (4.0)	-	100 (10.0)
H$_3$PO$_4$ (0.1 M)	46 (4.0)	-	105 (10.5)
H$_2$SO$_4$ (0.1 M)	-	-	-
NaCl (0.1 M)	84 (9.0)	-	-
CsCl (0.1 M)	85 (9.0)	-	-
NH$_4$Cl (0.1 M)	100 (10.0)	-	-
CaCl$_2$ (0.05 M)	85 (9.0)	-	-

[a] Values in brackets indicate experimental errors from at least two randomized measurements. A very similar effect of the varying media on compound **5·Cl** is also present, but was not the focus of further investigations.

A potential explanation for the behavior of compound **2** could be that additional non-classical interactions (cation/anion-π interactions) caused by the presence of H$^+$ and Cl$^-$

139

ions compete in a negative way with more common and stable intermolecular interactions
(classical H-bonding of amides and aromatic π-π stacking) necessary to promote gelation
in difference to compounds **1** and **3**. Further investigations revealed that compounds **1** and
3 were also able to promote effective gelation of HCl at concentrations even lower than the
CGC reported for pure aqueous environments as indicated in Table 1. Fascinated about
these results we were curious, if such properties can be extended to other acids. We could
observe positive results on additional gelation of AcOH (0.1 M) and H_3PO_4 (0.1 M) also,
but an increase of the gelator concentration by a factor of ca. 2 was necessary to promote
effective gel-formation. On the other hand no gelation of dilute H_2SO_4 (0.1 M) could be
observed as indicated in Table 1, resulting in the formation of turbid solutions at
concentrations between 10 and 200 mg/mL. Taking also a potential effect of the Cl^-
counterion into consideration, we could observe gelation of salts like NaCl, CsCl, $CaCl_2$
and NH_4Cl (0.1 M in respect to Cl^-) at increased concentrations (3.5-4 fold excess in
concentration is necessary) in comparison to the CGC of the pure aqueous phase and also
exclusively for compound **1**. The application of compound **3** resulted in precipitation of
materials at concentrations between 10 and 200 mg/mL.

Tab. 2 Determination of the optimum amount of HCl for enhancement of typical gelation-properties of
compounds **1** and **3** at the CGC of the gelators in pure water as indicated in Table 1. [a]

conc. (HCl) [M]	Gelation-time [min]		T_{gel} [°C]		Optical appearance	
	1	**3**	**1**	**3**	**1**	**3**
0.00	1080 (60)	2640 (240)	56 (1)	49 (1)	TPG	OG
0.10	20 (2)	50 (5)	60 (2)	63 (1)	OG	OG
0.25	20 (5)	65 (5)	59 (1)	56 (2)	OG	OG
0.50	40 (5)	180 (15)	51 (1)	43 (2)	OG	OG
1.00	140 (20)	-	42 (2)	-	SG	CS
2.00	-	-	-	-	CS	CS

[a] Values in brackets indicate experimental errors from at least two randomized measurements.
Abbreviations: TPG = transparent gel; OG = opaque gel; SG = soft gel (exhibits gravitational flow after
inverting a test tube within 30 min); CS = clear solution.

Such findings suggest that the presence of both H^+ and Cl^--ions is necessary to facilitate the formation of materials with enhanced properties in terms of CGC and hence only HCl was used as medium for further investigation. Additional positive effect of the presence of HCl was obvious by comparing the time necessary to promote gelation and the thermal stabilities of corresponding gel materials at comparable concentrations. A drastic reduction of the gelation time to about 20% of the value necessary for pure aqueous solution was visible for both compounds **1** and **3**. Furthermore thermal gel-to-sol transition temperatures (T_{gel}) were found to be increased by 4 and 14 °C respectively. The ideal content of HCl in aqueous solution was determined by testing different concentrations of the acid at the CGC of the corresponding gelator in pure water and investigations of the effect on typical gelation properties. The results are summarized in Table 2 and Figure 11 and indicate that a total concentration of HCl of 0.1 M promotes gelation in a most effective way ongoing with an enhance of typical properties like the gelation-time and T_{gel}-values. A maximum concentration of 1.0 and 0.5 M can be applied to promote gelation of compounds **1** and **3**, whereas the formation of clear solutions, which still promote an increase of the solutions viscosity, can be observed by applying higher concentrations of HCl. Very interesting to mention is a clear change in the optical appearance of hydrogels derived from **1**. In the presence of HCl, opaque hydrogels are formed indicating the formation of aggregates bigger than the wavelength of visible light (350-750 nm), whereas completely transparent gel-materials are formed in pure water (view Figure 11 F).

Tab. 3 Determination of mechanical properties by oscillatory rheology of gels derived from compounds **1** and **3** in pure water and 0.1 M HCl at the CGC of the gelators in pure water as indicated in Table 1. [a]

Compound	G' [Pa]		G'' [Pa]		Max. strain at break	
	H_2O	HCl	H_2O	HCl	H_2O	HCl
1	510 (96)	4646 (138)	72 (2)	634 (33)	15 (7)	4 (0.6)
3	218 (27)	1916 (461)	37 (6)	234 (74)	32 (9)	13 (0.2)

[a] Values in brackets indicate experimental errors from at least two randomized measurements.

Dynamic oscillatory rheology was conducted in order to prove the gel-state of materials and to compare overall mechanical stabilities towards external shear forces. Corresponding dynamic frequency sweep (DFS), dynamic strain sweep (DSS) and dynamic time sweep

(DTS) experiments reveal a strong enhancement of mechanical stabilities of gels in HCl as indicated by higher absolute values for G' (almost one order of magnitude increase; view Figure 11 D). On the other hand, the materials derived from HCl seem to be more brittle in nature as indicated by a smaller maximum strain at break of the gels (view Figure 11 C). Additionally the smart thixotropic behavior of compound **1** is also preserved macroscopically in the presence of 0.1 M HCl and proven by a three-step loop test, which has been described earlier (view Figure 11 E).
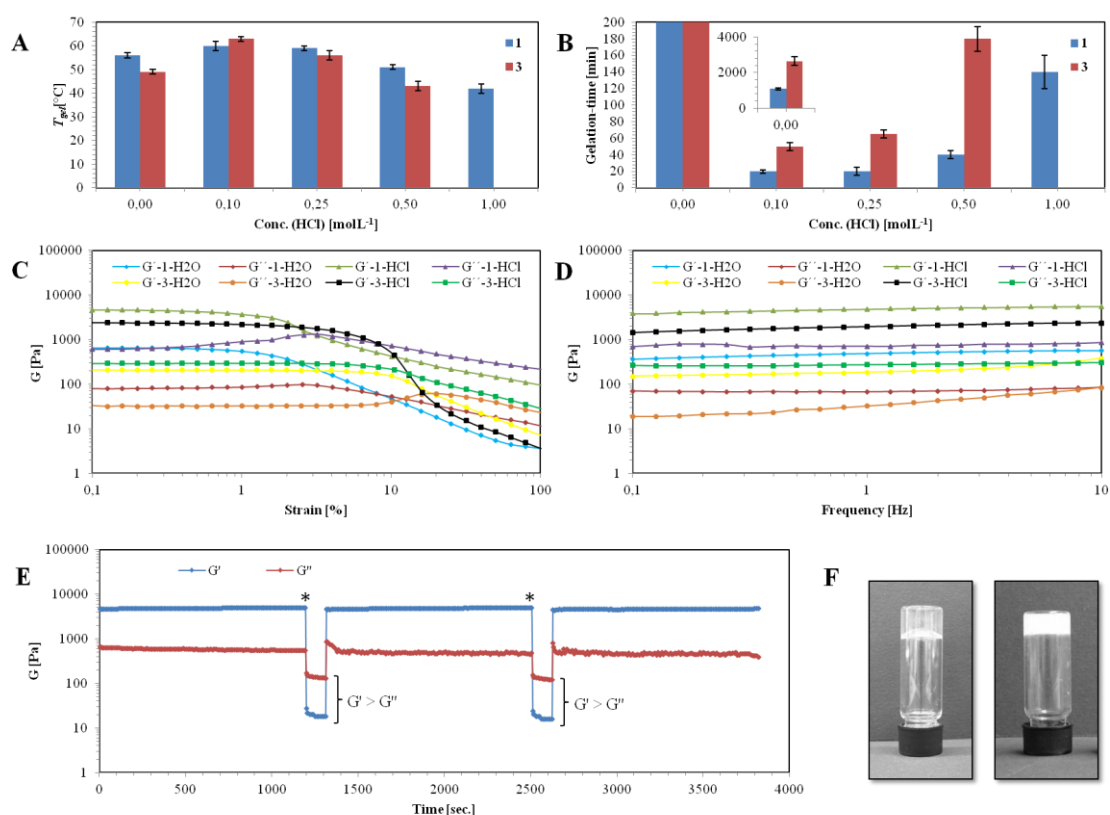
Fig. 11 (A+B): Representative bar graphs demonstrating the effect of HCl-concentration on typical gelation properties of compounds **1** and **3** at the corresponding CGC of the gelators in pure water as indicated in Table 1 (A: gelation-time; B: T_{gel}-values). (C+D): Comparative oscillatory rheology of gels derived from compounds **1** and **3** in pure water and 0.1 M HCl respectively at the CGC of the gelators in pure water as indicated in Table 1 (C: DSS-plots; D: DFS-plots). (E) Three-step loop test to demonstrate the smart thixotropic behavior of gels derived from **1** (25 mg/mL) in 0.1 M HCl. The asterixes indicate the application of a high shear strain (100 %). After the second cycle of relaxation 97 % of the original value in G' could be reached. (F): Representative digital photographs of upside-down vials containing gels derived from compound **1** (25 mg/mL) in pure water (left) and 0.1 M HCl respectively (right).

Optical microscopy of compound **1** (25 mg/mL) in both 0.1 M HCl and pure water revealed the presence of distinctive domains of birefringes under crossed nicols conditions dependent on the nature of the aqueous medium, indicating the formation of different anisotropic aggregates (view Figure 12 A-D).
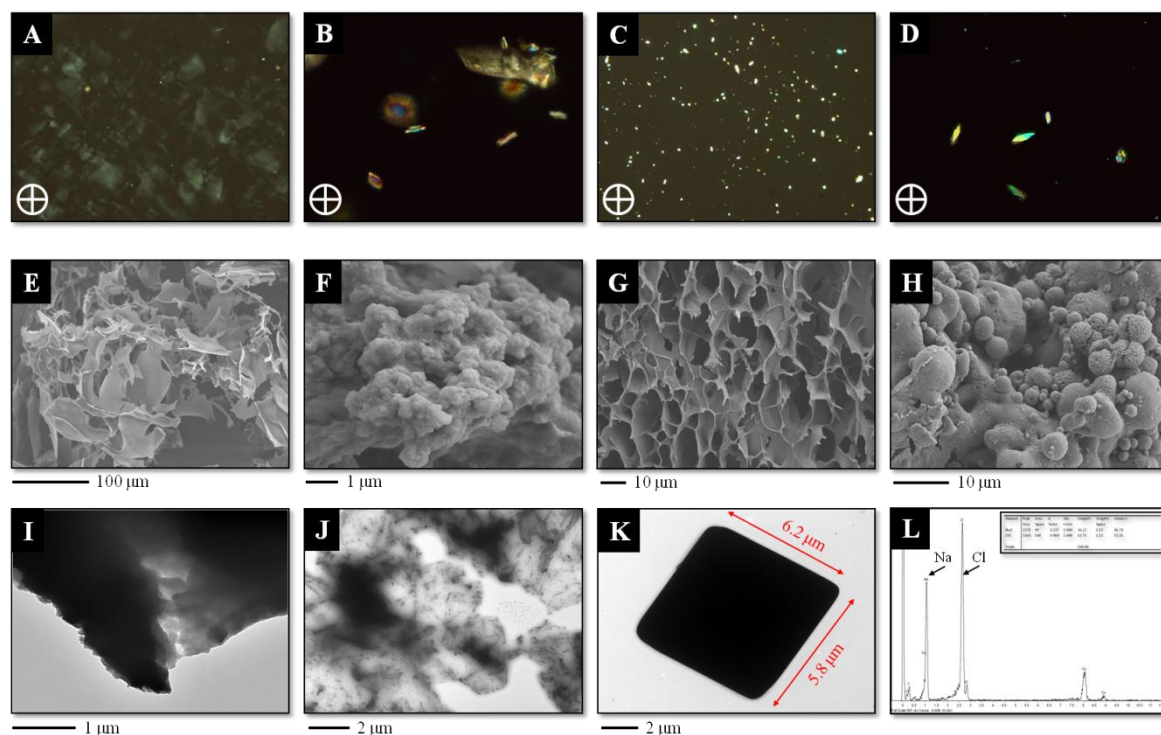
Fig. 12 Optical and morphological features of hydrogels prepared from ionenes **1** (A-F and I-K) and **3** (G and H) at the concentration of the CGC of the corresponding pure hydrogel as indicated in Table 1. (A, C) Optical images (10×) of the hydrogel films under crossed nicols. (B, D): Optical image (50×) of the hydrogel films under crossed nicols. (E-H) FESEM and (I-K) TEM microphotographs of the corresponding xerogels. (A, B, E, G, I) Materials derived from pure aqueous environment. (C, D, F, H, J, K) Materials derived from acidic environment (0.1 M HCl). (L) Elemental analysis profile of cubic structures derived from compound **1** (25 mg/mL) in 0.1 M HCl.

The higher birefringence for gel-materials in acidic environment at comparable concentrations suggests the formation of more extended networks as compared to pure hydrogels, which is in good agreement with their higher mechanical and thermal resistance

143

(*vide supra*). Additional electron microscopy of corresponding xerogels, obtained by the freeze-drying method, confirmed the induction of different morphologies caused by the nature of the aqueous environment (view Figure 12 E-K). FE-SEM images of the materials describe dense and macroporous networks formed by connected leaf-like layers with interlamellar distances in a range of 5-10 μm for the xerogels of **1** and **3** in pure water. In sharp contrast much rougher and denser agglomerates could be observed in the presence of 0.1 M HCl. Agglomerates resembling pebble stones (average diameter for individual particles ~ 1-5 μm) were characteristic for xerogels from compound **3**. TEM-images derived from compound **1** in pure water clearly reveal the overlapped lamellar structures consisting of large and homogeneous sheets, which is in good agreement with the findings obtained by FESEM. On the other hand materials derived from acidic environment reveal the presence of very dense and non-layered structures. Very interestingly additional very uniform cubic structures with average edge lengths of ca. 5-15 μm could be observed from xerogels of compound **1** in 0.1 M HCl. Subsequent elemental analysis of such cubes furnished the formation of NaCl-crystals during the preparation process of the gels/xerogels or during an aging-process. As expected, comparative FT-IR studies confirmed the participation of hydrogen-bonding amides and aromatic interactions during the gelation process in both pure aqueous and acidic environment as demonstrated for compound **1** (25 mg/mL) in Figure 13. Thus, hydrogen bonding in the ionene hydrogels shifted both CO and NH resonances to lower energy with respect to the solid ionene (e.g., from ca. 1656 to 1531 cm^{-1} for amide I bands, and from ca. 3390 to 3275 cm^{-1} for NH stretching bands) independent on the nature of the aqueous phase. At the moment computational studies are conducted in order to set up probable mechanisms for the effect of the presence of HCl in the gelation process and to explain its positive effect on typical gelation properties.
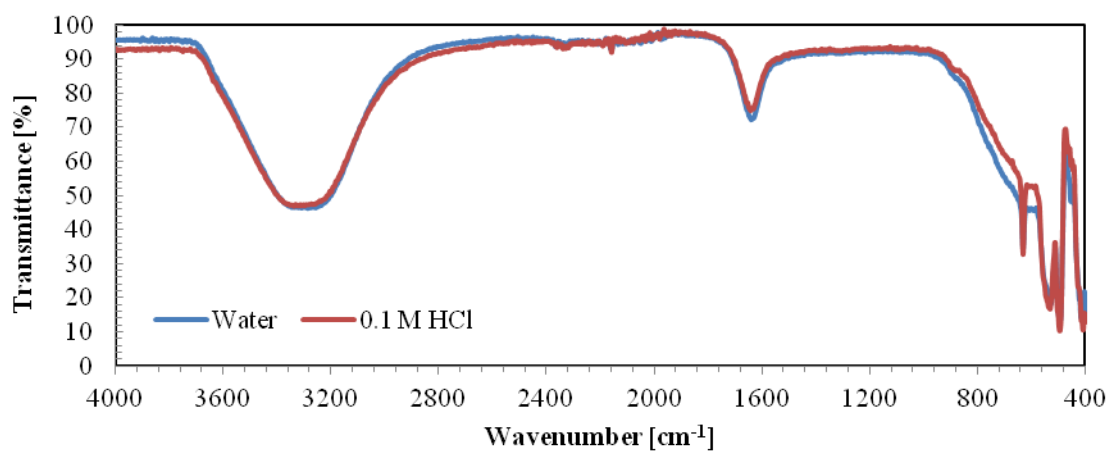
144

Fig. 13 Comparative FT-IR of hydrogels derived from compound **1** (25 mg/mL) in pure water and 0.1 M HCl.

→ Additional information on compound synthesis and characterization, and further computational studies can be found in the electronic supplementary information (ESI) on the enclosed CD.

3.5. References

[1]   R. R. Netz and D. Andelman, *Physics Reports*, 2003, **380**, 1-95.

[2]   A. Y. Grosberg, T. T. Nguyen and B. I. Shklovskii, *Rev. Mod. Phys.*, 2002, **4**, 329-345.

[3]   C. Poinsignon, *Mat. Sci. Eng. B*, 1989, **B3**, 31-37.

[4]   W. Jaeger, J. Bohrisch and A. Laschewsky, *Prog. Polym. Sci.*, 2010, **35**, 511-577.

[5]   C. Werner, *Advances in Polymer Science: Polymers for Regenerative Medicine*, Springer, Dresden, 2006.

[6]   S. Punyani and H. Singh, *J. Appl. Polym. Sci.*, 2006, **102**, 1038-1044.

[7]   H. Kourai, T. Yabuhara, A. Shirai, T. Maeda and H. Nagamune, *Eur. J. Med. Chem.*, 2006, **41**, 437-444.

[8]   A. N. Zelinkin, D. Putnam, P. Shastri, R. Langer and V. A. Izumrudov, *Bioconjugate Chem.,* 2002, **13**, 548-553.

[9]   E. Bortel, A. Kochanowski, B. Siniarska and E. Witek, *Polish J. Appl. Chem.,* 2001, **44**, 55-77.

[10] H. Noguchi, *Ionene Polymers. In Polymeric materials encyclopedia*; J. C. Salomone, Ed.; CRC Press, Boca Raton, London, New York, Tokyo, 1996, pp 3392-3421.

[11] A. Laschewsky, *Curr. Opin. Colloid Interface Sci.*, 2012, **17**, 56-63.

[12] S. R. Williams and T. E. Long, *Prog. Polym. Sci.*, 2009, **34**, 762-782.

[13] E. R. Littmann and C. S. Marvel, *J. Am. Chem. Soc.*, 1930, **52**, 287-294.

[14] C. F. Gibss, E. R. Littmann and C. S. Marvel, *J. Am. Chem. Soc.*, 1933, **55**, 753-757.

[15] M. Friedman, *J. Agric. Food Chem.*, 2003, **51**, 4504-4526.

[16] J. K. Oha, R. Drumright, D. J. Siegwart and K. Matyjaszewski, *Prog. Polym. Sci.*, 2008, **33**, 448-477.

[17] M. Yoshida, *Synthesiology*, 2012, **5**, 181-189.

[18] S. Schlick, *Ionomers: characterization, theory, and applications*. CRC Press, Boca Raton, 1996.

[19] M. R. Tant, K. A. Mauritz and G. L. Wilkes, *Ionomers: Synthesis, structure, properties, and applications*. Blackie Academic and Professional, London, 1997.

[20] A. Kowalenko, A. E. Kobryn, S. Gusarov, O. Lyubimova, X. Liu, N. Blinov and
M. Yoshida, *Soft Matter*, 2012, **8**, 1508-1520.

[21] Y. He, H.-K. Tsao and S. Jiang, *J. Phys. Chem. B*, 2012, **116**, 5766-5770.

[22] S. G. Lee, G. F. Brunello, S. S. Jang and D. G. Bucknall, *Biomaterials*, 2009, **30**,
6130-6141.

[23] S. S. Jang, W. A. Goddard, M. Y. S. Kalani, D. Myung and C. W. Frank, *J. Phys.
Chem. B*, 2007, **111**, 14440-14440.

[24] S. S. Jang, W. A. Goddard and M. Y. S. Kalani, *J. Phys. Chem. B*, 2007, **111**, 1729-
1737.

[25] E. Chiessi, F. Cavalieri and G. Paradossi, *J. Phys. Chem. B*, 2007, **111**, 2820-2827.

[26] Y. Misawa, N. Koumura, H. Matsumoto, N. Tamaoki and M. Yoshida,
Macromolecules, 2008, **41**, 8841-8846, and references therein.

[27] T. Takewaki, L. W. Beck and M. E. Davis, *Micropor. Mesopor. Mat.*, 1999, **33**,
197-207.

[28] T. M. Reincket and M. E. Davis, *Mat. Res. Soc. Symp. Proc.*, 2002, **724**, 209-214.

[29] N. Koumura, H. Matsumoto, H. Kawanami, N. Tamaoki and M. Yoshida, *Polym.
J.*, 2010, **42**, 759-765.

[30] E. Berwig, V. L. S. Severgnini, M. S. Soldi, G. Bianco, E. A. Pinheiro, A. T. N.
Pires and V. Soldi, *Polym. Degrad. Stabil.*, 2003, **79**, 93-98.

[31] S. K. Kundu, M. Yoshida and M. Shibayama, *J. Phys. Chem. B*, 2010, **114***, 1541-
1547.

[32] M. Yoshida, N. Koumura, Y. Misawa, N. Tamaoki, H. Matsumoto, H. Kawanami,
S. Kazaoui and N. Minami, *J. Am. Chem. Soc.*, 2007, **129**, 11039-11041.

[33] J. D. Tovar, *Acc. Chem. Res.*, 2013, **46**, 1527-1537.

[34] D. M. Guldi and N. Martín, *Carbon nanotubes and related structures. Synthesis,
characterization, functionalization, and applications*, Wiley-VCH, 2010.

[35] S. Taruta and M. Endo, *Chem. Soc. Rev.*, 2009, **38**, 1897-1903.

[36] J. Bachl, T. Huber, D. Kühbeck, E.-M. Schön, G. Brunner, B. Kraus, J. Heilmann,
J. A. Codelli, C. R. Bertozzi, C. Cativiela and D. D. Díaz, *Nanosci. Nanotech. Asia*,
2012, **2**, 200-209, and references therein.

[37] P. Angelikopoulos and H. Bock, *Phys. Chem. Chem. Phys.*, 2012, **14**, 9546-9557,
and references therein.

38 V. A. Sinani, M. K. Gheith, A. A. Yaroslavov, A. A. Rakhnyanskaya, K. Sun, A. A. Mamedov, J. P. Wicksted and N. A. Kotov, *J. Am. Chem. Soc.*, 2005, **127**, 3463-3472.

39 T. Fujinaga and N. Nakashima, *Polym. J.*, 2008, **40**, 577-589.

40 G. Romero and S. E. Moya, *Soft Matter*, 2012, *8*, 9727-9730, and references therein.

41 Z. Wang and Y. Chen, *Macromolecules*, 2007, **40***, 3402-3407.

42 X. Tong, J. Zheng, Y. Lu, Z. Zhang and H. Cheng, *Mater. Lett.*, 2007, **61**, 1704-1706, and references therein.

43 M. Asai, K. Sugiyasu, N. Fujita and S. Shinkai, *Chem. Lett.*, 2004, **33**, 120-121.

44 R. Shvartzman-Cohen, Y. Levi-Kalisman, E. Nativ-Roth and R. Yerushalmi-Rozen, *Langmuir*, 2004, *20*, 6085-6088.

45 R. Allen, Z. Bao and G. G. Fuller, *Nanotechnology*, 2013, **24**, 015709.

46 S. K. Kundu, T. Matsunaga, M. Yoshida and M. Shibayama, *J. Phys. Chem. B*, 2008, **112**, 11537-11541.

47 S. Bartoli and S. Roelens, *J. Am. Chem. Soc.*, 2002, **124**, 8307-8315.

48 D.-X. Wang and M.-X. Wang, *J. Am. Chem. Soc.*, 2013, **135**, 892-897.

49 P. Ballester, *Acc. Chem. Res.*, 2013, **46**, 874-884.

50 a) H. Omidian and J. G. Rocca, *U.S. Pat. Appl. Publ.*, 2008, US 20080089940 A1 20080417; b) J.-J. Xuan, Y.-D. Yan, D. H. Oh, Y. K. Choi, C. S. Yong and H.-G. Choi, *Drug. Deliv.*, 2011, **18**, 305-311; c) M. J. Molina, M. R. Gómez-Antón, B. L. Rivas, H. A. Maturana and I. F. Piérola, *J. Appl. Polym. Sci.*, 2001, **79**, 1467-1475.

51 For selected references see: a) M. Suzuki, S. Owa, M. Yumoto, M. Kimura, H. Shirai and K. Hanabusa, *Tetrahedron Lett.*, 2004, **45**, 5399-5402; b) M. Suzuki, M. Yumoto, H. Shirai and K. Hanabusa, *Org. Biomol. Chem.*, 2005, **3**, 3073-3078. c) M. Suzuki, M. Yumoto, M. Kimura, H. Shirai and K. Hanabusa, *Tetrahedron Lett.*, 2004, **45**, 2947-2950; d) M. Yamanaka and D. Higashi, *PCT Int. Appl.*, 2012, WO 2012121394 A1 20120913; e) I. Hwang, W. S. Jeon, H.-J. Kim, D. Kim, H. Kim, N. Selvapalam, N. Fujita, N. Shinkai and K. Kim, *Angew. Chem. Int. Ed.*, 2007, **46**, 210-2013.

4. Ultrasonication enhanced gelation-properties of an amphiphilic formamidine-based gelator[i]

Solution   Ultrasound enhanced gelation   Gel
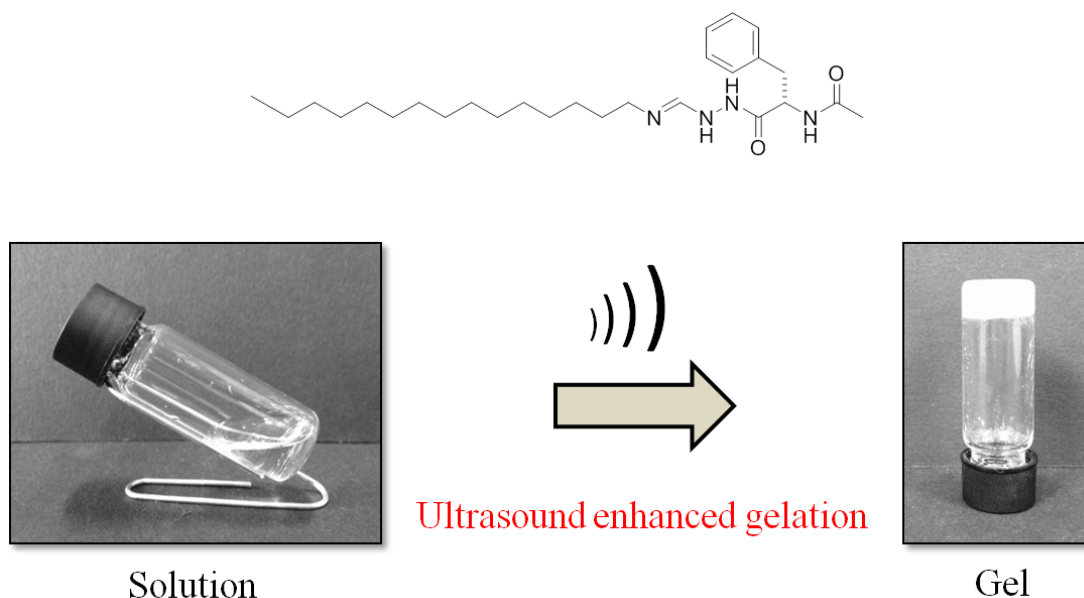
Enhancement of typical physical gelation properties of various organogels based on a formamidine compound by treatment of isotropic solutions with ultrasound is reported. The time necessary to promote gelation and critical gelation concentrations could be decreased significantly in comparison to values obtained by applying a classical heating-cooling protocol to induce gelation. On the other hand thermal stabilities as determined by thermal *gel*-to-so*l* transition temperature measurements and mechanical strength of model materials as determined by dynamic oscillatory measurements could be clearly improved. Additionally, an almost perfect linear correlation of typical gelation-properties with inductive Hammett-parameters in several aromatic solvents was explored giving rise of potential insight into prediction of certain behaviours of gel-materials. The injectable, smart thixotropic nature of the materials completes a versatile multi stimuli-responsive nature of the tested model systems, which also includes a colorimetric response against some metals-ions resulting in a potential application in the field of heavy-metal sensors. We are also delighted to report the first hydrogel formation of a gelator bearing a formamidine unit, which exhibits high temporal stability and ability of controlled drug release.

---

[i] In this chapter, all experiments were carried out by J. Bachl.

4.1. Introduction

Formamidines have been studied extensively during the last decades because of their facile preparation and high potential of biological or pharmacological activity.[1] Some prominent insecticides like chlordimeform[2, 3] and amitraz[3, 4] have been developed already since the late 1960s and have found broad industrial application, before some of them were found to exhibit carcinogenic potential. Also the concept of incorporating formamidine units into well studied drug-systems has been found to increase bioactivity in comparison to parent drugs and is hence a well accepted key modulation in medicinal chemistry.[5] On the other hand especially organo-metallic chemists also register interest on formamidines as complexing agents for metals in catalysis due to their high diversity of binding modes and structural variety.[6] Formamidines have been found to act as effective supporting ligands in e.g. zinc-catalyzed hydrosilylations,[7] iron-catalyzed epoxidations,[7] lanthanide-catalyzed Tishchenko reactions,[8] ruthenium-catalyzed olefin metathesis[9] or palladium-catalyzed cross additions[10] amongst others. In the fields of organocatalysis formamidines serve as important precursors for the preparation of *N*-heterocyclic carbenes (NHC),[11] which have proven their high activity and tremendous amount of reactions catalyzed for at least 20 years.[12] New developments on synthetic approaches towards multi-substituted formamidines even resulted in findings of gel-formation in protic organic solvents, which opens potential applications in the field of material science.[13] Viscoelastic gels,[14] which are one specific type of stimuli-responsive materials, have gained a lot of interest during the last decades due to their huge potential in fabricating new devices in the fields of biomedicine, catalysis, sensing, cosmetics, food and agriculture.[15] Gels, which are continuous in structure and solid-like on their rheological behaviour,[14 a)-c), 16] can be classified according to e.g. the nature of the solvent (organogels for organic solvents and hydrogels for water) or the types of interactions forming the network (chemical[17] or physical[18] gels). The solid-like appearance of the gels is a result of entrapment of liquid (major compound) in the interstices of a solid 3D matrix of large surface area (minor component) predominantly through surface tension and capillary forces.[18a), 19] In the case of gels based on low-molecular-weight (LMW) compounds, the formation of the solid matrix is a consequence of the entanglement of 1D suprapolymeric strands of LMW-molecules, which is typically induced by cooling hot isotropic solutions to room temperature.[18a), 20] Despite the classical heating-cooling (HC) protocol of gel-formation, some compounds are also known to

151

undergo transformation into stable gels by ultrasound (US) treatment,[21] although it was assumed previously that ultrasonic waves would disrupt self-assembly in solution.[22] The potential of ultrasound sonication lies in the formation of materials or architectures that are not accessible by other routes and is hence a valuable method for preparing functional soft materials. It is also known that ultrasonication can fasten or modulate the gelation kinetics and properties of certain gelator-systems.[23] In this context, we report a novel amphiphilic gelator molecule bearing a formamidine unit, which shows enhancement of typical gelation properties by US treatment in comparison to a standard HC protocol.

4.2. Experimental section

4.2.1.   Materials

Unless otherwise specified, all reagents, starting materials and solvents (p.a. grade) were purchased from commercial suppliers and used as received without further purification. Double-distilled water was purified additionally using a Millipore water-purifying system (Merck) prior usage. Xylene as mixture of isomers was used after double-distillation. Gasoline (95 octanes) and diesel were commercially available from Shell Company (Germany). See ESI† for detailed information about instrumentation, synthetic procedures, compounds and material characterization.

4.2.2.   Preparation of organogels *via* a heating-cooling cycle

Typically, a weighted amount of the formamidine-based gelator **1** and an appropriate organic solvent (0.5 mL) were placed into a screw-capped glass vial (4 cm length × 1 cm diameter) and gently heated with a heat gun until the solid material was completely dissolved. In some cases ultrasonication of the samples before heating could facilitate the dissolution of the compound. The resulting isotropic solution was then spontaneously cooled down to RT. No control over temperature rate during the heating-cooling process was applied. The material was preliminary classified as "gel" if it did not exhibit

gravitational flow upon turning the vial upside-down at RT. The state was further confirmed by rheological measurements.

4.2.3. Preparation of organogels *via* ultrasound treatment

An isotropic solution consisting of compound **1** and an appropriate solvent obtained by gentle heating was treated with ultrasound while still be warm using a VWR™ ultrasonic cleaner (USC200TH, 45 kHz, 120 Watt) keeping a constant temperature of 23±2 °C. During sonication stable gels were formed *in situ* during time intervals varying from a few seconds to several minutes, which were defined as the time necessary to promote gelation. Sole ultrasound treatment without applying heat did not facilitate gelation due to simple solubility issues of **1** in most organic solvents.

4.2.4. Preparation of hydrogels

Hydrogelation of the formamidine compound could be achieved by building a pH gradient in aqueous solution. The procedure of formation of hydrogels at optimized conditions is given as following: A certain amount of the formamidine (35 mg) is placed in a screw-capped glass vial when water (0.4 mL) was added. A minimum amount of 1M HCl (0.05 mL) is added to the mixture in order to dissolve the compound by gentle heating. Thereto 1M NaOH is added in portions of 0.01 mL (in total 0.04 mL) during treatment with ultrasound until a translucent gel-material at a final concentration of 71±8 mg/mL was formed *in situ*.

4.3. Results and discussion

4.3.1.   Compound design and synthesis

Several research groups have spent much effort on improving synthetic procedures towards the formation of substituted formamidine derivatives.[1, 13, 24] Especially formamidine acetals have found to be useful precursors in the synthesis of *N,N*-dimethyl formamidines, which can undergo exchange reactions of the dimethylamine fragment in the presence of suitable nitrogen-nucleophiles, to yield diverse mixed formamidine compounds.[13, 24a)]
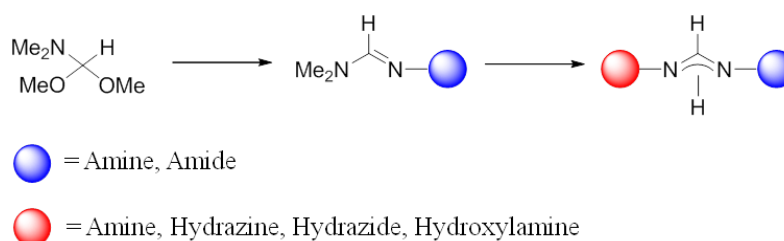
Fig. 1 Synthetic route for the production of mixed substituted formamidine-derivatives.

Taking advantage of such efficient synthetic routes, we were able to design an amphiphilic formamidine-based molecule (**1**), which consists of an apolar tail built by a chain of carbons on one side of the formamidine nucleus and a polar phenylalanine-based head group on the other side. Such structural motif is a key concept for the preparation of functional soft materials like gels, which draw tremendous interest because of their huge amount of potential applications in fields mentioned above. Additionally donation of the lone-pair of the hydrazide moiety increases significantly the stability towards hydrolysis as described earlier.[13]

4.3.2.   Gelation ability and effect of ultrasound treatment

The gelation ability of compound **1** was systematically investigated for 30 organic solvents of different nature (apolar, polar aprotic or polar protic) by applying a classical heating-

cooling cycle. Materials that did not exhibit gravitational flow according to the "stable-to-inversion" method[25] were preliminary classified as gels and their solid-like appearance was further confirmed using dynamic rheological measurements (*vide infra*). The formamidine was found to be highly soluble in DMF, THF and chlorinated solvents like CH_2Cl_2, $CHCl_3$ or 1,2-dichloroethane, while being insoluble in glycerine. Partial gels at maximum concentrations of 200 mg/mL have been formed in alcoholic solvents like MeOH, EtOH, *i*-PrOH, 2-butanol, 1-hexanol.
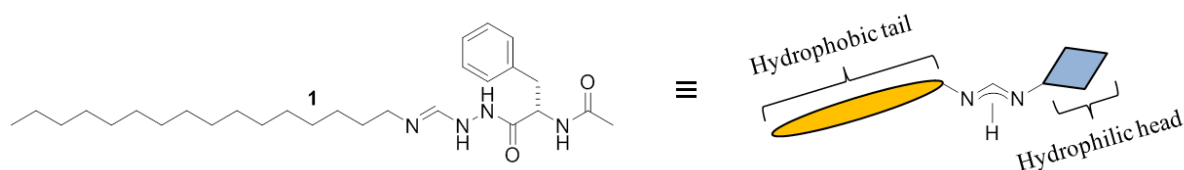
Fig. 2 Amphiphilic nature of compound **1**.

All 19 of the remaining solvents, including also two room temperature ionic liquids and several oil-based solvents, were able to produce stable gels in a concentration range varying from about 15-150 mg/mL for most samples, which opens the door for potential applications in removal of oil spills and fabrication of conducting materials. During investigations concerning other approaches towards the formation of stable gels different to the classical heating-cooling (HC) cycle, it was found that ultrasound (US)-treatment (see experimental section) of isotropic solutions of compound **1** and an appropriate organic solvent resulted in faster gelation kinetics of up to 99 % of the original value. Interestingly also the range of solvents gelled could be extended by the 5 alcoholic solvents mentioned above.

4.3.3. Enhanced gelation-properties: Considerations on appearance, concentration, thermal and mechanical stabilities

Efficient gelation of compound **1** could be observed in 80% of all tested organic solvents by US treatment of isotropic solutions, hence extending the scope of the classical HC procedure by 5 solvents. This finding shows the high efficiency of compound **1** to gel

various types of solvents with varying functionalities and polarity scales exhibiting a broad range of potential applications.

Fig. 3 A) Representative digital photographs of upside-down vials containing organogels derived form **1**. The materials have been prepared according to the US treatment described in the experimental section at their corresponding *CGC*. Abbriviations: 2-BuOH = 2-butanol; DOX = 1,4-dioxane; 1-HexOH = 1-hexanol; IL-1 = 1-butyl-3-methylimidazolium hexafluoro phosphate; IL-2 = 1,3-dibutylimidazolium hexafluoro phosphate; PheCl = chlorobenzene; PheCN = benzonitrile; R-oil = rapeseed oil; S-oil = silicon oil. B) Proof of transparency of gels derived from toluene (17 mg/mL) in comparison to gels derived from MeCN (9 mg/mL). Top: Intact gels; Bottom: gels destroyed using a spatula.

In general completely transparent (benzene, toluene, xylene) or translucient (chlorobenzene, benzonitrile, olive-, rapeseed-, silicon oil, gasoline and diesel) appearance of the gels derived from aromatic and most oil-based solvents could be observed independent on the method of material preparation at comparable concentrations. Gels derived from chlorobenzene and benzonitrile could be triggered towards the formation of completely transparent materials by reducing the concentration as possible by applying US treatment. On the other hand, the formation of aggregates bigger than the wavelength of visible light (ca. 380-780 nm) was observed in all other solvents, as indicated by the complete opacity of the organogels (view Figure 3). Independent of the nature of the solvent or the preparation method all gels remained their solid like structure for at least 6 month inside screw capped vials. Critical gelation concentrations (*CGC*), defined as the minimum concentrations of formamidine where gelation was observed, were established to be in a range of 15-150 mg/mL for most cases applying a classical HC protocol.

156
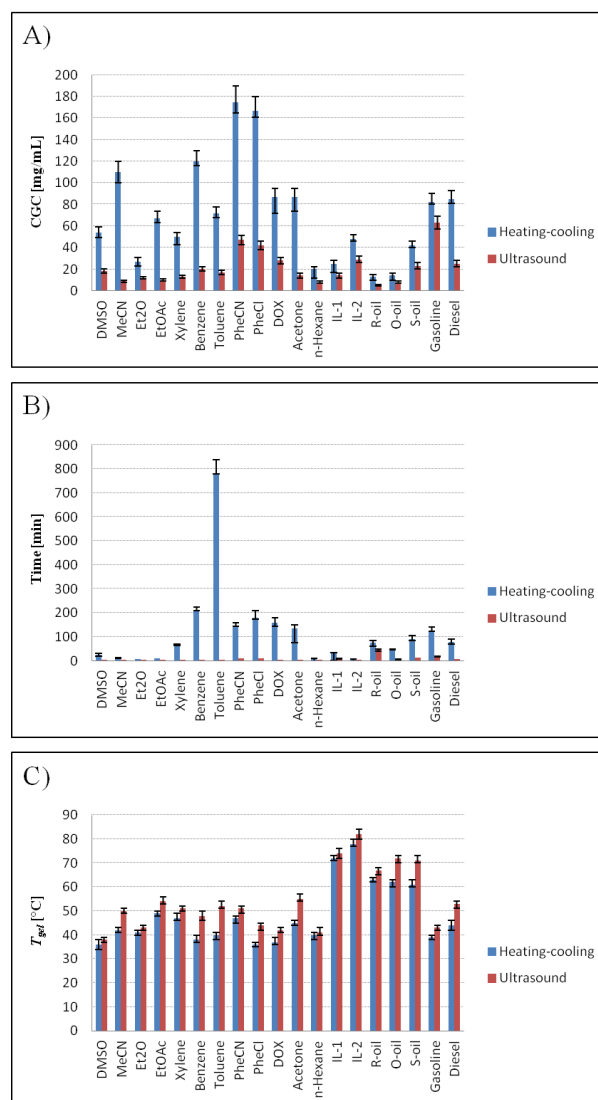
Fig. 4 Bar graphs showing the enhanced gelation properties of ultrasound treatment in comparison to a classical heating-cooling protocol of tested systems. A) *CGC*; B) time necessary for gelation; C) T_{gel} (values of plots B) and C) have been determined at comparable concentrations). Solvents, where no gelation was observed by the both preparation methods are not plotted. Abbriviations: 2-BuOH = 2-butanol; DOX = 1,4-dioxane; 1-HexOH = 1-hexanol; IL-1 = 1-butyl-3-methylimidazolium hexafluoro phosphate; IL-2 = 1,3-dibutylimidazolium hexafluoro phosphate; PheCl = chlorobenzene; PheCN = benzonitrile; R-oil = rapeseed oil; S-oil = silicon oil.

Astonishingly the introduction of US treatment of isotropic solutions resulted in a decrease of *CGC* values (view Figure 4) in all tested cases. Several hundreds of solvent molecules per gelator molecule can hence be effectively immobilized inside the gel-matrices. In solvents like silicon oil or 1-butyl-3-methylimidazolium hexafluoro phosphate the *CGC* decreases from 42 to 23 and 25 to 14 mg/mL (ca 45 %) respectively, whereas the decrease is even more visible in solvents such as EtOAc, benzene or acetone (about 80-85%).
157

Moreover, *CGC* values of as low as 5 mg/mL could be observed by simple application of the ultrasound protocol in some cases. The thermal stability of obtained organogels was evaluated using their thermal *gel*-to-*sol* transition temperatures (T_{gel}). T_{gel} values were obtained using a custom made set-up as described in the ESI (view Figure S1) as a variation of the "inverse-flow-method (IFM)"[26] and cross-checked using the classical IFM. However, the values determined by IFM strongly depend on factors such as cooling rate, aging time, thermal history, and degree of hysteresis[27] among others, and hence were correlated for model systems to the first endothermic transition observed by modulated DSC. In general all gels reveal a full thermo-reversible nature without changing the T_{gel} significantly even after several cycles. The obtained values are quite low in a range between ca. 35 to 50 °C, which is quite typical for LMW-based gels. Only in ionic liquids and oil-based solvents higher T_{gel}-values between about 60 to 80°C could be observed. But in all tested materials an increase in thermal stability was obvious comparing a classical heating-cooling protocol towards ultrasound treatment. In most cases only a slight increase (ΔT_{gel} of about 2-5 °C) could be observed whereas solvents like acetonitril, benzene, toluene, acetone, olive- and silicon oil revealed higher improvement of up to 12 °C (for tabular data on *CGC*, gelation time, optical appearance and T_{gel}-values see table 1, for detailed information on all tested systems see ESI). According to which solvents provide the highest differences on so far established gelation properties (*CGC*, gelation time, T_{gel}) between classical heating-cooling and ultrasound preparation of gels, two model systems were selected for further studies. Taking also the nature of the solvent into consideration an aromatic and apolar solvent, toluene, and a polar aprotic solvent, MeCN, were chosen. As usual in other physical gels, T_{gel} increases significantly with increasing gelator concentration (view Figure 5), indicating that self-assembly processes are driven by strong intermolecular interactions affording closely packed 3D networks. Gelator concentrations could be increased up to 300 (toluene) or 500 mg/mL (MeCN) respectively, affording homogeneous gels. A typical plateau region for both examples (ΔT_{gel} = 19 and 13 °C) was visible before the gels collapsed into partial and inhomogeneous gels with expelling some liquid on top over short periods of time lower than 30 min. However more realistic vision can be obtained by looking at the percental increase of a variable over the entire range of permitted concentration until reaching a plateau value of T_{gel}. The Ln-Ln plot of the percentage increases before the plateau regions, showed a good linear relationship between

the increment in the gelator concentration and the consequent increment in the T_{gel} with respect to the initial values at the *CGC* (view Figure 5 B)).

Tab. 1 Comparison of gelation properties derived from heating-cooling and ultrasonication enhanced protocol for gelation. [a]

Solvent	CGC[b] [mg/mL]	Gel-Time[b]	T_{gel}[b] [°C]	Appearance[b]	CGC[c] [mg/mL]	Gel-Time[c],[d] [min]	T_{gel}[c],[d] [°C]	Appearance[c]
DMSO	54 (5)	25 (5)	36 (2)	OG	18 (2)	4.5 (0.5)	38 (1)	OG
MeCN	110 (10)	12 (2)	42 (1)	OG	9 (1)	0.8 (0.1)	50 (1)	OG
Et₂O	27 (4)	7 (1)	41 (1)	OG	12 (1)	1.3 (0.1)	43 (1)	OG
EtOAc	67 (7)	10.5 (0.5)	49 (1)	OG	10 (1)	0.8 (0.1)	54 (2)	OG
Benzene	120 (10)	210 (15)	38 (2)	TPG	20 (2)	4 (0.5)	48 (2)	TPG
Toluene	72 (6)	780 (60)	40 (1)	TPG	17 (2)	2.5 (0.2)	52 (2)	TPG
Xylene	50 (4)	65 (5)	47 (2)	TPG	13 (1)	1.5 (0.2)	51 (1)	TPG
PheCl	167 (13)	180 (30)	36 (1)	TLG	42 (4)	9.5 (0.5)	44 (1)	TPG
PheCN	175 (15)	145 (15)	47 (1)	TLG	47 (4)	11 (0.5)	51 (1)	TPG
DOX	87 (8)	160 (20)	37 (2)	OG	28 (3)	5 (0.5)	42 (1)	OG
Acetone	87 (8)	135 (15)	45 (1)	OG	14 (2)	0.8 (0.1)	55 (2)	OG
Hexane	20 (2)	10 (0.5)	40 (1)	OG	8 (1)	1.3 (0.1)	41 (2)	OG
IL-1	25 (3)	30 (5)	72 (1)	OG	14 (2)	8.5 (0.5)	74 (2)	OG
IL-2	48 (4)	7 (1)	78 (2)	OG	29 (3)	3.5 (0.5)	82 (2)	OG
R-oil	13 (2)	75 (10)	63 (1)	TLG	5 (1)	45 (5)	67 (1)	TLG
O-oil	14 (2)	45 (5)	62 (1)	TLG	8 (1)	5.5 (0.5)	72 (1)	TLG
S-oil	42 (4)	90 (15)	61 (2)	OG	23 (3)	13 (1)	71 (2)	OG
Diesel	85 (8)	80 (10)	44 (2)	TLG	25 (3)	7.5 (0.5)	53 (1)	TLG
Gasoline	82 (8)	125 (15)	39 (1)	TLG	63 (6)	16.5 (1.5)	43 (1)	TLG

[a] Values in brackets indicate errors from at least 2 randomized experiments. [b] Values obtained *via* heating-cooling protocol. [c] Values obtained *via* ultrasound enhanced protocol. [d] Values determined at the corresponding *CGC* of the heating-cooling protocol. Abbriviations: OG = opaque gel; TLG = translucient gel; TPG = transparent gel; 2-BuOH = 2-butanol; DOX = 1,4-dioxane; 1-HexOH = 1-hexanol; IL-1 = 1-butyl-3-methylimidazolium hexafluoro phosphate; IL-2 = 1,3-dibutylimidazolium hexafluoro phosphate; PheCl = chlorobenzene; PheCN = benzonitrile; R-oil = rapeseed oil; S-oil = silicon oil.

Thus, within the end-limits defined by the *CGC*s and the maximum T_{gel} values, the slopes of these straight lines indicated that in toluene as solvent a slight 1.1-fold higher percentage increment of T_{gel} is observed in comparison to MeCN. A similar behaviour of

gelation time with increasing gelator concentration could not be observed as the gelation time stays pretty much constant during the whole range of concentration. Interestingly, during increasing gelator concentration in toluene as solvent a gradual growth of particle size could be observed, indicated by a change of optical appearance of the gels from complete transparent to translucent (from 200 mg/mL) and opaque (from 300 mg/mL), on the other hand gels derived from MeCN kept their opaque nature abroad the whole concentration range.
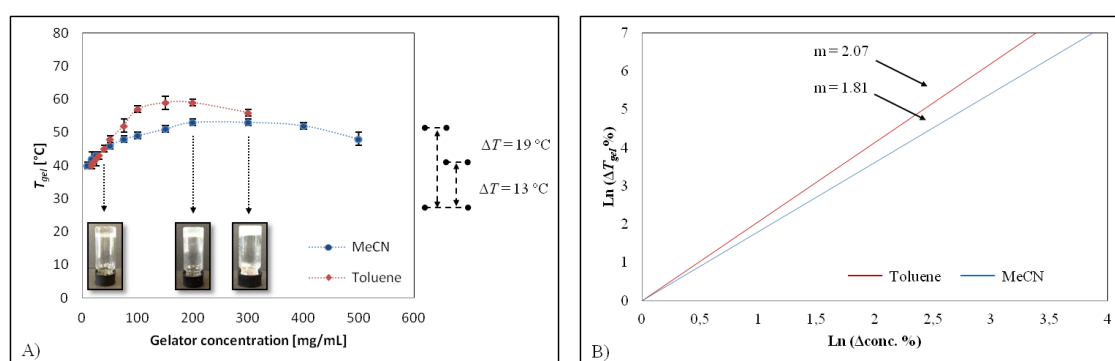

Fig. 5 A) Phase boundaries defined by the evolution of T_{gel} with increasing gelator concentration for gels formed by ultrasound treatment for both MeCN and toluene. Gradual growth of particle size in gels derived from toluene as visual from a change of optical appearance from transparent to opaque with increasing gelator concentration. B) Normalized Ln-Ln plot of the corresponding percental increase.

Oscillatory rheological measurements unequivocally confirmed the viscoelastic gel nature of the materials that did not show gravitational flow upon turning the vial upside-down. Thus, their storage modulus G' (energy storage modulus) and loss modulus G'' (energy loss modulus) were first measured at room temperature as a function of frequency (dynamic frequency sweep experiment, DFS) and shear strain (dynamic strain sweep experiment, DSS) to determine the linear viscoelastic regime associated to the material (view Figure 6 A)). Relatively constant tan δ (G''/G') values during the frequency sweep indicate a good tolerance of the gels to external forces. Within the linearity limits of deformation (solid-like response), the storage modulus was approximately one order of magnitude higher than the loss modulus during the flow experiment (e.g. $G' \approx 7.9 \pm 0.5$ kPa, $G'' \approx 1.1 \pm 0.1$ kPa, for the gel made in toluene at 17 mg/mL by US treatment). The viscoelastic and brittle nature of the materials was confirmed by the destruction of the gels at low frequency and about 5 % of strain. Further dynamic time sweep (DTS) measurements at 0.1% strain and 1

160

Hz frequency confirmed the stability (no phase transition) of the gel materials as a function of the ageing time at room temperature (view Figure 6 B)). In general, the tan δ values between random measurements of the same material were reproducible and decreased with the concentration of the gelator, suggesting an enhancement of the mechanical damping properties. In general gels derived from MeCN show an enhanced mechanical stability in comparison to toluene.
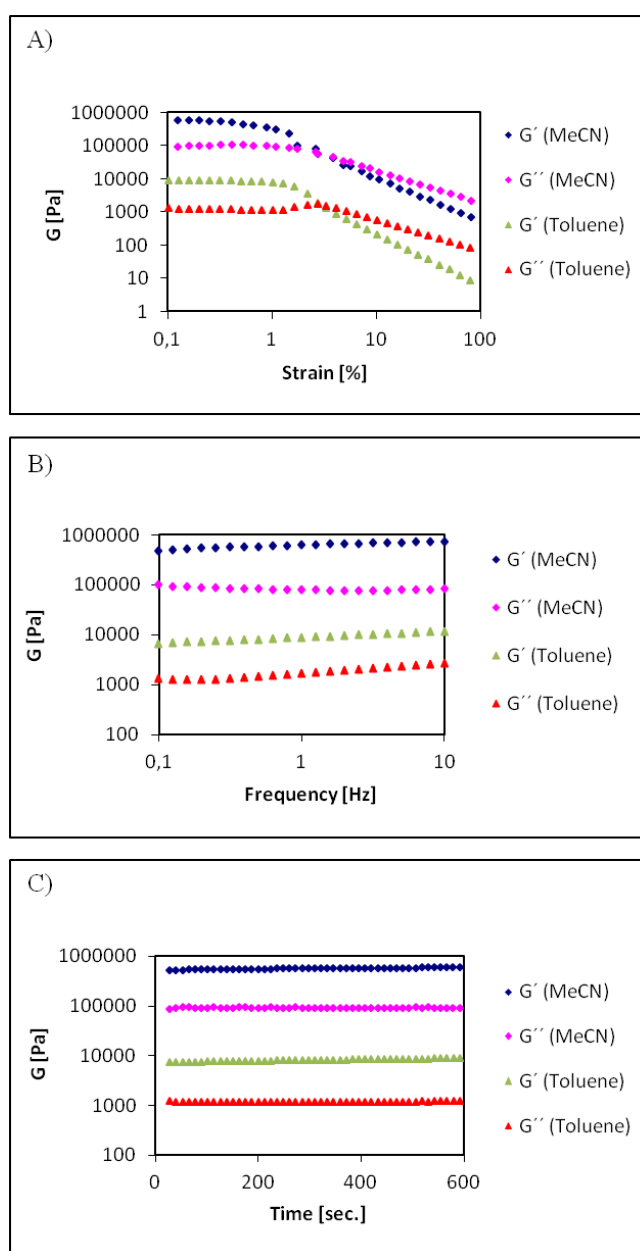
Fig. 6 Oscillatory rheological measurements of model gels: Representative A) DSS, B) DFS and C) DTS experiments of the gel made from **1** in MeCN and toluene. The gels were prepared by the ultrasound enhanced protocol at their *CGC* as indicated in Table 1.

161

Comparing the different methods for gel preparation at the concentration necessary to form stable gels in both cases, it is obvious for the 2 model solvents that gels prepared by US treatment show enhanced properties against the classical HC protocol in respect to the absolute value of G', the tan δ and the maximum % strain at break (at least visual for MeCN) of the material (view Table 2 and Figure 7).

Fig. 7 Comparing the 2 methods for gel preparation by oscillatory rheological measurements at the corresponding *CGC* (72 mg/mL) of the heating-cooling protocol in toluene as model system (Plots for MeCN can be found in ESI): A) DSS, B) DFS and C) DTS experiments.

Relative high values for tan δ of gels derived from the HC method indicate their low mechanical stability. These findings are in good agreement with other gelation properties mentioned earlier. Furthermore 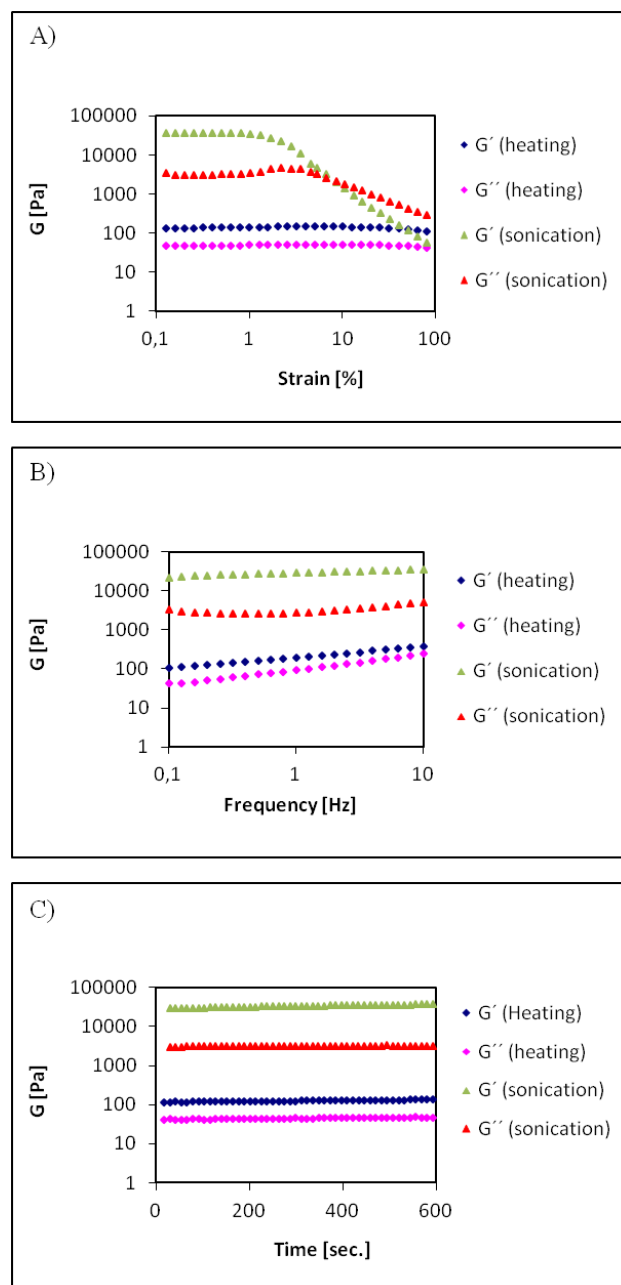we are delighted to report a smart thixotropic response of almost all gels (except form gels derived from gasoline and hexane) to both macroscopic shaking and external large straining almost independent on the nature of the solvent or the preparation method within seconds, which is considered a key property for real-life applications of gel-based materials.[28]

Tab. 2 Comparison of oscillatory rheological properties derived from heating-cooling and ultrasonication enhanced protocol for gelation. [a]

	MeCN		Toluene	
	HC	US	HC	US
G' [kPa]	720.3	3162.8	0.12	33.0
G'' [kPa]	206.1	672.5	0.04	3.1
tan δ	0.29	0.21	0.35	0.09
Strain [%]	2	6	>100	8

[a] Toluene and MeCN were used as model systems. Data were obtained from at least 2 randomized experiments at the corresponding *CGC* of the heating-cooling protocol as indicated in table 1. Errors obtained were always below 10 % of the absolute values.

Figure 8 shows a simple thixotropy three-step rheological loop test[29] for the organogel made of **1** in MeCN (9 mg/mL) prepared by the US enhanced gelation protocol. The experiment is based on successive cycles involving the following steps: 1) application of a shear strain and frequency as defined by DTS experiments (gel state, $G' > G''$, 0.1 % strain, 1 Hz frequency), 2) increase of the shear strain until the gel fractures (viscous solution, $G' < G''$, 100-1000 % strain, 1 Hz frequency) and 3) return at the same rate to the initial strain % value (recovered gel state, $G' > G''$). In the model example shown in Figure 8 the gel displayed more than 98 % recovery after the first and more than 85 % after the second cycle of the thixotropic loop test. Such fast and almost complete recovery of the gel-strength gives raise for potential applications in the field of injectable gels for lubrication purposes or biomedicine.
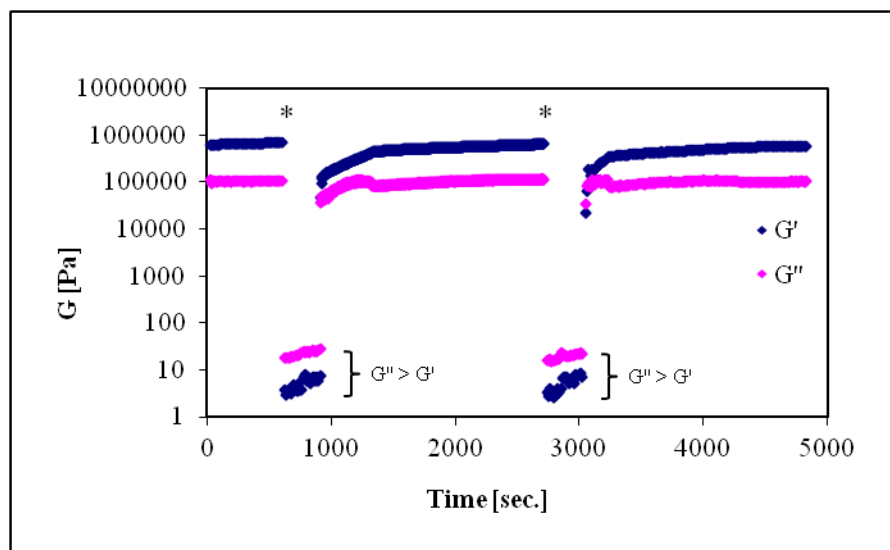
Fig. 8 Typical thixotropy loop test of the model gel made from **1** in MeCN (9 mg/mL). The strain for each step during shear was first increased from 0.1% (linear viscoelastic regime –gel state–) to 100% (rupture of the gel –solution state–) and subsequently returned to the original value (recovery of the gel state). Asterisks indicate the increase of the shear strain at the time scale.

4.3.4. Correlation with solvent parameters and multi-stimuli responsive nature

Taking a close look on the gelation behavior of formamidine compound **1** in aromatic solvents, it was found that the substituent of monosubstituted benzene derivatives has a significant influence on the *CGC* of gels obtained by the US enhanced protocol (view Table 3). As general trend it is obvious that *CGC*-values decrease for electron-donating substituents, which seems to correlate with resonance and inductive stabilization parameters. One suitable approach to quantify this observation with experimental data is using Hammett-parameters. The Hammett-equitation was developed based on empirical observations investigating the rate constants of the basic hydrolysis of substituted benzoic acid esters correlating the former with substituent induced effects that can be expressed by the difference of corresponding Gibb´s enthalpies.[30] Later on Taft expanded the studies, taking also sterical, inductive and resonance effects of the substituent into consideration making the parameters more accurate.[31] Recent computational and experimental studies revealed a clear correlation of aromatic stacking interactions with inductive Hammett-parameters σ^i.[32] Computational studies support a model describing aromatic rings as

164

positively charged σ-frameworks that are sandwiched between two regions of negatively charged π-electron density. Substituents on aromatic rings can either directly interact in stacking properties or influence the arene by polarization effects. Both experimental and theoretical investigations reveal a positive effect on the stacking affinity of arenes by electron-withdrawing substituents. A probable explanation could be a simply reduction of the repulsion caused by electron density, and a reciprocal effect caused by electron-donating substituents.[33] In our studies we found a clear and almost perfect linear relationship between σ^i –parameters and *CGC*, gelation time and T_{gel}-values in 5 aromatic solvents tested (view Figure 9). We assume that electron-withdrawing substituents increase intermolecular solvent-solvent interactions by positive influence on stacking-properties and hence weaken intermolecular gelator-solvents interactions responsible for effective gelation. On the other hand electron donating substituents of aromatic solvents enhance gelation properties by facilitating the formation of gelator-solvent interactions in comparison to unsubstituted benzene. A similar conclusion could be also drawn for gels prepared by the classical HC cycle, but the correlation with Hammett-parameters is not as perfect. The order of suitable aromatic solvents for gelation induced by compound **1** would hence be the following: Xylene > Toluene > Benzene >> Chlorobenzene > Benzonitril. This finding suggests a clear participation of intermolecular π-π-stacking interactions, which seem to be next to H-bonding interactions the driving forces for effective gelation ability of **1**.

Tab. 3 Correlation of gelation properties of compound **1** in aromatic solvents with corresponding σ^i – parameters[34] of the substituents. [a]

Solvent	σ^i	*CGC* [mg/mL]	Gel-Time [min]	T_{gel} [°C]
Xylene	-0.10	13 (1)	1.5 (0.3)	51 (1)
Toluene	-0.05	17 (2)	2.5 (0.3)	48 (1)
Benzene	0.00	20 (2)	3.5 (0.3)	46 (1)
PheCl	0.47	42 (4)	10.8 (0.5)	38 (1)
PheCN	0.59	47 (4)	12.5 (0.5)	36 (1)

[a] Abbriviations: PheCl = Chlorobenzene; PheCN = Benzonitril. Values for gelation time and T_{gel} of all systems have been determined at the highest *CGC* in PheCN for comparative purposes. For Xylene the σ^i – value caused by the CH_3-group has been simply doubled for approximation. Values in brackets indicate experimental errors.
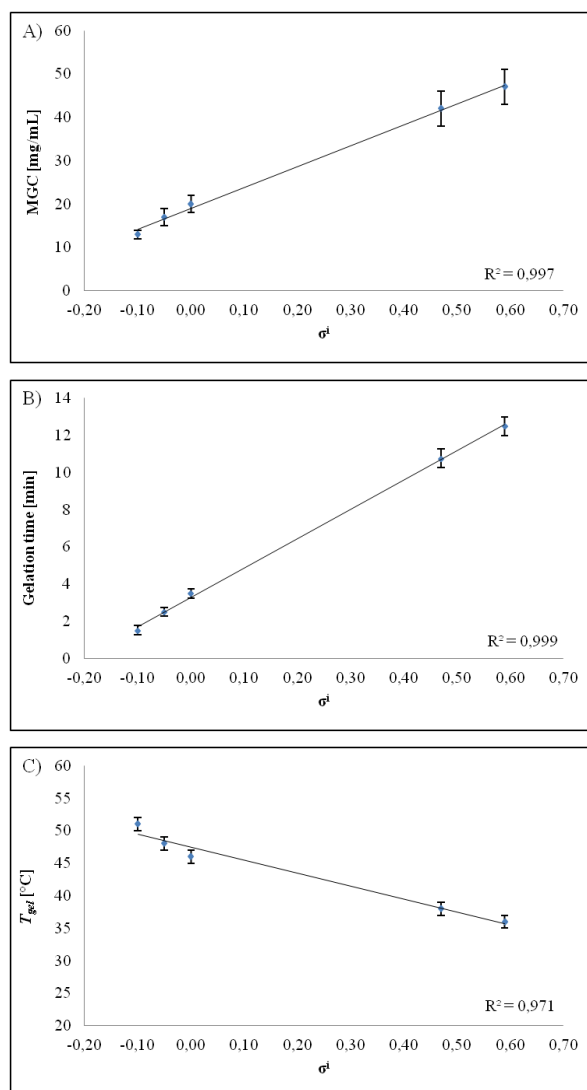
Fig. 9 Graphical plots of the linear correlation of corresponding aromatic solvent σ^i – parameters[34] with gelation properties of compound **1**. A) *CGC*, B) Gelation time and C) T_{gel}-plots.

The response towards external stimuli of physical gels is one of their key-features for potential applications. As mentioned above all gels reveal a full thermo-responsive nature without any visible changes in T_{gel} even after several cycles of heating and cooling independent on the nature of solvent and preparation method. Also a smart thixotropic response against vigorous mechanical shaking or application of large strain was observed in all gels except from hexane and gasoline. Furthermore we explored an injectable nature of the thixotropic materials after vigorous shaking/stirring as indicated in Figure 10. These findings complete a versatile multi-responsive map of gels derived from **1**. Figure 11

summarizes the results carried out using toluene (17 mg/mL) as model system (data for MeCN, which exhibits similar behavior, can be found in the ESI). An isotropic solution obtained by heating could be transformed into stable and fully thermo-reversible organogels upon cooling or ultrasound treatment.
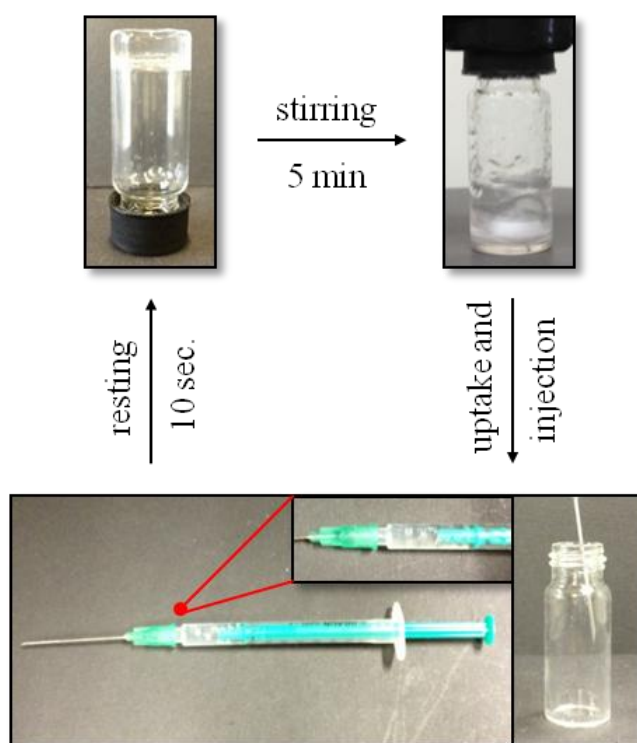
Fig. 10 Digital photographs demonstrating the thixotropic and injectable nature of gels from **1** in toluene (17 mg/mL) prepared by the ultrasonication enhanced gelation protocol. Vigorous stirring of the gel for 5 min results in the formation of a viscous solution, which can be uptaken using a syringe (1 mL volume) and injected into a vial afterwards, resulting in reformation of a stable gel within 10 sec.

In addition, vigorous shaking of the vial afforded a viscous solution, which could return to a stable gel state within seconds. Finally irreversible chemical response of gels within minutes was found against addition of HCl, various electrolytes (NaCl, KF, CsCl, Na_2SO_4, etc.) and many gelling and non-gelling organic solvents (except from apolar or aromatic solvents like cyclohexane, hexane, octane, toluene or benzonitrile). On the other hand stability of organogels could be preserved in the presence of water and NaOH, as well as halides (TBAF, TBAB and TBACl). Furthermore we observed a *gel*-to-*sol* phase transition

of organogels in the presence of aqueous metal-cations solutions with valences between I and IV.
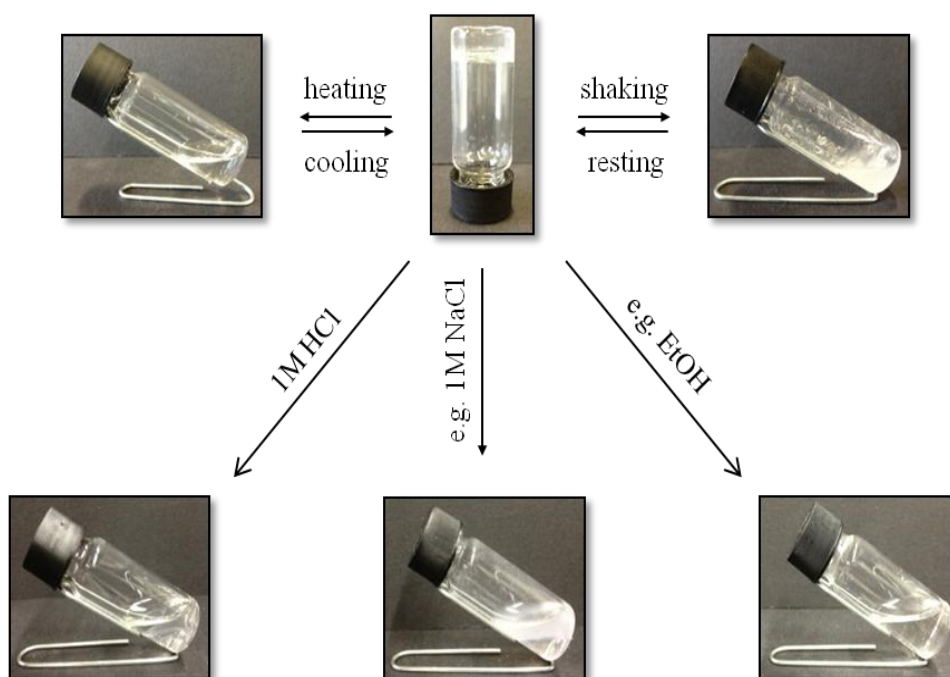

Fig. 11 Diagram showing the preparation of multi stimuli-responsive organogels from **1** in toluene (17 mg/mL) prepared by the ultrasound enhanced protocol.

Interestingly the addition of Cu(II) and Fe(III) resulted in a change of color of the toluene layer very different to the color of the aqueous metal solutions accompanied by a *gel*-to-*sol* phase transition. Confirmation of the visual inspection was carried out using UV-vis spectroscopy. The toluene layer after phase separation caused by the addition of e.g. Cu(II) exhibited a shift of the maximum wavelength λ_{max} from 808 to 418 nm. This finding could suggests either the formation of metal nanoparticles by reductive motifs of compound **1** or more likely, the formation of metal-formamidine complexes,[25,35] but in order to draw firm statements further studies like the growth of crystals still need to be carried out. On the other hand Ag(I) and Ce(IV) solutions caused a disruption of the gel by phase separation without any visible change of coloration indicating another mechanisms responsible for the *gel*-to-*sol* transition. Figure 12 documents the change in coloration with digital photographs and UV-spectra for the case of Cu(II). This interesting observation could give potential application of gels derived from **1** in the field of heavy metal sensing by applying simple spectroscopic techniques.
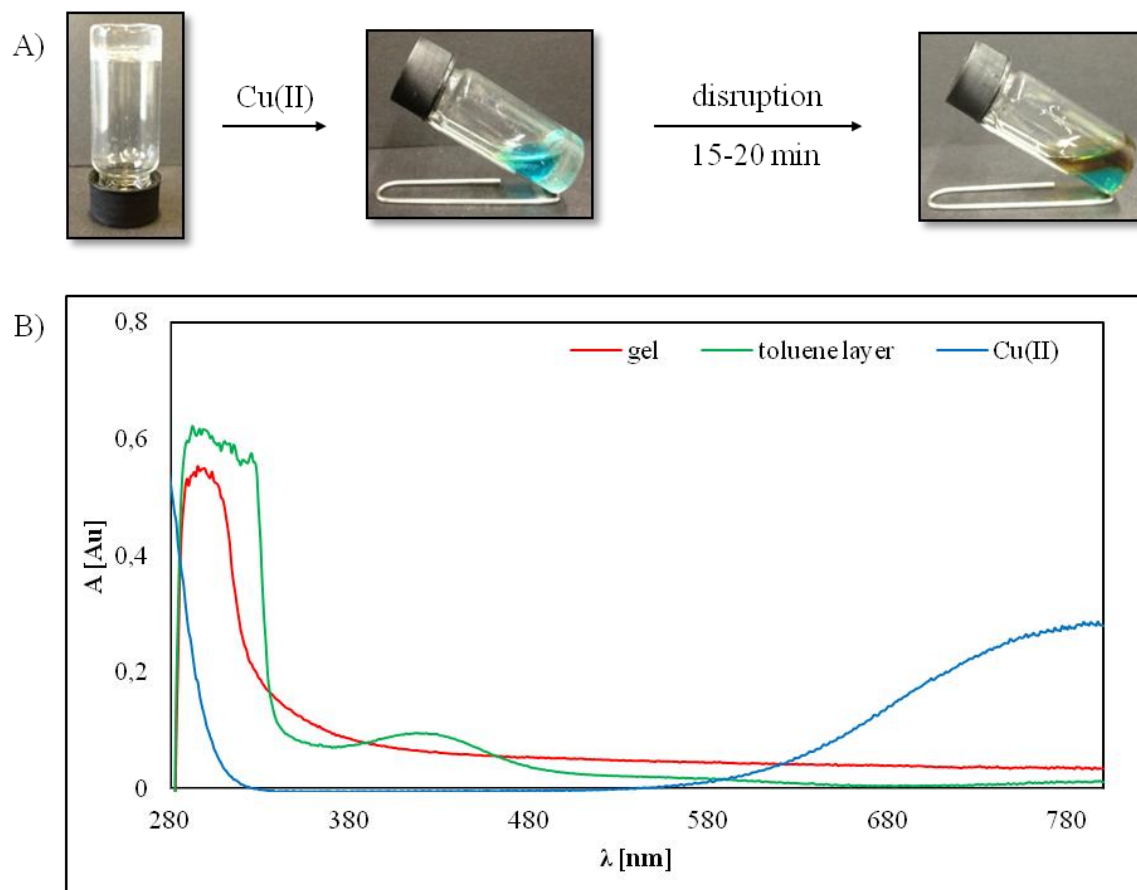
Fig. 12 Responsive nature of gels derived from toluene (17 mg/mL) against aqueous solutions of Cu(II). A) Digital photographs demonstrating the change of coloration of the toluene layer in comparison to metal-solution accompanied by a gel-to-sol phase transition. B) Corresponding UV-spectra of aqueous $CuSO_4$ * $5H_2O$-solution (0.1M), the gel derived from toluene (17 mg/mL) and the toluene layers (diluted by a factor of 1:10) after phase separation. Documentation for Fe(III) and Ce(IV) can be found in the ESI.

4.3.5.   Morphological and spectroscopic characterization

In order to gain visual insight into the morphologies of the organogels we conducted field emission scanning electron microscopy (FESEM) of the corresponding xerogels. A 3D appearance of the samples surface structure was revealed resembling kind of smooth and very dense lava-flows when toluene was used as solvent (view Figure 13 A-F). Commonly we observed several fibres fused together to form large longitudinal fibrillar structures with diameters varying from 0.5-20 μm (e.g. Figure 13 A, B). In contrast much smaller fibrillar structures with a diameter from 50-500 nm could be observed using more polar MeCN as solvents, resembling porous and much rougher surfaces similar to sponges and corals,

which can be found in the sea (Figure 13 G-L). In general more densely packed structures could be observed by increasing the concentration of the gelator, which is kind of predictable and in good agreement with their higher thermal stability and internal cohesiveness as indicated by their higher T_{gel}-values (e.g. Figure 13 C, D, I, J).
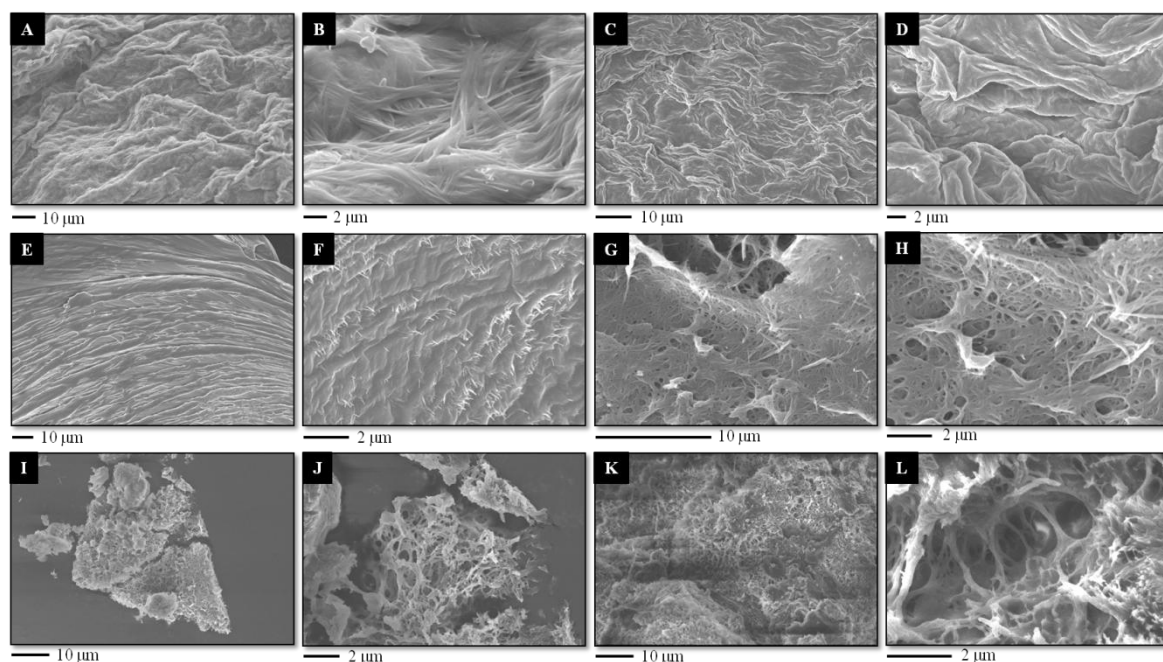
Fig. 13 SEM (A, B and G, H) and FESEM (C-F and I-L) images of cryogels prepared by the freeze-drying method from corresponding organogels. A, B: xerogel from toluene (17 mg/mL) prepared by ultrasound treatment; C, D: xerogel from toluene (72 mg/mL) prepared by ultrasound treatment; E, F: xerogel from toluene (72 mg/mL) prepared by classical heating-cooling protocol; G, H: xerogel from MeCN (9 mg/mL) prepared by ultrasound treatment; I, J: xerogel from MeCN (110 mg/mL) prepared by ultrasound treatment; K, L: xerogel from MeCN (110 mg/mL) prepared by classical heating-cooling protocol.

Such findings indicate differences in intermolecular solvent-gelator and gelator-gelator interactions, postulating a combination of H-bonding and π-π-stacking interactions as driving forces for gelation with different quantification dependent on the nature of the solvent. Comparing the two methods of preparation it can be seen that the solvent dependent morphology is preserved on the first view independent on the method of preparation (Figure 13 C-F and I-L). Paying more close attention it is obvious that differences can be spotted out. Gels prepared by the classical HC protocol in general exhibit less density of the networks (Figure 13 E, F and K, L). In the case of toluene as solvent the longitudinal structures are more wrinkled and fused in the case of US

170

treatment. Gels derived from MeCN show smaller pore-sizes when ultrasound is applied indicating a denser and more compact structure. These findings are in good agreement with other conclusions drawn previous and highlight the positive effect of ultrasound treatment on general gelation properties, including thermal and mechanical stabilities of the materials. Additionally transmission electron microscopy (TEM) imaging of cryogels derived from toluene reveal dense, characteristic fibrillar networks, consisting of bundles of twisted fibres with diameters varying from ca. 50-100 nm (smallest feature) and length on the scale of microns (see Figure 14). The high aspect ratio of the entangled networks is a consequence of a strong anisotropic growth process, which indicates a well ordered molecular packing to form unit nanofibers (for a selection of SEM/FESEM imaging in further solvents see ESI).
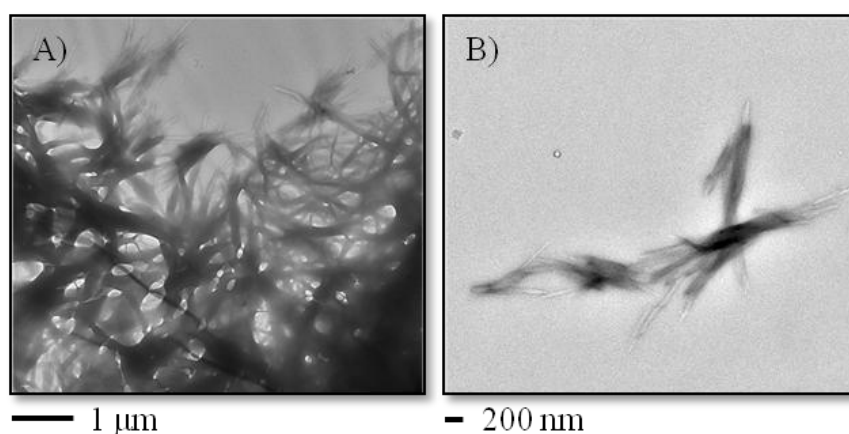
Fig. 14 Representative TEM photographs of xerogels obtained from gels in toluene (17 mg/mL) with magnifications of 2500x (A) and 4000x (B) respectively. Inset scheme (B) indication a thin fibre bundle of ca. 70 nm.

As expected, comparative FT-IR confirmed the participation of hydrogen-bonded amides during the gelation process. Thus hydrogen bonding in the organogels both slightly shifted CO and NH resonances to lower energies with respect to the solid state of the gelator **1** (e.g. from 1627 to 1617 cm^{-1} for amide I bands, and from 3287 to 3283 cm^{-1} for NH stretching bands respectively in MeCN as indicated in Figure 15). Although the *gel*-to-*sol* transition occurred with increasing temperature, the IR-bands arising from hydrogen-bonded amide groups decreased only marginally in the solution state indicating that these interactions are already significantly present in solution and also in the solid state. Also

noteworthy to mention is, that the preparation method and solvent has no significant influence on the development of IR band.
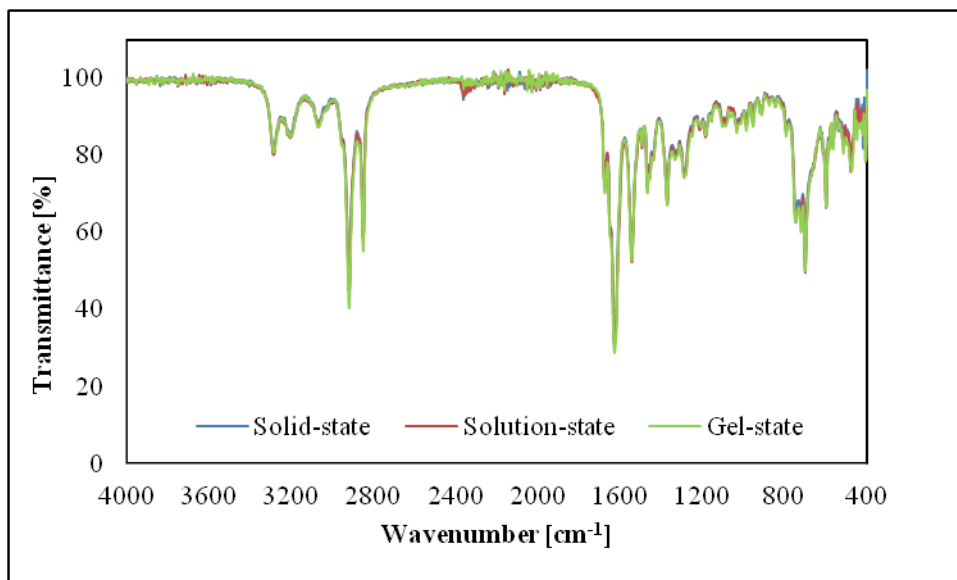
Fig. 15 Comparative FT-IR spectra derived from MeCN (9 mg/mL) prepared by ultrasound treatment showing solid state, gel-state and solution state (e.g. NH stretching bands are shifted to lower energies from 3287 cm^{-1} in the solid state to 3286 and 3283 cm^{-1} in the solution and gel state respectively.

4.3.6.   Hydrogel formation and characterization

Besides the formation of organogels in various organic solvents, compound **1** was also investigated on its potential of hydrogel formation. For this purpose many different methodologies have been explored, but remained unsuccessful. Neither a classical heating-cooling protocol in combination with ultrasound treatment, nor the use of water-soluble co-solvents (5-50% v/v) like acetone, DMF, DMSO, HFIP, or MeOH resulted in the formation of hydrogels, but in precipitation or insolubility of compound **1**. Also the potential formation of metallogels in the presence of various metal-salts (Ag(I), Cu(II), Fe(III) and Ce(IV)) remained inefficient. Only the good solubility of the formamidine in acidic media, probably due to simple protonation events, gave rise to the formation of hydrogels by building a simple pH-gradient from acidic to more basic media, by dissolving the compound in a minimum amount of 1M HCl and addition of small portions of 1M NaOH during ultrasound treatment. A detailed description of the procedure can be found in

172

the experimental section under optimized conditions. Hence stable and translucent hydrogels could be formed at an effective gelator concentration of 71±8 mg/mL at a pH between 4 and 5 as determined using a simple indicator paper test within 30 sec of ultrasound treatment, which has been confirmed by oscillatory rheological measurements (conditions can be found in the ESI). The hydrogels were found to be fully thermoreversible without significantly changing their physical properties after several cycles of heating and cooling as indicated by marginal changes of the T_{gel}-values (44±1 °C after the first cycle and 43±2 °C after the third cycle).
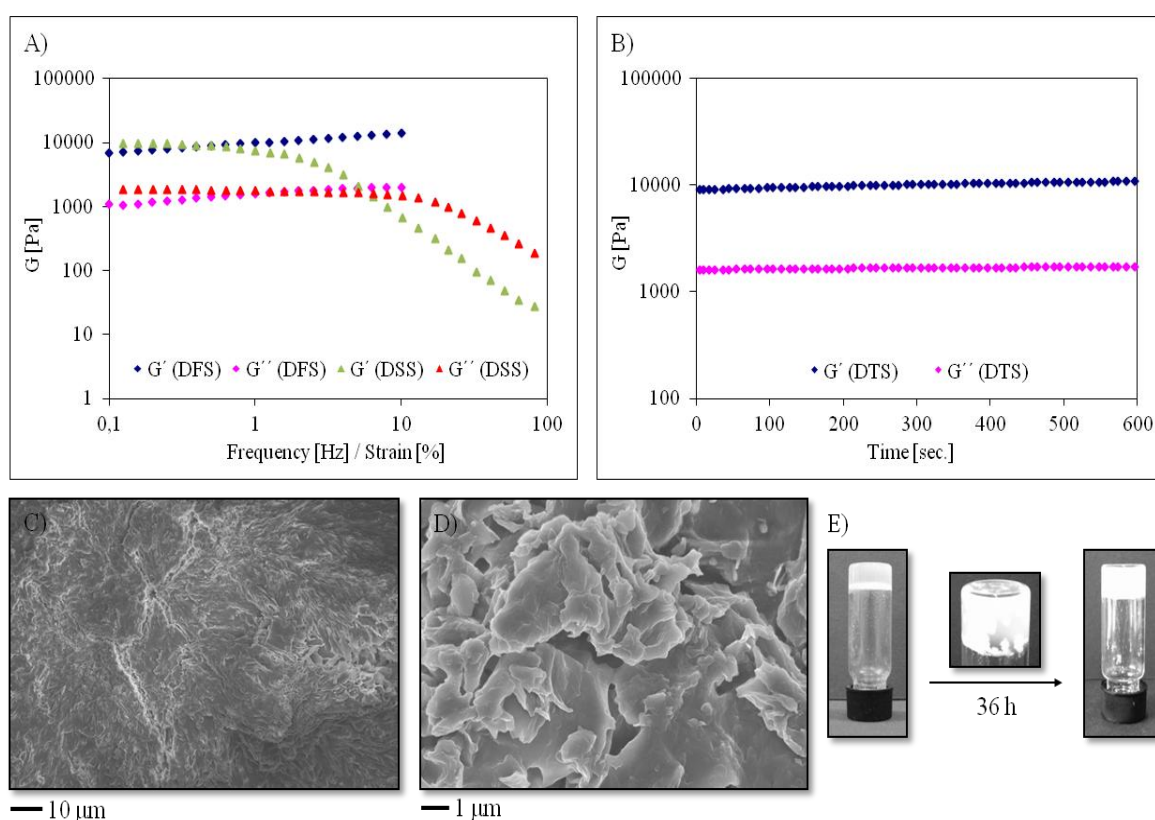
Fig. 16 Characterization of hydrogels derived from compound **1** (71 mg/mL). A), B) Dynamic oscillatory rheology of model gels: A) Representative DFS and DSS experiments; B) Representative DTS experiment. Hence the following experimental values have been obtained: G' = 11020±1482.8 Pa, G'' = 1493±230.6 Pa, tan δ = 0.14±0.040, critical strain at break = 10±2.7 %. C), D) Representative digital photographs of xerogels prepared by the freeze-drying method obtained by FESEM-imaging. E) Representative digital photographs describing the gradual change of the optical appearance of hydrogels from translucent to opaque nature.

Interestingly the optical appearance of the gels gradually changed from translucent to opaque within 36 h due to the growth of particles inside the gel as indicated by digital photographs in Figure 16 preserving their temporal stability of at least 2 months.

Interestingly, the hydrogels also exhibit a macroscopic smart thixotropic nature in analogy to the behaviour of the organogels, which still needs to be confirmed by the three-step loop test as described earlier. The morphology of freeze-dried samples visualized by FESEM imaging resembles smooth and dense lava-flows in similarity to samples obtained from toluene as solvent having approximately the same dimensions. As the biological activity of formamidines is likely influenced by their rate of hydrolysis[36] the stability of compound **1** in acidic aqueous methanol solutions (starting concentration = 5.29×10^{-4} M, 80% v/v in citrate buffer pH = 4.7, approximate pH inside the hydrogels) has been investigated. The first order rate constant for acid-mediated hydrolysis was determined to be $2.83 \pm 0.0012 \times 10^{-4}$ min^{-1} with a half-life $t_{1/2}$ of 41 h indicating a high stability in comparable to other similar systems studied earlier.[13] Interestingly the hydrogels remain a temporal stability of at least 2 month which indicates a drastic reduction of the hydrolysis inside the gel-matrix giving potential for applications in the field of biomedicine especially in controlled drug release.

4.4. Conclusions

In summary, we have described effective gelation of various organic solvents by an amphiphilic formamidine-based gelator molecule. A clear correlation of Hammett´s inductive σ^i parameters of several aromatic solvents was found, which can help to predict and trigger gelation properties in such solvents. Interestingly ultrasound treatment of isotropic solutions resulted in an enhancement of typical physical properties of gel-materials in all tested cases. For example, the time necessary to promote gelation could be reduced up to 85-99 % of the original value corresponding to a classical heating-cooling induced gelation protocol. Additionally a smart thixotropic behaviour with injectable nature of the systems was discovered with a recovery of the gel-sate after vigorous mechanical agitation within seconds. This finding completes a versatile multi stimuli-responsive nature of the materials including a responsive colorimetric behaviour against some metal-ions, which gives potential application in heavy-metal sensing. Herein we also report the first formamidine-based hydrogels, which could effectively be prepared by building a pH-gradient in aqueous media from acidic to more basic conditions. Hydrolysis kinetics in acidic aqueous solutions revealed half lives of about 41 h, which is comparable

to similar systems reported so far. Astonishingly the hydrolysis seems to significantly slow down in gel-materials as indicated by a temporal stability of at least 2 months. Such properties in combination with a potential biological activity of formamidine compounds give rise for potential applications in biomedical fields such as controlled release of drugs.

$\rightarrow$ For further information on compound synthesis and characterization, additional gelation properties and hydrolysis of **1** see the electronic supplementary information (ESI) on the enclosed CD.

4.5. References

[1] a) D. D. Díaz, and M. G. Finn, *Chem. Eur. J.*, 2004, **10**, 303-309 and refs. 2 and 3 therein; b) E. J. Kim, H. S. Shin, S. Y. Ryu, B. H. Lee and S. H. Cho, *Arch. Pharm. Res.*, 1995, **18**, 1-7; c) K. M. Chang and C. O. Knowles, *J. Agric. Food Chem.*, 1977, **25**, 493-501; d) J. Huang, T. Hamasaki and Y. Ozoe, *Arch. Insect Biochem. Physiol.*, 2010, **73**, 74-86; e) C. Hougaard, S. Hammami, B. L. Eriksen, U. S. Sorensen, M. L. Jensen, D. Strobaek and P. Christophersen, *Mol. Pharmacol.*, 2012, **81**, 210-219; f) B. Billick, D. E. Heck, D. M. Porterfield, R. P. Malchow, P. J. S. Smith, C. R. Gardner, D. L. Laskin and J. D. Laskin, *Biochem. Pharm.*, 2001, **61**, 1581-1586.

[2] a) F. Matsumura and R. W. Beeman, *Environ. Health Perspect.*, 1976, **14**, 71-82; b) E. A. Lund, R. M. Hollingworth and G. K. W. Kim, *Neurotoxicol. Insectic. Pheromones*, [Proc. Symp.] 1979, 119-137.

[3] R. M. Hollingworth, *Environ. Health Perspect.*, 1976, **14**, 57-69 and refs. therein.

[4] a) I. R. Harrison, A. Kozlik, J. F. Mc Carthy, B. H. Palmer, S. B. Wakerley, T. S. Watkins, D. M. Weigthon, *Pestic. Sci.*, 1973, **4**, 901-910; b) A. T. Proudfoot, *Toxicol. Rev.*, 2003, **22**, 71-74.

[5] K. Kik, K. Studzian, M. Wasowska-Lukawska, I. Oszczapowicz and L. Szmigiero, *Acta Biochim. Pol.*, 2009, **56**, 135-142.

[6] a) Z.-K. Chan, T.-R. Chen, J.-D. Chen, J.-C. Wang and C. W. Liu, *Dalton Trans.*, 2007, **31**, 3450-3458; b) P. C. Junk and M. L. Cole, *Chem. Commun.*, 2007, **16**, 1579-1590; c) P.-Y. Yang, F.-C. Chang, M.-C. Suen, J.-D. Chen, T.C. Keng and J.-C. Wang, *J. Organomet. Chem.*, 2000, **596**, 226-231; d) J. Tortajada, E. Leon, A. Luna, O. Mo and M. Yanez, *J. Phys. Chem.*, 1994, **98**, 12919-12926.

[7] S. Enthaler, K. Schröder, S. Inoue, B. Eckhardt, K. Junge, M. Beller and M. Drieß, *Eur. J. Org. Chem.*, 2010, **25**, 4893-4901.

[8] A. Zuyls, P. W. Roesky, G. B. Deacon, K. Konstas and P. C. Junk, *Eur. J. Org. Chem.*, 2008, **4**, 693-697.

[9] W.-Z. Chen, J. D. Protasiewicz, S. A. Davis, J. B. Updegraff, L.-Q. Ma, P. E. Fanwick and T. Ren, *Inorg. Chem.*, 2007, **46**, 3775-3782.

[10] N. Tsukada, S. Ninomiya, Y. Aoyama and Y. Inoue, *Org. Lett.*, 2007, **9**, 2919-2921.

[11] a) A. A. Danopoulos, K. Y. Monakhov and P. Braunstein, *Chem. Eur. J.*, 2013, **19**, 450-455; b) L. Benhamou, E. Chardon, G. Lavigne, S. Bellemin-Laponnaz and V. Cesar, *Chem. Rev.*, 2011, **111**, 2705-2733; c) R. Jazzar, H. Liang, B. Donnadieu, and G. Bertrand, *J. Organomet. Chem.*, 2006, **691**, 3201-3205; d) J. Zhang, X. Su, J. Fu and M. Shi, *Chem. Commun.*, 2011, **47**, 12541-12543.

[12] For excellent reviews on N-heterocyclic carbenes and their metal-complexes in catalysis see: a) W. A. Hermann, *Angew. Chem., Int. Ed.*, 2002, **41**, 1290-1309; b) D. Enders, O. Niemeier, A. Henseler, *Chem. Rev.*, 2007, **107**, 5606-5655; c) N. Marion, S. Diez-Ganzales and S. P. Nolan, *Angew. Chem., Int. Ed.*, 2007, **46**, 2988-3000; d) V. Cesar, S. Bellemin-Laponnaz and L. H. Gade, *Chem. Soc. Rev.*, 2004, **33**, 619-636; e) V. Nair, S. Bindu and V. Sreekumar, *Angew. Chem., Int. Ed.*, 2004, **43**, 5130-5135.

[13] D. D. Díaz and M. G. Finn, *Chem. Commun.*, 2004, **21**, 2514-2516.

[14] For selected publications, see: a) P. Terech and R. G. Weiss, *Chem. Rev.*, 1997, **97**, 3133-3160; b) D. J. Abdallah and R. G. Weiss, *Adv. Mater.*, 2000, **12**, 1237-1247; c) J. H. van Esch and B. L. Feringa, *Angew. Chem., Int. Ed.*, 2000, **39**, 2263-2266; d) O. Gronwald and S. Shinkai, *Chem. Eur. J.*, 2001, **7**, 4328-4334; e) K. Hanabusa, *Springer Ser. Mater. Sci.*, 2004, **78**, 118-137; f) X. Y. Liu, *Top Curr. Chem.*, 2005, **256**, 1-37; g) R. G. Weiss and P. Terech, *Molecular Gels: Materials with Self-Assembled Fibrillar Networks*; Springer: New York, 2006; h) M. George and R. G. Weiss, *Acc. Chem. Res.*, 2006, **39**, 489-497; i) G. C. Maity, *J. Phys. Sci.*, 2007, **11**, 156-171; i) S. Banerjee, R. K. Das and U. Maitra, *J. Mater. Chem.*, 2009, **19**, 6649-6687.

[15] For selected publications, see: a) D. J. Abdallah, R. G. Weiss, *Langmuir*, 2000, **16**, 352-355; b) M. de Loops, J. van Esch, R. M. Kellogg, B. L. Feringa, *Angew. Chem., Int. Ed.*, 2001, **40**, 613-616; c) J.-L. Pozzo, J.-P. Desvergne, G. M. Clavier, H. Bouas-Laurent, P. G. Jones, J. Perlstein, *J. Chem. Soc., Perkin Trans. 2*, 2001, 824-826; d) G. M. Whitesides, B. Grzybowski, *Science*, 2002, **295**, 2418-2421; e) B. Xing, M.-F. Choi, B. Xu, *Chem. Commun.*, 2002, **4**, 362-363; i) T. Kato, *Science*, 2002, **295**, 2414-2418; f) I. W. Hamley, *Angew. Chem., Int. Ed.*, 2003, **42**, 1692-1712; g) J. A. A. W. Elemans, A. E. Rowan, R. J. M. Nolte, *J. Mater. Chem.*, 2003, **13**, 2661-2670; h) W. Kubo, S. Kambe, S. Nakade, T. Kitamura, K. Hanabusa, Y. Wada, S. Yanagida, *J. Phys. Chem. B*, 2003, **107**, 4374-4381; i) M. George, R. G. Weiss, *Chem. Mater.*, 2003, **15**, 2879-

2888; j) K. Sugiyasu, N. Fujita, M. Takeuchi, S. Yamada, S. Shinkai, *Org. Biomol. Chem.*, 2003, **1**, 895-899; k) R. Ziessel, G. Pickaert, F. Camerel, B. Donnio, D. Guillon, M. Cesario, T. Prangé, *J. Am. Chem. Soc.*, 2004, **126**, 12403-12413; l) K. Sugiyasu, M. Numata, N. Fujita, S. M. Park, Y. J. Yun, B. H. Kim, S. Shinkai, *Chem. Commun.*, 2004, **17**, 1996-1997; m) H. M. Willemen, A. T. M. Marcelis, E. J. R. Sudolter, W. G. Bouwman, B. Deme, P. Terech, *Langmuir*, 2004, **20**, 2075-2080; n) J. H. Jung, S. Shinkai, *Top. Curr. Chem.*, 2004, **248**, 223-260; o) N. M. Sangeetha, U. Maitra, *Chem. Soc. Rev.*, 2005, **34**, 821-836; p) H.-F. Chow, J. Zhang, *Chem. Eur. J.*, 2005, **11**, 5817-5831; q) C. S. Love, V. Chechik, D. K. Smith, K. Wilson, I. Ashworth, C. Brennan, *Chem. Commun.*, 2005, **15**, 1971-1973; r) K. J. C. van Bommel, S. Shinkai, In *Molecular Gels: Materials with Self-Assembled Fibrillar Networks*; Springer: New York 2006; pp 857–893; s) I. A. Coates, A. R. Hirst, D. K. Smith, *J. Org. Chem.*, 2007, **72**, 3937–3940; t) H.-F. Chow, J. Zhang, C.-M. Lo, S.-Y. Cheung, K.-W. Wong, *Tetrahedron*, 2007, **63**, 363-373; u) J. Puigmarti-Luis, V. Laukhin, A. P. del Pino, J. Vidal-Gancedo, C. Rovira, E. Laukhina, D. B. Amabilino, *Angew. Chem., Int. Ed.*, 2007, **46**, 238-241; v) A. M. Smith, R. J. Williams, C. Tang, P. Coppo, R. F. Collins, M. L. Turner, A. Saiani, R. V. Ulijn, *Adv. Mater.*, 2008, **20**, 37-41; w) R. V. Ulijn, A. M. Smith, *Chem. Soc. Rev.*, 2008, **37**, 664-675; x) A. Vintiloui, J.-C. Leroux, *J. Controlled Rel.*, 2008, **125**, 179-192; y) C. Sanchez, M. Llusar, *Chem. Mater.*, 2008, **20**, 782-820.

[16] a) F. M. Menger, K. L. Caran, *J. Am. Chem. Soc.*, 2000, **122**, 11679-11691; b) O. Gronwald, E. Snip, S. Shinkai, *Curr. Opin. Colloid Interface Sci.*, 2002, **7**, 148-156; c) M. de Loos, B. L. Feringa, J. H. van Esch, *Eur. J. Org. Chem.*, 2005, **17**, 3615-3631; d) C. Sanchez, B. Julian, P. Belleville, M. Popall, *J. Mater. Chem.*, 2005, **15**, 3559-3592; e) E. Zaccarelli, *J. Phys. Condens. Matter*, 2007, **19**, 323101.

[17] a) T. Tanaka, *Sci. Am.*, 1981, **244**, 110-116; b) D. Derossi, Y. Kajiwara, Y. Osada, In *Polymer Gels: Fundamentals and Biomedical Applications*, Plenum Press, New York, 1991.

[18] a) F. Ilmain, T. Tanaka, E. Kokufuta, *Nature*, 1991, **349**, 400-401, and refs. therein; b) L. A. Estroff, A. D. Hamilton, *Chem. Rev.*, 2004, **104**, 1201-1218; c) P. Xie, R. Zhang, *J. Mater. Chem.*, 2005, **15**, 2529-2550; d) N. M. Sangeetha, U. Maitra, *Chem. Soc. Rev.*, 2005, **34**, 821-836; e) M. George, R. Mathew, R. G. Weiss, *Molecular Gels*, 2006, 449-

551; f) D. K. Smith, *Chem. Commun.*, 2006, **1**, 34-44; g) A. Ajayaghosh, V. K. Praveen, C. Vijayakumar, *Chem. Soc. Rev.*, 2008, **37**, 109-122.

[19] a) X. Huang, P. Terech, S. R. Raghavan, R. G. Weiss, *J. Am. Chem. Soc.*, 2005, **127**, 4336-4344; b) M. O. M. Piepenbrock, G. O. Lloyd, N. Clarke, J. W. Steed, *Chem. Rev.*, 2010 **110**, 1960-2004.

[20] Y. Osada and A. R. Khokhlov, In *Polymer Gels and Networks*; Marcel Dekker: New York, 2002.

[21] For selected publications, see: a) J. M. Mallicka, A. Sandeep, F. Monti, E. Bandini, M. Gazzano, C. Ranjith, V. K. Praveen, A. Ajayagosh and N. Armaroli, *Chem. Eur. J.*, 2013, 19, 12991-13001; b) T. Naota, H. Koori, *J. Am. Chem. Soc.*, 2005, **127**, 9324-9325; c) J. M. J. Paulusse, R. P. Sijbesma, *Angew. Chem., Int. Ed.*, 2006, **45**, 2334-2337; d) D. Bardelang, *Soft Matter*, 2009, **5**, 1969-1971; e) G. Cravotto, P.Cintas, *Chem. Soc. Rev.*, 2009, **38**, 2684-2697; f) N. Komiya, T. Muraoka, M. Iida, M. Miyanaga, K. Takahashi, T. Naota, *J. Am. Chem. Soc.*, 2011, **133**, 16054-16061; g) D. Bardelang, M. B. Zaman, I. L. Moudrakovski, S. Pawsey, J. C. Margeson, D. Wang, X. Wu, J. A. Ripmeester, C. I. Ratcliffe, K.Yu, *Adv. Mater.*, 2008, **20**, 4517-4520; h) S. Maity, S. Sarkar, P. Jana, S. K. Maity, S. Bera, V. Mahalingam, D. Haldar, *Soft Matter*, 2012, **8**, 7960- 7966; i) I. Maity, D. B. Rasale, A. K. Das, *Soft Matter*, 2012, **8**, 5301-5308.

[22] J. M. J. Paulusse, D. J. M. van Beek, R. P. Sijbesma, *J. Am. Chem. Soc.*, 2007, **129**, 2392-2397.

[23] a) S. Pan, S. Luo, S. Li, Y. Lai, Y. Geng, B. He and Z. Gu, *Chem. Commun.*, 2013, **49**, 8045-8047; b) J. Wu, T. Yi, Q. Xia, Y. Zou, F. Liu, J. Dong, T. Shu, F. Li and C. Huang, *Chem. Eur. J.*, 2009, 15, 6234-6243; c) X. Yu, Q. Liu, J. Wu, M. Zhang, X. Cao, S.Zhang, Q. Wang, L. Chen, T. Yi, *Chem. Eur. J.*, 2010, **16**, 9099-9106; d) Y. Cho, J. H. Lee, J. Jaworski, S. Park, S. S. Lee, J. H. Jung, *New J. Chem.*, 2012, **36**, 32-35.

[24] For selected publications, see: a) A. Porcheddu, G. Giacomelli and Ivana Piredda, *J. Comb. Chem.*, 2009, **11**, 126-130; b) Y. Han and L. Cai, *Tetrahedron Lett.*, 1997, **38**, 5423-5426; c) L. J. Mathias and C. G. Overberger, *Synth. Commun.*, 1975, **5**, 461-469; d) K. U. Sadek, A. Alnajjar, R. A. Mekheimer, N. K. Mohamed and H. A. Mohamed, *Green Sus. Chem.*, 2011, **1**, 92-97; e) A. S. Ripka, D. D. Díaz, K. B. Sharpless and M.

G. Finn, *Org. Lett.*, 2003, **5**, 1531-1533; f) D. D. Díaz and M. G. Finn, *Org. Lett.*, 2004, **6**, 43-46; g) S. Mehdi, M. Mohsen and H. Akbar, *J. Mol. Struct.*, 2012, **1027**, 156-161.

25 See the Supporting Information for detailed experimental procedures and characterization of compounds and materials.

26 J. E. Eldrige, J. D. Ferry, *J. Phys. Chem.*, 1954, **58**, 992-995.

27 a) L. Lu, T. M. Cocker, R. E. Bachman, R. G. Weiss, *Langmuir*, 2000, **16**, 20-34; b) J. Becerril, B. Escuder, J. F. Miravet, R. Gavara, S. V. Luis, *Eur. J. Org. Chem.*, 2005, **3**, 481-485.

28 P. Kirilov, F. Gauffre, S. Franceschi-Messant, E. Perez and I. Rico- Lattes, *J. Phys. Chem. B*, 2009, **113**, 11101-11108.

29 a) H. A. Barnes, *J. Non-Newtonian Fluid Mech.*, 1997, **70**, 1-33. b) G. Mezger, In *The Rheology Handbook*, Vincentz Network, Hannover, Germany, 2011.

30 a) L. P. Hammett, *Chem. Rev.*, 1935, **17**, 125-136; b) L. P. Hammett, *J. Am. Chem. Soc.*, 1937, **59**, 96-103.

31 (a) R. W. Taft, In *Steric Effects in Organic Chemistry*; M. S. Newman, Ed.; Wiley and Sons: New York, 1956; p 595 (Table V); (b) R. W. Taft and I. C. Lewis, *J. Am. Chem. Soc.*, 1958, **80**,2436-2443; c) W. J. Hehre, R. W. Taft, and R. D. Topsom, *Prog. Phys. Org. Chem.*, 1976,**12**, 159-187; d) S. H. Unger, and C. Hansch, *Prog. Phys. Org. Chem.*, 1976,**12**,91-118.

32 a) E. C. Lee, B. H. Hong, J. Y. Lee, J. C. Kim, D. Kim, Y. Kim, P. Tarakeshwar and K. S. Kim, *J. Am. Chem. Soc.*, 2005, **127**, 4530-4537; b) F. R. Fischer, W. B. Schweizer and F. Diederich, *Chem. Commun.*, 2008, **34**, 4031-4033; c) S. E. Wheeler, *J. Am. Chem. Soc.*, 2011, **133**, 10262-10274.

33 a) F. Cozzi, M. Cinquini, R. Annunziata and J. S. Siegel, *J. Am. Chem. Soc.*, 1993, **115**, 5330-5331; b) F. Cozzi, M. Cinquini, R. Annunziata, T. Dwyer and J. S. Siegel, *J. Am. Chem. Soc.*, 1992, **114**, 5729-5733; c) F. Cozzi, R. Annunziata, M. Benaglia, M. Cinquini, L. Raimondi, K. K. Baldridge and J. S. Siegel, *Org. Biomol. Chem.*, 2003, **1**, 157-162; d) F. Cozzi, R. Annunziata, M. Benaglia, K. K. Baldridge, G. Aguirre, J. Estrada, Y. Sritana-Anant and J. S. Siegel, *Phys. Chem. Chem. Phys.*, 2008, **10**, 2686-2694; e) F. Cozziand J. S. Siegel, *Pure Appl. Chem.*, 1995, **67**, 683-689; f) C. A. Hunter and J. K. M. Sanders, *J. Am. Chem. Soc.*, 1990,**112**, 5525-5534; g) C. A. Hunter, K. R.

Lawson, J. Perkins and C. J. Urch, *J. Chem. Soc., Perkin Trans. 2*, 2001, **5**, 651-669; h) S. L. Cockroft and C. A. Hunter, *Chem. Soc. Rev.*, 2007, **36**, 172-188; j) S. L. Cockroft, C. A. Hunter, K. R. Lawson, J. Perkins and C. J. Urch, *J. Am. Chem. Soc.*, 2005, **127**, 8594-8595; k) S. L. Cockroft, J. Perkins, C. Zonta, H. Adams, S. E. Spey, C. M. R. Low, J. G. Vinter, K. R. Lawson, C. J. Urch and C. A. Hunter, *Org. Biomol. Chem.*, 2007, **5**, 1062-1080.

34 C. Hansch, A. Leo and R. W. Taft, *Chem. Rev.*, 1991, **91**, 165-195 and ref. 32 therein.

35 a) D. D. Díaz, S. S. Gupta, J. Kuzelka, M. Cymborowski, M. Sabat and M. G. Finn, *Eur. J. Inorg. Chem.*, 2006, **22**, 4489-4493. b) Z.-K. Chan, C.-H. Lin, C.-C. Wang, J.-D. Chen, J.-C. Wang and C.-W. Liu, *Dalton Trans.*, 2008, **16**, 2183-2189.

36 (a) C. Anastasi, O. Hantz, E. DeClercq, C. Pannecouque, P. Clayette, N. Dereuddre-Bosquet, D. Dormont, F. Gondois-Rey, I. Hirsch and J.-L. Kraus, *J. Med. Chem.*, 2004, **47**, 1183-1192; (b) S.Vincent, C. Mioskowski and L. Lebeau, *J. Org. Chem.*, 1999, **64**, 991-997.

181

5. Transferring a concept from medicinal chemistry into soft matter: Replacing an amide with a triazole for modifying gelation properties[i]
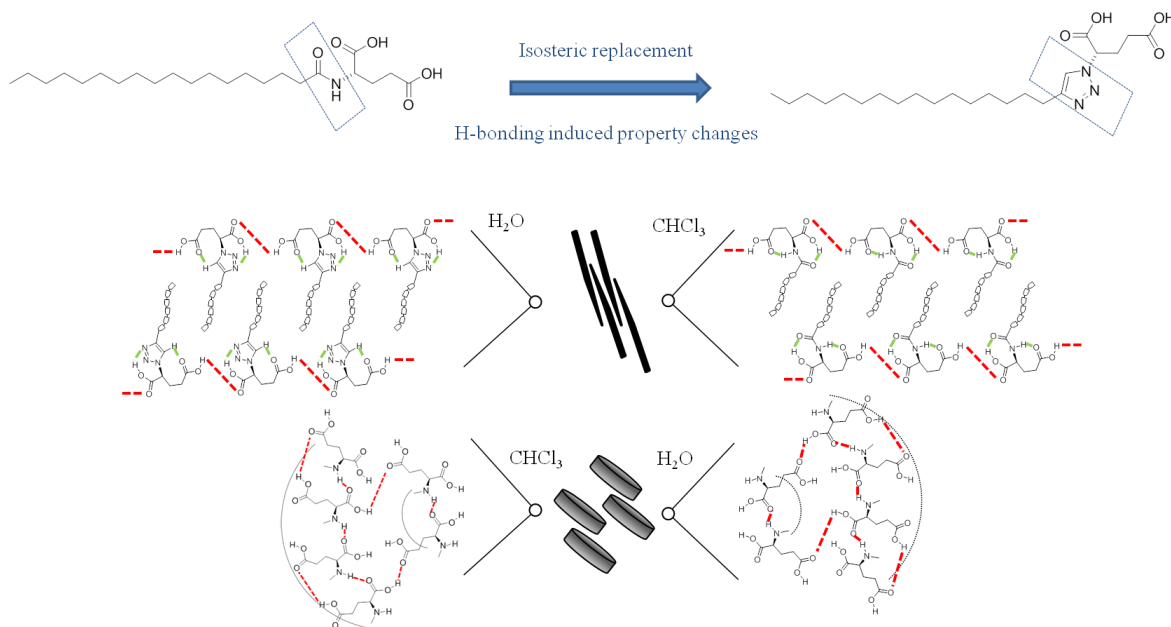
The well-known concept of isosteric replacement has been transferred successfully from medicinal chemistry into the field of soft gel-materials. The exchange of an amide moiety of a literature-known compound **C$_{18}$-Glu** with an 1,4-disubstituted 1,2,3-triazole via CuAAC furnished the novel compound **Click-Glu**. It was found that **Click-Glu** exhibits superior behaviour in terms of its gelation properties in polar-protic solvents. Not only *CGC* values could be decreased, but also mechanical and thermal stabilities could be improved. On the other hand an exact opposite behaviour was observed in aprotic solvents, where **C$_{18}$-Glu** revealed its superior properties. Explanations on this behaviour could be given by the differences in gelation mechanisms proposed for the two compounds based on varying gelator-solvent and gelator-gelator interactions, caused by the two linking moieties. Additional controlled drug release experiments using vancomycine revealed a triggering of the release rate depending on the compound used.

---

[i] In this chapter, all experiments were carried out by J. Bachl.

5.1. Introduction

Bioisosteric replacement[1] is a well accepted key concept in medicinal chemistry for already several decades. The origin of isosteres can be traced back to 1919 and is based on similar physicochemical behaviour of various atoms and molecules as described by Langmuir.[2] Taking also the octet-rule into consideration, isosteres were initially defined as those atoms or groups that have the same number and arrangement of electrons. Later on the concept was extended with the Grimm´s hydride displacement law[3] and Erlenmeyer´s redefinition of isosteres being atoms, ions and molecules in which the peripheral electron shells can be considered identical.[4] The term bioisosterism was initiated by Friedman[5] and extended later on by Burger[1 h)] for atoms or groups that posses similar shapes and volumes, approximately the same distribution of electrons and which exhibit similar physical properties and biological activities. Of special interest in modern research is the isosteric replacement of amide-bonds, because of its impact in peptide chemistry and the development of petide-mimetics. Many promising approaches introducing acyclic esters, thioamides, ureas, carbamates, and sulphonamides amongst others have been successfully applied to improve known drug-systems or to create new compounds and materials.[1a), 6] In order to increase stabilities against hydrolysis and enzymatic cleavage as well as to increase structural and conformational rigidity, heterocyclic isosteres for amide-bonds like 1,2,4-oxadiazoles,[7] 1,3,4-oxadiazoles[8] or triazoles[9] have found broad application. Especially 1,2,3-triazoles are of special interest, due to their facile and various preparation caused by the development of the copper-catalyzed cycloaddition of azides and alkynes (CuAAC) in 2002.[10] The CuAAC yields only the 1,4-disubstituted triazole ring and hence many effort was spent towards the formation of the 1,5-disubstituted analogue. It was found in 2005[11] that the 1,3-dipolar cycloaddition could be directed towards the formation of the 1,5-analogue using the $Cp*RuCl(PPh_3)_2$ catalyst, which makes this reaction a true regiocomplementary tool in organic synthesis. Triazoles are very suitable for isosteres as they are able to mimic either a *Z* or *E* configuration of the amide-bond depending on the substitution pattern.[9b), c), i)] Their planar structure exhibits the ability of hydrogen bonding due to the presence of both donor and acceptor groups, with a very similar relative position of the hydrogen bonding sites. The main difference between a 1,4-disubstituted triazole and a *Z* amide-bond is the larger distance between the substituents in the case of the former (~ 5.0 Å and ~ 3.9 Å respectively), which could be overcome by the larger overall dipolar

moment of the triazole in comparison to the amide ($\sim$ 5 D and $\sim$3.5 - 4.0 D[12] respectively).
The corresponding distances for the 1,5-disubstituted triazole and an *E* amide-bond are
near identical ($\sim$ 2.4 Å), but here differences in atom polarization occur.[9b)]
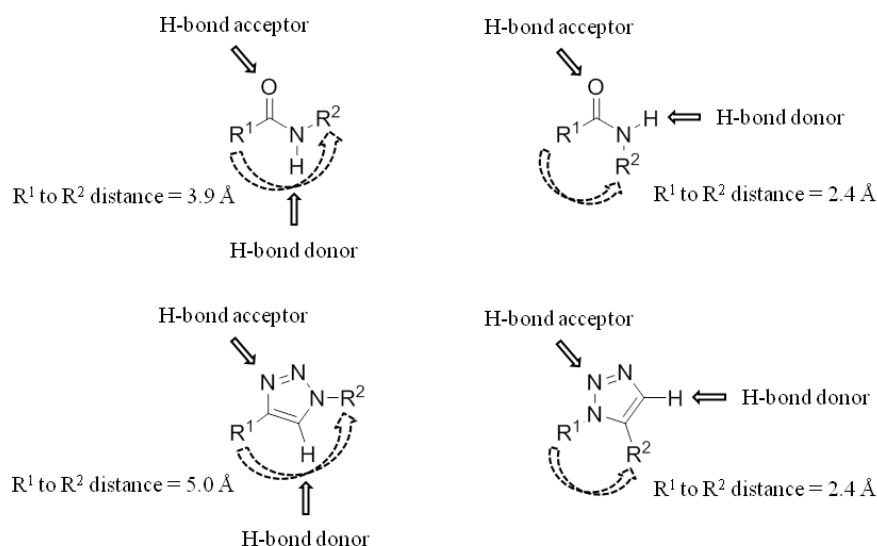
Fig. 1 Summary of features explaining the potential use of triazoles as bioisosteres for amide-bonds.[9 b)]

Furthermore computational studies suggest that a 1,4-disubstituted triazole could be
consistent with the geometry of a β-turn.[13] Besides the application of triazoles in petide-
mimetics and bioconjugation,[9b)-j)] they also found to be very useful structural motifs for the
fabrication of functional materials in material science.[14] Triazoles participate for example
in the manufacturing of sensors,[15] zeolites for gas uptake and catalysis[16] or even soft gel-
materials.[17] To the best of our knowledge no specific reports have been published so far on
the concept of isosteric exchange of an amide bond with a triazole in soft gel materials. In
this context we wanted to investigate the effects of exchanging an amide in a known low-
molecular-weight (LMW) model compound **C$_{18}$-Glu**[18] with a 1,4-disubstituted 1,2,3-
triazole resulting in compound **Click-Glu** on potential differences in gelation properties.

5.2. Experimental

5.2.1   Materials

Unless otherwise specified, all reagents, starting materials and solvents (p.a. grade) were purchased from commercial suppliers and used as received without further purification. Double-distilled water was purified additionally using a Millipore water-purifying system (Merck) prior usage. Xylene as mixture of isomers was used after double-distillation. See ESI† for detailed information about instrumentation, synthetic procedures, compounds and material characterization.

5.2.2   Preparation of gel-materials

Typically, a weighted amount of the corresponding gelator and an appropriate solvent (0.5 mL) were placed into a screw-capped glass vial (4 cm length × 1 cm diameter) and gently heated with a heat gun until the solid material was completely dissolved. In some cases ultrasonication of the samples before heating could facilitate the dissolution of the compound. The resulting isotropic solution was then spontaneously cooled down to RT. No control over temperature rate during the heating-cooling process was applied. The material was preliminary classified as "gel" if it did not exhibit gravitational flow upon turning the vial upside-down at RT. The state was further confirmed by rheological measurements.

5.2.3   Critical gelation concentration (*CGC*)

CGC values were estimated by continuously adding aliquots of solvent (0.02-0.1 mL) into vials containing the corresponding gelator and performing a typical heating-cooling for gel-formation until no gelation was observed. The starting point for *CGC* determinations was 200 mg/mL.

5.2.4 Thermal *gel*-to-*sol* transition temperature (T_{gel})

Tgel-values were determined using a custom made set-up (the sealed vial containing the gel-material (total volume of solvent = 0.5 mL) was placed in a mold of an alumina block which was heated up using an electric heating plate equipped with a temperature control couple at 1 °C/ 5 min, verification on the independence of the position inside the apparatus has been carried out and values obtained have been crosschecked with data from literature known compounds).

Fig. 2 Custom made set-up for T_{gel}-determinations. A) Front view showing the composition between electric heating plate, alumina block and digital thermo-couple. B) Top view of the set-up during experimentation containing vials (4 cm length x 1 cm diameter) with gel-materials. It is important to mention that the alumina block was constructed especially for one type of vials which fit smoothly inside the molds to ensure a good transmission of the heat-flow.

The hereby obtained values have been verified by the classical "inverse flow method" (IFM)[19] (the sealed vial containing the gel-material (total volume of solvent = 0.5 mL) was hung horizontally into an oil bath, which was heated up at 1 °C/ 5 min) and DSC measurements. Herein, the temperature at which the gel started to break was defined as T_{gel}. Each measurement was made at least by duplicate and the average value reported. T_{gel} values were found almost unaltered within a difference of 1-2 °C after several heating-cooling cycles.

187

5.2.5   Controlled release of vancomycin

A weighted amount of the corresponding gelator (50 mg, minimum amount of gelator to obtain stable gels for both compounds), vancomycin (2 mg) and water (1 mL) were placed into a screw-capped glass vial and gently heated until all solid materials were completely dissolved. The resulting isotropic solution was then spontaneously cooled to RT resulting in gel-formation with physically incorporated vancomycin. Obtained gel-materials were overlaid with PBS-buffer (1 mL, pH = 7.4) 12 h after formation, which was considered as the starting point of the experiments. At selected points of time aliquots (100 μL) were removed and stored at -20 °C, and the release buffer was completely replaced with fresh PBS to maintain infinite sink conditions. Drug concentration in the aliquots was determined at the end of the experiments by UV spectroscopy after calibration using the maximum absorbance at 280 nm. It was verified that degraded gel-materials exhibited a minimum absorbance in the region of drug detection.

5.3. Results and discussion

5.3.1   Gelation ability and optical appearance of the materials

The two potential gelator molecules bearing either an amide (**C$_{18}$-Glu**) or a 1,4-disubstituted 1,2,3-triazole (**Click-Glu**) moiety have been systematically investigated for their gelation ability in an aqueous environment and 25 different organic solvents by applying a classical heating-cooling cycle. Materials that did not exhibit gravitational flow according to the "stable-to-inversion" method[20] were preliminary classified as gels and their solid-like appearance was further confirmed using dynamic rheological measurements (*vide infra*). **C$_{18}$-Glu** was found to be completely soluble in THF and 1,4-dioxane, while being insoluble in viscous oil-type solvents and ionic liquids like BMIM·PF$_6$. Precipitation of the compound after cooling of hot isotropic solutions was observed in 1-hexanol, DMSO, DMF, EtOAc and acetone, while partial gel-formation occurred in most alcoholic solvents and aromatic solvents substituted with electron withdrawing groups.
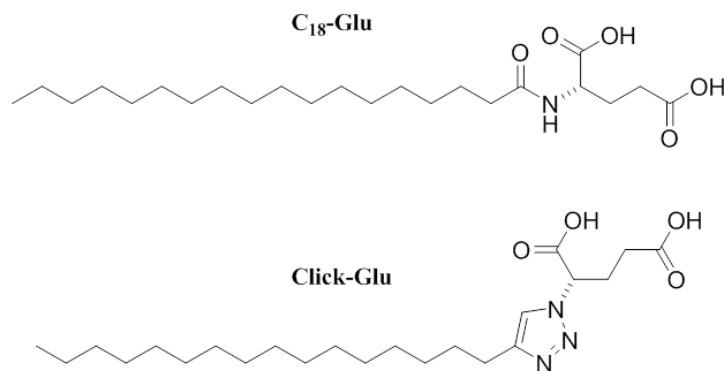
Fig. 3 Structures of model compounds **C₁₈-Glu** and **Click-Glu** for establishing the concept of isosteric exchange in soft gel-materials.

In the rest of the tested solvents including an aqueous environment formation of stable gels took place furnishing mostly complete opaque gels except from materials derived from glycerin, which revealed a translucient appearance.

Tab. 1 Comparison of gelation properties of **C₁₈-Glu** and **Click-Glu**. [a]

Solvent	C₁₈-Glu				Click-Glu			
	CGC [mg/mL]	Gel-Time [min]	T_{gel} [°C]	Appearance	*CGC* [mg/mL]	Gel-Time [min]	T_{gel} [°C]	Appearance
MeOH	33 (3)	10 (0.5)	41 (1)	OG	25 (2)	90 (15)	54 (1)	OG
Water	25 (2)	10 (0.5)	47 (1)	OG	17 (2)	3.5 (0.3)	65 (1)	OG
MeCN	110 (10)	2 (0.3)	67 (1)	OG	48 (4)	2 (0.3)	78 (2)	OG
Et₂O	18 (2)	3.5 (0.5)	69 (2)	OG	78 (8)	5 (0.5)	49 (2)	OG
CH₂Cl₂	100 (10)	2.5 (0.3)	62 (1)	OG	180 (15)	35 (5)	40 (2)	OG
CHCl₃	75 (8)	4 (0.5)	61 (1)	OG	95 (10)	7 (0.5)	43 (2)	OG
n-Hexane	25 (2)	2 (0.3)	84 (2)	OG	115 (10)	0.5 (0.1)	72 (2)	OG
Xylene	84 (8)	0.8 (0.3)	71 (1)	OG	95 (15)	0.5 (0.1)	56 (1)	OG
Toluene	90 (10)	1.3 (0.3)	80 (2)	OG	135 (10)	0.5 (0.1)	52 (1)	OG
Benzene	175 (20)	3.5 (0.5)	75 (2)	OG	200 (15)	1.5 (0.3)	64 (1)	OG
Glycerin	20 (2)	1.5 (0.3)	53 (1)	TLG	12 (1)	4.5 (0.5)	67 (1)	TLG

[a] Values for gelation-time and T_{gel} were determined at the concentrations of the material with higher corresponding *CGC*. Values in brackets indicate experimental errors from at least two randomized experiments. Abbreviations: OG = opaque gel; TLG = translucient gel.

The complete opacity of most gels is an indication for the formation of particle-aggregates bigger than the wavelength of visible light (~ 350-750 nm), while the translucient nature of

glycerin-gels indicates the formation of smaller particles. **Click-Glu** exhibits a quite similar behavior towards gelation in the tested solvents. Besides the formation of stable gels in the same solvents as **C₁₈-Glu** (sharing similar optical appearance as indicated in Figure 4), additional gelation of EtOH, *i*-PrOH and DMSO was observed extending the scope by 3 polar solvents (see Table 1 for a detailed summary). Interestingly **Click-Glu** also revealed *in situ* gelation of DMSO/water mixtures at concentrations of ca. 200 mg/mL during its synthesis as indicated in Figure 4 B.

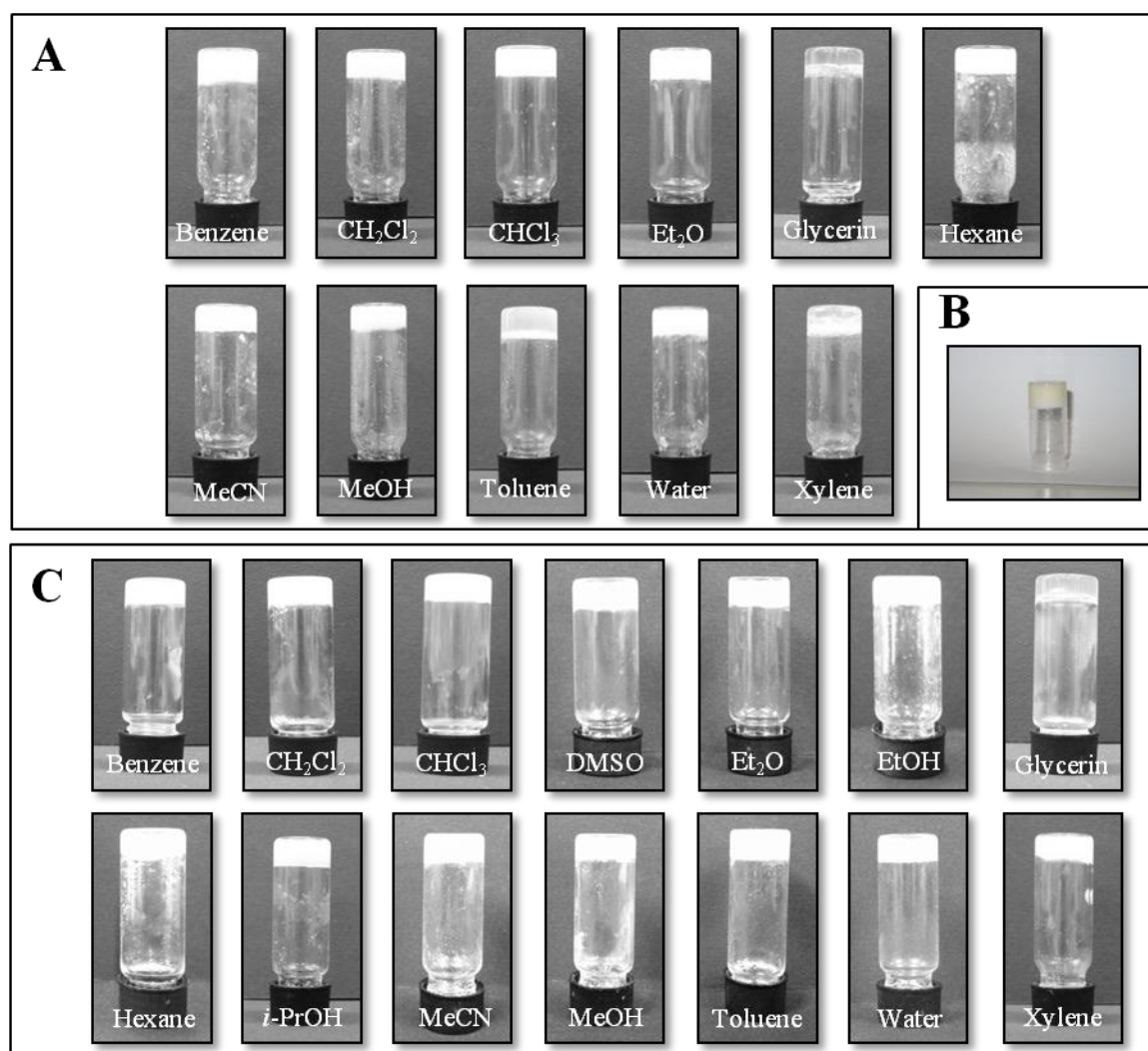**Fig. 4** Representative digital photographs of upside-down vials containing gels derived from compounds **C₁₈-Glu** (**A**) and **Click-Glu** (**C**) at the corresponding *CGC* in aqueous environment and various organic solvents as indicated in Table 1. **B**: Representative digital photograph demonstrating *in situ* gelation of **Click-Glu** during its synthesis in DMSO/water (2:1 v/v) at a concentration of ca. 200 mg/mL.

5.3.2 Considerations on CGC-values, temporal, thermal and mechanical stabilities and stimuli-responsive nature

Critical gelation concentrations (*CGC*), defined as the minimum concentrations of compound where gelation was observed, were established to be in a range of 10-200 mg/mL for most cases applying a classical heating-cooling protocol for gel-formation. Interestingly it was found that **Click-Glu** exhibited lower *CGC*-values in comparison to **C$_{18}$-Glu** when polar protic (water, MeOH and glycerin) and polar aprotic solvents (e.g. MeCN) were used (see Figure 5).
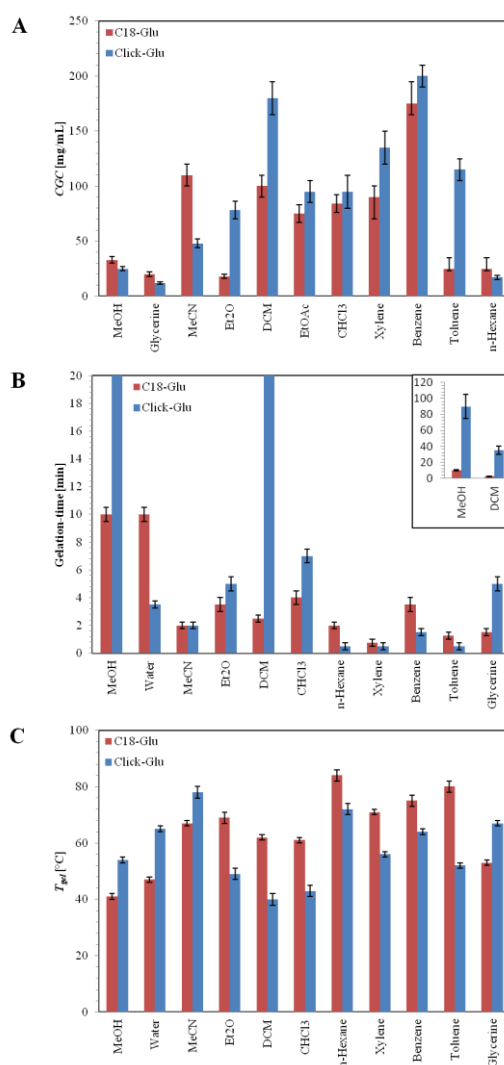

Fig. 5 Bar graphs indicating differences in gelation properties of **C$_{18}$-Glu** and **Click-Glu**. **A** *CGC*-values; **B** Gelation-time; **C** *T$_{gel}$*-values. For comparative purposes: Values for gelation-time and *T$_{gel}$* were determined at the concentration of the material exhibiting a higher corresponding *CGC*.

191

On the other hand an opposite behavior was observed in apolar (Et_2O, $CHCl_3$, CH_2Cl_2 and hexane) and aromatic solvents (benzene, toluene and xylene) (between 10 and 75 %).This finding already indicates the potential influence on the gelation-ability and kinetics of the isosteric replacement of an amide-moiety with a triazole. Independent on the nature of the solvent or the compound all gels exhibited a full thermo-reversible nature and a temporal stability for at least 12 months. The time necessary to promote gelation is relative fast for both compounds and is located in a range between several tens of seconds and several tens of minutes. In general no clear correlation at comparable concentrations between the gelation-time and the type of compound can be drawn, but it seems as if gelation-kinetics are significantly slower in polar solvents (see Figure 6 C, D).
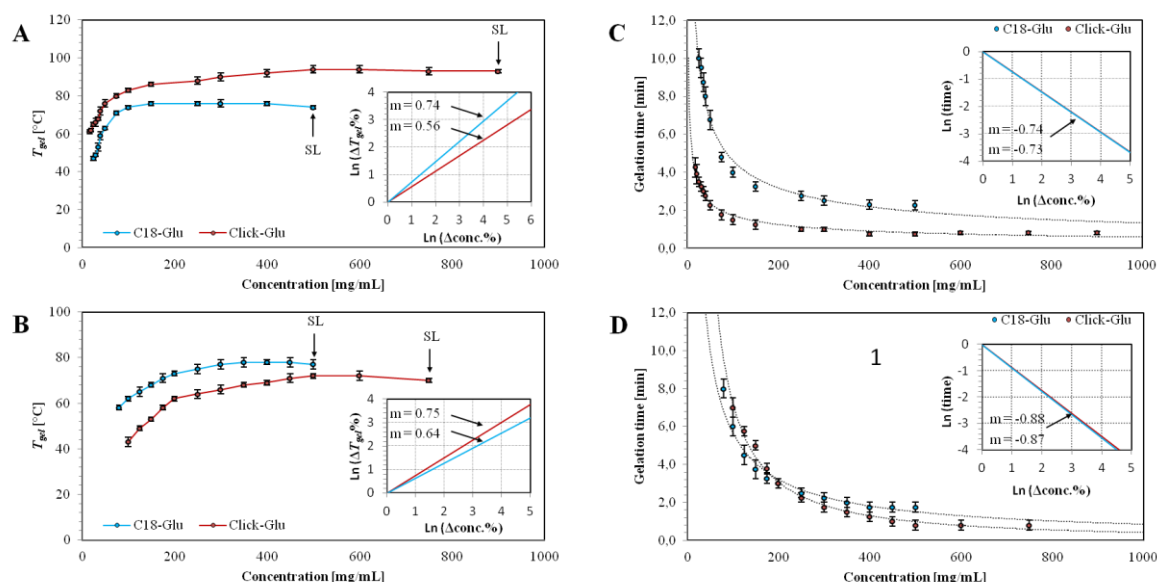
Fig. 6 A, B Evolution of T_{gel} with increasing gelator concentration (**A**: water as solvent; **B**: $CHCl_3$ as solvent). Inset-plots: Normalized Ln-Ln plots of the corresponding percental increments. **C, D** Gelation kinetics of compounds **C_{18}-Glu** and **Click-Glu** (**C**: water as solvent; **D**: $CHCl_3$ as solvent). Inset-plots: Normalized Ln-Ln graphs of the gelation-time against percental increments of concentration. Abbreviations: m = slope; SL = stability limit.

The thermal stability of obtained gel-materials was evaluated using their thermal *gel*-to-*sol* transition temperatures (T_{gel}). T_{gel}-values were obtained using a custom made set-up as described in the experimental section (view Figure 2) as a variation of the "inverse-flow-method (IFM)"[19] and cross-checked using the classical IFM. However, the values

determined by IFM strongly depend on factors such as cooling rate, aging time, thermal history, and degree of hysteresis[21] among others, and hence were correlated for model systems to the first endothermic transition observed by modulated DSC (see ESI). The obtained values are quite low in a range between ca. 40 to 70 °C and quite independent on the nature of the solvent, which is quite typical for LMW-based gels. In similarity to the trends observed for *CGC*-values, it was found that **Click-Glu** exhibits higher T_{gel}-values at comparable concentrations in polar protic and polar aprotic solvents, whereas **C$_{18}$-Glu** revealed superior behaviour in apolar and aromatic solvents (results are summarized in Table 1 and Figure 5, detailed information can be found in the ESI). Up to 40 % increase of the T_{gel}-values could be observed when the compound and the solvent-polarity matched. Remarkable in this context is the ability of both compounds to form gel-materials where T_{gel}-values are very close to or even exceed the boiling point of the corresponding solvent. In *n*-hexane (b.p. = 69 °C) for example the T_{gel}-values for **C$_{18}$-Glu** and **Click-Glu** are as high as 84±2 and 72±2 °C respectively. For further investigation on other typical gelation properties, two model solvents have been selected for convenience. Dependent on the results carried out so far and on the nature of the solvent, water as polar protic solvent and CHCl$_3$ as apolar solvent have been selected. As usual in other physical gels, T_{gel} increases significantly with increasing gelator concentration (view Figure 6) independent on the nature of the solvent or the compound, indicating that self-assembly processes are driven by strong intermolecular interactions affording closely packed 3D networks in both cases. Gelator concentrations could be increased up 500 mg/mL for **C$_{18}$-Glu** in both water and CHCl$_3$, affording homogeneous gels. For **Click-Glu** concentrations could be even increased up to 700 (CHCl$_3$) and 900 (water) mg/mL respectively. A typical plateau region for all examples (ΔT_{gel} = 20-33 °C) was visible before the gels collapsed into partial and inhomogeneous gels with expelling some liquid on top over short periods of time lower than 4 h. However more realistic vision can be obtained by looking at the percental increase of a variable over the entire range of permitted concentration until reaching a plateau value of T_{gel}.[22] The Ln-Ln plot of the percentage increases before the plateau regions, showed a clear linear relationship between the increment in the gelator concentration and the consequent increment in the T_{gel} with respect to the initial values at the *CGC* (view Figure 6). Thus, within the end-limits defined by the *CGC*s and the maximum T_{gel} values, the slopes of these straight lines indicated that in water as solvent a slight 1.3-fold higher percentage increment of T_{gel} is observed when **C$_{18}$-Glu** is used as

gelator (view Figure 6 A). The opposite trend is visible in CHCl$_3$ as solvent where a 1.2-fold higher percentage increment can be observed for **Click-Glu** (view Figure 6 B). However absolute maximum values for T_{gel} are higher for **Click-Glu** in water and higher for **C$_{18}$-Glu** in CHCl$_3$. Corresponding Ln-Ln plots of gelation-time vs. concentration revealed that for an equivalent increment in concentration with respect to the *CGC* materials based on either **C$_{18}$-Glu** or **Click- Glu** in water as solvent evolve nearly identical**,** but materials based on **Click-Glu** show faster absolute gelation-kinetics at the corresponding *CGC* (view Figure 6 C). In CHCl$_3$ as solvent both absolute and incremental gelation-kinetics are nearly identical for **C$_{18}$-Glu** and **Click-Glu** (view Figure 6 D).

Oscillatory rheological measurements unequivocally confirmed the viscoelastic gel nature of the materials that did not show gravitational flow upon turning the vial upside-down. Thus, their storage modulus G' (energy storage modulus) and loss modulus G'' (energy loss modulus) were first measured at room temperature as a function of frequency (dynamic frequency sweep experiment, DFS) and shear strain (dynamic strain sweep experiment, DSS) to determine the linear viscoelastic regime associated to the material (view Figure 7 A).

Tab. 2 Summary of rheological properties of compounds **C$_{18}$-Glu** and **Click-Glu** in two model solvents. [a]

Compound	Solvent	G' [kPa]	G'' [kPa]	tan δ	Strain [%] [b]
C$_{18}$-Glu	H$_2$O	15±1.8	4±0.2	0.30±0.01	6±1.3
C$_{18}$-Glu	CHCl$_3$	778±6.0	101±1.9	0.13±0.00	4±0.8
Click-Glu	H$_2$O	102±10.6	19±0.4	0.19±0.02	9±1.4
Click-Glu	CHCl$_3$	109±1.7	45±4.0	0.41±0.03	2±0.7

[a] Water (25 mg/mL) and CHCl$_3$ (100 mg/mL) were used as model systems. Data were obtained from at least 2 randomized experiments at the concentration of the material exhibiting the higher corresponding *CGC* as indicated in Table 1. [b] Maximum strain at break of the gel-material.

Relatively constant tan δ (G''/G') values during the frequency sweep indicate a good tolerance of the gels to external forces. Within the linearity limits of deformation (solid-like response), the storage modulus was approximately one order of magnitude higher than the loss modulus during the flow experiment (e.g. $G' \approx 778.4 \pm 5.9$ kPa, $G'' \approx 100.8 \pm 1.9$ kPa, for the gels made form **C$_{18}$-Glu** in CHCl$_3$ at 100 mg/mL). The viscoelastic and brittle nature of the materials was confirmed by the destruction of the gels at low frequency and

between about 2-10% of strain. Further dynamic time sweep (DTS) measurements at 0.1% strain and 1 Hz frequency confirmed the stability (no phase transition) of the gel materials as a function of the ageing time at room temperature (view Figure 7 B). In general, the tan δ values between random measurements of the same material were reproducible and decreased with the concentration of the gelator, suggesting an enhancement of the mechanical damping properties. Comparative oscillatory rheology measurements at the concentration of the material exhibiting a higher *CGC* revealed a similar behavior as already observed from *CGC* and T_{gel}-determinations. **C$_{18}$-Glu** provides more mechanical stable materials in aprotic solvents like CHCl$_3$ as indicated by higher absolute *G′*-values, lower tan δ and higher maximum strain at break. An exact opposite behavior can be observed in polar solvents like water where **Click-Glu** exhibits superior properties (view Table 2 and Figure 7).
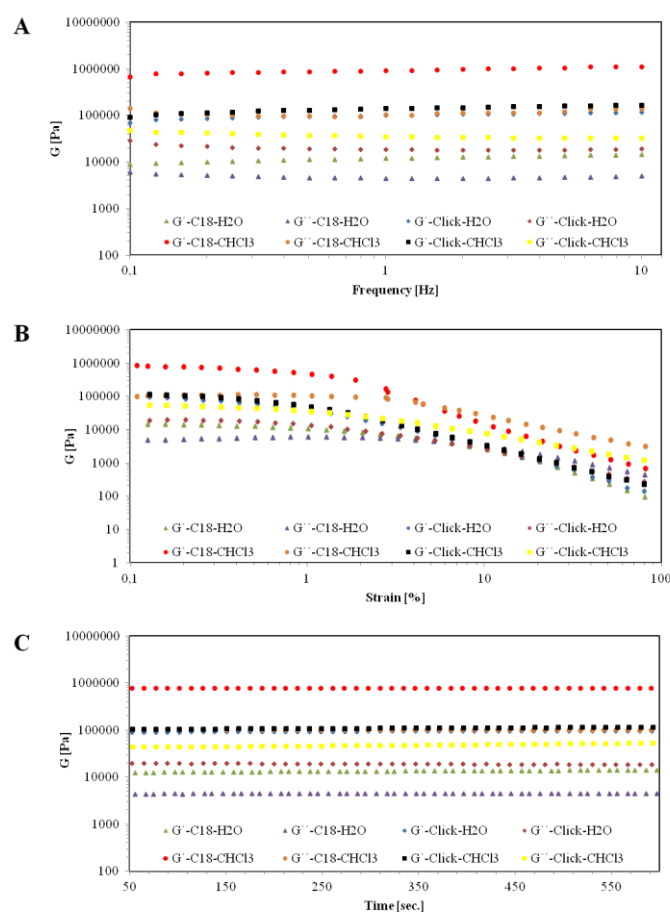

Fig. 7 Representative plots of oscillatory rheological experiments of **C$_{18}$-Glu** and **Click-Glu** in the two model systems water (25 mg/mL) and CHCl$_3$ (100 mg/mL) at the concentration of the material with the higher corresponding *CGC* as indicated in Table 1. **A**: DFS-plots. **B**: DSS-plots. **C**: DTS-plots.

195

The response towards external stimuli of physical gels is one of their key-features for
potential applications. As mentioned above all gel-materials independent on the type of
compound used or the nature of the solvent exhibited full thermo-reversible behavior
without any remarkable changes in T_{gel}-values even after several cycles of heating and
cooling. Figure 8 summarizes a versatile multi-responsive map of gels derived from **Click-
Glu** in water (17 mg/mL). Irreversible *gel*-to-*sol* phase transitions could be observed by
mechanical agitation and addition of certain chemical substances. Gel-materials were
dissolved in the presence of NaOH, while being stable towards neutral and acidic
conditions. Also treatment with certain electrolytes (e.g. Na_2SO_4, NaCl and CsF), buffered
solutions (phosphate buffer saline (PBS; pH = 7.4) and borate buffer (pH = 9.2)) and
organic solvents (THF and 1,4-dioxane) resulted in phase transition. A smart response
towards metal-ions (Ag^+, Cu^{2+}, Fe^{3+} and Ce^{4+}), halides (TBACl, TBAB and TBAF), other
organic solvents (*n*-hexane, toluene, cyclohexane, EtOAc, MeCN, MeOH, DMSO, DMF,
acetone and CH_2Cl_2), ultrasound treatment or UV-irradiation could not be observed. Gels
derived from **Click-Glu** in $CHCl_3$ behaved approximately the same, as also gels derived
from **C$_{18}$-Glu** in both water and $CHCl_3$, except from being stable against electrolytes and
PBS-buffered solutions. In general the response towards external stimuli is quite fast being
in a range between 30-240 min resulting in complete dissolution or destroyal of
corresponding gel-materials (view ESI for detailed information on other model systems).
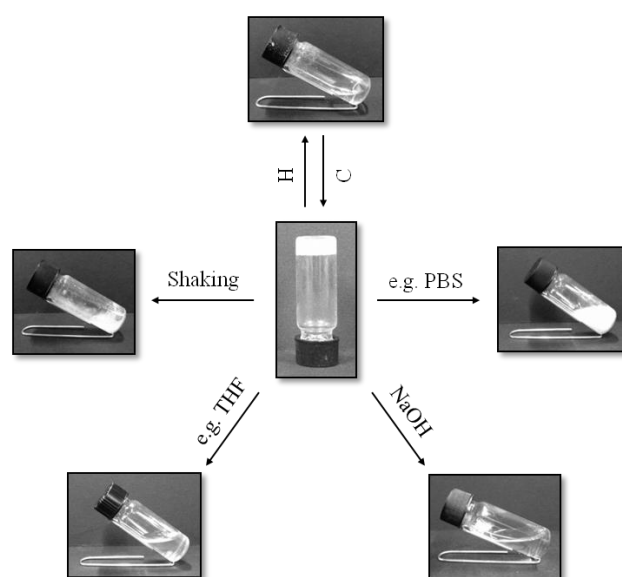

Fig. 8 Representative diagram showing the preparation of multi-stimuli responsive gels derived from **Click-
Glu** in water (17 mg/mL). Abbreviations: C = cooling; H = heating.

5.3.3 Morphological and spectroscopic considerations

In order to gain visual insight into the morphologies of the organogels we conducted field emission scanning electron microscopy (FESEM) of the corresponding xerogels (view Figure 9 A-H). The morphologies of materials based on **C$_{18}$-Glu** are very similar to those reported before. [18] In polar-protic environment formation of nanodiscs-like structures is revealed with diameters in a range of 1-5 μm, whereas ribbon-like microstructures that tend to form layered lamellar assembles are observed in CHCl$_3$. The ribbons exhibit widths of ca. 5-10 μm and lengths of 15-50 μm and consist of several nanofibers (smallest feature of diameter: 30-50 nm) fused together.
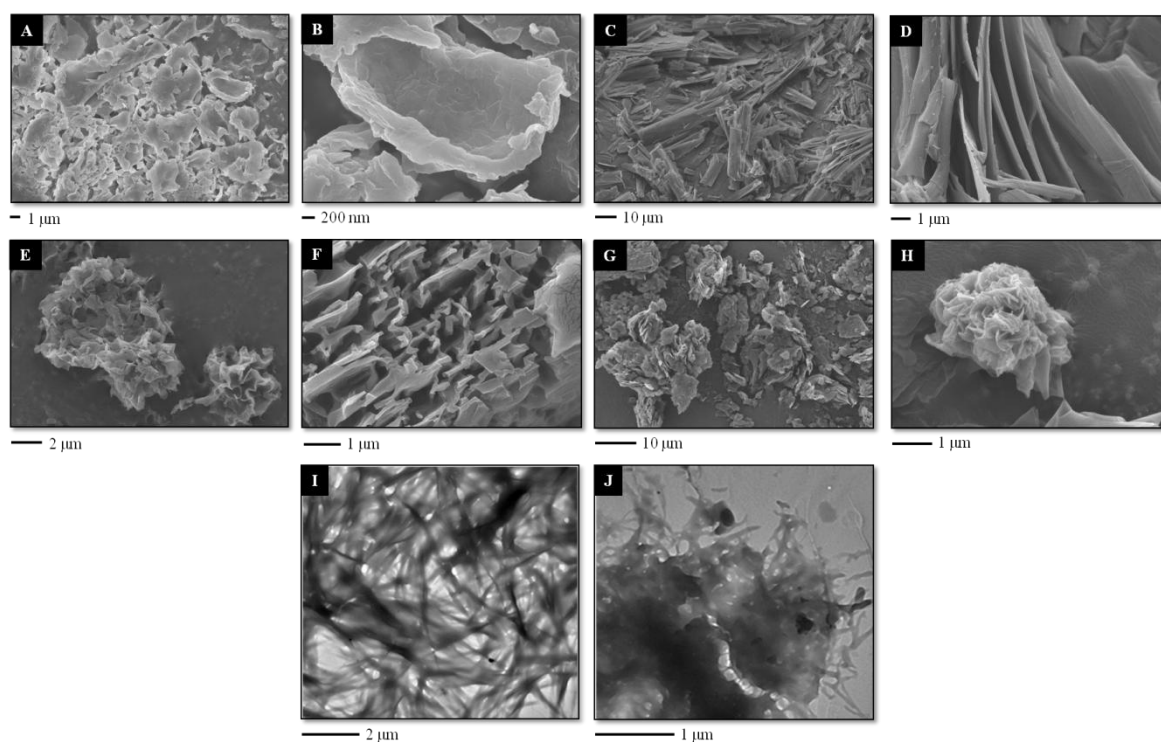
Fig. 9 FESEM (**A-H**) and TEM (**I-J**) images of cryogels prepared by the freeze-drying method of materials derived from **C$_{18}$-Glu** and **Click-Glu** at comparable concentrations. **A, B, I**: **C$_{18}$-Glu** in water (25 mg/mL); **C, D**: **C$_{18}$-Glu** in CHCl$_3$ (100 mg/mL); **E, F, J**: **Click-Glu** in water (25 mg/mL); **G, H**: **Click-Glu** in CHCl$_3$ (100 mg/mL).

An exact opposite trend is visible for materials based on **Click-Glu**. In aqueous environment wrinkled lamellar structures are formed consisting of intercalated ribbons

exhibiting dimensions of several μm in length and 100-500 nm in width. On the other hand in CHCl$_3$, the formation of disk-like structures is revealed with diameters between several hundreds of nm and few μm. Additionally transmission electron microscopy (TEM) imaging of cryogels derived from water reveal dense, characteristic fibrillar very dense networks, consisting of bundles of twisted fibers with diameters in a range of tens of nm (smallest feature) and length on the scale of microns (view Figure 9 I, J). The high aspect ratio of the entangled networks is a consequence of a strong anisotropic growth process, which indicates a well ordered molecular packing to form unit nanofibers (for a broader selection of SEM/TEM imaging in further solvents see ESI). When **Click-Glu** is used as gelator the density of the fiber-bundles is much higher in respect to materials where **C$_{18}$-Glu** is used as a gelator. The same observation was made during gas-adsorption measurements using N$_2$ where **C$_{18}$-Glu** revealed an approximate 2.4-fold higher porosity as the **Click-Glu** analogue (53.4 and 22.6 m^2/g respectively; more detailed information can be found in the ESI).

As reported before[18] the formation of different nanostructures could be explained by different hydrogen-bonding (H-bonding) patterns caused by an either polar-protic or apolar environment. For **C$_{18}$-Glu** in protic environment it is supposed, that intermolecular chiral H-bonds between the amide NH-bond and the CO-group of the acid moiety next to the chiral centre occur and hence molecules assemble in spiral molecular bilayers like nanodiscs. Additionally free acid-groups can form inter- and intra-layered intermolecular H-bonds between adjacent acid-groups in the spiral structure.[18, 23] In CHCl$_3$ intramolecular H-bonds are favored and the formation of both intramolecular H-bonds between amide and acid-moieties and then intermolecular H-bonds between free acid-groups could lead to the assemble of nanofibers through hydrophobic and hydrophilic interactions.[18] Due to the isosteric replacement of an amide by a triazole it seems as the more favorable solvent-driven H-bonding patterns change and hence triggering towards desired molecular architectures could be possible as indicated by the exact opposite formation of nano-structures in the case of **Click-Glu**. In order to confirm the statements concluded from morphological observations FT-IR was conducted. Examining the powdered and xerogels states of materials derived from **C$_{18}$-Glu** in CHCl$_3$ and water significant differences can be found as illustrated in **Fig. 11**. In CHCl$_3$ a clear shift in the amide-II band from 1544 cm^{-1} in the powdered state to 1539 cm^{-1} in the xerogel state is visible indicating that the amide NH-group forms H-bonds, which is further confirmed by the shift of the ν_{NH}-band from

3310 to 3332 cm^{-1}. The participation of amide CO-groups in H-bonding is suggested by a shift in the amide-I band from 1649 to 1644 cm^{-1}. No shift of the $\nu_{C=O}$ bands of the carboxylic acid-groups at 1730 and 1717 cm^{-1} indicate free, laterally H-bonded and bifurcated acid-groups, which are necessary for the formation of intra- and inter-layered H-bonds between intermolecular acid and/or amide groups.[18, 24]
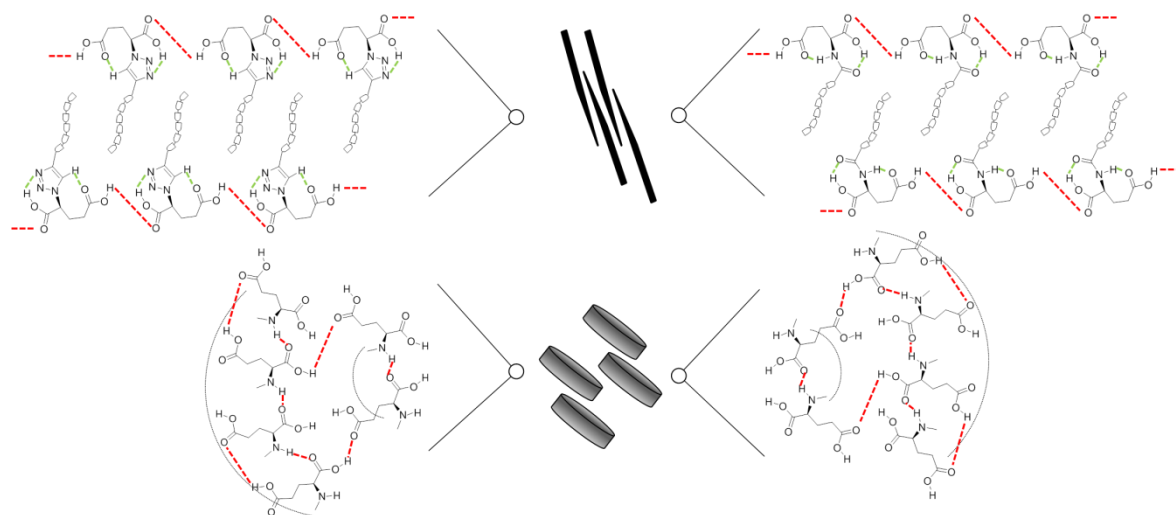

Fig. 10 Potential models of favoured H-bonded self-assembly into nanofibers and ribbons dependent on the nature of the solvent and molecular H-bonding moieties in **C$_{18}$-Glu** and **Click-Glu** respectively. Red lines indicate intermolecular H-bonding and green lines indicate intramolecular H-bonding.[18]

In water on the other hand, the amide-II band is only slightly shifted in xerogel-state from 1544 to 1545 cm^{-1} indicating only a small participation of NH-groups in H-bonding, which is supported by the marginal shift of the ν_{NH}-band from 3310 to 3311 cm^{-1}. No shift of the signals was observed for the amide-I band centered at 1644 cm^{-1}. Interestingly $\nu_{C=O}$ bands of the carboxylic acid-groups centered at 1730 and 1717 cm^{-1} were significantly shifted to 1700 and 1689 cm^{-1} respectively indicating a strong participation of the carboxylic acid moieties in H-bonding. Hence results obtained by FT-IR confirm the potential models of H-bond driven gelation mechanisms illustrated in Figure 10 suggesting that **C$_{18}$-Glu** forms solely intermolecular H-bonds in water, whereas both intra- and intermolecular H-bonds occur in CHCl$_3$. Examining powdered and gel-states of materials derived from **Click-Glu** it is obvious that they behave in an opposite way as compared to materials based on **C$_{18}$-Glu**. In water as solvent ν_{CH}-bands of the triazole moiety significantly shift from 3155 to 3069 cm^{-1} indicating strong participation of the donor-H in H-bonding.
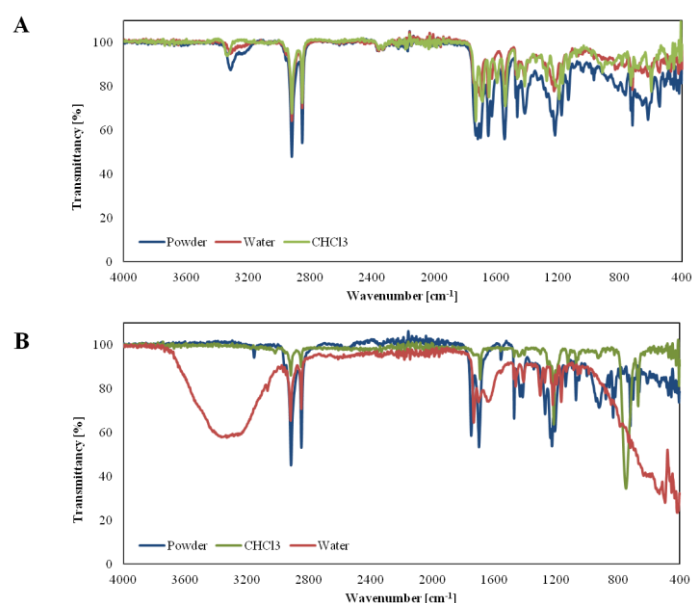
Fig. 11 Comparative FTIR of powder, gels or xerogels of **C₁₈-Glu** (**A**, xerogels) and **Click-Glu** (**B**, gels) respectively illustrating potential mechanisms of H-bonded driven gelation.

Additionally $\nu_{C=O}$ bands centered at 1749 and 1699 cm^{-1} are shifted towards 1733 and 1674 cm^{-1} respectively in the gel-state indicate the participation of the carboxylic acid moieties in H-bonding. On the other hand in CHCl₃ as solvent only little participation of the triazole H-donor is visible as indicated by a marginal shift from 3155 to 3154 cm^{-1}. Additionally the strong $\nu_{C=O}$ bands are not shifted in comparison to the powdered state indication free and laterally H-bonded necessary to intermolecular H-bonds as mentioned above and confirming the mechanisms of H-bonding dependent on the solvent as mentioned above. Hence it is obvious that **Click-Glu** forms solely intermolecular H-bonds in CHCl₃, whereas both types of H-bonding occur in water.

5.3.4   Considerations on controlled release of vancomycin

As mentioned earlier triazoles are very important building blocks for the development of novel drug-systems or fabrication of biomimetic materials such as peptide-mimetics and have hence found broad application in medicinal chemistry. On the other hand, supramolecular gels and in specific hydrogels have been recognized as promising materials in the fields of catalysis, sensing, cosmetics, environmental remediation and also

biomedicine.[25] The physical properties of hydrogels, resembling those of natural systems,[26] combined with the concept of incorporating a triazole could result in the formation of materials, which are very attractive for bioscience and biotechnology. Many gel-systems have already proven to be suitable systems in controlled drug release.[27] In this context investigations on controlled drug release using hydrogels based on **C$_{18}$-Glu** and **Click-Glu** were carried out. The hydrochloric acid salt of vancomycin was selected as model drug. Vancomycin is a type of glycopeptide antibiotic and used in the treatment of infections caused by Gram-positive bacteria. It is one of the quite rare natural haloorganic compounds and was first isolated in 1953.[28] Hydrophilic drugs like vancomycin are known to predominately distribute into the solvent phase rather than in the gel resulting in a relative quick and mostly complete release during drug release experiments, which makes this type of drug very interesting for potential application.[29]
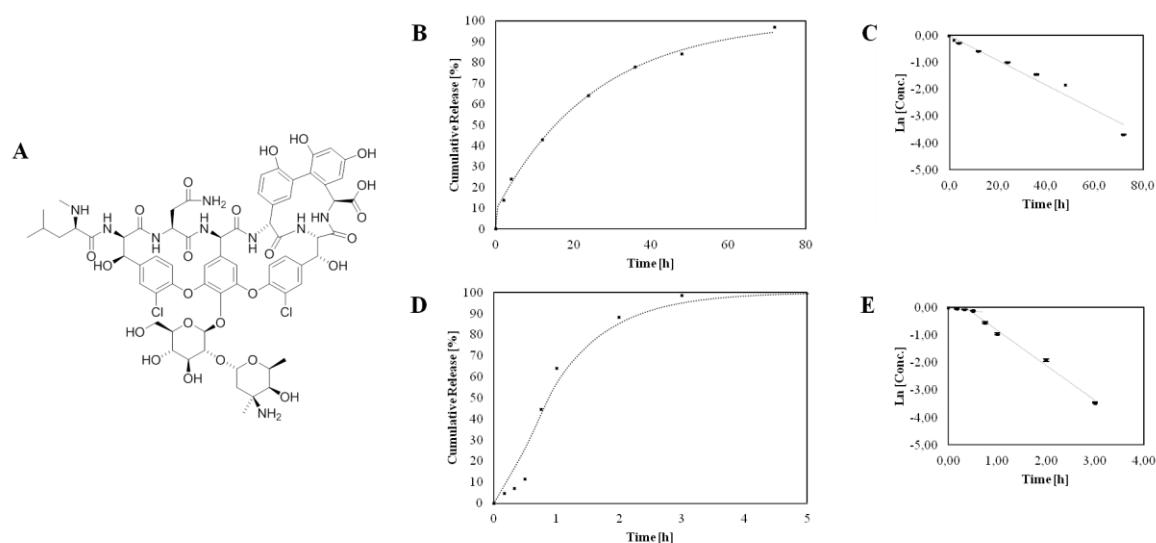
Fig. 12 Chemical structure of vancomycin (**A**) and controlled drug release studies from hydrogels based on **C$_{18}$-Glu** (**B, C**) and **Click-Glu** (**D, E**) at 50 mg/mL against PBS.

As mentioned earlier hydrogel-materials based on **Click-Glu** dissolve in the presence of PBS-buffer (< 3 h), whereas materials based on **C$_{18}$-Glu** remained stable for at least 7 d. This feature of selective degradation of the materials could have interesting influences in the release rate of drugs and is a key-advantage against conventional hard non-hydrogel materials like PLGA or hydroxyapatite.[29c)] Controlled release experiments of vancomycin (for detailed information see the experimental section) revealed a quite fast and complete

201

release of the drug from materials based on **Click-Glu** within 3 h as expected by a complete dissolution of the materials in the presence of PBS. On the other hand much slower, but complete release was observed in materials based on **C$_{18}$-Glu** after 72 h (view Figure 12). Release kinetics could be easily and smoothly fitted against 1st order rate-laws in the case of **C$_{18}$-Glu** resulting in $k_{obs} = 4.6 \pm 0.18 \times 10^{-2}$ h^{-1}. Release from **Click-Glu** materials revealed a two step process with a relative slow start (until 45 min from the start of the experiments) $k_{Obs} = 22.3 \pm 2.67 \times 10^{-2}$ h^{-1} before the material significantly starts to dissolve and a relative fast step $k_{Obs} = 135.1 \pm 34.17 \times 10^{-2}$ h^{-}1 afterwards. In an overall view vancomycin is released ca. 17-fold faster from **Click-Glu** based hydrogels mainly due to dissolution of the materials in the presence of PBS.

5.4. Conclusions

In summary we were able to successfully transfer the known concept of isosteric replacement of amides with triazoles from medicinal chemistry into the field of soft gel-materials. The two model compounds **C$_{18}$-Glu** and **Click-Glu** revealed significant differences in gelation properties during the studies carried out. **Click-Glu** revealed superior behavior with respect to *CGC*, T_{gel} and mechanical stabilities in polar protic solvents whereas **C$_{18}$-Glu** exhibited improved properties in apolar and aromatic solvents. Investigations on the morphology of the model-compounds in water and CHCl$_3$ conducted by electron microscopy give indication for inter- and/or intramolecular H-bonding driven changes for the formation of nanostructures dependent on both solvent-polarity and the nature of the compounds. Further confirmation of the participation of certain H-bonding interactions was obtained by FT-IR experiments. Additional controlled drug release studies of vancomycin reveal potential applications of both systems in biomedicine and biotechnology.

→ For further information on compound synthesis and characterization, further gel characterization and gas-sorption experiments see the electronic supplementary information (ESI) on the enclosed CD.

5.5. References

[1]   a) G. A. Patani and E. J. LaVoie, *Chem. Rev.*, 1996, **96**, 3147-3176; b) H. Kubinyi, *J. Braz.Chem. Soc.*, 2002, **13**, 717-726; c) T. Fujita, *Biosci. Biotech. Biochem.*, 1996, **60**, 557-566; d) C. D. Siebert, *Chem. Unserer Zeit*, 2004, **38**, 320-324; e) S. R. Langdon, P. Ertl and N. Brown, *Mol. Inf.*, 2010, **29**, 366-385; f) C. W. Thornber, *Chem. Soc. Rev.*, 1979, **8**, 563-580; g) C. A. Lipinski, *Annu. Rep. Med. Chem.*, 1986, **21**, 283-291; h) A. Burger, *Prog. Drug Res.*, 1991, **37**, 287-371; i) C. Hansch, *Drug Dev. Res.*, 1981, **1**, 267-309.

[2]   I. Langmuir, *J. Am. Chem. Soc.*, 1919, **41**, 1543-1559.

[3]   a) H. G. Grimm, *Z. Electrochem.*, 1925, **31**, 474-480; b) H. G. Grimm, *Naturwissenschaften*, 1929, **17**, 557-564.

[4]   H. Erlenmeyer and M. Leo, *Helv. Chim. Acta*, 1932, **15**, 1171-1186.

[5]   H. L. Friedman, *NASNRS*, 1951, **206**, 295-358.

[6]   a) A. F. Spatola in *Chemistry and Biochemistry of Amino Acids, Peptides and Proteins*, Weinheim, New York, 1983, 267-357; b) A. Giannis and T. Kolter, *Angew. Chem. Int. Ed.*, 1993, **32**, 1244-1267; c) A. Da Settimo, G. Primofiore, A. M. Marini, F. Da Settimo, V. Nuti, C. Martini, L. Trincavelli and A. Lucacchini, *Farmaco*, 1997, **52**, 421-428; d) C. L. Jenkins, M. M. Vasbinder, S. J. Miller and R. T. Raines, *Org. Lett.*, 2005, **7**, 2619-2622; e) J. Bieschke, S. J. Siegel, Y. Fu and J. W. Kelly, *Biochemistry*, 2008, **47**, 50-59; f) C. I. Fincham, M. Higginbottom, D. R. Hill, D. C. Horwell, J. C. O´Tool, G. S. Ratcliff, D. C. Reese and E. Roberts, *J. Med. Chem.*, 1992, **35**, 1472-1484; g) A. Reiner, D. Wildemann, G. Fischer and T. Kiefhaber, *J. Am. Chem. Soc.*, 2008, **130**, 8079-8084; h) P. Chen and J. Qu, *J. Org. Chem.*, 2011, 76, 2994-3004; i) P. Claudon, A. Violette, K. Lamour, M. Decossas, S. Fournel, B. Heurtault, J. Godet, Y. Mely, B. Jamart-Gregoire, M.-C. Averlant-Petit et al., *Angew. Chem. Int. Ed.*, 2010, 49, 333-336; j) C. S. J. Walpole, R. Wrigglesworth, S. Bevan, E. A. Campbell, A. Dray, I. F. James, K. J. Masdin, M. N. Perkins and J. Winter, *J. Med. Chem.*, 1993, 36, 2373-2380; k) V. Di Marzo, G. Griffin, L. De Petrocellis, I. Brandi, T. Bisogno, W. Williams, M. C. Grier, S. Kulasegram, A. Mahadevan, R. K. Razdan et al., *J. Pharmacol. Exp. Ther.*, 2002, **300**, 984-991; l) A. Duranti, A. Tontini, F. Antonietti, F.

Vacondio, A. Fioni, C. Silva, A. Lodola, S. Rivara, C. Solorzano, D. Piomeli et al., *J. Med. Chem.*, 2012, **55**, 4824-4836; m) K. M. Patil, R. J. Naik, Rajpal, M. Fernandes, M. Ganguli and V. A. Kumar, *J. Am. Chem. Soc.*, 2012, **134**, 7196-7199; n) D. B. A. De Bont, K. M. Sliedregt-Bol, L. J. F. Hofmeyer and R. M. J. Liskamp, *Bioorgan. Med. Chem.*, 1999, 7, 1043-1047; o) F. Navas III, F. L. M. Tang, L. T. Schaller and M. H. Norman, *Bioorgan. Med. Chem.*, 1998, **6**, 811-823.

7   a) S. A. Boyd, A. K. L. Fung, W. R. Baker, R. A. Mantei, H. H. Stein, J. Cohen, J. L. Barlow, V. Klinghofer, J. L. Wessale, K. M. Verburg, J. L. Polakowski, A. L. Adler, S. V. Calzadilla, P. Kovar, Z. Yao, C. W. Hutchins, J. F. Denissen, B. A. Grabowski, S. Cepa, D. J. Hoffmann, K. W. Garren and H. D. Kleinert, *J. Med. Chem.*, 1994, **37**, 2991-3007; b) K. E. Andersen, A. S. Joergensen and C. Braestrup, *Eur. J. Med. Chem.*, 1994, **29**, 393-399; c) F. I. Carrol, J. L. Gray, P. Abraham, M. A. Kuzemko, A. H. Lewin, L. W. Boja and M. J. Kuhar, *J. Med. Chem.*, 1993, **36**, 2886-2890; d) L. J. Street, R. Baker, J. L. Castro, M. S. Chambers, A. R. Guiblin, S. C. Hobbs, V. G. Matassa, A. J. Reeve, M. S. Beer, D. N. Middlemiss, A. J. Noble, J. A. Stanton, K. Scholey and R. J. Hargreaves, *J. Med. Chem.*, 1993, **36**, 1529-1538; e) P. G. Dunbar, G. J. Durant, Z. Fang, Y. F. Abuh, A. A. El-Assadi, D. O. Ngur, S. Periyasamy, W. P. Hoss and W. P. Messer Jr., *J. Med. Chem.*, 1993, **36**, 842-847; f) K. E. Andersen, B. F. Lundt, A. S. Joergensen and C. Braestrup, *Eur. J. Med. Chem.*, 1996, **31**, 417-425; g) J. C. Legeay, J. J. Vanden Eynde and J. P. Bazureau, *Tetrahedron Lett.*, 2007, **48**, 1063-1068.

8   a) G. W. Adelstein, C. H. Yen, E. Z. Dajani and R. G. Bianchi, *J. Med. Chem.*, 1976, **19**, 1221-1225; b) W. R. Tully, C. R. Gardner, R. J. Gillespie and R. Westwood, *J. Med. Chem.*, 1991, **34**, 2060-2067; c) B. S. Orlek, F. E. Blaney, F. Brown, M. S. G. Clark, M. S. Hadley, J. Hatcher, G. J. Riley, H. E. Rosenberg, H. J. Wadsworth and P. Wyman, *J. Med. Chem.*, 1991, **34**, 2726-2735; d) Z. Li, P. Zhen and X. Liu, *Mini Rev. Med. Chem.*, 2011, **11**, 1130-1142.

9   a) S. K. Thompson, A. M. Eppley, J. S. Frazee, M. G. Darcy, R. T. Lum, T. A. Tomaszek, L. A. Ivanhoff, J. F. Morris, E. J. Sternberg, D. M. Lambert, A. V. Fernandez, S. R. Petteway, T. D. Meek, B. W. Metcalf and J. G. Gleason,

Bioorg. Med. Chem. Lett., 1994, **4**, 2441-2446; b) G. C. Tron, T. Pirali, R. A. Billington, P. L. Canonico, G. Sorba and A. A. Genazzani, *Med. Res. Rev.*, 2008, **28**, 278-308; c) Y. L. Angell and K. Burgess, *Chem. Soc. Rev.*, 2007, **36**, 1674-1689; d) M. Corredor, J. Bujons, M. Orzáes, M. Sancho, E. Peréz-Payá, I. Alfonso and A. Messeguer, *Eur. J. Med. Chem.*, 2013, **63**, 892-896; e) G. Appendino, S. Bacchiega, A. Minassi, M. G. Cascio, L. De Petrocellis and V. Di Marzo, *Angew. Chem. Int. Ed.*, 2007, **119**, 9472-9475; f) A. Tam, U. Arnold, M. B. Soellner and R. T. Raines, *J. Am. Chem. Soc.*, 2007, **129**, 12670-12671; g) D. J. Pedersen and A. Abell, *Eur. J. Org. Chem.*, 2011, **13**, 2399-2411; h) A. Brik, J. Alexandratos, Y.-C. Lin, J. H. Elder, A. J. Olson, A. Wladower, D. S. Goodsell and C. H. Wong, *Chem. Bio. Chem.*, 2005, **6**, 1167-1169; i) J. M. Holub and K. Kirshenbaum, *Chem. Soc. Rev.*, 2010, **39**, 1325-1337; j) V. D. Bock, D. Speijer, H. Hiemstra and J. H. van Maarseveen, *Org. Biomol. Chem.*, 2007, **5**, 971-975.

[10] a) V. V. Rostovtsev, L. G. Green, V. V. Fokin and K. B. Sharpless, *Angew. Chem. Int. Ed.*, 2002, **41**, 2596-2599; b) C. W. Tornoe, C. Christensen and M. Meldal, *J. Org. Chem.*, 2002, 67, 3057-3064.

[11] L. Zhang, X. Chen, P. Xue, H. H. Y. Sun, I. D. Williams, K. B. Sharpless and V. V. Fokin, *J. Am. Chem. Soc.*, 2005, 127, 15998-15999.

[12] a) W. D. Kumler and C. W. Porter, *J. Am. Chem. Soc.*, 1934, **56**, 2549-2554; b) W. W. Bates and M. E. Hobbs, *J. Am. Chem. Soc.*, 1951, **73**, 2151-2156; c) N. G. Vassilev and V. S. Dimitrov, *J. Mol. Struct.*, 1999, **484**, 39-47; d) R. Antoine, I. Compagnon, D. Rayane, M. Broyer, P. Dugourd, G. Breaux, F. C. Hagemeister, D. Pippen, R. R. Hudgins and M. F. Jarrold, *Eur. Phys. J. D*, 2002, **20**, 583-587.

[13] K. Oh and Z. A. Guan, *Chem. Commun.*, 2006, **29**, 3069-3071.

[14] a) J. E. Moses and A. D. Moorhouse, *Chem. Soc. Rev.*, 2007, **36**, 1249-1262; b) M. Juricek, P. H. J. Kouwer and A. E. Rowan, *Chem. Commun.*, 2011, **47**, 8740-8749; c) A. J. Dirks, J. J. L. M. Cornelissen, F. L. van Delft, J. C. M. van Hest, R. J. M. Nolte, A. E. Rowan and F. P. J. T. Rutjes, *QSAR Comb. Sci.*, 2007, **26**, 1200-1210.

[15] a) J. J. Bryant and U. H. F. Bunz, *Chem. Asian J.*, 2013, **8**, 1354-1367; b) Y. H. Lau, P. J. Rutlegde, M. Watkinson and M. H. Todd, *Chem. Soc. Rev.*, 2011, **40**, 2848-2866.

[16] a) J.-S. Qin, D.-Y. Du, W.-L. Li, J.-P. Zhang, S.-L. Li, Z.-M. Su, X.-L. Wang, Q. Xu, K.-Z. Shao and Y.-Q. Lan, *Chem. Sci.*, 2012, **3**, 2114-2118; b) S. Wang, T. Zhao, G. Li, L. Wojtas, Q. Huo, M. Eddaoudi and Y. Liu, *J. Am. Chem. Soc.*, 2010, **132**, 18038-18041; c) R.-B. Lin, D. Chen, Y.-Y. Lin, J.-P. Zhang and X. M. Chen, *Inorg. Chem.*, 2012, **51**, 9950-9955.

[17] For selected articles view: a) K. Ghosh, A. R. Sarkar and A. P. Chattopadhyay, *Eur. J. Org. Chem.*, 2012, **7**, 1311-1317; b) K. Kuroiwa, T. Shibata, A. Takada, N. Nemoto and N. Kimizuka, *J. Am. Chem. Soc.*, 2004, **126**, 2016-2021; c) R. T. Chen, S. Marchesan, R. A. Evans, K. E. Styan, G. K. Such, A. Postma, K. M. McLean, B. W. Muir and F. Caruso, *Biomacromolecules*, 2012, **13**, 889-895; d) G. Ghini, L. Lascialfari, C. Vinattieri, S. Cicchi, A. Brandi, D. Berti, F. Betti, P. Baglioni and M. Mannini, *Soft Matter*, 2009, **5**, 1863-1869; e) D. D. Díaz, J. J. M. Tellado, D. G. Velázquez, A. G. Ravelo, *Tetrahedron Lett.*, 2008, **49**, 1340-1343; f) J. Zhang, H.-F. Chow, M.-C. Chan, G. K.-W. Chow and D. Kuck, *Chem. Eur. J.*, 2013, **19**, 15019-15025; g) D. Liu, D. Wang, M. Wang, Y. Zheng, K. Koynov, G. K. Auernhammer, H. J. Butt and T. Ikeda, *Macromolecules*, 2013, **46**, 4617-4625; h) V. Bhalla, H. Singh, M. Kumar and S. K. Prasad, *Langmuir*, 2011, **27**, 15275-15281; i) S. M. Park, Y. S. Lee and B. H. Kim, *Chem. Commun.*, 2003, **23**, 2912-2913; j) A. Hemamalini and T. M. Das, *New J. Chem.*, 2013, **37**, 2419-2425; k) O. Roubeau, A. Colin, V. Schmitt and R. Clérac, *Angew. Chem. Int. Ed.*, 2004, **43**, 3283-3286; l) R. M. Meudtner and S. Hecht, *Macromol. Rapid Commun.*, 2008, **29**, 347-351; m) J. P. Byrne, J. A. Kitchen, O. Kotova, V. Leigh, A. P. Bell, J. J. Boland, M. Albrecht and T. Gunnlaugsson, *Dalton Trans.*, 2014, **43**, 196-209; n) X. Yan, D. Xu, X. Chi, J. Chen, S. Dong, X. Ding, Y. Yu, F. Huang, *Adv. Mater.*, 2012, **24**, 362-369; o) S.-L. Yim, H.-F. Chow, M.-C. Chan, C.-M. Che and K.-H. Low, *Chem. Eur. J.*, 2013, **19**, 2478-2486; p) J. Yuan, H. Zhang, G. Hong, Y. Chen, G. Chen, Y. Xu and W. Weng, *J. Mater. Chem. B*, 2013, **1**, 4809-4818; q) J. Yuan, X. Fang, L. Zhang, G. Hong, Y. Lin, Q. Zheng, Y. Xu, Y. Ruan, W. Weng, H. Xia and G. Chen, *J. Mater. Chem.*, 2012, **22**, 11515-11522; r) V.

Mishra, S.-H. Jung, J. M. Park, H. M. Jeong and H.-I. Lee, *Macromol. Rapid Commun.*, 2013, DOI: 10.1002/marc.201300585; s) N.-T. Huynh, Y.-S. Jeon, M. Zrinyi and J.-H. Kim, *Polym. Int.*, 2013, **62**, 266-272; t) D. D. Díaz, K. Rajagopal, E. Strable, J. Schneider and M. G. Finn, *J. Am. Chem. Soc.*, 2006, **128**, 6056-6057.

18 P. Gao, C. Zhan, L. Liu, Y. Zhou and M. Liu, *Chem. Commun.*, 2004, **10**, 1174-1175.

19 J. E. Eldrige, J. D. Ferry, *J. Phys. Chem.*, 1954, **58**, 992-995.

20 See ESI for further information.

21 a) L. Lu, T. M. Cocker, R. E. Bachman, R. G. Weiss, *Langmuir*, 2000, **16**, 20-34; b) J. Becerril, B. Escuder, J. F. Miravet, R. Gavara, S. V. Luis, *Eur. J. Org. Chem.*, 2005, **3**, 481-485.

22 See chapter 3 in this thesis.

23 a) Y. J. Zhang, M. Jin, R. Lu, Y. L. Song, L. Jiang, Y. Y. Zhao and T. J. Li, *J. Phys. Chem. B*, 2002, **106**, 1960-1967; b) K. Sakamoto and M. Hatano, *Bull. Chem. Soc. Jpn.*, 1980, **53**, 339-343.

24 M. Kogiso, T. Hanada, K. Yase and T. Shimizu, *Chem. Commun.*, 1998, **17**, 1791-1792; L. Sun, L. J. Kepley and R. M. Crooks, *Langmuir*, 1992, **8**, 2101-2103; J. Dong, Y. Ozaki and K. Nakashima, *Macromolecules*, 1997, **30**, 1111-1117.

25 a) D. Derossi, Y. Kajiwara, Y. Osada, *Polymer Gels: Fundamentals and Biomedical Applications*, Plenum Press, New York, 1991, and references therein; b) J. H. Jung, S. Shinkai, *Top. Curr. Chem.*, 2004, **248**, 223-260; c) N. M. Sangeetha, U. Maitra, *Chem. Soc. Rev.*, 2005, **34**, 821-836; d) R. V. Ulijn, A. M. Smith, *Chem. Soc. Rev.*, 2008, **37**, 664-675; e) A. R. Hirst, B. Escuder, J. F. Miravet, D. K. Smith, *Angew. Chem. Int. Ed.*, 2008, **47**, 8002-8018; f) M. O. M. Piepenbrock, G. O. Lloyd, N. Clarke, J. W. Steed, *Chem. Rev.*, 2010, **110**, 1960-2004; g) D. D. Diaz, D. Kühbeck, R. J. Koopmans, *Chem. Soc. Rev.*, 2011, **40**, 427-448.

26 G. H. Pollack in *Cells, gels and the engines of life: A new, unifying approach to cell function*, Ebner & Sons, 2001.

27 For reviews see: a) B. Jeong, S. W. Kim and Y. H. Bae, *Adv. Drug Deliv. Rev.*, 2002, **54**, 37-51; b) M. Goldberg, R. Langer and X. Jia, *J. Biomat. Sci.*, 2007,

18, 241-268; c) N. A. Peppas, *J. Bioact. Compat. Pol.*, 1991, **6**, 241-246; d) H. J. Chung and T. G. Park, *Nano Today*, 2009, **4**, 429-437; e) K. Kabiri, H. Omidian, M. J. Zohurrian-Mehr and S. Doroudiani, *Polym. Composite.*, 2011, **32**, 277-289. For selected references see: f) I. C. Kwon, Y. H. Bae and S. W. Kim, *Nature*, 1991, **354**, 291-293; g) K. Kataoka, H. Miyazaki, M. Bunya, T. Okano and Y. Sakurai, *J. Am. Chem. Soc.*, 1998, **120**, 12694-12695; h) Z. Wu, X. Zhang, H. Guo, C. Li and D. Yu, *J. Mater. Chem.*, 2012, **22**, 22788-22796; i) A. Wang, Y. Cui, J. Li and J. C. M. van Hest, *Adv. Func. Mat.*, 2012, **22**, 2673-2681; j) P. Zou, J. Suo, L. Nie and S. Feng, *J. Mater. Chem., 2012*, **22**, 6316-6326; k) Y. Takemoto, H. Ajiro, T.-A. Asoh and M. Akashi, *Chem. Mater.*, 2010, **22**, 2923-2929; l) J. A. Saez, B. Escuder and J. F. Miravet, *Chem. Commun.*, 2010, **46**, 7996-7998.

[28] a) P.-A. Ashford and S. P. Bew, *Chem. Soc. Rev.*, 2012, **41**, 957-978; b) B. K. Hubbard and C. T. Walsh, *Angew. Chem. Int. Ed.*, 2003, **42**, 730-765; c) A. J. Zhang and K. Burgess, *Chem. Int. Ed.*, 1999, **38**, 634-636.

[29] a) A. Gutowska, Y. H. Bae, J. Feijen and S. W. Kim, *J. Control. Rel.*, 1992, **22**, 95-104; b) A. Gutowska, J. S. Bark, I. C. Kwon, Y. H. Bae, Y. Cha S. W. Kim, *J. Control. Rel.*, 1997, **48**, 141-148; c) D. J. Overstreet, R. Huynh, K. Jarbo, R. Y. McLemore and B. L. Vernon, *J. Biomed. Mat. Res.*, 2013, **101**, 1437-1446; d) B. Jeong, Y. H. Bae and S. W. Kim, *J. Control. Rel.*, 2000, **63**, 155-163.

209

E List of Abbreviations

1D	1-dimensional	**DNA**	deoxyribonucleic acid
2D	2-dimensional	**DOPA**	3,4-dihydroxy-*L*-phenylalanine
3D	3-dimensional	**DSC**	differential scanning calorimetry
ADP	adenosine diphosphate	**DSS**	dynamic strain sweep
AFM	atomic-force microscopy	**DTS**	dynamic time sweep
Asp	aspartic acid	**ECM**	extracellular matrix
ATP	adenosine triphosphate	**EDC**	*N*-(3-dimethylaminopropyl)-*N'*-ethylcarbodiimide hydrochloride
azoPhe	*p*-(phenylazo)-*L*-phenylalanine	**ESI**	electronic supplementary information
Boc	*tert*-butoxycarbonyl	**EtOH**	ethanol
Bzl	benzyl	**FE**	field emission
CD	compact disc	**FT**	Fourier transformed
CGC	critical gelation concentration	*G'*	storage modulus
CuAAC	Cu-catalyzed azide alkyne cycloaddition	*G''*	loss modulus
DABCO	1,4-diazabicyclo[2.2.2]octane	**H-**	hydrogen-
DFS	dynamic frequency sweep	**HC**	heating-cooling
DFT	density function theory	**HFIP**	hexafluoro isopropanol
DMF	dimethyl formamide	**HG**	hydrogel
DMSO	dimethyl sulfoxide	**HOBt**	1-hydroxybenzotriazole

IFM	inverse flow method	**PNIPAAm**	poly(*N*,*N'*-isopropylacrylamide)
IR	infrared	**POP**	pure organic phase
k_{obs}	rate constant	**PPDA**	*para*-phenylenediamine
LCST	lower critical solution temperature	**PSG**	phase selective gelation
LED	light emitting diode	**PSOG**	phase selective organogelator
LMW	low molecular weigth	**QD**	quantum dot
MD	molecular dynamics	**RFT**	riboflavin tetraacetate
MeCN	acetonitrile	**RGD**	arginine-glycine-aspartic acid
MeOH	methanol	**RNA**	ribonucleic acid
MGC	minimum gelation concentration	**rpm**	rounds per minute
MPDA	*meta*-phenylenediamine	**RT**	room temperature
MW	molecular weight	**SAFIN**	self-assembled fibrillar network
NaDC	sodium deoxycholate	**SEC**	size exclusion chromatography
NMR	nuclear magnetic resonance	**SEM**	scanning electron microscopy
NP	nanoparticle	**SWNT**	single-walled carbon nanotube
OG	organogel	**tan** δ	loss factor
OPDA	*ortho*-phenylenediamine	**TEM**	transmission electron microscopy
PBMA	poly(butylmethacrylate)	**TFA**	trifluoroacetic acid
PBS	phosphate buffer saline	**TFSA**	bis(trifluoromethanesulfonyl)amide
PDEAM	poly(*N*,*N'*-diethylaminoethyl methacrylate)	**TGA**	thermo-gravimetric analysis
PEG	poly(ethylene glycol)	T_{gel}	gel-to-sol transition temperature
Phe	phenylalanine	**TMV**	tobacco mosaic virus

211

TOF	turnover frequency	**UV**	ultra-violet
TON	turnover number	**vis**	visible
US	ultrasound		

F Curriculum Vitae

Persönliche Angaben

Name: Bachl	
Vorname: Jürgen Walter	
Geschlecht: männlich	
Geburtsdatum/-ort: 29.04.1986 in Furth im Wald, Bayern	
Familienstand: ledig	
Staatsangehörigkeit: Deutsch	
Adresse: Fichtenweg 5, 93485 Rimbach	
Mobil: 0171-7782497	
Mail: bachl_j@web.de	

Schule und Studium

06/2005	Abitur (Note 2,6) am Benedikt-Stattler-Gymnasium in Bad Kötzting
10/2005	Beginn des Chemiestudiums and der Universität Regensburg
09/2008	Bachelor of Science (B. Sc.) in Chemie (Note 2,2) an der Universität Regensburg mit der Arbeit „Entwicklung eines lipophilen molekularen Schalters zum Einbau in Liposome" (Note 1,3 unter Betreuung von Prof. Dr. Burkhard König)
09/2010	Master of Science (M. Sc.) in Chemie (Note 1,7) an der Universität Regensburg mit der Arbeit „Synthesis, characterization and evaluation of supramolecular gels as nanoreactors in photochemical processes" (Note 1,3 unter Betreuung von Prof. Dr. David Díaz Díaz)
Seit 10/2010	Promotion an der Universität Regensburg mit dem Thema „Engineering new supramolecular gels: From catalysis to drug delivery" unter Betreuung von Prof. Dr. David Díaz Díaz.

213

02/2013 - 04/2013	Forschungsaufenthalt am Institut für organische Chemie der Universität Zaragoza unter Betreuung von Prof. Carlos Cativiela

Stipendien, Förderung und Anstellungen

02/2010 - 09/2010	Anstellung als wissenschaftliche Hilfskraft an der Universität Regensburg
12/2010 - 06/2011	Forschungsstipendium des „Ministerio de Ciencia e Innovación-FEDER (CTQ2010-17436)"
07/2011 - 06/2013	Festanstellung als wissenschaftlicher Mitarbeiter an der Universität Zaragoza mit Arbeitsstelle in Regensburg
07/2013 - 10/2013	Festanstellung als wissenschaftlicher Mitarbeiter an der Universität Regensburg

Forschungsschwerpunkte in Stichworten

Organische Synthese – Polymere – Farbstoffe – „Click-Chemie" – Nachhaltige Chemie – Weiche Materialien – (Photo-) Katalyse – Anwendungen in der Biomedizin – Funktionale Materialien – Kolloide – Formamidine – Hydro-/Organo-/Metallogele – Peptide – Supramolekulare Chemie – Reaktivität in geordnet-strukturierten Systemen – Kohlenstoff-Nanoröhren – Komposit-Materialien

Konferenzen und Symposien

08/2012	Posterpräsentation bei „4th Congress of the European Association for Chemical and Molecular Sciences (EuCheMS)" in Prag mit dem Beitrag „*Exploring organophotocatalysis in nanostructured soft gel materials: Comparison with homogeneous and micellar solutions*"

Publikationsliste

2010	Bachl, J.; Díaz, D. D. in *N,N'-1,2-Phenylenebis[4-*

	(chloromethyl)benzamide], *Molbank*, **2010**, M705
2010	Bachl, J.; Díaz, D. D. in *N,N'-1,2-Phenylenebis[4-(azidomethyl)benzamide]*, *Molbank*, **2010**, M707
2012	Bachl, J.; Wolfbeis, O.; Cativiela, C.; Díaz, D. D. in *(Z)-N-(7-Cyano-9,9,15,15-tetramethyl-9,10,11,13,14,15-hexahydro-6H-benzo[4'',5'']imidazo[1'',2'':1',2']pyrido[3',4':5,6]pyrano[2,3-f]pyrido[3,2,1-ij]quinolin-6-ylidene)pent-4-ynamide*, *Molbank*, **2012**, M783
2012	Kapoor, I.; Schoen, E.-M.; Bachl, J.; Kuehbeck, D.; Cativiela, C.; Saha, S.; Banerjee, R.; Roelens, S.; Marrero-Tellado, J. J.; Díaz, D. D. in *Competition between gelation and crystallization of a peculiar multicomponent liquid system based on ammonium salts*, *Soft Matter*, **2012**, *8*, 3446-3456
2012	Bachl, J.; Huber, T.; Kuehbeck, D.; Schoen, E.-M.; Brunner, G.; Kraus, B.; Heilmann, J.; Codelli, J. A.; Bertozzi, C. R.; Cativiela, C.; Díaz, D. D. in *Hybrid bioactive hydrogels containing single-walled carbon nanotubes covalently integrated via strain-promoted azide-alkyne cycloaddition*, *Nanoscience and Nanotechnology Asia*, **2012**, *2*, 200-209
2013	Fatás, P.; Bachl, J.; Oehm, S.; Jiménez, A. I.; Cativiela, C.; Díaz, D. D. in *Multistimuli responsive supramolecular organogels formed by novel low-molecular-weight peptides bearing side-chain azobenzene moieties*, *Chemistry - A European Journal*, **2013**, *19*, 8861-8874
2013	Bachl, J.; Hohenleutner, A.; Dhar, B. B.; Maitra, U.; Koenig, B.; Díaz, D. D. in *Organophotocatalysis in nanostructured softgel materials as tunable reaction vessels: Comparison with homogeneous and micellar solutions*, *Journal of Material Chemistry A*, **2013**, *1*, 4577-4588
2013	Kuehbeck, D.; Schoen, E.-M.; Bachl, J.; Gotor-Fernández, V.; Díaz, D. D. in *Gelatin protein-mediated direct aldol reaction*, *Helvetica Chimica Acta*, **2013**, angenommen
2014	Saha, S.; Bachl, J.; Kundu, T.; Díaz, D. D.; Banerjee, R. in *Amino acid-based multiresponsive low-molecular-weight metallo-hydrogels with*

	load-bearing and rapid self-healing ability, *Chemical Communication.*, **2014**, *50*, 3004-3006.
2014	Bachl, J.; Zanuy, D.; López-Pérez, D. E.; Revilla-López, G.; Cativiela, C.; Alemán, C.; Díaz, D. D. in _Synergistic computational-experimental approach to improve ionene polymer-based functional hydrogels_, *Advanced Functional Mateials*, **2014**, angenommen.

Erfahrungen in Lehre und Koordination

Betreuung von Bachelorarbeiten

2011	Jäger, Stefanie: „_Gelation properties of Phe-Phe dipeptide derivatives (I)_", Institut für Organische Chemie, Universität Regensburg
2011	Kolb, Anika: „_Gelation properties of Phe-Phe dipeptide derivatives (II)_", Institut für Organische Chemie, Universität Regensburg
2011	Mayr, Judith: „_Synthesis, characterization and evaluation of different surfactant free, ionic polymer isomers, forming hydrogels_", Institut für Organische Chemie, Universität Regensburg
2011	Keseberg, Pia: „_Effects of non-covalent inclusion of phthalocyanines on the properties of low and high molecular weight gels_", Institut für Organische Chemie, Universität Regensburg

Betreuung von Forschungspraktika

2010	Smith, Justin: „_Studies of several gel-related projects: catalytic hydrogel beads, gel-phase photo chemistry, and orthogonally synthesized biopolymer matrices for pollutant removal_", Institut für Organische Chemie, Universität Regensburg
2010	Gillick, Paul: „_New azo-containing low-molecular-weight peptides and their evaluation as organogelators_", Institut für Organische Chemie, Universität Regensburg

2011	Minderjahn, Julia: „*Nanochemistry- Synthesis and characterization of soft functional materials*", Institut für Organische Chemie, Universität Regensburg
2013	Feldner, Tobias: „*Synthesis, characterization and evaluation of a novel formamidine-based organogelator for potential heavy metal-sensing*", Institut für Organische Chemie, Universität Regensburg
2013	Betreuung eines Saalpraktikums der organischen Chemie für Biologen und Lehramtsstudenten im 4. Semester, Institut für Organische Chemie, Universität Regensburg

Fachbezogene Mitgliedschaften

Gesellschaft deutscher Chemiker (GdCh)

Sprachkenntnisse

Deutsch (Muttersprache), Englisch (Fremdsprache - etwa Level C1), Spanisch (Fremdsprache - Basiskenntnisse).

Sonstige Kenntnisse

Ausgeprägte EDV-Kenntnisse im Umgang mit gängigen Office-Programmen und zusätzliche Kenntnisse im Umgang mit fachbezogener Auswerte-Software der analytischen Chemie.

Außeruniversitäres und Interessen

seit 1986	Mitglied des Fingerhaklvereins Gau Bayerischer Wald e.V. zur Erhaltung des Volksbrauchtums
seit 1992	Mitglied des Sportvereins SV Rimbach e.V.

2003 - 2010	Nebentätigkeit als Kinderbetreuer im Feriendorf Wildgatter (Grafenwiesen)
seit 2009	Mitglied des Dartvereins DC Riascherl Briada e.V.
seit 2014	Mitglied des Fischereivereins Furth im Wald e.V.

Interessen: Wandern, Sport (allgemein), Reisen, Angeln.

Academic Reference

Prof. Dr. David Díaz Díaz

Institit für Organische Chemie

Universität Regensburg

Universitätsstrasse 31

D-93053 Regensburg

e-Mail: david.diaz@chemie.uni-regensburg.de

phone: +49 (0)941 943 4373

219

G Acknowledgements

First of all, I would like to thank my supervisor Prof. Dr. David Díaz Díaz for the allocation of an exciting research project, for excellent support, for being always available when personal or professional requests occurred and for the creation of a nice working atmosphere during the past years.

Special thanks goes to Prof. Dr. José Juan Marrero Tellado for acting as my second examiner.

I also wanted to express my gratitude to Prof. Wegener and Prof. Cativiela for financial support.

Moreover, I wanted to thank Prof. Carlos Cativiela for enabling the stay in his laboratories at the ISQHC in Zaragoza (Spain) and supervision during the exchange program.

The years in the Díaz group were very pleasant based on a nice atmosphere in the laboratories. Therefore, special thanks goes to my labmates Dr. Eva Schön and Dr. Dennis Kühbeck.

I also want to express my gratitude to Peter Kreitmeier, Georg Aldolin, Klaus Döring, Helena Konkel and Roxane Harteis for technical support and HPLC analysis.

Additionally I want to thank PD Dr. Rainer Müller for providing lab-space during renovation and for being my third referee.

H Declaration

Herewith, I declare that this present dissertation is a presentation of my original work prepared single-handed. Wherever contributions from others are involved, all of them are marked clearly, with reference to the literature, license, and acknowledgement of collaborative research.

Regensburg, 08 April 2014

_____

Bachl Jürgen